Micro- and sub-microstructuring and characterisation of technical surfaces by means of laser direct writing including a novel approach for laser beam profiling

by

Hauke Buse

A Doctoral Thesis

Submitted in partial fulfilment of the requirements for the award of
Doctor of Philosophy of Loughborough University

March 2011

CERTIFICATE OF ORIGINALITY

This is to certify that I am responsible for the work submitted in this thesis, that the original work is my own except as specified in acknowledgements or in footnotes, and that neither the thesis nor the original work contained therein has been submitted to this or any other institution for a degree.

Signature

Date

Abstract

Within recent years, numerous fields of engineering, like mechanics, optics and electronics, have been influenced and revolutionised by the technique of micro- and nano-structuring. For example, special optical elements for beam shaping, surface structures for the reduction of friction or modern "lab on chip" devices have been produced.

Within this thesis a universal system has been developed facilitating the production of such structured surfaces with dimensions down to 500 nm. This system is not only capable of structuring surfaces by means of lithographic processes; it further allows the inspection of surfaces by scanning their topography.

To realise such a system, two different technologies have been evaluated: Scanning Near-field Optical Lithography (SNOL), a very sophisticated technique which uses a thin fibre tip to expose a photo resist-covered surface, and confocal scanning technology. Here, the confocal scanning is accomplished using an adapted optical component, the optical pickup unit (OPU), from a gaming console, which turned out to be the most suitable and cost-efficient solution for the realisation of this system. Several test series have been carried out during this work, to verify the performance of the confocal system, both to structure photo resist surfaces and to characterise unknown surfaces.

This present work will show the ability of the developed system to produce structures down to the sub-micron range and to characterise unknown surfaces with sub- micron precision. Various patterns have been written into photo resist-coated substrates to structure their surface. Beginning with diffractive optical elements (DOE) for beam shaping, followed by Dammann gratings for two-dimensional beam shaping and optical gratings for light guidance as well as producing technical surfaces imitating the properties of sharkskin or simple micro-mechanical structures, the developed confocal system has shown itself to be flexible and widely-applicable.

During the development of the confocal system, a strong need for a beam profiling system analysing the light beam diverging from the OPU, was recognised. Due to the fact that no commercially available system was capable of characterising beam sizes within the range of the diffraction limit, a novel method for beam profiling was invented. This method makes use of the fibre tips already applied within the SNOL system, producing tomographical scans of the beam spot.

Acknowledgements

Thank you, professors Mike Jackson and Rob Parkin for making my PhD project possible and for the support you have given throughout the project.

Thank you, professor Horst Kreitlow for your help, inspiration and guidance during our years of work.

Special thanks to

Arno Hinrichs, Sebastian Menke and Arnold Terviel for your help with electronical and mechanical problems.

Finally, I offer my greatest gratitude for my family for the continuous love and support during my project.

In memory of my beloved Father

Table of content

List of publications

2006 DGAO - German branch of the European optical society (EOS) proceedings "Production of diffractive optical elements by means of near field lithography" ISSN 1614-8436

2006 Scientific reports – Wissenschaftliche Berichte der Hochschule Mittweida "Einsatz der Nahfeldlithografie/ -mikroskopie zur Strukturierung bzw. Charakterisierung von DOE´s sowie zur Vermessung von Laserstrahlprofilen"
ISSN 1430-3698 / 1437-7624

2007 DGAO - German branch of the European optical society (EOS) proceedings "Implementation and application of a "triple wavelength laser diode into a lithography setup" ISSN 1614-8436

 2007 TI-Technologie Informationen 2-2007 ; Published by the technology transfer institutes of the Universities of Lower Saxony "Vorbild Natur –Oberflächen mit Haifischhaut- Effekt

2008 DGAO - German branch of the European optical society (EOS) proceedings "Charakterisierung von Laserstrahlfoki mittels SNOM Faserspitzen und Anwendungen einer 405 nm Optical Pickup Unit" ISSN 1614-8436

2010 Lasers in engineering „Method for characterisation of laser beams diverging from large NA by means of optical fibre tips" (accepted: 23.08.2010)

List of tables

List of figures

All pictures / figures are own work unless otherwise noted within figure annotation

1. Introduction

The following preview gives an overview of this thesis and the benefits of the results to science and industry. In addition, it introduces the thesis structure as well as the content of the individual chapters.

1.1. Scientific benefit

Novel device for structuring as well as characterising of technical surfaces

The system developed and described within this work, combining the possibilities of structuring and characterising (technical) surfaces (Fig 1.1), represents a novelty within the lithographic instrumentation sector.
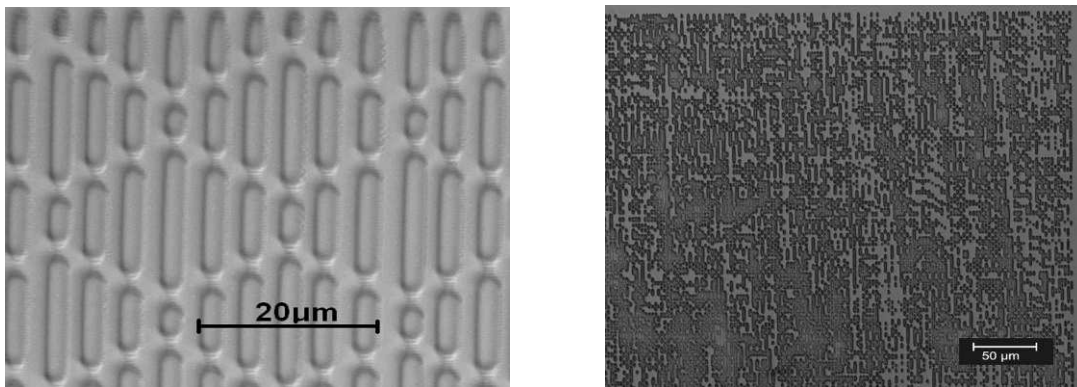
Fig. 1-1: Examples of technical surfaces showing structured photo resist laser with shark skin like properties (left) and a diffractive optical element (DOE) for beam shaping (right)

Moreover, this thesis shows that continuous surface profiles, as shown in Figure 6-28, can be realized by means of this lithographic system.

Development of a system that combines the possibilities of structuring and characterising surfaces using Scanning Near-field Optical Lithography (SNOL), as described in Chapter 3, was the main task within the first year of research.

1

SNOL is a technique which is based on SNOM (Scanning Near-field Optical Microscopy), where a very small light-guiding fibre tip is used to scan and characterize surfaces in order to measure the topography with nanometre resolution. By means of SNOL, photo resist-coated glass substrates are structured by local exposure of the resist surface with laser light (He-Cd – λ: 442nm) guided by these fibre tips.

The development included the construction of a mechanical x-y system consisting of high-precision linear stages to move the photo resist-coated substrates according to the structure which has to be written into the resist surface and the construction of the scanning head holding the optical fibre tip itself.

A technique called "tube-etching" for the preparation of the necessary optical fibre tips will be explained. This delivers fibre tips with repetitious accuracy and better geometries (bigger cone angles) than could be gained compared to the formerly-used production technique (please refer to Chapter 4 and the publication "DGAO proceedings 2006" within the Appendix).

It was recognised that this technology is useful to realize surface inspection and structuring within the nanometre range, but due to its very fragile fibre tip, the substrate/sample has to be moved slowly beneath the tip. Thus it is only profitable for small areas of some hundred microns square. For larger areas (e.g. 2mm square), it will take too long to complete a pattern. To overcome this disadvantage, confocal scanning was positively evaluated as an alternative technique. This technique, presented in Chapter 4, uses a focussing lens to expose the photo resist. Because the main section of an optical disc player (CD, DVD or BluRay©), the optical pickup unit (OPU), contains all necessary parts for reading out data from the optical discs, and since the availability of the Blu-ray© optical disk technology in 2007, a confocal setup taken from a commercial Blu-ray© device was created. By adapting the OPU, a further decrease in the mechanical dimensions and an increased optical resolution has been gained. The ability to operate at a larger distance from the substrate's surface and the increased energy absorption of the used photo resist at 405nm leads to increased writing speeds.

Moreover, the confocal scanning technique is cheaper to realize due to the substitution of the expensive He-Cd laser (λ: 442nm) by a semiconductor laser (λ:

405nm) implemented in the Blu-ray© device.

The scope of the third year of the research, described in Chapter 5, has been the possible enhancement of the confocal setup by the implementation of a solid immersion lens (SIL) to increase the resolution and to decrease the feature size of the written structures. During this research it was found that the existing SI–lens was not adaptable to the optical writing head and other SI-lenses were not commercially available.

In addition to this, a review of the recent literature showed that a significant research effort is taking place in the field of SIL–technology creating the next generation of optical storage.

Hence, the aim of the research was to build a flexible, low-cost, multi-purpose system for the characterisation and structuring of technical surfaces.

This microcontroller-based system is described in Chapter 6 and is capable of using different types of optical writing heads, especially SIL-based ones, which will be commercially available in the future. The suitability of the developed confocal system is shown by various examples of surface structuring and characterisation at the end of Chapter 6.

Novel method for the profiling of small optical foci

During this thesis a novel method for beam characterisation has been developed. Since the fundamental workpieces of lithography, the photo resist covered substrates, will only be exposed in very small spots to produce fine structures, knowledge of the laser beam profile in respect of the intensity distribution within the beam is essential for the design of a system for the structuring and characterisation of technical surfaces.

Several methods already exist to characterise the geometrical behaviour of light originating from an OPU:

- Knife edge method,
- Slit method,
- Pinhole method and
- CCD cameras.

Unfortunately, none of these methods is sufficiently suitable for waves propagating from lenses with high numerical apertures (Blu-ray[©]: NA=0.85) with focal dimensions within the range of 400nm and below, without magnification of the focal region.

Therefore a beam profiler has been developed within this work using optical fibre tips. Former works of Herzog et al. 1997, Goldberg et al. 1995 and Lila et al. 1998 demonstrate the use SNOM fibre tips for the measurement of the beam properties of laser diodes close (some micron) to the out-coupling facets of the laser active layer. The presented profiling technique however differs from this method by using fibre tips in the far field of the focal area of a focussed laser beam. Hence, this beam profiler works by moving a thin fibre tip (as used for SNOM / SNOL purposes) across the focal area of the laser spot collecting light at its very small aperture (some hundred nm). The other end of the fibre leads to a photomultiplier tube (PMT) quantifying the radiation.

Finally, a computer with an analogue to digital (AD) converter attached to the PMT converts the radiation signals to digital values.

This novel measuring device uses specially developed software to scan the laser spot topographically. It is able to visualize the power distribution within the laser spot three dimensionally (please refer to chapter 4 and the publications "Scientific reports- Hochschule Mittweida 2006" and the "Proceedings of the German Branch of the European Optical Society (EOS) 2007" within the Appendix).

1.2. Industrial benefit

Current research activities, especially in the field of photovoltaics (PV) and (automotive) lighting, show a strong need for structured technical surfaces (Haase and Stiebig 2007). To enhance the incoupling efficiency of solar cells via structuring their surfaces is a present objective of research, since common etching processes, as used in Si-based PV, either lead to undefined surface structures (Kluth 1999) or are not suitable for polymer-based PV.

In the field of (automotive) lighting, e.g. headlights, many attempts were made to guide light to the place where it is needed. Classical ways for light guidance and beam shaping utilize lenses, whereas modern ways try to combine various functions into planar optics, such as diffractive optical elements (DOE) (US Patent 5890796). Lithographic processes and the subsequent moulding procedures are the commonly used methods for the realisation of those structures.

In addition to this, a constant demand for techniques giving information about surface characteristics, e.g. topographies, is known from laboratory work.

The major emphasis of this thesis was to develop a system for both the structuring and characterisation of technical surfaces by means of laser direct writing and laser scanning respectively. The setup should be, and is, able to include both functions:

Structuring of surfaces by illuminating photo resist covered substrates

As well as:

Characterisation of surfaces by scanning their topography

The system presented in this thesis is intended to be more cost-effective compared to commercial products, which provide either characterisation (e.g. Scanning electron microscopy (SEM), Atomic force microscopy (AFM) ...) or structuring (e.g. Laser direct writing, spatial light modulator- (SLM) based devices).

Such a low-cost system is very lucrative for e.g. research and development departments to produce engineering samples and small batches of structured surfaces and/or to characterise surface finishes within the sub–micron scale.

1.3. Thesis structure

Chapter 1

An overview of the aim of the thesis and the benefits for industry and science is presented.

Chapter 2

The nature of surface structuring as well as lithography as a suitable technique to realise structured surfaces is presented. Examples of surface structuring within industrial and scientific applications are introduced. These include beam-shaping elements, like diffractive optical elements, as well as functional surfaces. Moreover, a brief survey of techniques for surface characterisation is given.

Chapter 3

This chapter deals with the first of the two techniques considered for the structuring and characterisation of technical surfaces: Scanning Near-field Optical Lithography (SNOL), a technique derived from Scanning Near-field Optical Microscopy (SNOM). The concept of the optical near-field will be described together with the necessary components of the SNOL system and the preparation of the fibre tips which have a vital function within this technology. Examples of structuring and characterisation by means of SNOL complete this chapter.

Chapter 4

Confocal laser direct writing is the subject of Chapter 4. This technique is explained by means of the Blu-ray optical disc technology which was introduced to the market in 2007. Two test rigs consisting of the main optical component of such Blu-ray devices as well as the peripheral components are presented. Examples of structuring and characterisation by means of this technique complete this chapter.

Chapter 5

A possible enhancement of the test rig described in Chapter 4 is presented. With the aid of a special lens which is placed in front of the focussing lens of the main

optical component of the Blu-ray device, the resolution of the entire optical system can be increased. The concept of the so-called solid immersion lens (SIL) and its necessary regulating devices are presented.

Chapter 6

This chapter deals with the integration of the confocal device (PS3 optical pickup unit) into a microcontroller-based system. This system has been developed due to the necessity for a standalone device without Windows/Labview latency times, incurred by "windows internal" procedures (hard disc accesses etc.). Those latency times led to errors concerning the uniformity of the structures. Moreover, a μC-based adaptive focal control is presented. The entire setup is controlled by software written in C#, which allows the user to have full access to the individual hardware components to either structure a photo resist-covered surface with a desired pattern or to characterise an "unknown" surface.

Chapter 7

Conclusions and the potential for future developments are discussed in this final chapter.

2. Structured technical surfaces / Diffractive Optical Elements

This chapter is divided into three parts. The first shows the possibilities for realising structured technical surfaces followed by two explanatory parts concerning structured technical surfaces in general and a special kind of technical surface: Diffractive Optical Elements.

2.1. Basics of surface structuring

Surface structuring, often called "finishing", is one of the most important steps within the manufacturing process of technical (metal) workpieces. The techniques (Fig.2-1) of surface structuring used vary depending on the desired surface behaviour and the available tooling.

Fig. 2-1: Diagram showing individual techniques of surface structuring (EPA 2010, Dzur 2007)

In order to achieve special characteristics, e.g. reduced friction or specific optical behaviour, the surface of metallic- workpieces can be structured.

For structure sizes ("fineness") within the range of some millimetres and/or large affected areas, this could be done by classical methods like milling, grinding or honing. Mostly, these techniques produce random structures (Fig.2-2).

Fig. 2-2: *Honed car-engine cylinder, note the crosswise grooves on the sliding surface (Endyn 2010)*

For higher resolution and exactly defined structures, like preservative patterns, imprinting injection moulding (Fig. 2-3 shows a glass stamp used for injection moulding) or mask-based etching are suitable techniques.
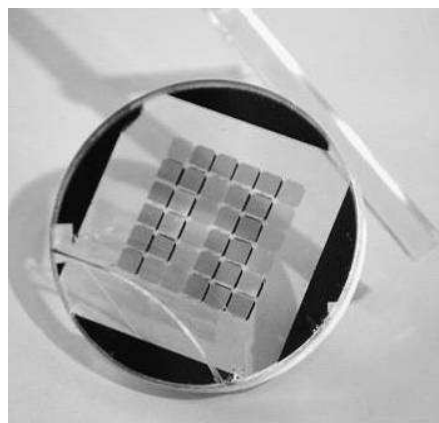
Fig. 2-3: *Glass stamp for injection moulding with various pattern*

For this purpose stamps or masks are needed to transfer the desired pattern to the surface of the workpiece. These stamps can be made by means of lithographic processes.

2.1.1. Basics of lithographic photo resist structuring

Lithography (lithos = stone + graphein = to write). This technique was invented in 1798 by Alois Senefelder (Encyclopaedia Britannica, 2009a) and lithography has been mentioned since 1803 in France. In the beginning, lithography was used only for nonartistic purposes e.g. text. The music publisher Andre from Offenbach am Main initiated the use of lithography for the copying of sculptural representations thereby beginning the development of the artist-lithographer (Fig. 2-4).

Figure removed due to copyright restrictions

Fig. 2-4: *Stone used for lithography printing (left) and a printing made with this stone (right) (John Grossman Collection 2009)*

Lithography grew in popularity because it is the procedure that produces copies that are very similar to the "hand-written" works. The artist needs neither specific chemical knowledge (as with etching or aquatint), nor to engrave a copper plate. In addition lithographic printing machines were economical mass printing devices that produced copies in almost unlimited numbers.

Modern procedures

Lithography was developed further with the introduction of photolithography, a technique which, with modifications, is used in other fields; indeed, neither printed

circuit boards (PCB) nor, for example, microelectronics are realisable without photolithography.

In the semiconductor industry, structure information is exposed onto a layer of photo resist (applied by spin-coating onto a substrate, for example a wafer) by means of photolithography (Fig. 2-5). Spin-coating is a procedure for the application and regular distribution of photo resist onto a substrate (refer to next sub-chapter 2.1.1.1.1).

Several types of lithographic techniques have been developed, as shown in Fig. 2-5 below:

Figure removed due to copyright restrictions

Fig. 2-5: *Trends of lithographic techniques used in industrial applications (Ito and Okazaki 2009)*

Fig. 2-5 shows various technologies under investigation for the development of pilot and production lines of Large-Scale Integrated (LSI) circuitry. These include: KrF excimer laser lithography with a wavelength of 248 nm; ArF excimer laser lithography with a wavelength of 193 nm; F2 excimer laser lithography with a wavelength of 157 nm; PSM, phase-shifting mask applied to KrF, ArF and F2; EPL, electron-projection lithography; PXL, proximity X-ray lithography; IPL, ion-projection lithography and EBDW, electron-beam direct writing (Ito and Okazaki, 2009).

2.1.1.1. Process of photo resist structuring

The main application of lithography within this work is the production of structured technical surfaces, e.g. phase modulating photo resist structures, a.k.a. the production of diffractive optical elements (DOE) as well as the production of similar functional surfaces. Fig. 2-6 shows the process steps in photo resist structuring. The chemical structure of the photo resist is being changed by local optical irradiation; especially, the molecular chains are cut (positive resist type) or cross-linked (negative resist type). The resist used within this project is a positive-resist type, so the regions that were exposed to the laser light will be removed by the developer (University of Rochester, 2010).
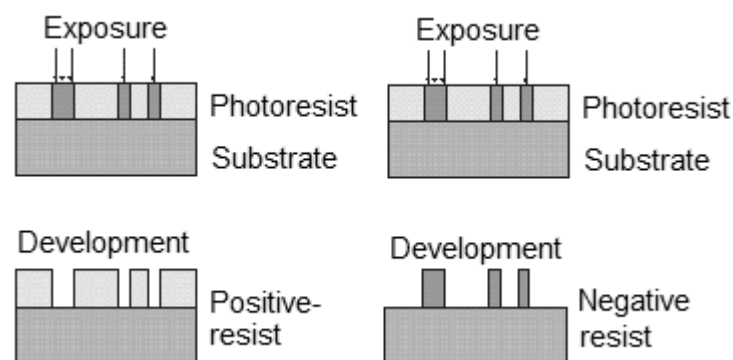
Fig. 2-6: *Principle of photolithography shown for positive and negative photo resist*

The production process for these resist structures contains the following steps:

2.1.1.1.1. Covering the glass substrate with a photo resist layer

A layer of photo resist is applied to the glass substrate (Size: 2"x 2") using a spin coater (Fig. 2-7). The thickness of this layer can be adjusted by changing the revolution speed and the viscosity of the photo resist.
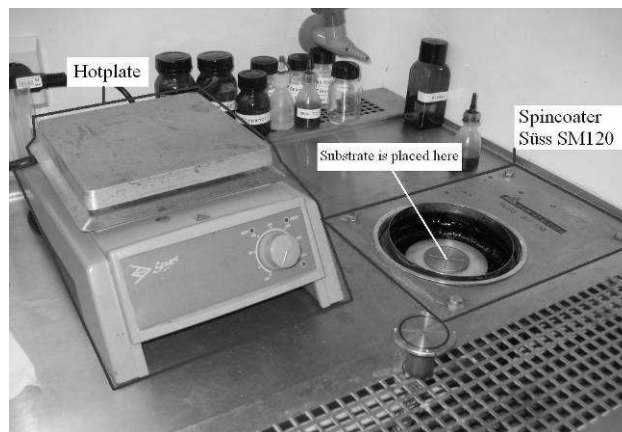
Fig. 2-7: *Working setup for substrate coatingicnl Hotplate and Spincoater*

The resist used here, the Shipley Microposit S1800 Series (S1805) resist, can be exposed by means of light sources in the spectral output range of 350-450 nm. Fig. 2-8 shows the absorbance spectrum of the photo resist. The wavelengths used in this project (405 nm and 442 nm) are indicated.

Fig. 2-8: *Absorbance vs. Wavelength (red line shows ~405 nm and ~442 nm) (Datasheet Shipley Microposit 2006)*

The photo resist thickness versus spin speed, displayed in Fig.2-9, provides the information required to tune in properly the desired resist thickness.

To achieve a 0,5-micron layer, a spin speed of 1000rpm (10sec) followed by 3000rpm (30sec) has been chosen.

Figure removed
due to copyright
restrictions

Fig. 2-9: *Photo resist thickness vs. Spin speed (red line shows 3000rpm)(Datasheet Shipley Microposit 2007)*

Solvent is removed from the photo resist in a bake process on a hotplate (Fig. 2-7) lasting 90 seconds (Soft bake) at approx. 100° C. Soft baking reduces the solvent content in order to:

- Avoid mask contamination and/or sticking to the mask,

- Prevent popping or foaming of the resist by Nitrogen (N2) created during   exposure,

- Improve resist adhesion to the substrate,

- Minimize dark erosion during development,

- Prevent dissolving one resist layer by a following multiple coating and

- Prevent bubbling during subsequent thermal processes (coating, dry etching) (Microchemical 2007).

After the spin coating procedure, the average solvent concentration within the photo resist layer is between 20% (thin films) and about 40% (thick films). Soft baking can reduce the remaining solvent concentration in the photo resist layer by solvent diffusion and evaporation. Thereby, the solvent evaporation rate drops during the soft bake time for two reasons:

- The evaporation rate is proportional to the surface solvent concentration,
- The solvent diffusion towards the resist surface drops strongly in solvent poor-resist.

Figure 2-10 plots the evolution of the average solvent concentration for two film thicknesses during soft bake at various temperatures. The formation of a strong solvent concentration gradient (not shown here) can be observed, especially in thick resist films.

Figure removed due to copyright restrictions

Fig. 2-10: *Soft bake-time vs. concentration of remaining solvent (Microchemicals 2007)*

2.1.1.1.2. Exposure of the photo resist

The exposure of the photo resist is subdivided into two classes:

- Photomask-based (parallel procedure)
- Mask-free/ laser direct writing (serial procedure)

Photomask-based exposure techniques use ultraviolet light, which illuminates the photo resist layer through a mask that hides the areas which should not be exposed and which has openings at the areas that should be exposed. This technique is well-known from the production process of printed circuit boards (PCB) within the electronics industry.

The mask- based procedure can be divided into three categories:

Contact method
The photo mask and the photo resist-covered substrate are pressed together by pressure or vacuum (Fig. 2-11).
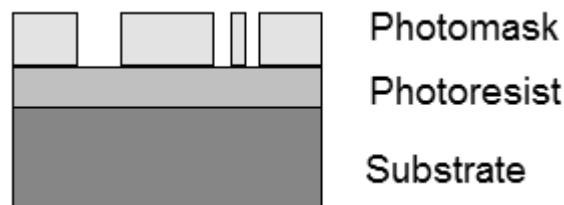
Fig. 2-11: *Mask-based lithography procedure –contact method*

Fig. 2-12 shows a commercial lithography system, using the "contact method" at the Fachhochschule Emden, Wilhelmshaven site (next page).

16
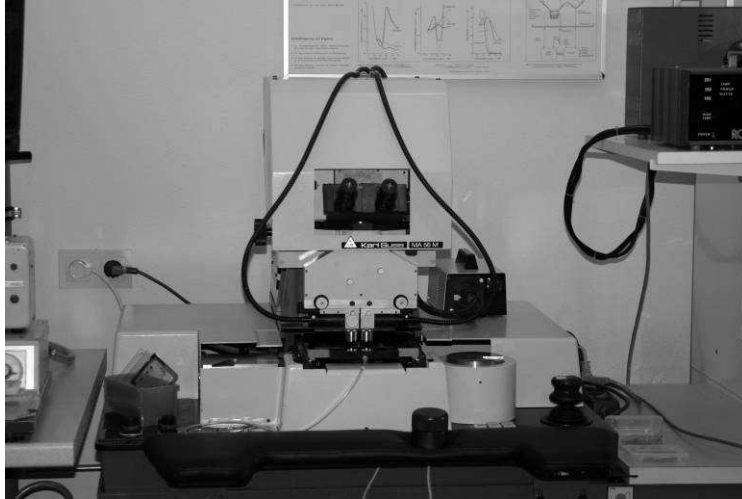
Fig. 2-12: *Suess MA 56M lithography system for mask-based "contact mode" lithography*

By utilizing this method, a resolution within the sub-micron range can be reached. The drawback of this method is the possibility of damage to the resist layer and/or the photo mask due to their mutual contact.

Proximity method

Between the photo-mask and photo resist-covered substrate is a small, defined distance of about 10-50 microns (Fig. 2-13).
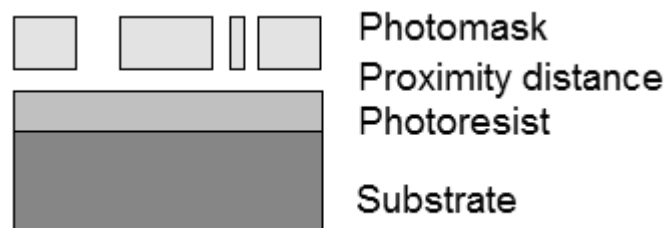
Fig. 2-13: *Mask-based lithography procedure –proximity method*

Here the resolution is degraded due to a diffraction effect, although the surfaces of the mask and resist layers are protected from damage, e.g. scratches.

Projection method

This method (Fig.2-14; Fig. 2-15) uses lenses to reduce the mask image by a constant factor, commonly by 10:1 or 4:1, and is applicable for resolutions down to some hundred nanometres. The reduced image is projected onto the photo resist-covered substrate and exposes the resist locally (Menz and Mohr 1997).

Figure removed due to copyright restrictions

Fig. 2-14: *Process of photo-mask-based exposure using reduction lenses (Toppan 2009)*

Fig. 2-15: *Lithography system for mask-based "projection mode" lithography built at the Fachhochschule Emden , Wilhelmshaven site*

Photo masks

These photo masks are specially made for the individual applications. Commonly, these photo masks are made by laser direct writing. This technique offers a high throughput and is suitable for the mass production of, for example, integrated circuits.

Within this work, the mask-free or laser direct writing technique is being used. It has the advantage of individual structuring possibilities due to the independence of the photo masks. Thereby the desired diffractive structure is illuminated by means of the lithography setup presented in Chapter 3 and 4 into the photo resist. Parameters as illumination intensity; spot size and dealing-speed determine the dose "D" of the light flooded in:

$$D = \frac{E \cdot t}{A} \qquad \left[mJ / cm^2 \right] \qquad\qquad (2.1.1.1.4.1)$$

where:

E   : Energy of Light

t   : Exposure time

A   : affected Area

Within this work, the illumination energy of one single pixel, measuring 1micron square, is approx. 700nW and the illumination duration is 4ms. This results in an illumination dose of approx. 270 mJ/ cm^2.

Greyscale (multilevel) photo masks

Lithography in general makes use of the fact that the dose of light used for the exposure of the photo resist is dependent on the energy of the light source (here the laser). By using a special type of photo mask, greyscale photo masks, staircase profiles (or depending on the number of steps: even quasi-continuous profiles) can be produced, as shown in Fig. 2-16.
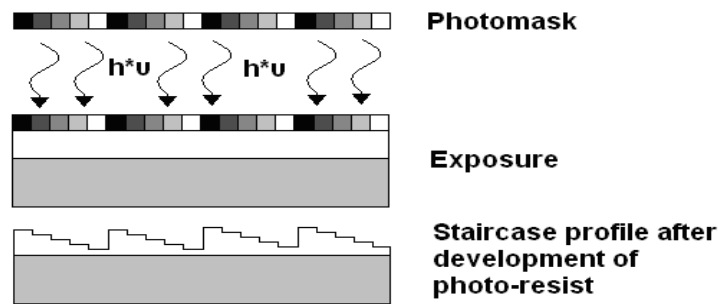
Fig. 2-16: *Schematic view of greyscale lithography*

Profiles of this nature are especially important in the field of diffractive optical elements (DOE) to enhance their diffraction efficiency of (please refer to chapter 2.3 for details).

Mask-free/ laser direct writing (serial procedure)

This technology uses focussed laser beams (other methods use a focussed ion beam or focussed electron beam for laser direct writing) with wavelengths of 442 nm and below (depending on the used laser source used) for point-wise or line-wise exposures of photo resist-covered substrates. Its main application is the production of photo masks for use in parallel lithographic processes. Figure 2-17 shows the general setup of a laser direct writing system:
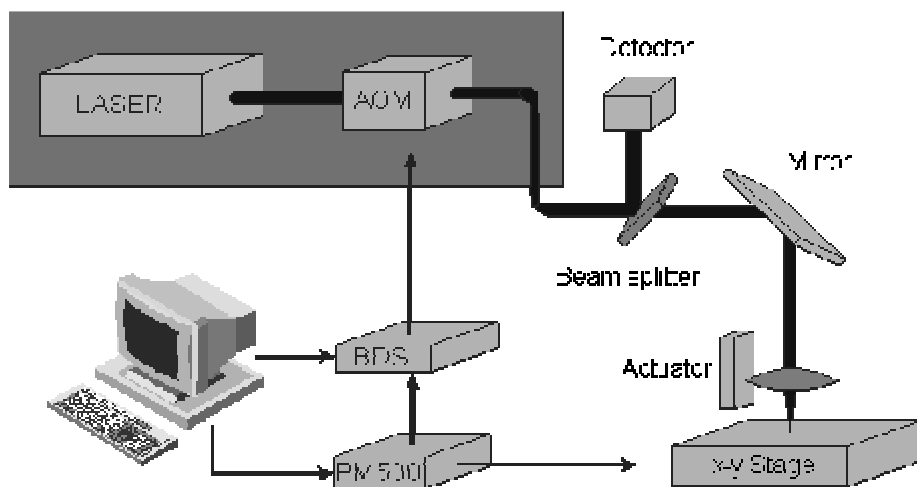
Fig. 2-17: *Schematic view of the direct writing lithography setup used at the Fachochschule Emden*

In 1995, Uve Samuels constructed a laser direct writing setup as a part of his PhD thesis; this setup (Fig. 2-18) has done good work for years but may now need replacing with a higher-resolving and more compact system.
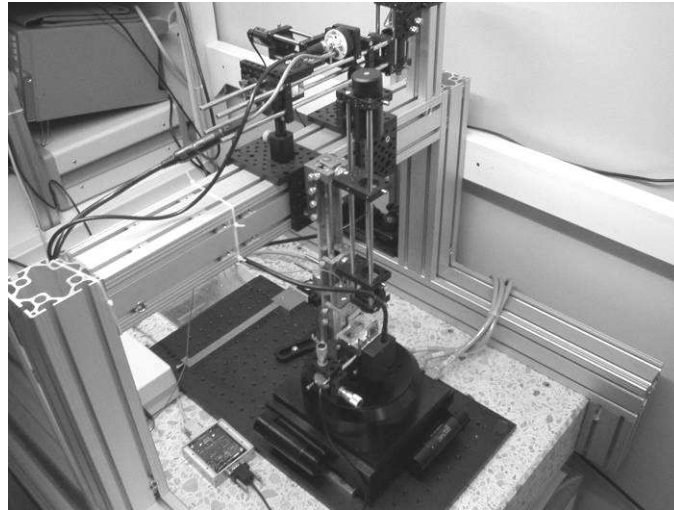
Fig. 2-18: *Direct laser writing lithography setup at Fachhochschule Emden*

State of the art systems for industrial laser direct writing use spatial light modulators (SLM) or modulated and scanned beam (MSB) techniques.

SLM-based exposure (Micronic Laser Systems/Sweden)

According to Figure 2-19, Micronic describes this technology as follows:
"The light source is a pulsed excimer laser with 248 nm wavelength and a high repetition rate. The SLM has a flat, mirror-like surface composed of mechanical micro-mirrors and the reflected light exposes the photo resist on the mask blank. By applying a voltage to areas that are intended to be unexposed, electrostatic forces cause the micro-mirrors to be slightly deflected in those areas. These areas scatter the light outside of the Fourier aperture, in practice the aperture stop of the projection system. The stage with the mask blank moves continuously and the interferometer commands the laser to flash when it reaches the position for the next field. Because of the short flash time, around 20ns, the movement of the stage is frozen and a sharp image of the SLM is produced in the resist.

The SLM is reloaded with a new pattern in time for the next flash. The patterns are stitched together from the fields" (Micronic laser systems 2010).

Figure removed due to copyright restrictions

Fig. 2-19: *Scheme of exposure of photo resist-covered substrate by means of the SLM technique (Micronic laser systems 2010)*

This technology is capable of producing structure sizes/resolutions down to 200 nm, with special objectives like the Corning Tropel, µCat Objective family (Bentley 2002).

MSB-based exposure (Heidelberg Instruments/Germany)

The intensity of the laser beam (mostly between 363 nm (Excimer laser source) or 442 nm (He-Cd laser source)) is modulated by an acusto optic modulator (AOM) (please refer to chapter 3) while an acusto optic deflector (AOD) deflects the beam and scans perpendicular to the moving substrate (Fig. 2-20). By this, stripes are exposed on the photo resist-covered substrates that have the width of a scan. By stitching multiple stripes together, the whole substrate area can be exposed (Heidelberg Instruments 2010).

Figure removed
due to copyright
restrictions

Fig. 2-20: *Scheme of exposure of photo resist-covered substrate by means of the MSB technique (Heidelberg Instruments 2010)*

This technology is capable of producing structure sizes/resolutions down to 600 nm (considering the laser direct writer DWL 4000).

Remark

Other methods of photo resist exposure deal with the application of a scanning electron microscope (SEM); by this, the electron beam is led across the photo resist-covered substrate grid-wise, exposing the photo resist. The electron beam is blanked at areas which are not intended to be exposed. For cost reasons (price range: min. 100k€), this technology is not being considered within this work.

2.1.1.1.3. Developing photo resist

After illumination, the substrate is developed by placing it into a developer solution (Shipley Microposit MF-319). The removal of the photo resist increases with the size of the illumination dose at the place of exposition. The thickness 'Δd' of the removed photo resist depends on the energy of illumination 'E':

$$\Delta d = f\,(E) \tag{2.1.1.1.3.1}$$

Previous work by Bartolini (1977) has shown the following relationship (room temperature conditions):

$$\Delta d \approx \Delta r\, T\, \alpha_0\, E + r_2\, T \tag{2.1.1.1.3.2}$$

where:

Δd	: Difference in photo resist layer thickness (µm)
$\Delta r = r_1 - r_2$	: Difference in etching rates of exposed to unexposed molecules
T	: Time of development (ms)
α_0	: Resist constant
E	: Energy of illumination (mJ=1mWs)
r_1	: Etching rate of unexposed molecules (µm/ ms)
r_2	: Etching rate of exposed molecules (µm/ ms)

Two conclusions can be derived from this approximation:

- The dissolving velocity of the photo resist is proportional to the intensity of the laser light used for exposure and the duration of exposure ´t´. Thus lower laser intensity can be compensated with longer exposure.

- Exposed areas of photo resist are removed faster than unexposed areas (valid for positive photo resist) so different surface profiles can be produced by different development durations.

2.1.1.1.4. Hard bake / Post bake (optional)

To enhance the chemical as well as the mechanical stability of the photo resist surface and to force the evaporation of remaining solvents, a second baking process can be applied. Therefore the substrate is heated for 90s on a hotplate (Fig.6) at 140ºC.

2.1.1.1.5. Transfer of the resist structure (optional)

The transfer of the photo resist structure to the underlying (glass) substrate can be carried out by dry- or wet-etching, sandblasting or by changing the refractive index of the affected areas by ion exchange. Structures transferred into glass are very stable against environmental impacts and are resistant to very high laser light intensities. These substrates can be used as injection moulding stamps (refer to Fig.2).

Wet etching

A solvent is used to remove material from the substrate within the non-masked regions that are not "protected" by the photo resist. The solvents vary according to the different substrate surface materials.

Glass substrates are commonly etched using Hydrofluoric acid (HF):

$$SiO_2 + 4\,HF \rightarrow SiF_4 + 2\,H_2O \tag{2.1.1.1.5.1}$$

or mixtures of HF and Nitric acid (HNO_3):

$$\text{I:} \quad 3\,Si + 4\,HNO_3 \rightarrow 3\,SiO_2 + 4\,NO + 2\,H_2O \tag{2.1.1.1.5.2}$$
$$\text{II:} \quad 3\,SiO_2 + 18\,HF \rightarrow 3H_2SiF_6 + 6\,H_2O \tag{2.1.1.1.5.2}$$
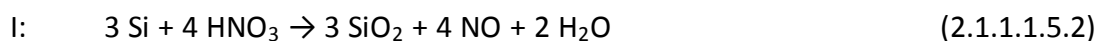
Dry etching

Dry etching processes are divided into three different methods:

- sputter etching (Fig. 2-20),
- reactive ion etching and
- vapour phase etching.

<u>Sputter etching</u> uses an Argon-filled vacuum chamber (Fachhochschule Emden uses: Balzers PLS 570) with a pressure of $7*10^{-3}$ mbar, as shown in Fig.2-21.

Figure removed due to copyright restrictions

Fig. 2-21: *Setup for sputter etching of photo resist-masked substrates (Zengerle 2006)*

The substrate with the photo resist mask is placed between two electrodes. Applying a high voltage to one of the electrodes generates an electromagnetic field and plasma is formed. Ar^+ ions are accelerated within the electromagnetic field and "shot" onto the substrate, whereby thin layers of the substrate material can be removed.

<u>Reactive ion etching</u> uses mixtures of gases instead of Argon gas to generate a chemically reactive plasma. The setup is similar to the setup used for sputter etching and presented within Fig. 2-22. A special type of this process is called

"Deep Reactive Ion Etching" (DRIO). This process is split into two parts of operation:

- Etching of the base material by using reactive gases e.g. SF_6,
- Protecting the etched zones by depositing a polymer.

Figure removed due to copyright restrictions

Fig. 2-22: *Schematic process steps of the deep Reactive Ion Etching Process (DRIE) (Nadim and Williams 2004)*

These operations can be executed periodically depending on the desired depth.

Vapour phase etching is used to etch Substrates by using fumes of e.g. Hydrofluoric acid (HF). The substrates are placed inside a hermetically sealed container and fumes of HF react with the glass surface causing the removal of material (Lee et al. 1997).

Variation of the refractive index by ion exchange

By dipping a masked substrate into molten silver nitrate (AgNO3), the index of refraction is changed by Δn (Fig. 2-23). This process is based upon the thermal diffusion of the Ag+ cations from the liquid phase into the substrate material. The Sodium (Na+) or Potassium (K+) Ions are removed and substituted by the heavier Silver. Silver ions are more polarisable than Na+ or K+, thus the index of refraction is increased by the concentration of silver ions diffusing into the glass (Thoma 2006).
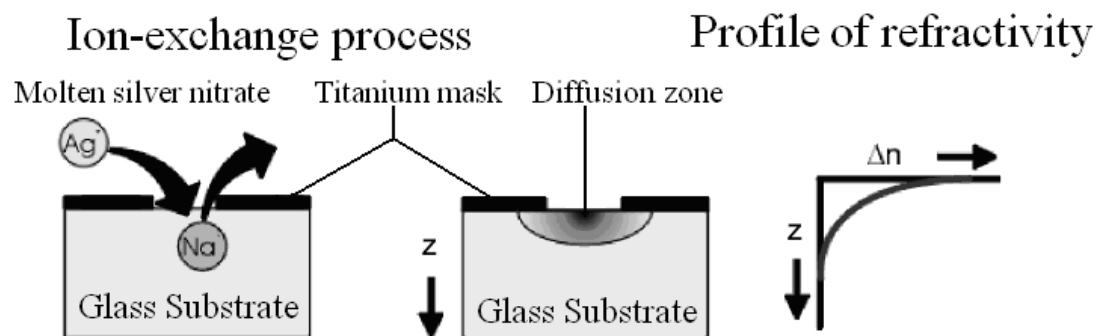
Fig. 2-23: *Process of ion exchange within glass substrates by means of silver ions*

2.2. Structured technical surfaces

This section should give a brief overview about the application of structured technical surfaces within different fields of engineering.

2.2.1. Structures for photovoltaic / solar cells

(This application has been discussed with Dr. Ingo Riedel, a specialist in organic solar cells, University of Oldenburg, Germany, and is intended to be realized within a funded research project)

Solar cells convert the energy of sunlight directly into electrical energy. The conversion efficiency of industry grade (Si) solar cells is about 12%-18% (Reuk 2009). By increasing the optical path length of light within the "active" zone inside a solar cell (Fig. 2-24), the efficiency can be enhanced.
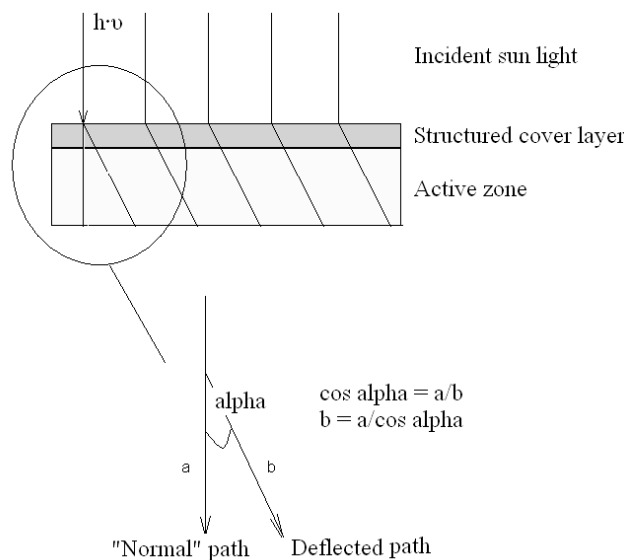
Fig. 2-24: *Scheme showing a method to enhance optical path length of solar cells*

This cover layer can be an adhesive plastic film with special structures, which deflect the light into a defined direction. These structures can be realized by using gratings or so called "off-axis" zone plates. Chapter 2.3.4 will explain the concept of "off-axis" zone plates on the basis of another application.

29

2.2.2. Functional surfaces – shark skin

This application presents an adaptation of the dermal denticles of sharks (Fig. 2-25). Sharkskin is known for its streamlined structure enabling sharks to reach high velocities underwater.

Figure removed due to copyright restrictions

Fig. 2-25: *Scanning microscope image of shark skin (University of Cape Town 2010)*

To reproduce such structures and to cover (e.g.) the hulls of ships with these structures would lead to decreased energy consumption of these ships and a reduction in barnacle sticking to the hull.

2.2.3. Lab on chip (LOC) applications

"Lab on chip" systems are a new method for carrying out biological and chemical analysis. They are miniaturised integrated measurement units. The example shown in Fig. 2-26 and 2-27 has been developed and realized by a lithographic technique at FHOOW. It shows a fluid combiner with fibre connectors for the analysis of the adsorbed spectra.
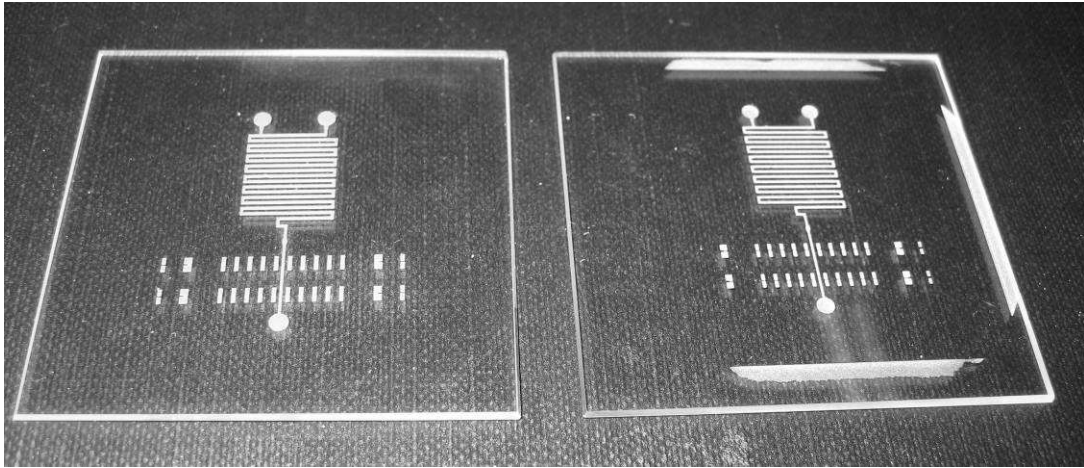
Fig. 2-26: *Photomask (left) and reproduction (right) of the LOC device (substrate size 2" x 2")*
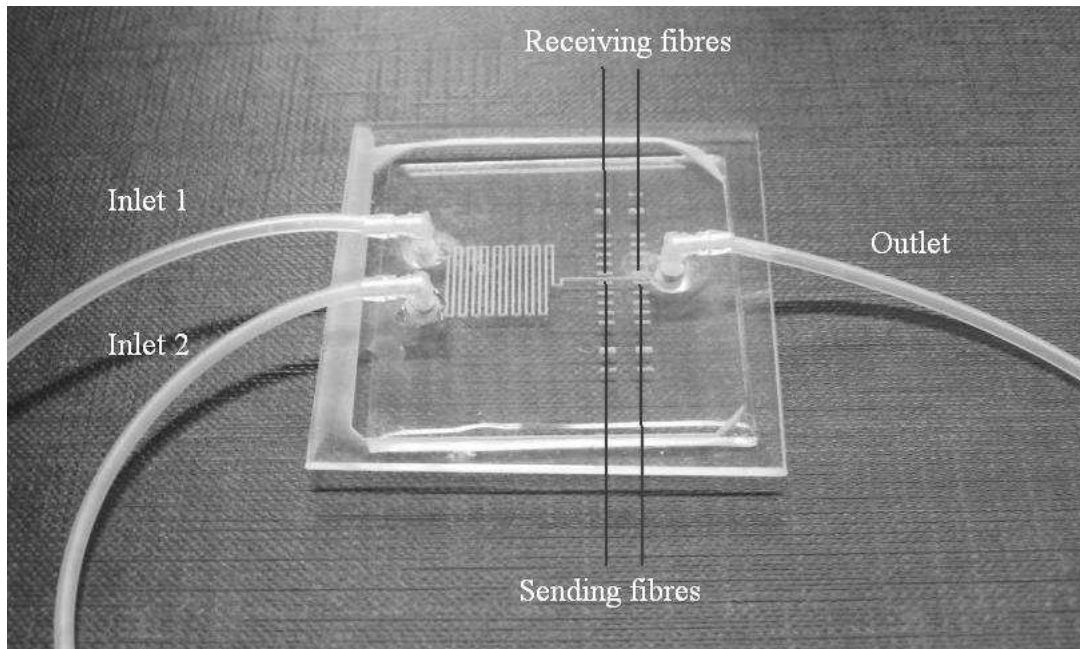
Fig. 2-27: *LOC device with attached supply hoses (Note that the optical fibres are not attached within this picture)*

2.2.4. Micromechanics

A rapidly growing (Fig. 2-28) field of lithographic surface structuring is called Micro-Electro-Mechanical Systems (MEMS).

Fig. 2-28: *Market analysis for 26 different MEMS products (Nexus 2009)*

The Encyclopaedia Britannica defines this technology as follows:

"Mechanical parts and electronic circuits combined to form miniature devices, typically on a semiconductor chip, with dimensions from tens of micrometers to a few hundred micrometers (millionths of a metre). Common applications for MEMS include sensors, actuators, and process-control units."

Examples of Micro-Electro-Mechanical Systems

According to the Encyclopaedia Britannica (2009b) the first product to make a market breakthrough was the automotive air-bag sensor, which combines inertia sensors to detect a crash and electronic circuits to deploy the air bag. Fig. 2-29 shows the inner assembly of such an inertial sensing unit:

Figure removed
due to copyright
restrictions

Fig. 2-29: *Core of a 3-axis MEMS accelerometer. The complex structure represents capacitors which change their capacity due to movement (Guillou 2010)*

Another application of the MEMS technology deals with the realisation of "micro-machines "as for example, micro- turbines shown in Fig. 2-30.

Figure removed
due to copyright
restrictions

Fig. 2-30: *Micro-turbine realised using MEMS technology (MIT 2010)*

2.3. Diffractive optical elements (DOE)

Diffractive Optical elements (DOEs) are optical devices for beam shaping, forming and modulation without any loss, quickly, passively and with high-efficiency. DOE`s can transform every wavefront in an user- definable, arbitrary other wavefront as shown in Fig. 2-31.
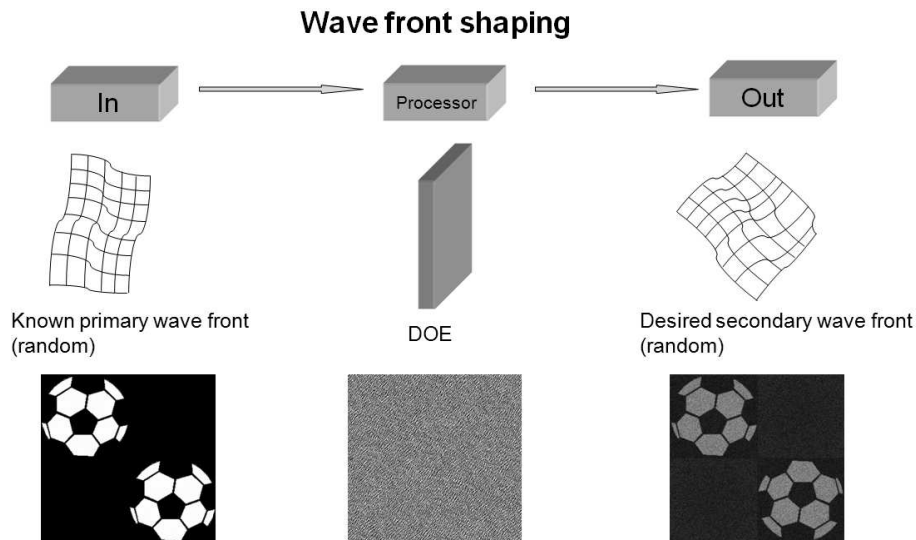
Fig. 2-31: *Schematic of wavefront shaping by means of DOEs*

DOEs generally feature small sizes, have a small weight, are usable with multiple functions (for example realization of a multiple beam splitter with supplementary focussing of the single rays) and are mostly cheap to produce, for example projection caps for laser pointers. In addition, DOEs lead to new, often very "smart", solutions that were not, or only with very high expenditure, feasible with refractive optics (for example ray homogenizing of excimer lasers). Attention is to be paid to the fact, that DOEs are strongly wavelength-dependent and therefore only usable for laser applications or monochromatic sources of light.

2.3.1. Definition

In comparison to refractive optics, which use the refraction of light, DOEs use the diffraction phenomenon of gratings and the overlay of light waves forming an

interference pattern (Hologram). With a hologram, it is possible to produce spatial pictures of objects. This technique was invented by D. Gabor in 1948 (Gabor, 1971). The 3D impression of this holographic picture seems like the impression of the real object itself. To create such an interference pattern, an object is illuminated with a coherent light source. Thereby, every point of the object sends out elementary waves (Huygens) whose entirety presents the wave radiated from the object, as illustrated in Figure 2-32. This wave front contains all the optical information of the object. With normal photography the spatial impression disappears, because only intensity-information is stored, but not the phase of the light wave. Holography stores the phase and the amplitude of the light wave. In order to get a relationship between the phases, the object wave is overlapped with a so-called reference wave.
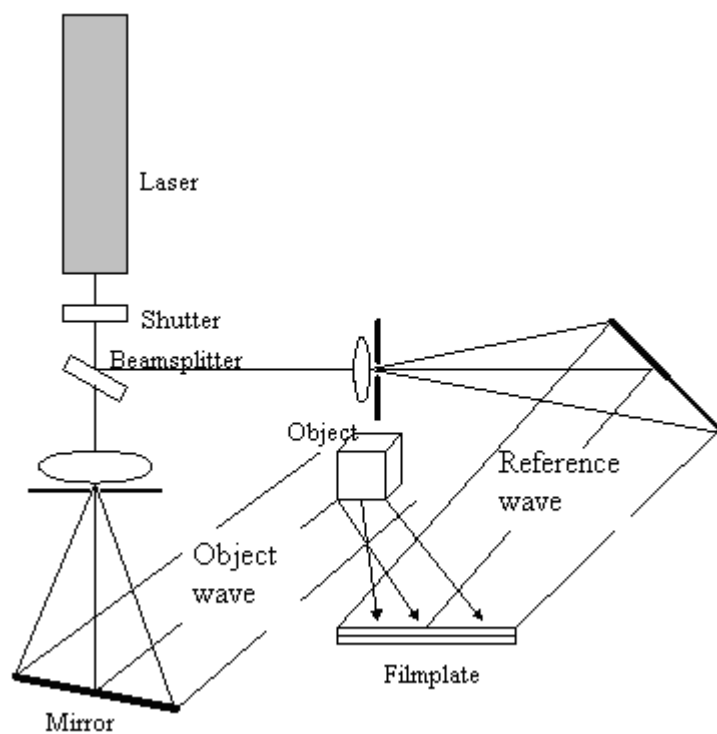
Fig. 2-32: *Exposure of a (transmission) hologram (according to Olsen 1996)*

A complex interference pattern, which is stored on a film, is created by the overlap of the object wave with the reference wave. Places with identical phase lead to constructive interference, places with different phase to destructive interference. According to Figure 2-33, the original picture is reproduced by illuminating the

developed hologram (only) with the reference wave. At the complex interference pattern of the hologram, the reference wave is bent and the observer can see a spatial virtual picture.
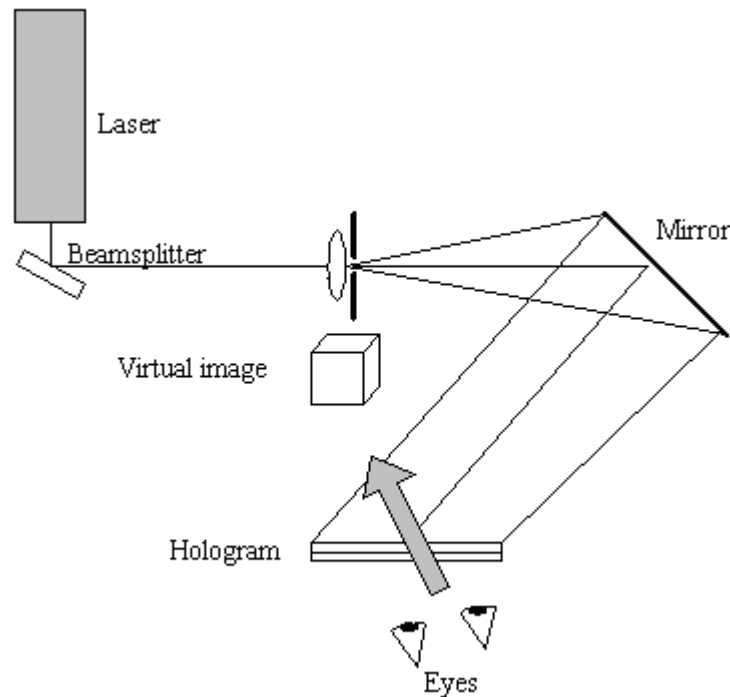
Fig. 2-33: *Reconstruction of a (transmission) hologram (according to Olsen 1996)*

The interference structure in the photographic plate (hologram) deflects the light of the reference wave as if the object would be still behind the photographic plate. Considering this phenomenon and comparing object and interference structure lead to the development of iterative algorithms that make it possible to calculate a hologram (Interference structure). These calculated interference structures are known as DOEs.

Diffraction Theory

Diffraction occurs when a light wave enters a barrier, which has an opening size within the range of the wavelengths of the light being used.

Fig. 2-34: *Diffraction at a double slit barrier. The numbers mark the diffractive order (according to JGU 2010)*

The diffraction phenomenon can be described by the double slit experiment (schematically shown in Fig.2-34). In this, a plane wave hits a barrier with two small openings. Small elementary waves are generated at the opening according to Huygens Law ("each point of a wavefront generates a new ´elementary wave´"). Diverging from "classic" geometrical optics, the light behind the barrier is not spotted in two points at the screen, but a characteristic pattern is formed caused by the wave nature of light. This pattern shows the individual diffractive orders.

2.3.2. Diffractive Amplitude Elements (DAE) vs. Diffractive Phase Elements (DPE)

DOEs and holograms change the complex amplitude and phase of a coherent radiation field with the aid of the ability of the light to diffract and interfere. Illuminating a hologram with the reference wave leads to the rise of the transformed wave front. DOEs are divided into Diffractive Amplitude Elements (DAE) and Diffractive Phase Elements (DPE) according to the way in which they work. The effect of the DAE is based on an extraction of partial rays with only the amplitude being changed. Photo resist-covered DAEs allow a fundamental

diffraction efficiency of 50% since their interference structure is arranged by absorptive and transmittive structures, e.g. zone plates, as shown in Figure 2-35.
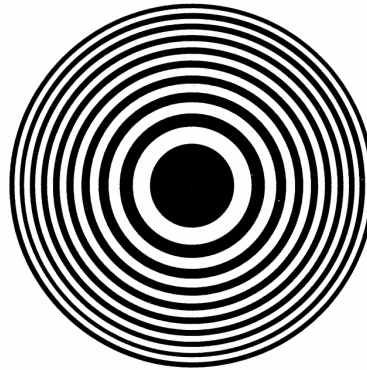
Fig. 2-35: *Example of a binary zone plate*

In order to reduce the optical losses through the DAE, transparent elements were developed: DPEs that change the phase of the incident wavefront through their surface structure.

In order to change the phase of the wavefront efficiently, the profile and the used wavelength must be synchronized (Fig. 2-36).

Figure removed due to copyright restrictions

Fig. 2-36: *One-dimensional, continuous Diffractive Phases Element (DPE) (Stankovic 2002)*

The height 'h0' is given by the quotient of the wavelength used and the difference of the refractive indexes. If the optimal height 'h0' is not realized during the production of the DPE, the intensity decreases in the wanted diffraction order (m = 1), and light becomes deflected into other diffraction orders (m = 0; +2; -1; +3; …). This behaviour is described in Figure 2-37.

Fig. 2-37: *Effect of the height Δh on the diffraction efficiency of a continuous DPE (Stankovic 2002)*

Due to the difficulty in manufacturing Continuous DPEs, the production process is simplified by the quantization of the continuous phase profile (Fig. 2-38). For quantized DPEs, only a discrete number 'Z' of height intervals are realized. Thus, not the whole phase deviation (2π) is realized but rather π (Z-1)/ (Z*2). The maximum height 'D' of a quantized DPE is given by the following equation:

$$D = (Z-1)/Z * \lambda /(n_r - n_0)$$

(2.3.2.1)

The approximation of the continuous phase distribution through Z levels leads the intensity I to decrease in the wanted orders (m = 1). For a 1-dimensional DPE with optimal step-heights Di = D/(Z-1) it follows that:

$$I(m,Z) = (\sin c((m-1)+1/Z))^2$$

(2.3.2.1)

The relative intensity being calculated from that is, for some selected diffraction orders, indicated in Table 1.

Fig. 2-38: *Examples of quantized DPEs, here binary and 4 levcel structures (Stankovic 2002)*

Table 1: *Percental diffraction efficiency in dependence of the modulation density (according to Stankovic 2002)*

	m= -1	m= 0	m= +1	m= +2
Z=2	4,5	40,5	40,5	4,5
Z=3	2,7	17,1	68,1	4,3
Z=4	1,7	9	81,1	3,2
Z=8	0,4	1,9	95	1,2

2.3.2.1. Calculation of diffractive structures

In order to calculate a complex, digital, interference pattern, an algorithm is required to find a solution iteratively and by coincidence. The calculation of the phase function can be done with the aid of iterative Fourier algorithms. This method was improved by Wyrowski and Fienup and is known as the Iterative Fourier Transformation Algorithm (IFTA) (Wyrowski and Bryngdahl 1988). The iteration process of the IFTA is schematically represented in Figure 2-39. The IFTA is very efficient and allows large amounts of data, but it is very sensitive to variations of the starting values.
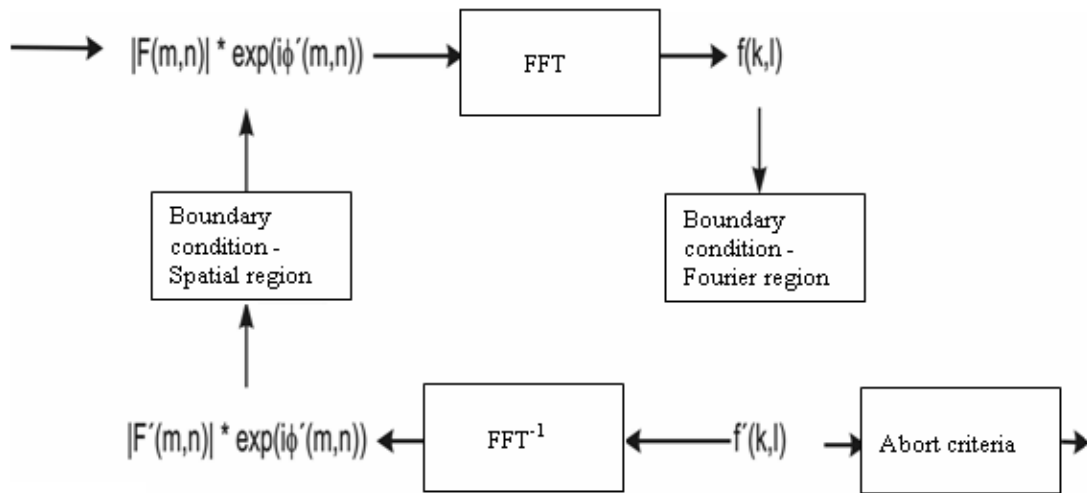
Fig. 2-39: *Scheme of the IFTA algorithm*

Figure removed
due to copyright
restrictions

Fig. 2-40: *Intensity distribution (Sample)*   *Resulting DOE from Fig. 2-40*

Based on this algorithm software, (Fig. 2-41) was created at the Fachhochschule Emden to transform intensity distributions (e.g. a picture) to the corresponding phase distribution (Fig. 2-40), the DOE.
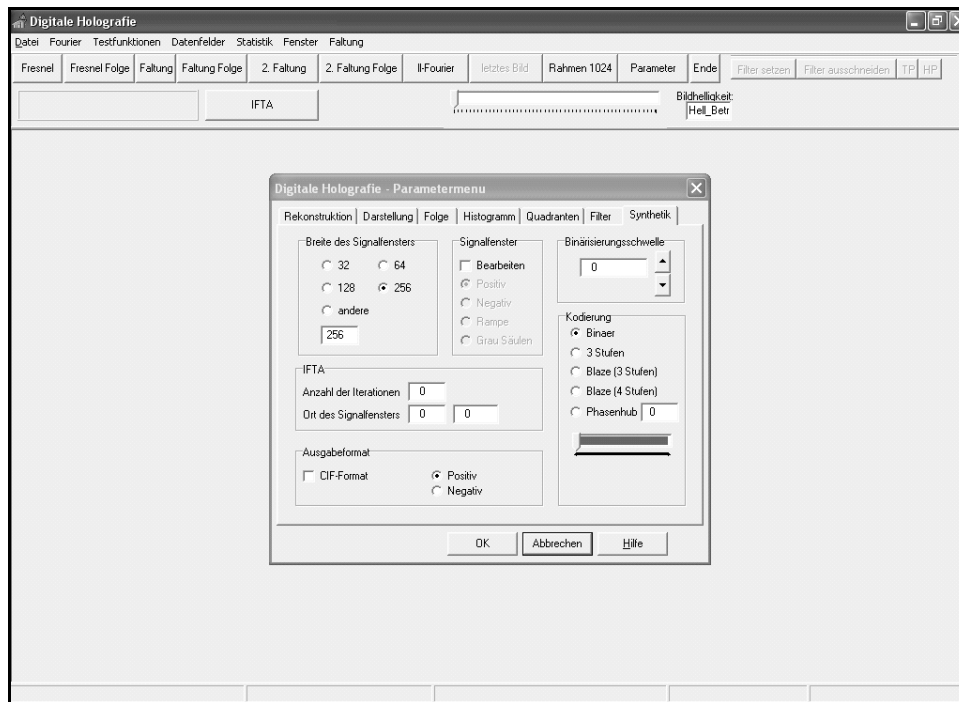
Fig. 2-41: *Software to calculate DOE´s with the aid of the IFTA algorithm*

Such software offers an exensive freedom of design and the calculation of every arbitrary intensity distribution. Binary Diffractive Optical Elements are possible, as well as blazed 3 or 4 level DOEs.

2.3.3. Dammann gratings

Dammann gratings (Fig. 2-42) (Dammann and Gortler 1971) present a special class of binary DOEs which have the same diffractive intensities in all diffractive orders. An incident beam is shaped by the Dammann grating to an array of equipollent spots. These gratings can be used to produce a multi-spot beam splitter or in the telecommunications industry (Schlarb 2003).
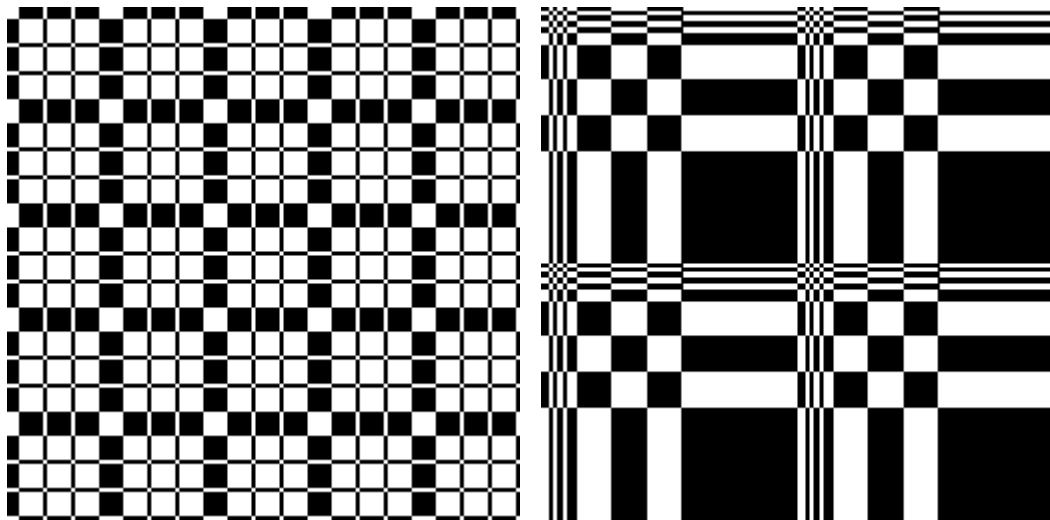
Fig. 2-42: *Examples of Dammann gratings for beam splitting*

2.3.4. Beam splitter for high power application

Based on the concept of a special optical element called a "zone-plate" (please refer to Chapter 2.3.2), a special beam splitter (Fig. 2-43) has been developed at the Fachhochschule, Emden for coupling out a small portion of laser light from a laser beam with up to 4 KW optical power. This beam splitter uses an off-axis variant of a zone plate structure and has been designed to couple 0.1% out of the "main" beam for monitoring purposes, e.g. by using photodiode sensors, to ensure the beam quality.
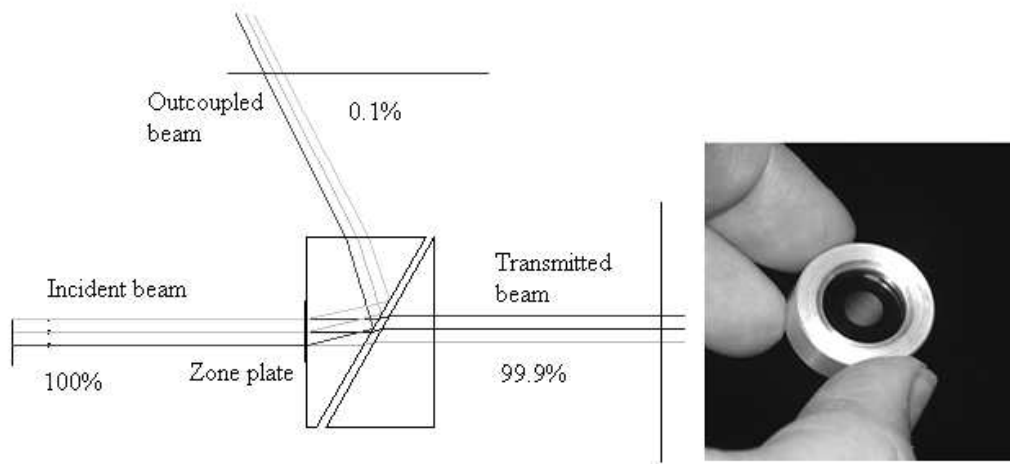
Fig. 2-43: *Simulated beam path of the 0.1% beam splitter and the beam splitter mounted in an aluminium ring*

The off-axis variant of the zone plate deflects and focuses the desired portion of light out of the incident laser beam. Differing from the "normal" zone plates, which focus light along the optical axis, off-axis zone plates (OAZP) can be calculated to deflect light at a defined angle, in this case 13.5º.The calculated OAZP, as shown in Figure 2-44, is exposed to photo resist and transferred into the glass structure by using ion exchange (refer to chapter 2.2.1.1.5).
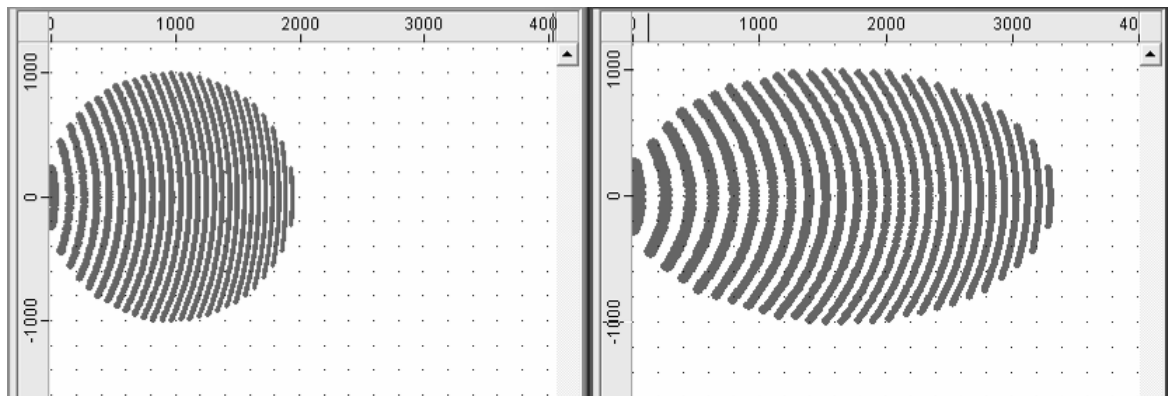
Fig. 2-44: *Calculated OAZP for 0.1% beam splitter (different variants)*

2.4. Characterisation of (structured) technical surfaces

Several techniques exist to characterise the surface of technical objects. All these techniques offer information about the topology of the considered surfaces. The oldest one is optical microscopy; newer technologies are scanning electron microscopy (SEM), atomic force microscopy (AFM) and laser scanning methods like Autofocus or laser triangulation.

2.4.1. Optical microscopy

Once invented around 1600 AD, the optical microscope allowed the nature of matter below the resolution of the human eye to be examined. It uses lenses to produce an enlarged image of objects located within the focal plane of the lens assembly. Figure 2-45 shows the beam path inside an optical microscope. Note that the "virtual image" is only visible with the eyes, not on a screen, since the eyes trace the light straight back to the virtual image.
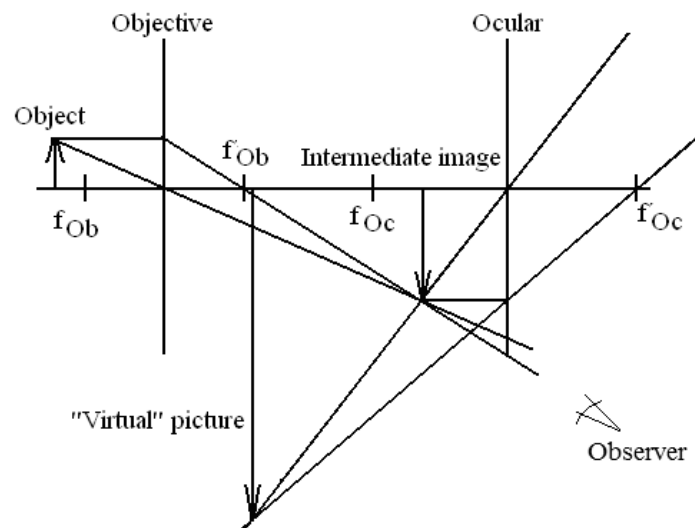
Fig. 2-45: *Beam path inside an optical microscope*

Due to diffraction limitations the smallest object size would be in the range of 300-400 nm.

2.4.2. Scanning electron microscopy (SEM)

The interaction of sample surfaces with a focussed electric beam is used to produce an image of the samples topography. The beam, generated by an electron gun, is led across the sample grid-wise, and the signal of the backscattered (secondary) electrons can be displayed. The sample topography is gained by the secondary scattered electron signal; the material contrast is given by the backscattered electrons (Fig. 2-46). The smallest object size would be in the range of some nanometres.
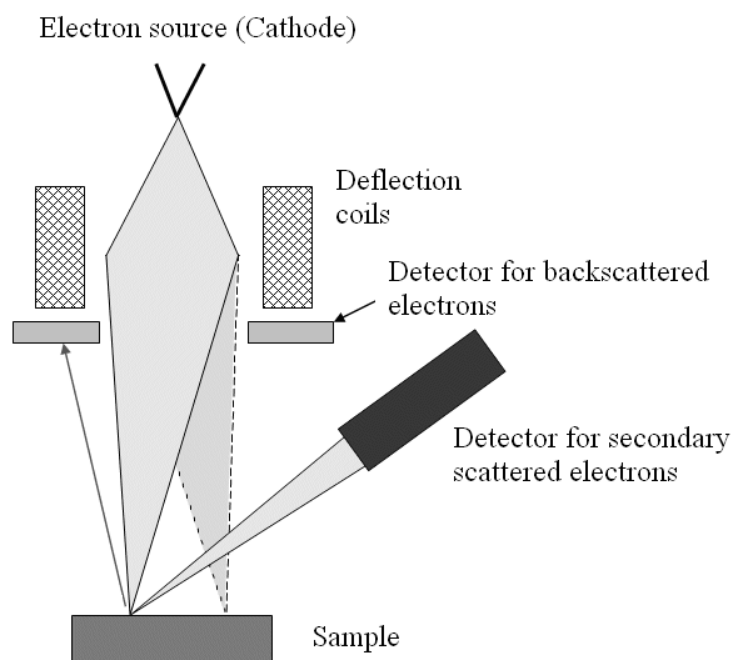
Fig. 2-46: *Simplified model of a scanning electron microscopy (SEM) (according to Ziel 2007)*

2.4.3. Atomic force microscopy (AFM)

Unlike the methods of microscopy mentioned above, AFM is not a "non-contact" technology. It uses a very thin tip (curvature radius of about 10-50 nm) (Fig. 2-47), which is led grid-wise across the sample surface, to determine the topography of the object surface with a resolution of some tens of nanometres.

Figure removed due to copyright restrictions

Fig. 2-47: *Cantilever spring holding a tip for Atomic force microscopy (AFM) (University of Neuchâtel 2010)*

Information about the topography is gained by the detection of the bending of a cantilever spring, which holds the thin tip, as a response to external forces. In case of contact between the tip and the samples surface, these forces are within the range of 0.1 - 1 nN. To detect this very small bending (some 0.01 nm), a laser beam is focused on the back of the cantilever. The reflected laser beam illuminates a photo diode (PD), typically a 4 quadrant PD. The illuminated area on the PD changes depending on the cantilever movement (Fig. 2-48).
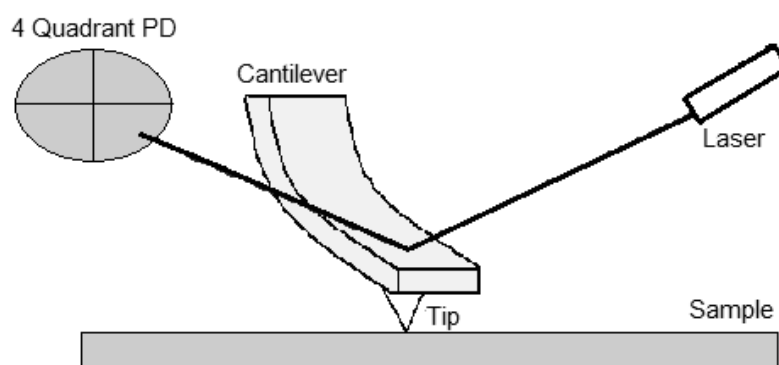
Fig. 2-48: *Simplified model of an atomic force microscopy (AFM)*

47

The AFM achieves atomic resolution on some surfaces and has an important advantage in case of non-conductive materials, where the use of the SEM is not possible or difficult.

2.4.4. Laser-scanning methods

Several measurement techniques use laser beams to characterise the surface of (technical) objects. Most of these make use of diverging distances between the (laser-) sensor and the sample surface. This distance variation (caused by the surface topography itself) is used to produce a three dimensional image of the samples surface and can be determined by the "time of flight" of the light from the sensor to the surface and back. Other methods make use of phase variations between the outgoing laser beam (from the sensor) and the reflected beam (reflected by the sample surface). In all of these techniques, the laser beam is led grid-wise (except methods using line-wise scanning, e.g. light-section) across the sample surface. The following two methods for surface characterisation by laser scanning had been used earlier and are now explained in more detail:

2.4.4.1. Autofocus method

This technique is widely used within photographic cameras (Olympus 2009) or optical instrumentation in general, to automatically focus on objects. It works by changing the focal position of the reflected beam (Fig. 2-49 green lines) according to the surface topography.
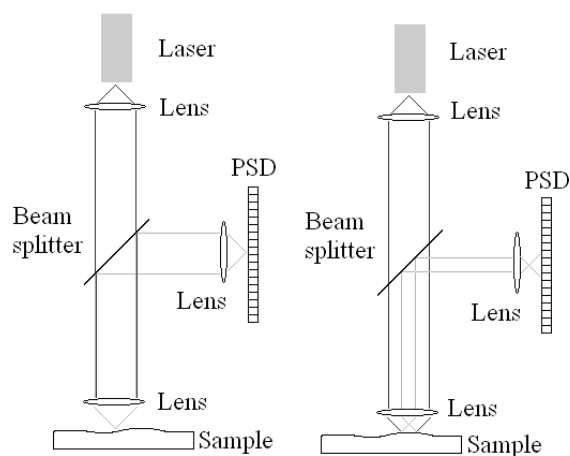
Fig. 2-49: *Schematic view of an autofocus method for surface characterisation*

2.4.4.2. Laser triangulation

Like the Autofocus method described above, the laser triangulation sensor also uses a position-sensing device (PSD) to determine the variation of the point of incidence (Δx) of a reflected laser beam (Fig. 2-50). This variation is caused by a height difference ´Δd´ on the sample´s surface.
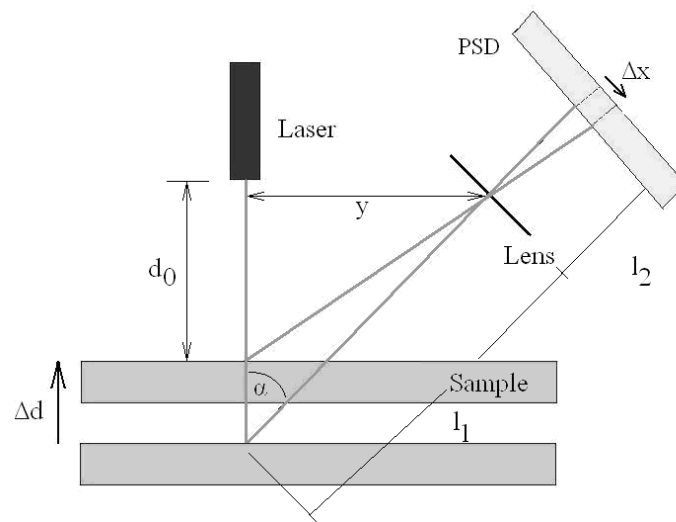
Fig. 2-50: *Scheme of triangulation sensor used for distance measurement*

Due to the triangular geometry of the measuring setup, the height ´Δd´ can be defined by:

$$\Delta d = y \cdot \frac{\dfrac{d_0}{y} + \dfrac{\Delta x}{l_2}}{1 - \dfrac{d_0}{y} \cdot \dfrac{\Delta x}{l_2}} \qquad (2.4.4.2.1)$$

Summary

This chapter has given an overview of surface structuring by means of lithographic techniques and the necessary equipment to realize functional surfaces. Examples of structured surfaces have been shown, special kinds of surface have been described in detail and diffractive optical elements reviewed. The next chapter will present a technology for producing such structured surfaces: Scanning Near-field optical Lithography, a technology using a thin, light-guiding, fibre tip, which is led across the photo resist surface to expose the resist locally.

3. Structuring and surface characterisation by means of near-field techniques

The spatial resolution of surface structures produced by lithographic processes is given by diffraction limitations. To overcome them, one approach can be the use of near-field techniques. This can lead to realizable structure sizes below the wavelength of the used (laser) light.

3.1. Near-field vs. far field theory

A field of light ("Wavefront") heading to a sample structure is modulated spatially by the sample structure itself (Fig. 3-1), regardless of how small the structure is in comparison to the optical wavelength. Only that object information which originates from structure sizes larger than λ/2 is capable of spreading-out beyond the near-field.
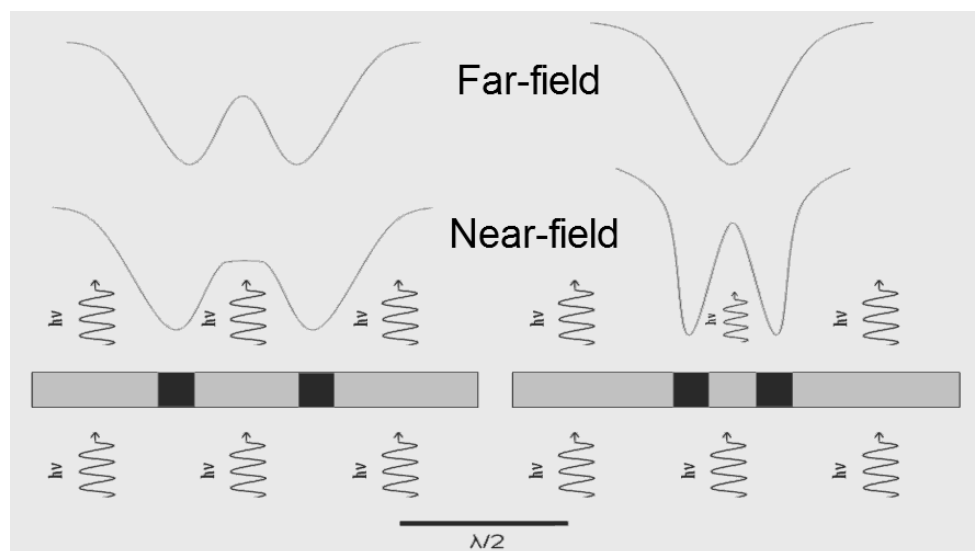
Fig. 3-1: *Near-field principle for two different openings (according to EPJ 2002)*

51

The amplitude of a wavefront which contain the information about structures, that are smaller than λ/2, decrease exponentially. The characteristic length of this decrease is given by λ/2. A structure arising from two corpuscles separated by a distance ´l´ is visible through a conventional microscope for l > λ/2. In Contrast there is no spatially resolved figure of the two corpuscles possible for l < λ/2. The objective of a conventional optical microscope is mounted in a distance from the sample much bigger than λ/2 to the sample - in the so-called ´far-field´. The Rayleigh criteria (Abbe-limit):

$$\Delta x = \frac{0,61 * \lambda}{NA}$$

(3.1.1)

where:

Δx: minimum distance between two objects, at which both appear partially separated

λ :   wavelength

NA: numeric aperture

can be broken if it also succeeds in detecting the exponentially decreasing fields – so-called evanescent fields.

For this purpose the detector must be located in the near-field of the sample, this means no mounting further away from the sample than λ/2 (EPJ 2002).

3.1.1. Concept of Scanning Near-field Optical Lithography (SNOL)

An adaptation of the procedure explained in Chapter 3.1 is Scanning Near-field Optical Lithography (SNOL). SNOL is used to expose the photo resist layer. A very small fibre tip (Fig. 3-2) is used, which is led over the surface at some 10 nm distance. This technique is based on SNOM (Scanning Near-field Optical Microscopy), where a small fibre tip is used to scan and characterize surfaces in order to measure the 3D shape with nanometre resolution (please refer to Chapter 3.2 for details).
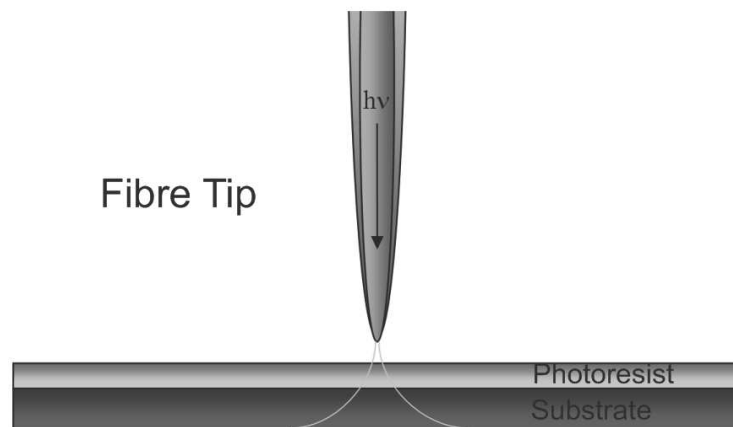
Fig. 3-2: *Scheme of the SNOL technique(according to: Hecht et al. (2000))*

Initially announced by Betzig et al. in 1992 (Betzig et al 1992) for the polarity change of local magnetic domains and further investigated for the exposure of conventional photo resist by Krausch et al. (Krausch et al. 1995) and Cotton et al. (Cotton 2008), SNOL became a potential candidate to break the diffraction limitation within the lithography business. Current research of Leggett (Leggett 2006) and Credgington et al. at UCL (Credington et al. 2010) show that structures within the range of some tens of nm can be produced using the thin aperture (approx. 50 nm) of a fibre tip and the small distance to the surface

3.1.1.1. Construction of the SNOL Systems

An optical fibre tip that has a very small extension (ideally around 100 nm) acts as a light source for the structured illumination of the photo resist with structure solutions of some 100 nm. In order to achieve the targeted resolution, this tip must be moved to within a few nm of the test surface. This is realised by the use of a Nanomotor© from the company Klocke. The distance between the optical fibre tip and the test surface is controlled with the aid of the shear force mechanism and readjusted above a control unit.
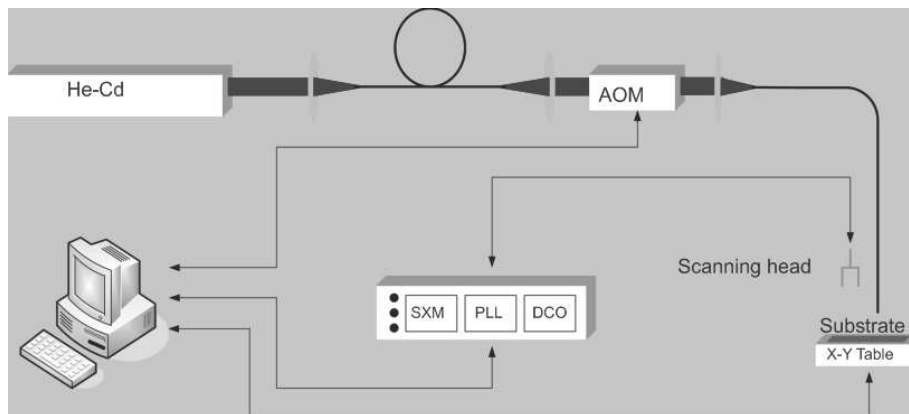
Fig. 3-3: *Block diagram SNOL system at FHOOW Emden*

The construction (Fig. 3-3 and 3-4) of the system up to the fibre coupling took place on a base of the Newport Company which guaranteed an oscillation-free operation.
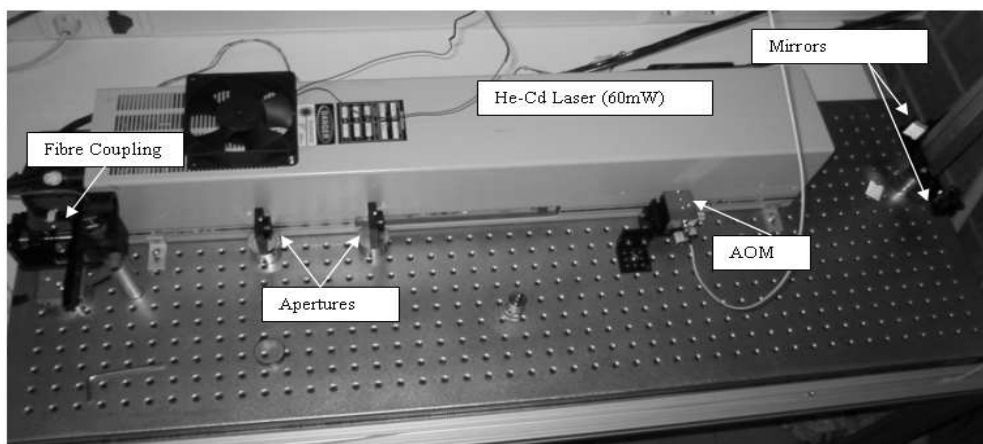
Fig. 3-4: *The components of the laser unit mounted on Newport base*

The coupling of the laser beam into the monomode-fibre is shown in Figure 3-5:
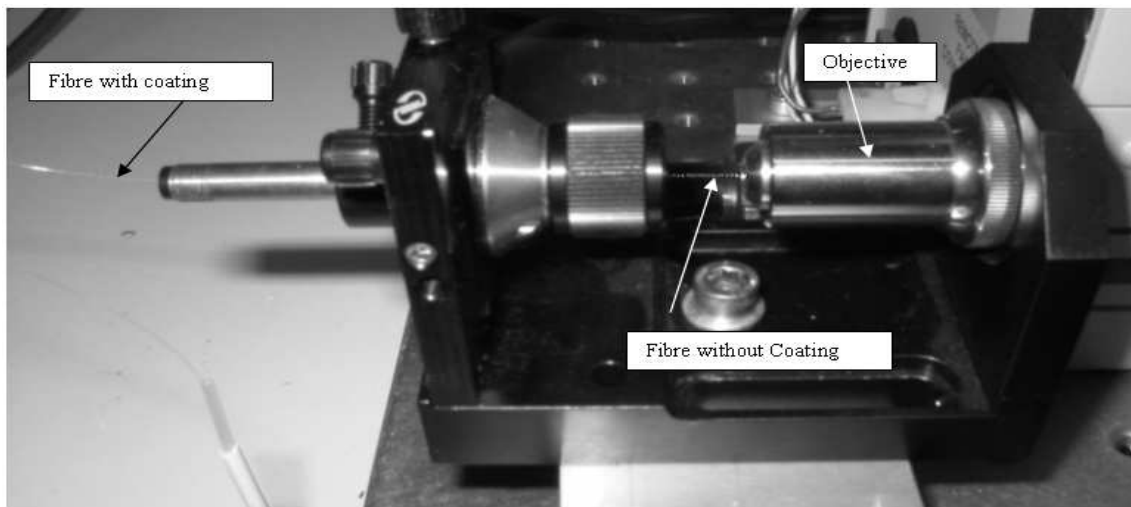
Fig. 3-5: *Fibre coupling unit showing*

For the additional oscillation damping, the scanning unit (which is spatially separated from the laser unit) was mounted into an aluminium case. Figure 3-6 shows some 3D CAD drawings of this housing.
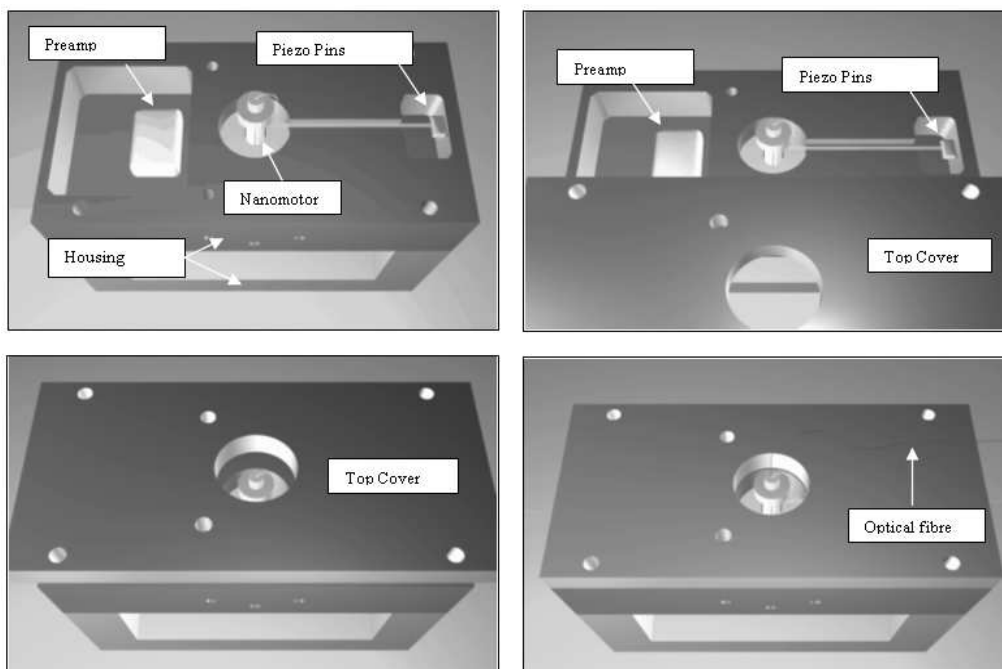
Fig. 3-6: *3D CAD drawings of SNOL scanning unit*

55

The completely assembled SNOL system is shown in Figure 3-7:
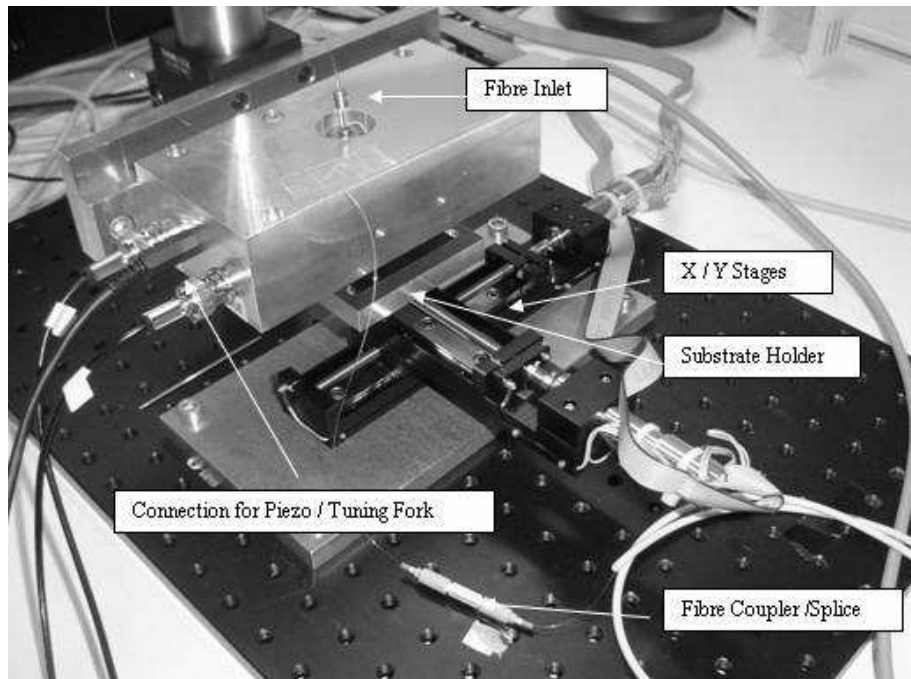
Fig. 3-7: *SNOL Setup showing primary components*

The fibre tip mounted to the dither piezo and to the tuning fork is shown in Figure 3-8 below:
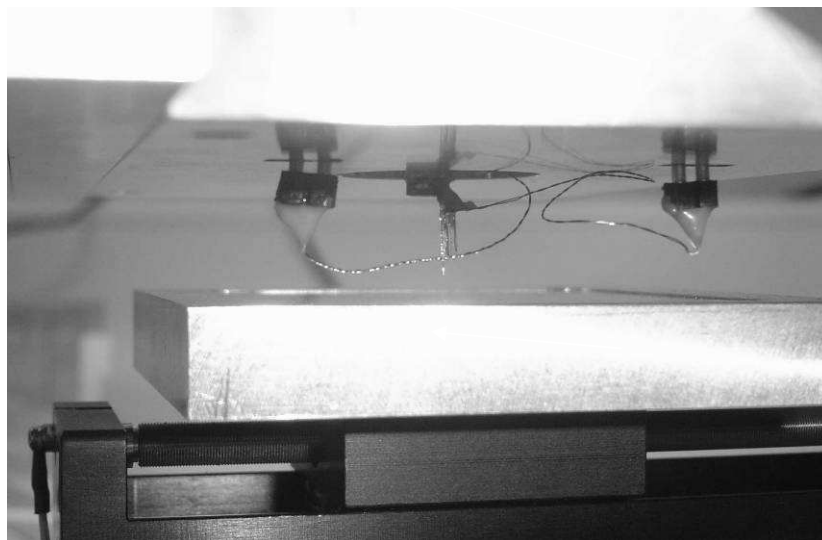
Fig. 3-8: *Mounted fibre tip at the bottom of the SNOL Setup*

3.1.2. Distance regulation

The good resolution of the SNOL Systems is based on the near-field effect and presupposes a distance from the photo resist surface to the source of light (the fibre tip which is considerably smaller than the wavelength of the light). This condition must be met during the entire scan - even if the topography of the sample varies strongly, and can achieved using the shear force mechanism.

3.1.2.1. Shear force interaction

The distance control of the fibre tip works according to the principle of the shear force interaction. Thereby, the tip is stimulated by a digitally operated oscillator to produce an oscillation parallel to the substrate surface (Fig. 3-9). The amplitude of the oscillation is measured using the Lock-in Principle with the PLL-electronics (Phase Locked Loop).

With a sufficiently small distance (approx. 20 nm) between fibre tip and the sample, shear forces, which cause a distance-dependent damping of the oscillation amplitude, occur. Information about surface unevenness can be gained from this damping.
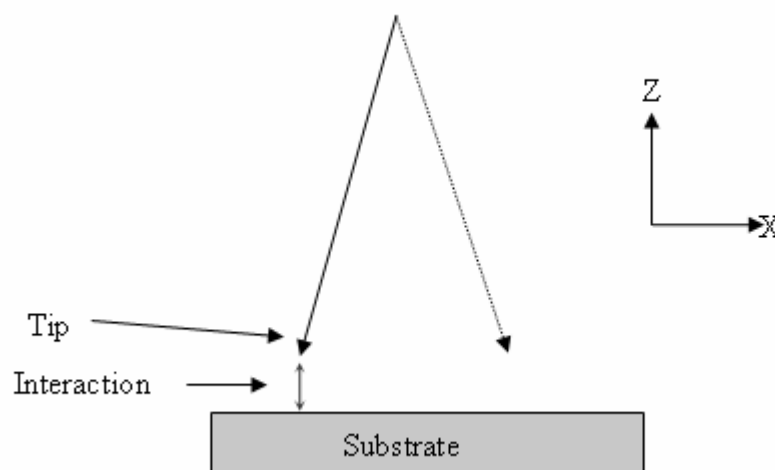
Fig. 3-9: *Scheme of shear force interaction*

57

As a simple theoretical approach, the description of the tip oscillation can be based on the equation for a harmonic oscillator with periodic stimulation can be taken as a basis (Klocke 2007):

$$\ddot{x} + 2(p_0 + p(z))\dot{x} + \omega_0^2 x = A_0 \cdot e^{i\omega t}$$

(3.1.2.1.1)

The term $p_0+p(z)$ describes the damping that consists of an "own part" ´p_0´ and a part, proportional to the reciprocal of the sample-tip distance ´z´:

$$p(z) = \frac{\gamma}{z}$$

(3.1.2.1.2)

X describes the lateral deflection of the tip, ω_0 the resonance frequency of the un-damped system, ω and $_{A0}$ the frequency and the amplitude of the external stimulation.

With the implementation approach:

$$x = A(\omega, z) \cdot e^{i\omega t}$$

(3.1.2.1.3)

the oscillation amplitude of the tip is:

$$(\omega_0^2 - \omega^2 + 2i\omega(p_0 + p(z))) \cdot A(\omega, z) = A_0$$

$$\rightarrow |A(\omega, z)| = \frac{A_0}{\sqrt{(\omega_0^2 - \omega^2)^2 + 4\omega^2(p_0 + p(z))^2}}$$

(3.1.2.1.4)

The resonance frequency of the system is chosen as the stimulation frequency of the fibre-tip, and it is determined at a large z-distance experimentally (Fig. 3-10).
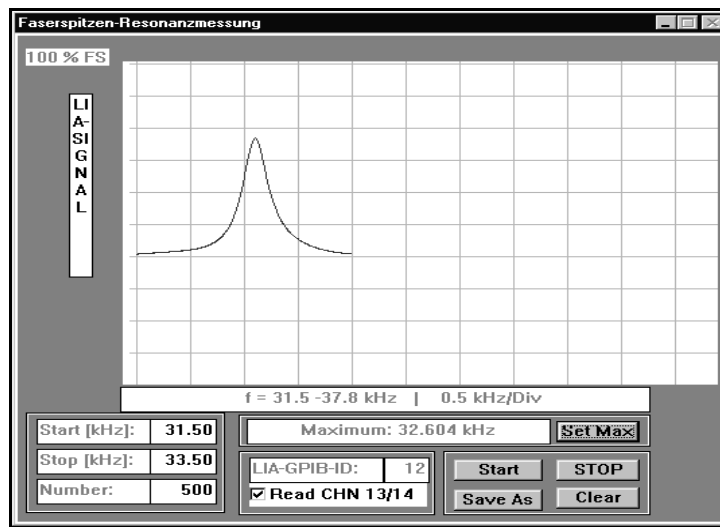
Fig. 3-10: *Measurement of the resonance frequency (Screenshot)*

For great values of ´z´ the linear distance-dependent damping term can be neglected, and thus the resonance frequency results from the maximum of the amplitude function (Klocke 2007)::

$$\omega_r = \sqrt{\omega_0^2 - 2\,p_0^2}$$

(3.2.1.1.5)

The oscillation is stimulated with ω= ω$_r$- thus the amplitude is given by:

$$A(z) = \frac{A_0}{2 \cdot \sqrt{p_0^2 + (p_0 + \dfrac{\gamma}{z})^4 (\omega_0^2 - 2\,p_0^2)}}$$

(3.2.1.1.6)

For z<< 1 this can be developed into a Taylor-row:

$$A(z) = \frac{A_0}{2 \cdot \sqrt{\gamma^2(\omega_0^2 - 2p_0^2)}} \cdot z + 0(z^2)$$

<div align="right">(3.2.1.1.7)</div>

The amplitude signal results can be seen as being proportional to the distance between the tip and the sample surface (about z < 15 nm). With reference to measurements (Fig. 3-11) that were carried out at the University of Aachen (Germany), the following amplitudes (shown in Table 2) were determined (Klocke, 2007).

Figure removed due to copyright restrictions

Fig. 3-11: *Amplitudes vs. Surface distance [according to Klocke 2007)*

Table 2: *Amplitudes vs. Surface distance (Values taken from Fig. 3-11)*

Z distance in nm	Amplitude A(z)
0	0,05
1,25	0,5
2,5	0,62
5	0,84
7,5	0,91
10	0,97
15	0,98
20	1

According to the equation (3.2.1.1.7) it follows that:

$$\gamma = \sqrt{\frac{A_0{}^2}{\sqrt{\left(\frac{A(z)}{z}\right)^2 \cdot 4 \cdot \omega_o^2}}} \qquad\qquad (3.1.2.1.8)$$

In the distance-dependent damping term ´γ´ (With A_0 = 500 nm, p_o was ignored due to the assumption $\omega_r \approx \omega_0$. (Klocke 2007): The damping in dependence to the distance z is given in Table 3.

Table 3: *Damping in relation to the distance z to the substrate surface*

Z distance in nm	Amplitude A(z)	Damping (γ)
0	0,05	0,000
1,25	0,5	3,461
2,5	0,62	5,583
5	0,84	8,241
7,5	0,91	11,411
10	0,97	14,274
15	0,98	21,192
20	1	27,691

The correlation between the damping and distance z is shown in Figure 3-12:
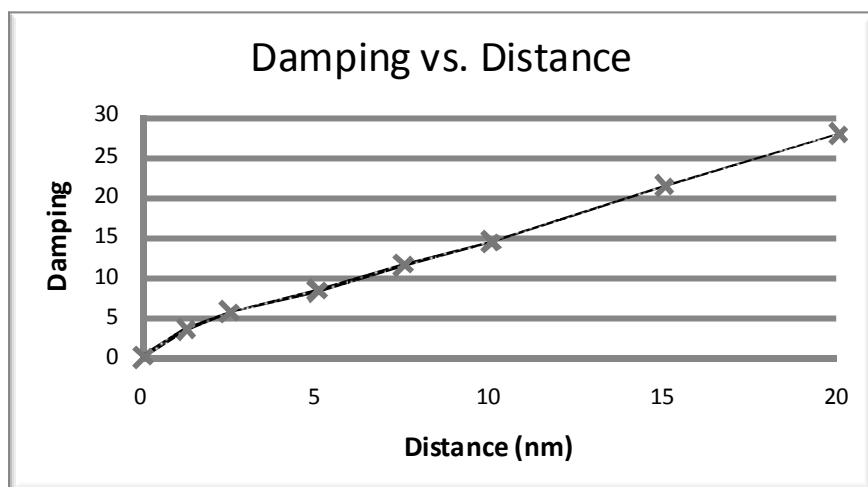
Fig. 3-12: *Correlation between Damping and Distance to the samples surface*

The mechanism which leads to the oscillation damping is not yet completely clear. Different ideas have been published in the literature (Betzig et. al (1991), Ruiter et al (1997), Hoppe et al (2004)). , which, however, do not completely describe the phenomenon. Possible reasons have been sought in different electrical and chemical properties of the materials. On the one hand, the oscillation is supposed to be influenced here due to mirror loads. On the other hand, the damping is caused by the immersion of the top into an absorbance layer, the thickness of which is determined by the surface materials. There are references to an interaction with an absorbance layer, in particular any existing water. Moreover, the processes are not explainable with measurements in a vacuum, with low temperatures or in liquid helium. Other approaches result from the analysis of approximation curves, in which the phenomena that occur are only explainable through the mechanical contact of the tip with the sample. Similarly, a long-range Van-der-Waals interaction is conceivable as an explanation (Klocke 2007). Therefore different approaches with different dominant effects depending on external factors such as the tip form, the test surface and vibratory excitation must be considered.

3.1.2.1.1. Detection of shear force interaction

Shear force interaction, thus the damping of tip oscillation in accordance to the surface distance was proposed for distance regulation of SNOM systems in 1991 by Betzig et. al (Betzig et al. 1991), further investigated by Ruiter et al in 1997 (Ruiter et al 1997) and spectroscopy of the shear force interaction has been carried out by Hoppe et al in 2004 (Hoppe et al 2004).The detection of the oscillation amplitude (caused by the dither piezo) occurs with the aid of a quartz tuning fork, to which the fibre tip is attached (scanning head). The bottom of the fork is stuck to a carrier tube (Fig. 3-13).
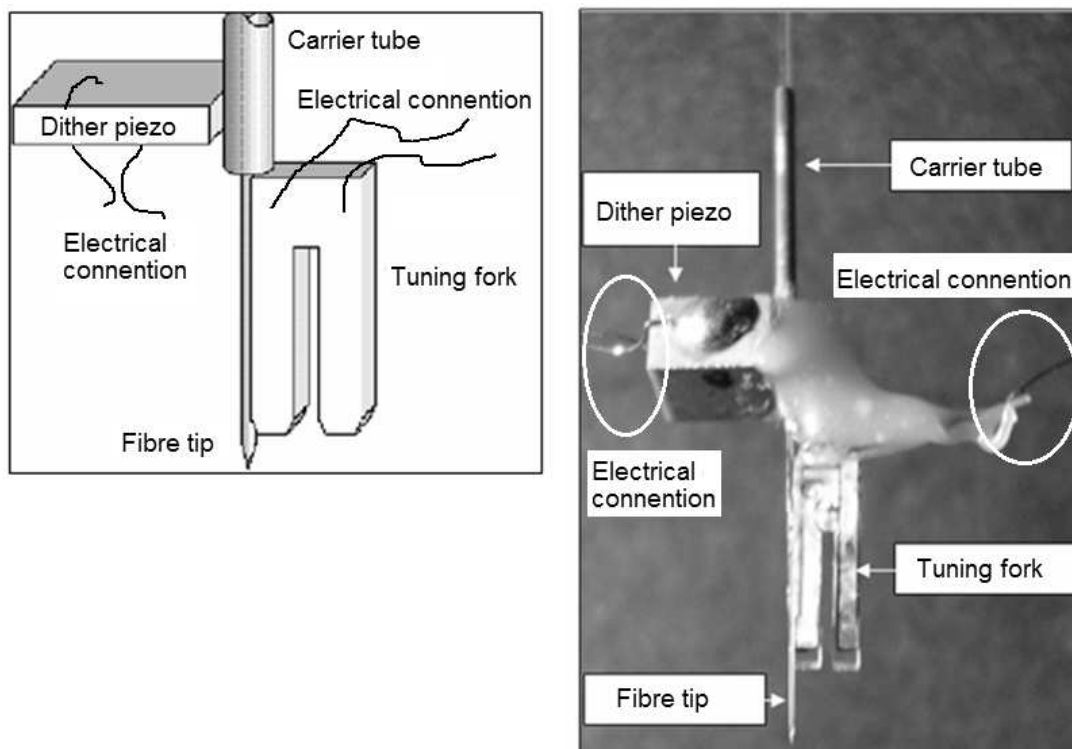
Fig. 3-13: *Left: Scheme of the scanning head; right: Tuning fork with piezo and fibre tip attached*

The vibratory excitation of the scanning head is caused by a piezo-crystal (with two electrodes) attached to the carrier tube. This material makes use of the inverse piezoelectric effect: It deforms under the influence of an electric voltage.
By connecting a sinusoidal voltage (some hundred mV) to the piezo, the tuning fork and the attached fibre-tip are stimulated into a harmonic oscillation.

The tuning fork also has electric contacts to measure a voltage, correlating to the oscillation amplitude (some hundred micro volts). This electrical voltage is amplified with an operational amplifier mounted near to the sensor, 1000 times and sent to the Phase-Locked-Loop (PLL) device. There, an amplitude-dependent D.C. voltage is produced with the aid of the stimulation signal as a reference frequency. The principle of operation of the PLL-electronics is represented in Figure 3-14:
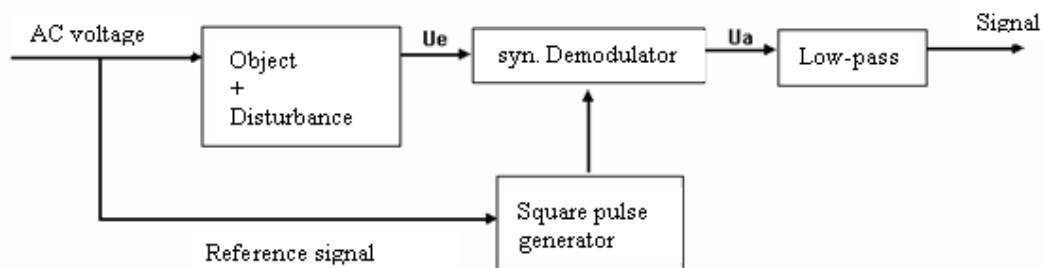
Fig. 3-14: *Schematic circuit diagram of a Lock-In amplifier*

The resonance frequency featured by the freely oscillating system, consisting of a fibre tip tuning fork, a dither-piezo and a fixture is chosen to stimulate the scanning head. According to the preparation of the tuning fork, the resonance frequency (32.7 kHz) deviates insignificantly. The following figure 3-15, below, shows a typical measurement curve to define the resonance frequency.

Figure removed due to copyright restrictions

Fig. 3-15: *Resonance curve of oscillating tip [according to Klocke 2007)*

Next to the resonance frequency of the freely oscillating system, quality is an important factor. This is defined as the quotient of the resonance frequency (fr) and the width of the resonance curve at $1/\sqrt{2}$ times the resonance amplitude (see Fig. 3-15). Experimental investigations show that if the quality is too high, the

system reacts to external influences, like the shear force interaction, too slowly. With a lower quality, the oscillation amplitude is also smaller, thus worsening the signal-noise ratio.

3.1.3. Nanomotor

Since the shear force interaction occurs only at distances below 20 nm, the z-movement of the fibre tip has to be corrected continuously according to the test topography, in order also to be able to examine tests with stronger surface roughness. To receive the best possible resolution the positioning-accuracy should be at least a nanometre. On the other hand, a macroscopic approximation (about a distance of some millimetres) of the tip onto the sample must also be possible. That means that the range of fine adjustment must be smaller by a factor of 10^6 than the necessary shift for the coarse movement. The Nanomotor$^®$ (Fig. 3-16) from Klocke Nanotechnik meets these requirements. It carries the scanning head formed by the tuning fork, fibre tip and dither-piezo.

Figure removed due to copyright restrictions

Fig. 3-16: *Scheme of Scanning head attached to the Nanomotor (Klocke 2007)*

The Nanomotor$^©$ is a type of a "Linear motor" whose mode of operation is based on the inverse piezoelectric effect: A small cylindrical tube (piezo crystal, 4 segments) with electrodes (insulated against each other) attached inside and outside (Fig. 3-16: x+/-, y+/- connections) shows a longitudinal extension by

applying an electric voltage. A fine positioning with sub-nanometre precision is achieved, combined with a stroke of more than 1 cm (at a high voltage). For greater distances, coarse steps can be made by using the pulse wave mode. This leads to a relative shift between the piezo-crystal and the carrier tube in coarse steps, which results in a movement of the fibre-tip relative to the sample.

3.1.4. Acousto-optic modulator (AOM)

Acousto-optic modulators are used to control of the intensity and direction of a laser beam electronically. The basic principle of an AOM is based on the reflection of laser light at a diffraction grating produced by ultrasonic waves:

A high-frequency source powers a piezo transceiver that couples an ultrasonic wave into a germanium crystal (Fig. 3-17).
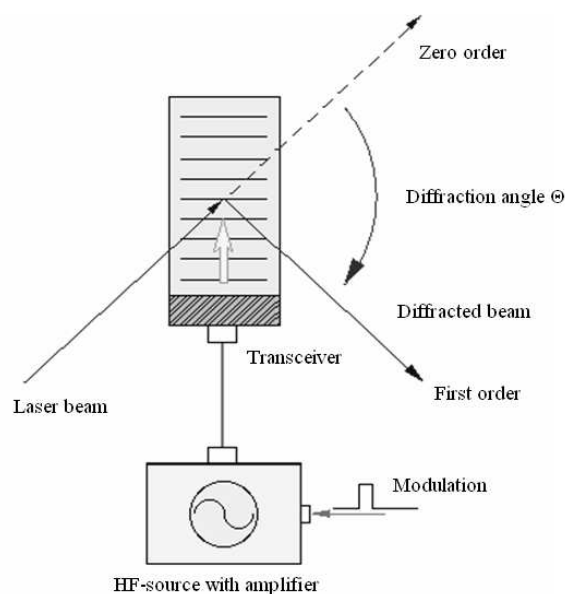
Fig. 3-17: *Schematic construction of an AOM used within SNOL setup*

The incident laser radiation is bent at this grating, and by tuning the frequency, the first diffraction order is forced to have the highest intensity at the output (except for the zero diffraction order which, however, is neglected here due to the impossibility of its regulation).

The angle of the diffraction order (Θ) is almost proportional to the stimulating frequency; the higher the frequency of the HF source becomes, the larger the angle between zero and the first diffraction order becomes (Yariv and Yeh 1984).

$$\Theta = \frac{\lambda \times f_a}{V_a}$$

(3.1.4.1)

Here, λ describes the wavelength of the laser in air, f_a the frequency of the stimulation and V_a the velocity of propagation in the crystal (5,5 mm per µs at germanium).

3.1.5. Translation Stages

In order to scan the substrate in the X-Y direction for point-wise exposure of the photo resist layer, the use of linear stages is necessary (Fig. 3-18). These stages are controlled by software written in Labview$^{©}$.
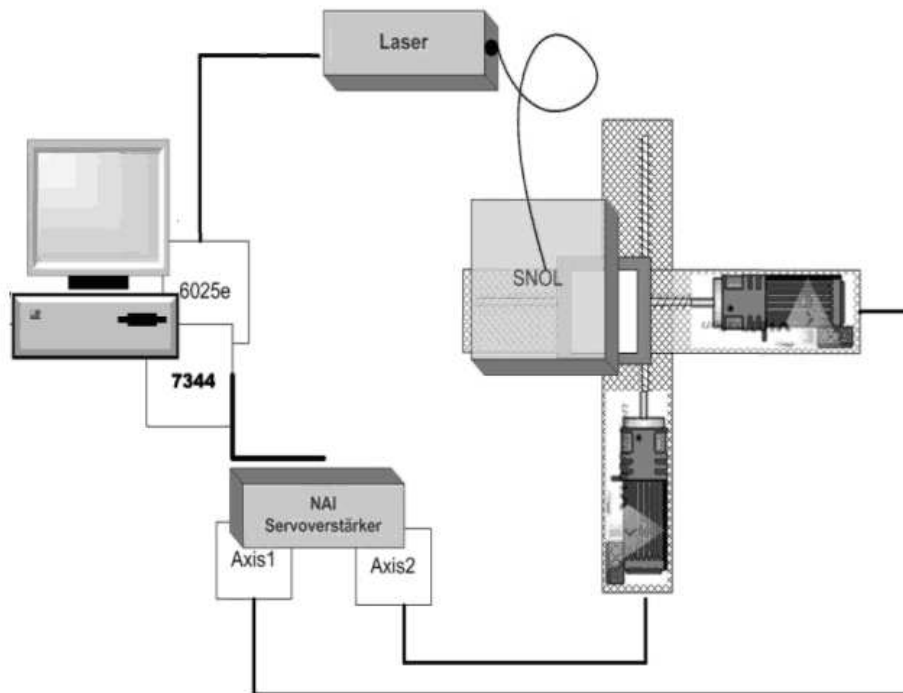
Fig. 3-18: *Scheme of X-Y Stages and the enclosed periphery*

This software also enables triggering light impulses by controlling the AOM through the fibre tip to expose single defined points into the substrates photo resist layer. The hardware components to realize this setup are:

- Interface Cards: Motion Controller 7344 (National Instruments)

  Analog/digital I/O 6025e (National Instruments)

- Servo controller: MC-4SA (National Aperture, Inc.)

- Translation Stages : MM-4-EX80 (National Aperture, Inc.)

- Connector Box: SCB-68 (National Instruments)

3.1.6. SNOL-fibre tips

A key component of the SNOL system, as well as of the beam characterisation system (mentioned in chapter 4.4), is a thin fibre tip. It was necessary to prepare these fibre tips, due to poor commercial availability. The next chapter will give an overview of the production methods.

3.1.7. Optical fibre

The type of optical fibre used to produce the SNOM/SNOL tips is a single-mode fibre manufactured by Newport (Fig. 3-19). Its cut-off wavelength is optimised for the use of He-Cd Lasers.

Figure removed
due to copyright
restrictions

Fig. 3-19: *Structure and technical data of the optical fibre "Newport F-SA" (Newport 2004)used for the production of fibre tips*

3.1.7.1. The production of the SNOL fibre tips

There are two possible procedures in order to shape the end of an optical fibre, according to the requests that a SNOL- Fibre tip should be conical:

- The optical fibre can be pulled with a puller, or
- Etched chemically.

69

The pulling method procedure

During the pulling procedure the optical fibre is preloaded before it is heated up with a CO_2-laser or locally using a heating-film and forced to melt. Immediately after the melting process begins, the puller pulls the optical fibre to give it additional strength (Fig. 3-20) so that the fibre is tapered first and finally tears itself apart generating a tip. The properties of the optical fibre tips produced in this way vary according to the different parameters of the Puller - as for example the pulling force (Schlarp 2003).

Fig. 3-20: *Scheme of the pulling method with particular process steps (Schlarp 2003)*

Commonly, all pulled SNOL- tips show a very lean geometry. Figure 3-21 shows an example of a pulled fibre tip.
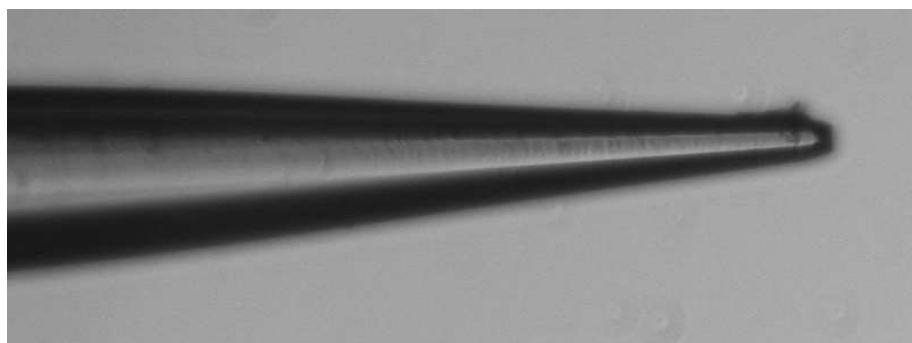
Fig. 3-21: *Example of a pulled fibre (note the lean geometry of the tip)*

70

This lean figure is disadvantageous for the SNOM - or SNOL operation - because the strength, which is caused by the shear force interaction, will not be able to be well transferred to the tuning force well. More rigid fibres (therefore fibre tips with bigger cone angles) are considerably more suitable.

Furthermore, these pulled fibre tips feature a very small transmission due to the long shape of the tip. Bigger cone angles and correspondingly a higher transmission property are reached by etched SNOL- Fibre tips (Essaidi et al. 1998). The SNOL- Fibre tips used in this work were manufactured by etching.

The etching method procedure

A few different methods are used to produce fibre tips by etching. The procedure used here is the so-called "Tube-etching" method (Fig. 3-22). Tube-etching is a further development of the standard etching method, invented by Turner in 1984, published by Stöckel et al. and Lambelet et al. (Stöckle et al. 1999; Lambelet 1998; Suh and Zenobi 2000). This procedure allows the production of considerably smoother top surfaces. In the Tube-etching procedure, the coating of the optical fibre is not removed before the etching. Due to gravity-drawn degradation of the glass products, a concentration slope arises in the hydrofluoric acid, which causes convection. The convection carries the hydrofluoric acid into the upper zone of the tip, which thus develops conically (Schlarp 2003).

Fig. 3-22: Schematic representation of the „Tube- etching method" (according to *Stöckle et al. 1999)*

3.1.7.1.1. The results of the fibre tip production

A 3 mm length of the fibre was immersed into 20 ml of hydrofluoric acid. A light mineral oil was used to realise a separate phase above the hydrofluoric acid, to prevent corrosion by hydrofluoric acid fumes at the upper regions the fibre. The temperature during the production of the tips corresponded to room temperature. In order to gain data for a reproducible etching-process, a series of measurements of the chronological progress of the reaction was taken. Optical fibres etched for different times were compared with an optical microscope and analyzed. Within the following series of figures (Fig. 3-23), the etching time increases in steps of 30min:
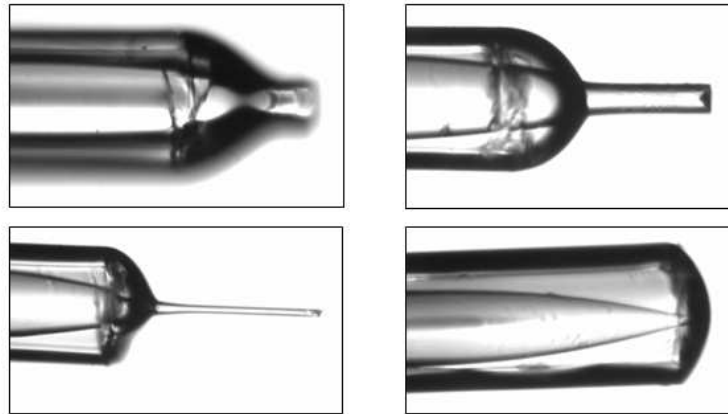
Fig. 3-23: *Fibre tip after 30 min – 120 min etching time*

By the completion of the Tube-etching process, the coating of the optical fibre is still attached around the etched tip and was removed with dichloromethane (Fig.3-24).
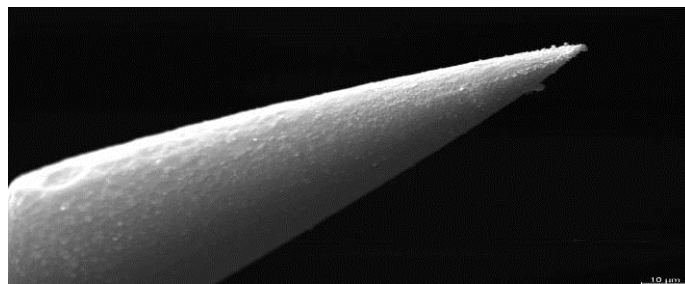
Fig. 3-24: *Fibre tip after coating removal (Taken with SEM, scale bar: 10 µm)*

3.1.7.1.2. The beam path inside the fibre tip

Due to total internal reflection (TIR) at the boundary of the core (higher refractive index) and the air (lower refractive index), the light is guided along the optical fibre tip (Paesler and Moyer 1996; Kramper 2002).
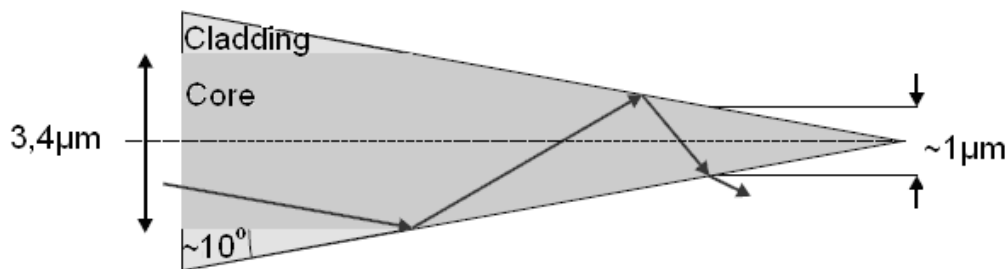
Fig. 3-25: *Out-coupling of light from a fibre tip (schematic)*

Figure 3-25 illustrates this behaviour: At the tip of the fibre, where the cladding is removed by etching, the light can escape from the core, after TIR caused by the difference in refractive index at the core-air boundary. To ensure a very small opening, the tapered tip can be metal coated leaving a small opening (aperture) in the range of hundreds of nm by metalising the tip at a steep angle, creating a metal-free region end of the tip (Madsen et al. 1998).

Fig. 3-26: *Preparation of an aperture by partial metallisation of the fibre tip (according to Schlarb 2003)*

73

Moreover, Haumann et al. (2005) report the stand-alone device for the electrolytic fabrication of aperture probes using electrolytic etching of silver coated fibre tips. However this technique is capable of producing apertures in the range of ~100 nm. The most sophisticated method for production of aperture fibre tips smaller than 100 nm is focussed ion beam milling.

By means of this technique, more precise and reproducible results in aperture formation can be gained. It works by complete metallisation of the tip and subsequent opening of a small region by focussed ion beam (FIB) milling (Muranishi et al. (1998), Veerman et al. (1998)). Figure 3-27 shows an example of a fibre tip realised by FIB milling. Throughout this thesis non-metallised tips have been used.

Figure removed due to copyright restrictions

Fig. 3-27: Optical fibre tip with aperture generated by focussed ion beam milling *(Veerman et al. (1998)*

3.1.8. Results from surface structuring by SNOL

Scanning near-field lithography (SNOL) is a very accurate method for surface structuring, but due to the very small and fragile fibre tip, the tip must be moved very closely (~ max. 100 nm) and slowly across the surface of the substrate.

Therefore, it is only profitable for small areas, as of some hundred microns square. For larger areas it will take too long to complete a structured pattern. The following pictures (Figs. 3-26 and 3.27) will show some examples of the test series made with the SNOL system.
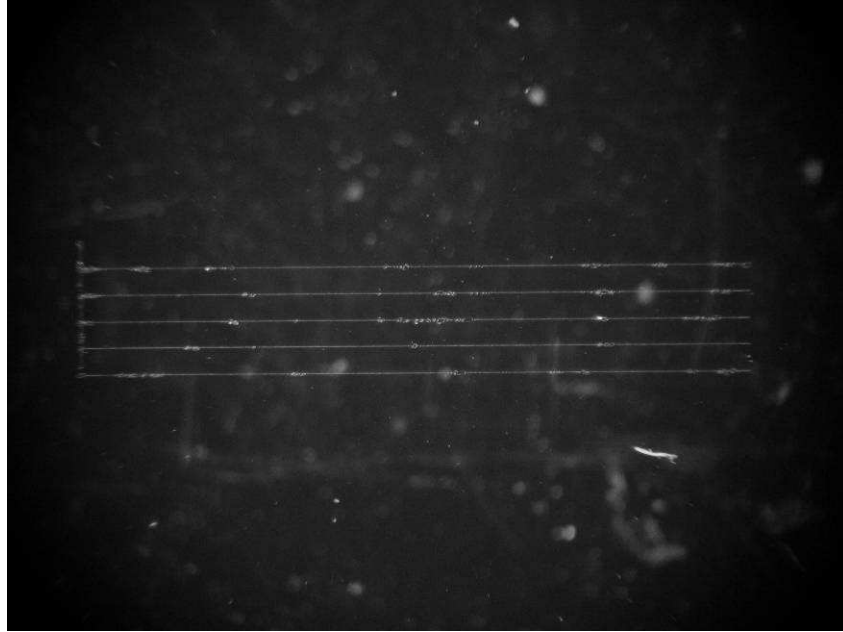
Fig. 3-28: *Very early test with parallel lines (20 mm length)*
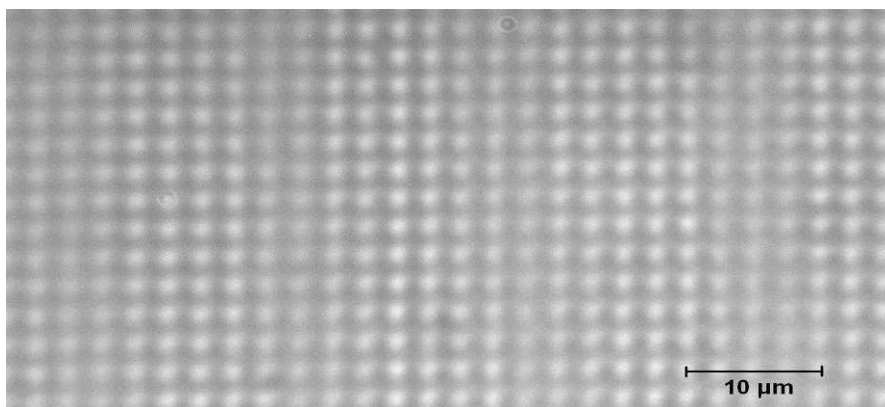
Fig. 3-29: *Dot pattern structure made using the SNOL technique*

3.2. Surface characterisation by means of near-field techniques

The high resolution of the SNOL technology can be used not only for structuring of surfaces by exposure of the photo resist; it is also capable of giving information about the nature of objects by scanning the surface.

3.2.1. Scanning Near-field Microscopy (SNOM)

In 1972, Ash and Nicholls first reported a near-field microscope in the microwave band. They used a construction with an aperture and achieved a solution of λ/60 at a wavelength of λ=3 cm (Ash and Nicholls, 1972). With this experiment and with experiences of tunnel microscopy, Pohl et al. realized the first optical near-field microscope in the year 1984 (Pohl et al., 1984).

The SNOL technique has been developed from Scanning Near-field Microscopy (SNOM). The setup is nearly the same as the one used for the SNOL technique. Thereby, non-diffraction-limited information about a sample's surface can be gained by:

- The damping of the oscillating fibre tip, or
- Reflected or collected light out of / from the fibre tip.

3.2.1.1. Possible configurations of near-field microscopy

A fibre tip (nano-aperture) produces the near-field which is altered by the sample and then measured in the far field. The reverse is also realizable:

A laser illuminates the test from behind and a nano-aperture absorbs the near-field of the sample in order to lead it to the detector. These two methods are referred correspondingly as illumination-mode and collection-mode of SNOM. The combination of both possibilities is known as Reflection-Mode-SNOM.

Fig. 3-30: *SNOM used in: a) Illumination mode, b) Collection mode and c) Reflection mode (according to Schlarp 2003)*

The configuration (Fig. 3-28) used within this thesis was the "collection mode". Therefore, the opposite end of the fibre tip was connected to a photomultiplier tube (Hamamatsu H5784) to detect the light collected by the fibre tip. The data gained was converted by an interface card (NI 6025e) and visualized by a Labview application. Figure 3-29 shows the schematic arrangement of the components used.
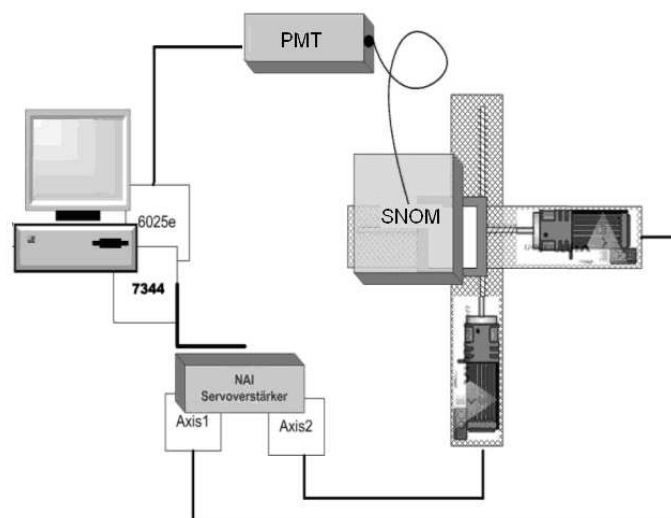
Fig. 3-31: *Scheme of the SNOM system using "collection mode" configuration*

3.2.1.1.1. Examples of characterisation with SNOM

Non-periodic structures, as for example writing, are well suited to the evaluation of near-field microscopes. Letters that appear in the 100 nm range, as shown in Figure 3-30, are not readable because of insufficient resolution.

Fig. 3-32: *Examples of SNOM, note that the smallest letters are about 500 nm high (left) Topography gained by the damping signal, Signal of the reflected light (right) (Marti 2009)*

Figure 3-31 shows an example of SNOM taken at the Fachhochschule Emden. The test pattern was an object used for SEM calibration (Plano S) with periodic squares of ~10 µm (scale bar: 9,87 µm).
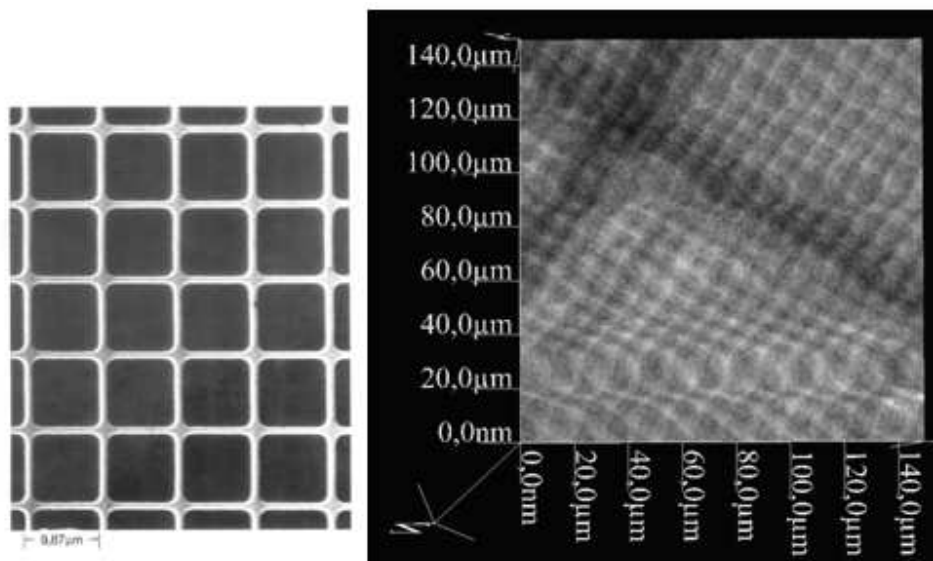
Fig. 3-33: *SEM picture of the SEM calibration object (left)(Plano 2009) scanned with SNOM (right) in collection mode*

Summary

This chapter has introduced scanning near-field lithography (SNOL) for structuring technical surfaces by exposing photo resist surfaces locally. A technique for the characterisation of surface topographies - scanning near-field optical microscopy (SNOM) - has been described. Both technologies are very suitable for structuring and characterizing small areas (in the range of some tens of micrometers), due to the slow movements of the substrate below the fibre tip. Within the next chapter, a technique will be presented enabling higher speeds of substrate movement for better process times.

4. Structuring and surface characterisation by means of confocal techniques

The method used so far for the structuring of technical surfaces was scanning near-field lithography (SNOL). This method is very accurate, but due to the very small and fragile fibre tip, the tip must be moved very closely (20 nm) and slowly across the surface of the substrate. Therefore, it is only profitable for small areas of some hundred microns square. For larger areas the time taken to complete a structured pattern would be too long. This drawback can be overcome by using a "lens-based" system: A confocal setup can be built using a commercial Blu-ray© device, as the optical pickup unit (OPU) of the Blu-ray device can be seen as a "special" kind of confocal arrangement.

A larger distance from the substrate surface is offered by this technique, and therefore the substrate can be moved faster beneath the lens of the OPU. Moreover, it is cheaper to realize due to the substitution of the expensive He-Cd laser by the semiconductor laser used in the Blu-ray© device.

Therefore, and last but not least because of the more compact set up implemented in the new technology, it has been decided to develop the confocal system in the form of the Blu-ray device. During the work on this thesis, it was found that a possible enhancement of the developed test rig leads to a system using the near-field effect discussed in Chapter 3.

4.1. Surface structuring by means of confocal techniques

This chapter will explain the techniques and systems developed for the structuring of technical surfaces. It represents the major part of this thesis and the chapter "Beam characterisation with optical fibre tips" introduces a novel method of beam profiling.

4.1.1. Concept of confocal techniques

In a standard optical microscope, the picture is a superposition of a sharp figure of points in the focal plane and an unsharp image of points outside this focal plane. In a confocal microscope, the stimulating light is focused onto the sample (Webb 1996). Light from this focus is shown normally through the same objective onto an aperture and guided from there onto a detector (commonly a photodiode) (Fig. 4-1).
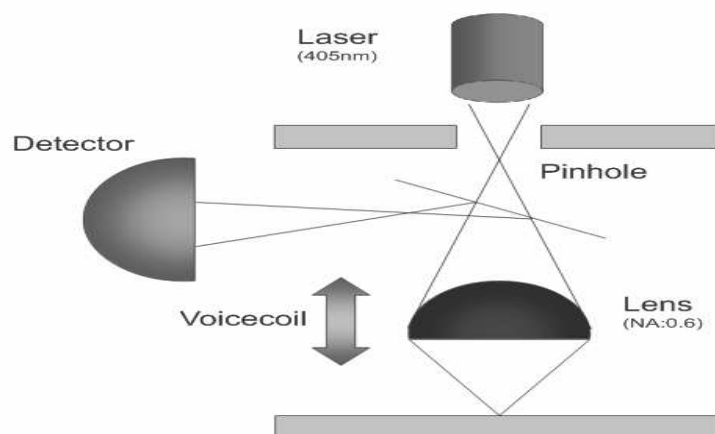
Fig. 4-1: *Principle of a confocal microscope showing the beam path starting from the Laser through the beam splitter and lens to the surface and backwards through the lens and beam splitter to the detector*

Therefore, the focus of stimulation and of detection is positioned confocally. Optical information that does not emerge from the focal plane is suppressed in a twofold way: Firstly, it is not significant since the light intensity is weak outside of

the focus and, secondly, light from outside the focal plane does not become focused on the aperture, so that it is almost completely blocked (Webb 1996).

4.1.2. First test rig using confocal technique

To evaluate the suitability of this technology for surface structuring and characterisation, a test rig (Fig. 4-2) was constructed.
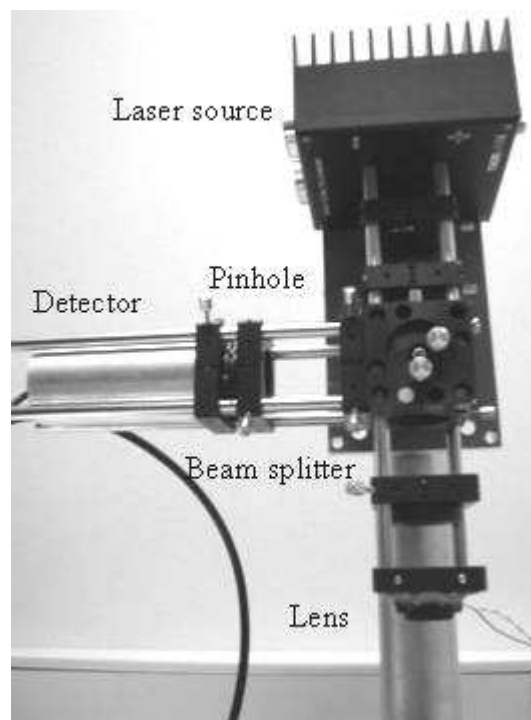
Fig. 4-2: *Test rig of a confocal apparatus (early state)*

This test rig is made of Mikrobank© elements commercially available from Linos©. The advantage of this assembly is the possibility to adjust the distances between the individual components very accurately. The laser source is realized by a 405 nm (Sanyo DL-4146-101S) laser diode and the detector used within this system is a Centronic OSD5-5T photodiode with internal transimpendance amplification. The peripheral system is based on the instrumentation used within the SNOM/SNOL studies (Chapter 3) and has been adapted to the actual needs (Fig.4-3). The used software used for the structuring and characterisation of technical surfaces was created with Labview©; please refer to Appendix 1 for a detailed description.
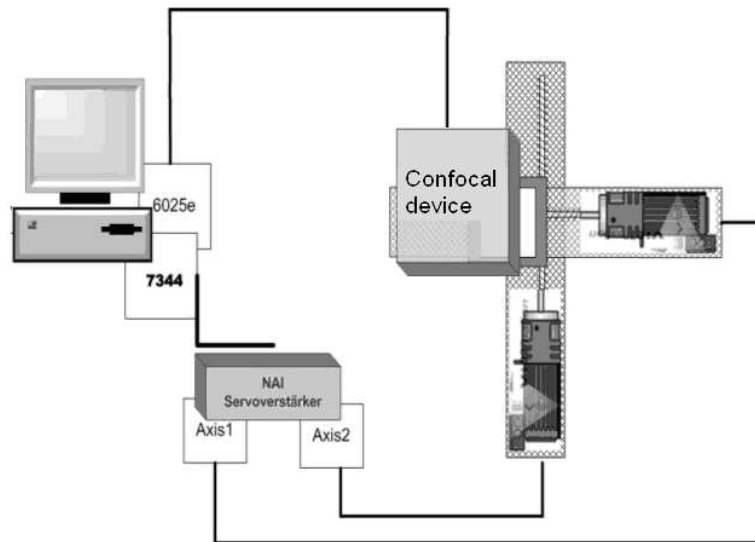
Fig. 4-3: *Scheme of confocal test rig system for structuring and characterisation*

Surprisingly good results in structuring and surface characterisation had been obtained by this system.

Figure 4-4 shows a test pattern consisting of a matrix of single dots exposed onto a photo resist surface.
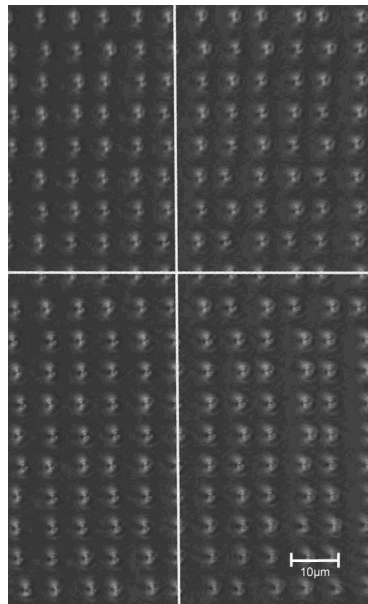
Fig. 4-4: *Microscopic image of a dot matrix test pattern made by the confocal setup*

In the next step, the feasibility of this setup for the characterisation of surfaces has been tested. Thus, the surface of a commercially produced moiré grating (Grid: 40 line pairs / mm) was scanned grid-wise and the detector signal was stored and visualized (Fig. 4-5).
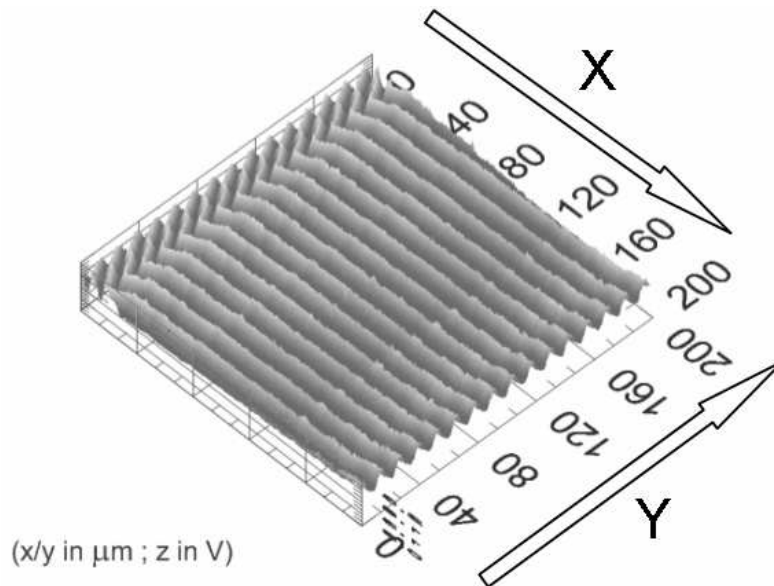
Fig. 4-5: *Surface scan of a moiré grating (40 line pairs/ mm) made by the confocal setup*

4.2. Introduction of the Blu-Ray$^©$ technology

Due to the increasing demand for higher memory densities for high-definition (HD) movies and/or interactive applications (Fig. 4-6) (Blu-Ray Disc Founders 2007) a new generation of optical storage was developed. It uses a shorter wavelength, higher aperture lenses and a smaller distance between the lens and the optical disc.

Fig. 4-6: *Evolution of consumer optical discs (Blu-Ray Disc Founders 2007)*

Two standards were available until 2008:

- **HD-DVD** (high definition digital versatile disc), developed by Toshiba and NEC (using a 405 nm Laser and a <u>NA: 0.65 lens</u>) (Toshiba 2009) was available from 2005-2008.

And

- **Blu-ray**, developed by (amongst others) Sony and Philips (using a 405nm Laser and a <u>NA: 0.85 lens</u>), which was the winner of the "race" for the next-generation optical disc standard.

Together, they all use the same principles for writing and reading optical discs (diameter 120 mm) as those already used in compact disc (CD) players. These principles and how they have been used in this work will be explained further on. The name Blu-ray Disc (official logo shown in Fig. 4-7) is derived from the blue-violet laser used to read and write this type of disc.

Figure removed
due to copyright
restrictions

Fig. 4-7: *Official logo of Blu-ray discs*

The Blu-ray standard has been developed by members of the so-called "Blu-ray Disc Association", an industry consortium, founded in 2002. The founding members were: Matsushita, Pioneer, Philips, Thomson, LG Electronics, Hitachi, Sharp, Samsung and Sony. Companies that signed up as cooperative members include e.g. Apple, TDK, Dell, Hewlett Packard, The Walt Disney Company, Warner Bros. and Universal Music Group (BRDAA 2010).

These optical discs can store:

- About 9 hours of high-definition (HD) video on a 50 GB disc, or
- about 23 hours of standard-definition (SD) video on a 50 GB disc.

On average, a single-layer disc can store a High Definition feature of 135 minutes using MPEG-2, with additional space for 2 hours of bonus material in standard definition quality. A dual-layer disc will extend this capacity up to 3 hours in HD quality and 9 hours of SD bonus material (Blu-Ray Disc Founders 2007).

4.2.1. Basics of Blu-ray© Devices

The fundamental concept of a Blu-ray device is similar to that of a standard CD or DVD Player. The basic setup of such an optical disc drive device is shown in Figure 4-8. An optical disc drive uses focused laser light to detect the lengths of a helical arranged series of pits and lands inside an optical disc. Thus "pits" and "lands" (Figure 4-9) form the information layer of the optical disc; the pits are the "dimples" on the disc, and the land the remaining surface.

Figure removed due to copyright restrictions

Fig. 4-8: *General system setup for a compact disc player optical pickup unit (OPU) (Scarrf 2010)*

Focussed light from a laser diode (Compact disc: 790 nm, DVD: 650 nm; Blu Ray 405 nm) is sent through several lenses, a polarizing beam splitter and a special polarizing device called a quarter-wave plate. Then it is focused through the clear

plastic surface of the compact disc and onto the shiny aluminium layer inside the disc. A portion of light is reflected back through so that it passes through the quarter-wave plate a second time before encountering the polarizing beam splitter. By travelling through the quarter-wave plate twice, the polarization of light switches from horizontal to vertical (or vice versa) so that instead of returning all the way to the laser, the light turns 90° at the polarizing beam splitter and is directed onto an array of photodiodes. Thus, only light which is back-reflected from the optical disc's surface can reach the photodiode. These photodiodes measure the amount and spatial distribution of the reflected light. From this reflected light, the electronics of optical disc players can determine whether the laser beam is hitting a pit or a land on the disc's aluminium layer. Every change from a pit to a land (or vice versa) results in a logical 1. By reading out the information gained by the photodiodes A-D how well focused or aligned (photodiodes E and F) the laser beam is to the aluminium layer and its pits can also be determined (Bloomfield 2008).

Figure removed due to copyright restrictions

Fig. 4-9: *Binary data structure of a compact disc created by pits and lands(CT Magazine 1998)*

Differing from the common setups used for CD or DVD players, Blu-ray devices use focussing lenses with higher numerical aperture and laser light with shorter wavelength (405 nm) to create smaller spots.

To ensure the downward compatibility to CD-Rom and/or DVD, the use of dual or triple wavelength laser diodes is feasible.

4.3. Essential components of the confocal setup

This chapter deals with the introduction and explanation of the components used to build the confocal setup for the structuring and characterisation of technical surfaces. During the work on this thesis, two different types of optical drives have been used for "donating" the optical pickup unit (OPU) as the key component for the developed system. The second optical drive (PS3) will be explained in full detail since it was used for the final version of the confocal-based setup.

4.3.1. Pioneer BDR 101A

Due to the rarity of 405 nm laser diodes, the introduction of Blu-ray was delayed for some time and the availability of such a device was very poor. One of the first devices on the market was the Pioneer BDR 101A ("A" marks the black model, Figure 4-10 shows the grey version).

Figure removed due to copyright restrictions

Fig. 4-10: *Pioneer BDR 101 (Pioneer Cooperation Japan 2008)*

It supports the following optical storage types (Pioneer Cooperation Japan 2008):

- Read Speed: 8x (DVD) / 2x (Blue-ray Disc (BD))
- Write Speed: DVD:8x(±R),2x(-R DL),2.4x(+R DL)/BD:2x(-R)
- CD / DVD Rewrite Speed: 4x (DVD-RW) / 8x (DVD+RW) / 2x (BD-RE)

The drive uses two different laser diodes: one for Blu- ray (405 nm) and one for the DVD compatibility (650 nm). The key component of this optical drive is represented by the optical pickup unit (OPU) (Fig. 4-11).
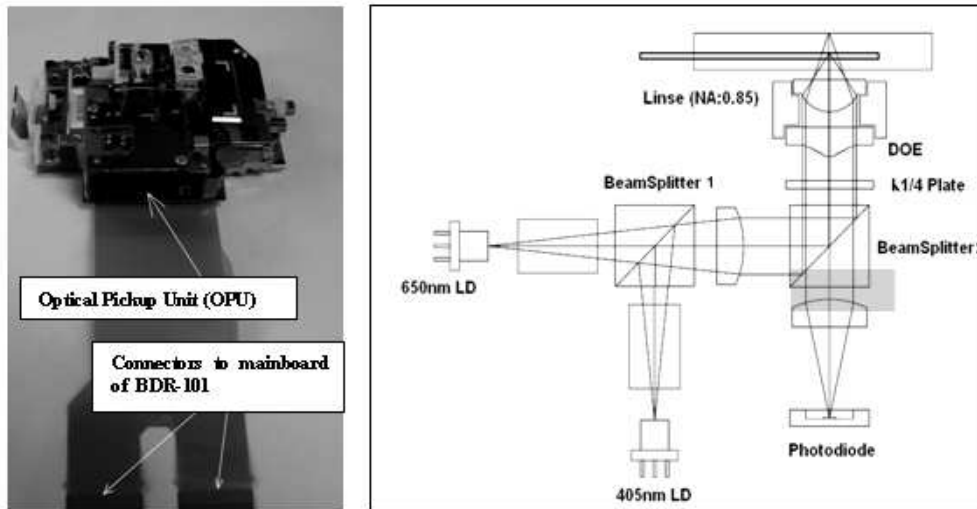
Fig. 4-11: *Optical pickup unit (OPU) of the Pioneer BDR 101 Blu- ray drive*

The peripheral setup (Fig. 4-12) of the test rig discussed within the last chapter has been modified to work with the OPU. Therefore, a second Computer with a USB AD/DA conversion Interface box (NI 6009) and a laser diode driver (Thorlabs LDC 202B) providing the electrical power for the laser diode was added to the setup.
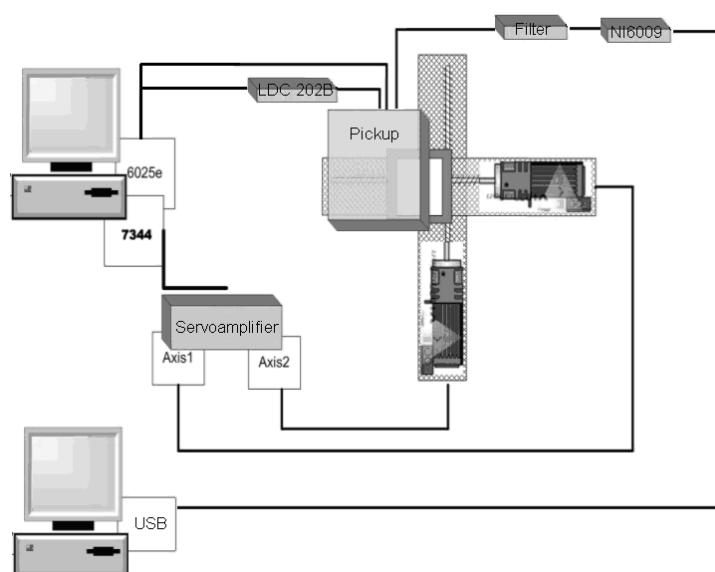
Fig. 4-12: *Scheme of the complete BRD 101 Blu-ray setup*

Due to the fact that the photo detectors originally used in the pickup head were connected by a multi-pin, flat band cable (Fig. 4-11), it was impossible to ascertain which pins lead to which quadrants of the photo diode. Unfortunately, all attempts at "reverse engineering" failed in order to avoid destroying other circuits, especially the 405 nm laser diode which is also connected via this cable. The Pioneer Company stated that the information is confidential and they will not provide the pin-out of the unit. Therefore the original photodiode configuration was removed and replaced by an on-chip amplified photodiode (Fig. 4-13) (Burr Brown Corporation 2007).
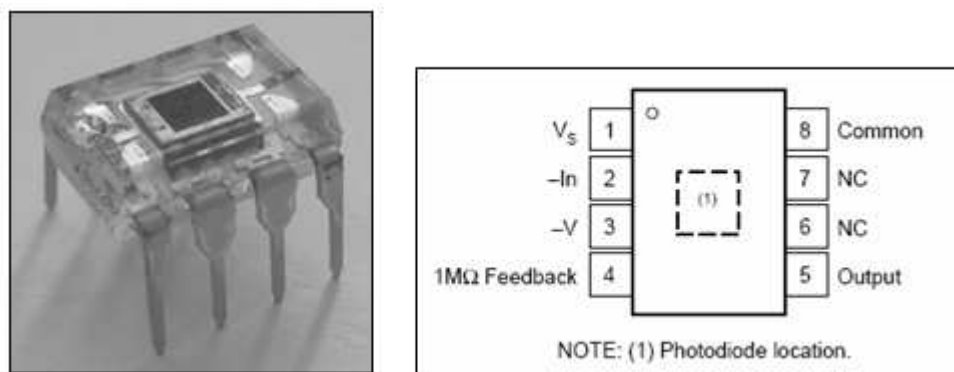
Fig. 4-13: *Burr Brown OPT 202 photodiode and its pin out*

Because of its flat surface and large detection area, this diode was ideal for mounting inside the pickup (Fig.4-14) instead of the original photodiode.
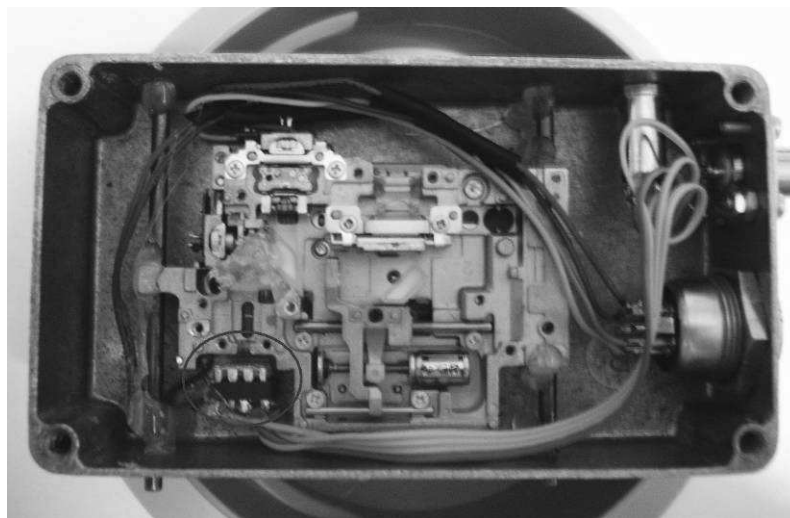
Fig. 4-14: *OPT 101 mounted in the pickup with attached OPT202 (red circle)*

91

Signal conditioning (Fig. 4-15) is done by an `RC` low pass with a cut-off frequency of 200Hz to reduce noise and an inverting amplifier, which amplifies the pre-amplified signal from the photodiode again.
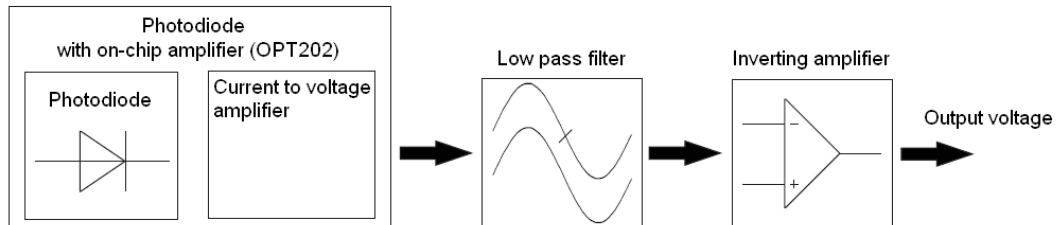
Fig. 4-15: *Scheme of signal conditioning of the photodiode signal*

The following pictures (Fig. 4-16 and Fig. 4-17) show the developed setup.
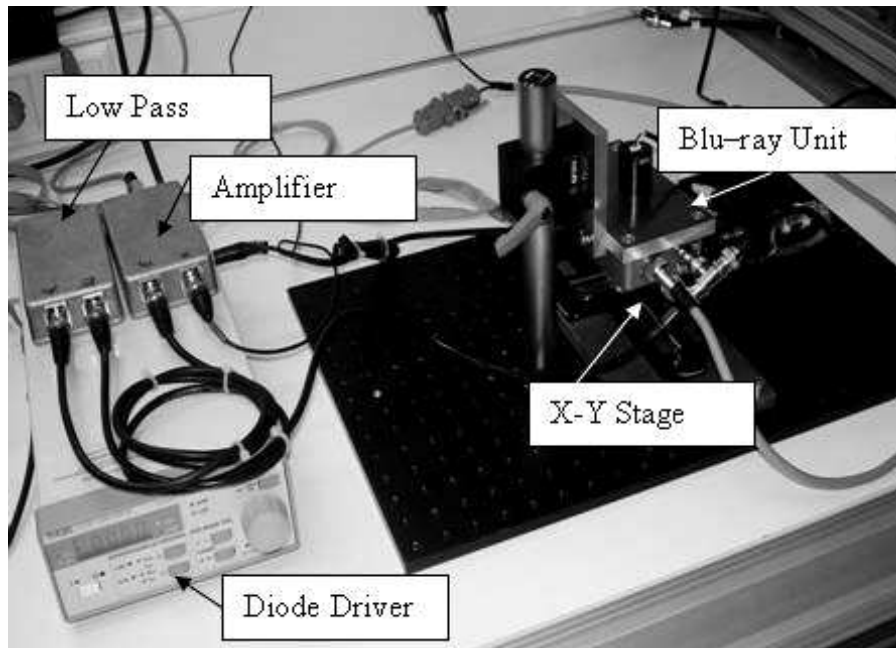
Fig. 4-16: *Pioneer BDR 101-based confocal setup*
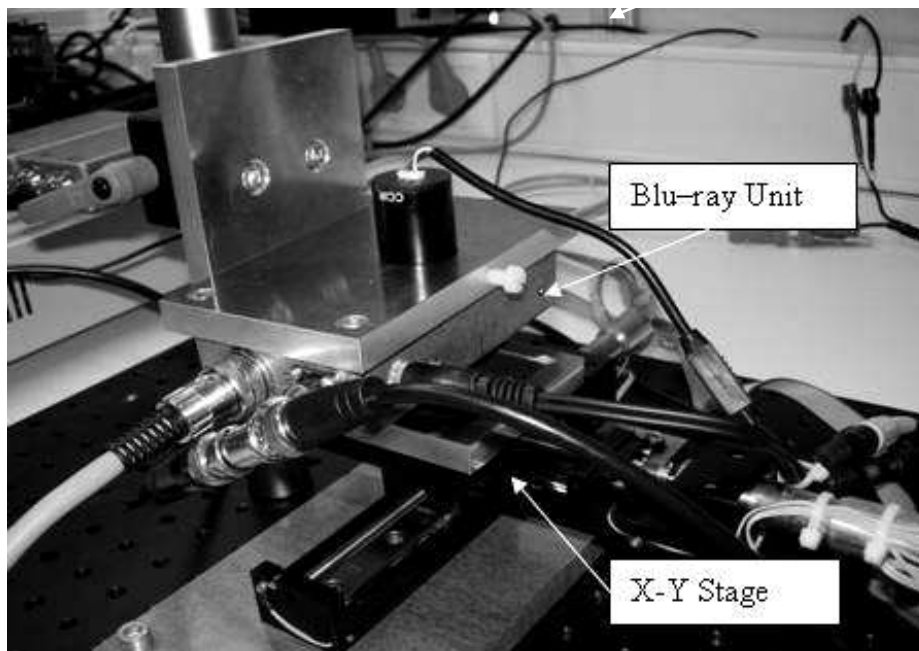
Fig. 4-17: *Close-up of the Pickup housing mounted above translation stages*

4.3.1.1. Results of structuring

The figures below show some examples of structuring with the Pioneer BDR 101-based confocal device. It is obvious that the photo resist is not exposed homogeneously (Fig. 4-18, please note the nonhomogeneous exposure of the photo resist from the left to the right side of the substrate) and that the arrangement of the dots is not uniform (Fig. 4-19, please note the non-uniform patterning; the dots are not aligned properly).
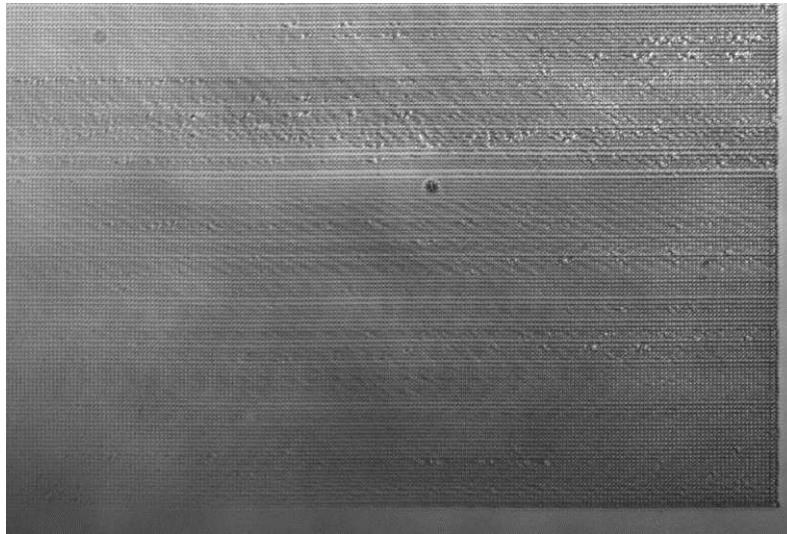
Fig. 4-18: *Dot pattern test structure (magnified 10x)*
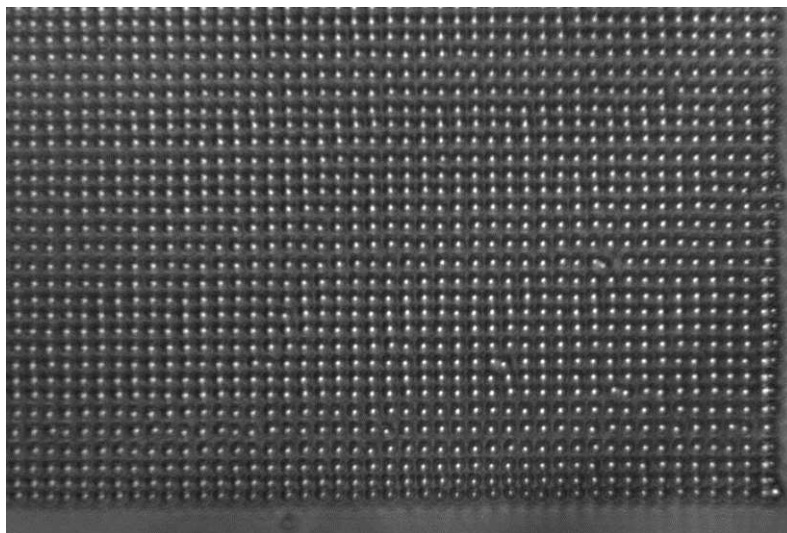
Fig. 4-19: *Same dot pattern test structure (magnified 40x- one dot is ~ 1micron)*

94

It has been found, that the nonhomogeneous exposure is caused by different heights within the photo resist surface, and that the Labview based Software which is providing the pattern data to the laser diode, is corrupted by the Windows$^{©}$ latency times resulting in non- uniform patterning.

This leads to the conclusion that an adaptive focal control and a hardware based pattern data system is necessary.

4.3.2. Multi wavelength Optical Pickup Unit extracted from Playstation© 3

Another electronic device using Blu-ray technology came to market in 2007: The Sony Playstation 3. It was decided to buy the optical part (optical pickup unit, the "OPU") of the optical disc drive unit. "Reverse engineering" of this device was necessary to understand its function and to adapt it for use in a lithography device. No official information concerning the internal technique is available for the playstation, esp. the optical drive unit, since all of this is confidential.

The Playstation© 3 entertainment unit

Figure removed due to copyright restrictions

Fig. 4-20: *The Sony Playstation 3 game console (Sony Cooperation 2008a)*

The Sony PlayStation 3 (Fig. 4-20), officially labelled PLAYSTATION®3 (abbreviated PS3), is the third home video game console produced by Sony Computer Entertainment. The PS3 competes with Microsoft's Xbox 360 and Nintendo's Wii as part of the seventh generation of videogame consoles (Wiki 2008). The console was first released on November 11, 2006 in Japan, on November 17 in North America and on March 23 2007 in Europe. The PS3´s primary storage media is the Blu-ray Disc, while it also supports SACDs, DVDs, and CDs due to its "downward compatibility" (BBC 2008, USA Today 2008, Sony Cooperation 2008b).

4.3.2.1. The Optical Drive Unit

The Blu Ray drive unit is a KES 400AAA (factory code) (Fig. 4-21) built by Sony Cooperation and is downward compatible to CD-Rom (780 nm) and DVD (650 nm). Moreover it is able to play the Blu ray optical discs (405 nm). Figure 4-21 shows the main drive unit consisting of the Disc motor for driving the optical disc at rotational speeds up to 2000 min-1 (Bennet 2006).

Figure removed due to copyright restrictions

Fig. 4-21: *PS3 main drive unit with OPU (according to Wright and Goldwasser 2008)*

4.3.2.2. Optical Pickup Unit (OPU)

Figure 4-22 shows the top view of OPU with the objective lens assembly and electronic devices for laser power regulation ect. The large connector interconnects the electronic components of the OPU to the main electronics of the PS3.

97

Figure removed
due to copyright
restrictions

Fig. 4-22: *Top view of the Sony KES 400AAA Optical Pickup unit (Daedallaser 2009)*

By removing the bottom cover, the inner parts of the OPU are visible (Fig. 4-23):
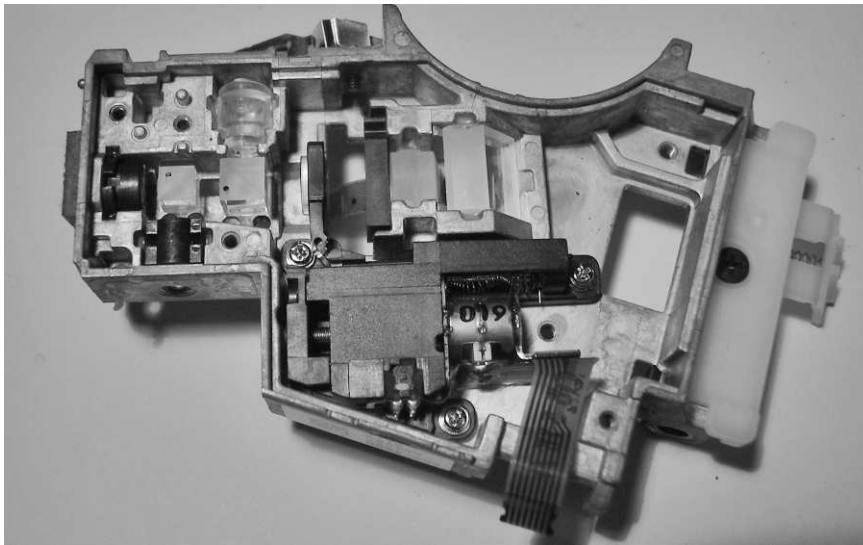
Fig. 4-23: *Bottom view of the Sony KES 400AAA Optical Pickup unit*

With the help of patent publications (U.S. Patent 2006/0067196) and by "reverse engineering", the following beam path of the OPU could be discovered (Fig. 2-24):

Figure removed
due to copyright
restrictions

Fig. 4-24: *Reconstructed beam path within the PS3 OPU*

It shows the different wavelengths coming from the laser diode travelling through the optical components of the OPU. The main parts of the assembly will be explained in more detail in the following:

4.3.2.2.1. Adjustable lens

The most conspicuous part is a lens which is attached to a motor. Figure 4-25 shows this lens after removal from the OPU.
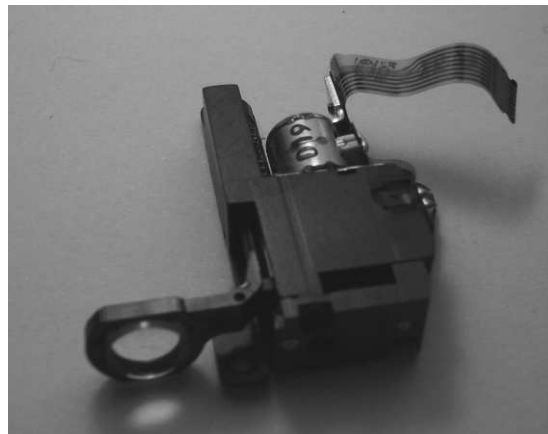
Fig. 4-25: *Lens attached to stepper motor taken out of the PS3 OPU*

The assembly consists of a micro-stepper motor (about 6 mm long) which moves the mounted lens via a screw drive on a linear track. This assembly allows the use of multi layer optical discs due to the possibility of changing the focal length available at the objective lens.

4.3.2.2.2. Grating

To ensure a correct alignment of the lens above the surface of the optical disc, it is necessary to detect the tracks in which the "pits" and "lands" (the binary data) are structured on the disc. Therefore the laser beam is split into a major (high intensity) beam and to "sub" beams (lower intensity).This is realized by an optical grating (Fig. 4-26):
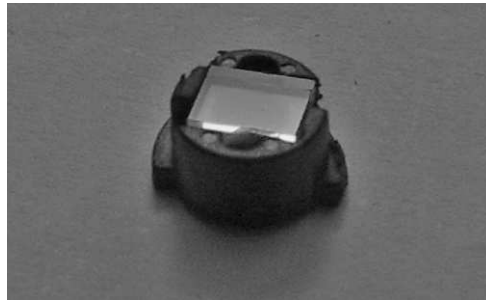
Fig. 4-26: *Optical grating taken out of the PS3 OPU*

To learn more about the working manner of the optical grating, a laser beam was sent through it and the focal spot produced was displayed on a screen showing the major beam with two adjacent, smaller, sub-beams (Fig. 4-27).

Fig. 4-27: *Image of the focal spot magnified 100x over a distance of approx .2m*

This grating has been removed from the OPU within the lithography test rig, because the sub beams would disturb the exposure of the photo resist, due to possible "cross exposure".

4.3.2.2.3. LCD wavefront corrector

This part comprises of a small liquid crystal display, approx. 4 mm square with a flexible cable attached (Fig. 4-28).
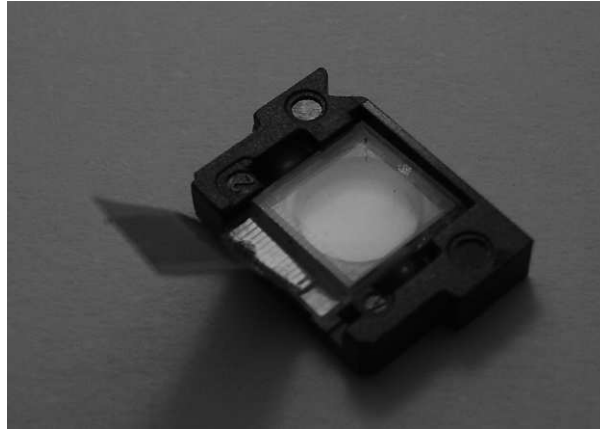
Fig. 4-28: *Wavefront corrector consisting of a small LCD*

Its purpose is to correct the the optical errors in the wavefront e.g. aberration, spherical aberration, astigmatism, and coma. U.S. Patent Application Publication #2006/0067196 A1: "Optical pickup and optical disk drive using same" (Sony) shows the segmented electrode pattern of the LCD wavefront corrector (Fig. 4-29):

Fig. 4-29: *Electrode pattern of the wavefront corrector (U.S. Patent 2006/0067196)*

Since this component is not necessary for the presented work, please refer to the patent publication for further details on its operating mode.

4.3.2.2.4. Objective lens assembly

The most sophisticated, and for this work most important, part of the optical pickup unit is the lens assembly shown in Figure 4-30.
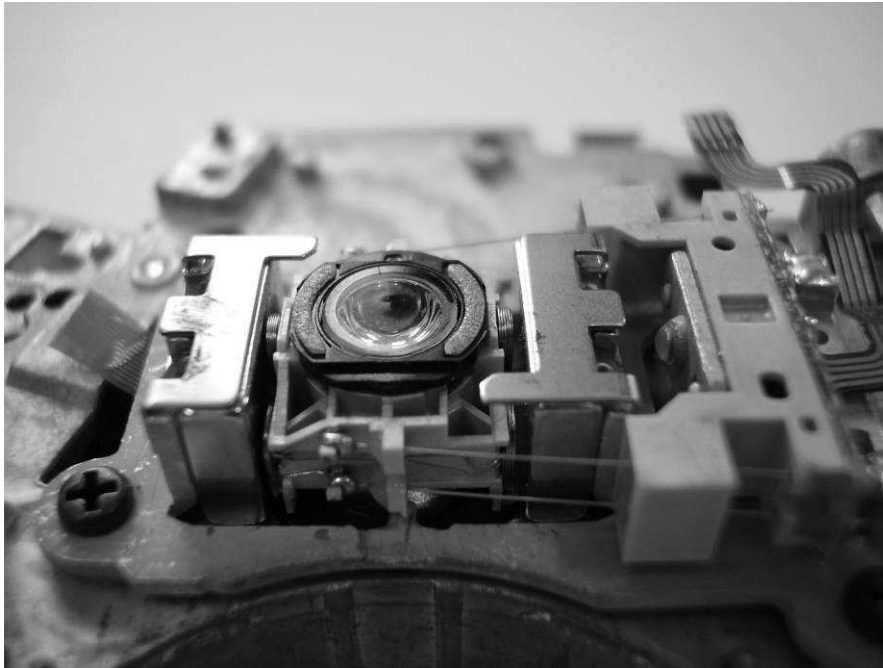
Fig. 4-30: *Optical lens assembly of the PS3 OPU*

The three main parts of the assembly are:

- The actuator for alignment of the lens above the optical disc surface,
- The focussing lens and
- The diffractive optical element for adaptation of the beam path for different wavelengths.

Actuator

In order to adjust the lens while moving across the surface of the optical disc, the lens is mounted in a frame (Fig. 4-31) which is moving in a magnetic field build by the permanent magnets. It is held by wire springs that also supply electric current to the coils. This current induces a magnetic field in the coils and the coils move up or downward in the static magnetic field, depending on the polarity of the current passing through them. The whole assembly is called the optical pickup unit (OPU) or simply ´the pickup´.
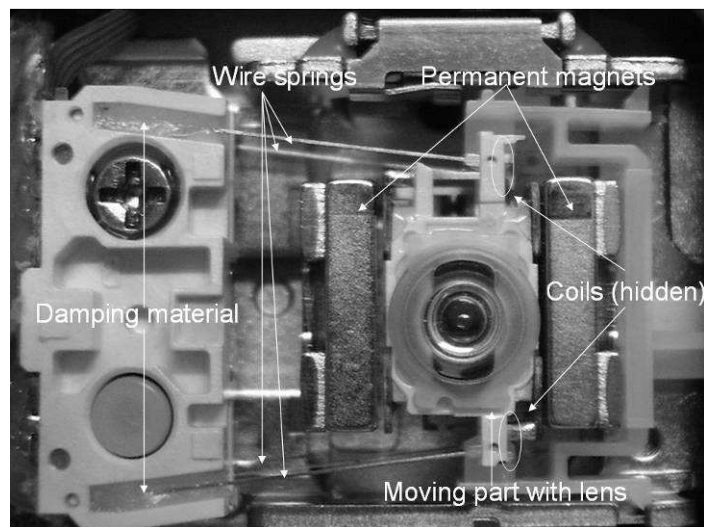
Fig. 4-31: *The actuator of an optical disc drive*

The working principle of this actuator is based on the Lorentz-force, according to the Dutch physician H. A. Lorentz (1853-1928). Please refer to Appendix 4 for a detailed explanation of the Lorenz-force.

A test setup was created to characterize the z-adjustment of the pickup by a frequency generator driving the coils and an optical detector detecting the light emitted by the laser diode. Due to a permanent increase of the current´s frequency, which is driving the coils, a Bode-plot (Fig. 4-32) has been taken, showing that there is a resonance frequency at 70Hz.

Fig. 4-32: *Bode-plot of the pickup showing the resonance frequency at 70Hz*

Therefore, the frequency of adjustment should be in the range of max. 60Hz, i.e. that the position of the lens is corrected due to surface roughness a maximum of 60 times a second.

Another test of the pickup deals with the linearity of the displacement related to the driving current (Fig. 4-33). The coil is made of copper wire with a diameter of 60µm +/- 5µm and an electrical resistance of ~12Ω. The linearity of movement was measured depending on the driving current by means of a measuring microscope. The slope is determined as follows:

Δz / Iz : 15,5 ±0,5 µm/ mA
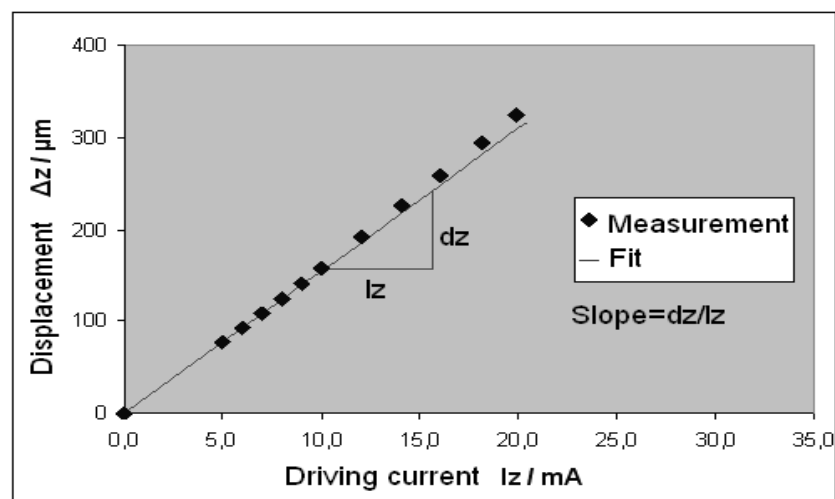
Fig. 4-33: *Displacement vs. driving current of the OPU actuator*

Focussing lens

The focussing lens of Blu-ray devices consist of a numeric aperture (NA) of 0.85. The NA (dimensionless number) is defined as the sine of half the angle of the cone of light . See Figure 4-34 ; where f describes the focal length of the lens from each point of the object that can be accepted by the objective multiplied by the refractive index (n) of the medium in which the object is immersed (Encyclopaedia Britannica 2009c).

$$N_A = n * \sin\Theta \qquad (4.3.2.2.4.1)$$
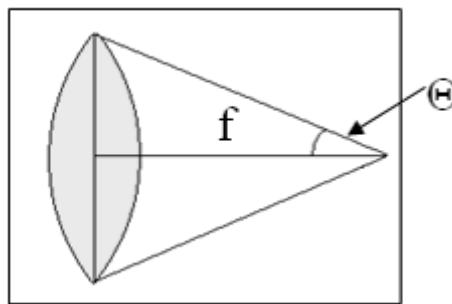
Fig. 4-34: *Definition of the opening angle"Θ with focal length "f"*

NA is an important parameter in microscopy because it indicates the resolving power of a lens; the size of the finest detail that can be resolved proportional to λ/NA, where λ is the wavelength of the light (Encyclopaedia Britannica 2009). This diffraction-restricted resolution of optical instruments was calculated by Lord Rayleigh by using the wave character of light (Hecht 2001).
The equation:

$$\Delta x = \frac{0,61 * \lambda}{NA} \qquad (4.3.2.2.4.2)$$

testifies, that the minimum distance Δx between two objects, at which both appear partially separated, is proportional to the wavelength λ and inversely proportional to the numeric aperture NA.

105

Furthermore the numerical aperture should be as large as possible for two different reasons (Monos 2009):

- The spatial resolution improves for larger NA,
- The collection efficiency, i.e. the brightness of the image, increases very quickly with NA, quadratically for small apertures. The fraction of light collected for an isotropic light source is:

$$\frac{\Omega}{4\Pi} = \frac{1}{2}(1 - \cos\alpha) = \frac{1}{2}(1 - \sqrt{1 - (NA/n)^2})$$

(4.3.2.2.4.3)

With: n = refractive index of material (air: 1); Ω = collection angle

So the increase is quadratic for low NA and becomes even faster for larger NA´s, as shown in Figure 4-35:
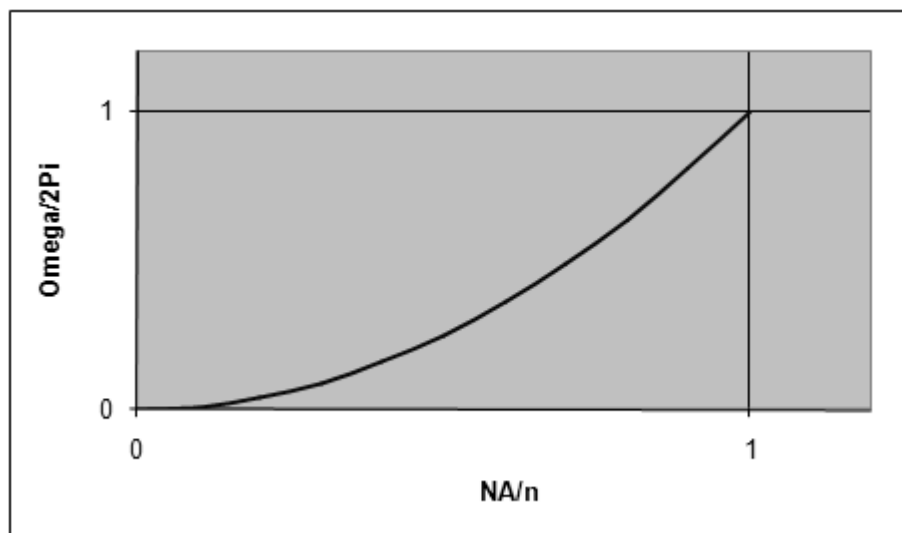
Fig. 4-35: *Variation of the collection angle with numerical aperture NA*

Consequently, a lens with a larger numerical aperture will be able to visualize finer details and collect more light and will generally provide a brighter image than a lens with a smaller numerical aperture. To achieve focus spot diameters in the

range of 500 nm and below, it is necessary to increase the NA. In comparison to the CD (NA: 0,4) or DVD (NA:0,6), the spot size of the Blu-ray optics is one third that of the size of a CD optics spot, respectively half as big as a DVD spot. Thus the feature sizes of "pits" and "lands" of the optical Blu-ray discs are much smaller than in the conventional techniques (Fig. 4-36):

Fig. 4-36: *Comparison of different optical discs (according to Yamada 2004)*

The focussing lens of the PS3 optical pickup unit consists of an complex formed asphere (Fig. 4-37).
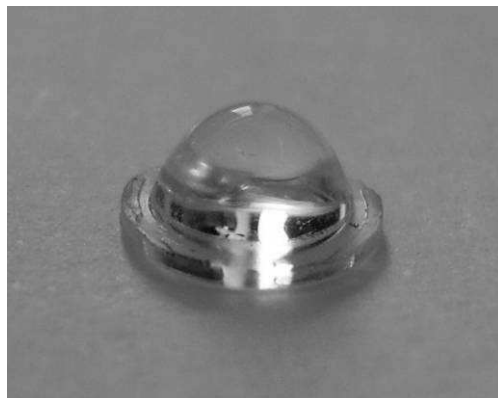
Fig. 4-37: *Focussing lens taken out of the PS3 OPU*

For simulation purposes, the extracted lens has been measured to build a model of it. Aspheres in general (Fig. 4-38) are distinguished from the spherical lenses by the form of their surface. This surface is not specified by <u>one</u> shape parameter, as for example the radius of a ball (spherical lens), rather, it is described through <u>several</u> parameters, mostly in the form of constants.

Figure removed due to copyright restrictions

Fig. 4-38: *Construction of an aspher (Kreischer 2007)*

Often, an asphere is formed by rotation of a conic section around its main axis. An ellipse, a parabola or a hyperbola can be used as the basis. The description of such a curve can be done in Cartesian coordinates, in more general equation form or in direct polar coordinates. The most frequently-used form is an axis-symmetrical curve that rotates around its optical axis (and so around the symmetry axis). The (general) formula can be represented as follows (Tokai, 2007):

$$z(r) = \frac{c * r^2}{1 + \sqrt{1 - (1 + k) * c^2 * r^2}} + A * r^4 + B * r^6 + C * r^8 + D * r^{10}$$

(4.3.2.2.4.4)

With:

r =   radial distance from vertex

c=   vertex curvature (1/radius of curvature)

k=   conical constant

Z =   sag height

A, B, C, D=   Coefficients of a polynomial development of the function which describes the surface of the asphere.

By measuring the focussing lens, we gained the geometrical outline of the lens (Fig. 4-39):

Figure removed
due to copyright
restrictions

Fig. 4-39: *Plotted data gained by measuring the PS3 focussing lens*

By this, the aspheric parameters could be retrieved:

Data removed

With these parameters, a model (Fig. 4-40) of the lens could be generated and the simulation has produced with the aid of the Zemax© optical design software.

Fig. 4-40: *Zemax© (Zemax 2009) generated model of the PS3 focussing lens*

By simulating the focussing system (the lens), the entire setup could be understood better and the possibility to enhance the system was given.

For a basic understanding of the focussing system, the next sub chapter will give a quick overview of the mathematical description of the lens assembly.

Basics in optical calculation

The propagation of a laser beam through a thin lens (Fig. 4-41) should give an overview of the parameters and terms used in the following chapter:
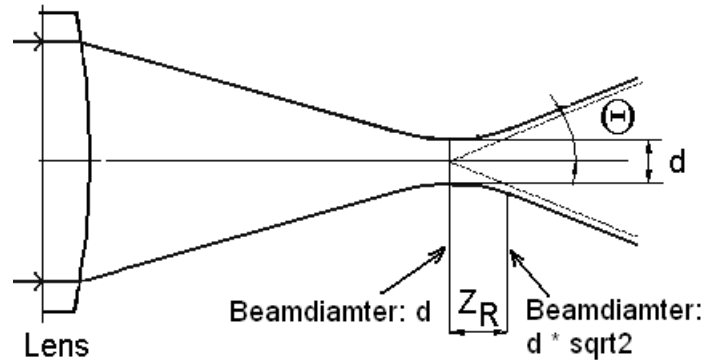
Fig. 4-41: *Scheme of a laser beam propagating through a thin lens (according to Siegman, 1986)*

The Numerical Aperture, already described, is given by:

$$NA = n * \sin \Theta$$

(4.3.2.2.4.4)

By using lenses with high NA, very small focus diameters d can be achieved. The following equation (Imlau 2003; according to the Abbe criterion d= (1/2*λ)/NA) describes the relation between focus diameter d, wavelength λ, refractive index n and the numerical aperture NA:

$$d = \frac{\lambda}{NA} * \frac{n}{2}$$

(4.3.2.2.4.5)

Table 4: *Parameters of different optical discs*

	CD	DVD	BD
Wavelength (nm)	780	650	405
NA	0,45	0,6	0,85
n (Protective layer)	1,5	1,5	1,5

Applied to the parameters (Table 4) of Compact Disc (CD), Digital Versatile Disc (DVD) and Blu-ray Disc (BD) the following (theoretical) focus diameters are calculated (Table 5):

Table 5: *Comparison of different spot sizes*

	CD	DVD	BD
Diameter of focus (nm)	Data removed	Data removed	Data removed
Radius of focus (nm)	Data removed	Data removed	Data removed

While the protecting layers of these optical discs are made of polycarbonate (PC) or polymethylmethacrylate (PMMA) with refractive indexes around n~1.5, the surrounding media in this work is air with a index of n=1, as shown in Fig. 4-42 below (according to: Datarius 2010).

Fig. 4-42: *Comparison of the surface structure of optical discs (here: Blu-ray disc) with "non-protective layer" structures of photo-resist covered substrates*

So with a refractive index of n=1.0 the best possible focal diameter changes from

Data removed

The region in which the focus is still within its width of +/- $\sqrt{2}$ * d is called Raleigh Length Z_R (see Fig.33) and can be calculated in different ways. The historical way is given by Damask (2004):

$$Z_R = \frac{\pi * r^2}{\lambda}$$
(4.3.2.2.4.6)

Data removed

A more complex way is presented by Young et al. (1993):

$$Z_R = 2 * \Delta z = \frac{\lambda}{4 * n * \left(1 - \sqrt{1 - (NA/n)^2}\right)}$$
(4.3.2.2.4.7)

It follows that $\underline{Z_R = xxx\ nm}$

In order to achieve constant spot diameters, it is necessary to position the lens within this distance (Z_R) above the substrate surface. Chapter 5 will give a solution for the active focal control to ensure the perfect position of the lens above the substrate surface.

4.3.2.2.5. Diffractive optical element for adaptation of the beam path

To explain the working method of this part of the optical assembly, the author likes to quote an edited excerpt of Wright and Goldwasser (2008) of United States Patent Application 20070035837 "Optical pickup and optical disc apparatus":

"The diffractive optical element diffracts the light (@660 nm), so that the diffracted light is incident on the objective lens at an optimal divergent angle, whereas the second diffractive part of the diffractive optical element diffracts the light beam (at 405 nm) so that the diffracted light is incident on the objective lens in an optimal amount, and at an optimal divergent angle. As a result, the spot shape and the amount of the light beam, having each of the wavelengths can be made appropriate with respect to (the type of media used)".

Figures 4-43 and 4-44 show the position of the zone plate within the lens assembly as well as the zone plate itself:
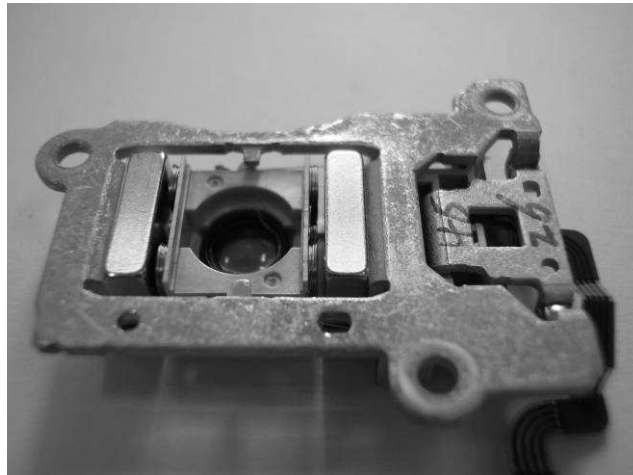
Fig. 4-43: *Close-up of the bottom of the objective lens assembly showing the position of the zone plate in the centre of the lens holder*
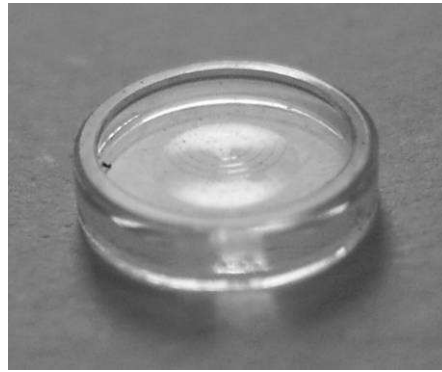
Fig. 4-44: *The diffractive optical element (DOE) extracted from the PS3 OPU*

As already mentioned, Blu-ray devices use blue light (405 nm) and a numerical aperture (NA) of 0.85. A cover layer thickness of 0.1 mm is chosen to compensate for the disk tilt margin. Blu-ray devices are expected to be backward-compatible and to allow the reading and recording of DVDs, despite the fact that their optical parameters are very different. The cover layer thickness, the light wavelength and the NA of a DVD are 0.6 mm, 650 nm and 0.6 respectively (Komma 2004). Chromatic aberration is also an important issue in a BD system, since the focal depth is smaller and the dispersion of the lens material is more significant at shorter wavelengths.

The chromatic aberration of a refractive positive lens can be corrected using a diffractive optical element (DOE) that acts as a positive lens (Maruyama 1995). In a Blu-ray and DVD-compatible pickup, red light for the DVD also passes through the DOE (Fig. 4-45).

Fig. 4-45: *Diffraction variation caused by an optical grating (Tanaka et al. 2003)*

Spherical aberration caused by the difference in thickness of the protective cover layer can be eliminated utilizing the difference in wavefront curvature between incident blue and red rays (Tanaka *et al.*, 2003, Mori *et al.* 2005). This difference in wavefront curvature, however, causes coma aberration with lens movement of the tracking servo, and requires individual photo detectors for BD (405 nm) and DVD (650 nm). A BD-DVD compatible lens able to converge parallel blue and red rays is needed to stabilize tracking servo control and to enable the use of a common photo detector for detecting signals from both types of disc. The third-order spherical aberrations (SA3) caused by the difference in cover layer thickness between BD and DVD can be corrected by utilizing the diffraction angle difference of the red and the blue light (Tanaka *et al.* 2003). This SA3 of DOE, however, causes incorrect SA3 cancellation when the wavelength of the blue light deviates from the designed standard wavelength (Maruyama 1995). To address this, phase-steps to correct the chromatic SA3 were utilized. The DOE pattern and refractive lens surfaces are divided into inner and outer regions (Fig. 4-46).

Fig. 4-46: *Configuration of a lens system showing elements for beam path correction (Tanaka* et al*. 2003)*

The inner regions are designed to focus the second-order diffracted parallel blue ray through the 0.1 mm cover layer and the first-order diffracted parallel red ray through the 0.6 mm cover layer. The DOE corrects the SA3 that is caused by the difference in cover layer thickness by utilizing the wavelength and the diffraction-order difference. The outer regions are designed only for BDs (Blu-Ray Disc Founders 2004, Komma 2004).

4.3.2.2.6. Detection circuit/ photodiode assembly

To detect the laser diode´s reflected signal, the PS3 unit uses two special photodiode assemblies, as shown in Figure 4-48. Due to the fact that the photo detectors originally used in the pickup head were connected by a multi-pin, flat band-cable (Fig. 4-47), it was impossible to ascertain which pins lead to which quadrants of the photo diode.

Fig. 4-47: *PS3 OPU with attached original photo diode detectors (red rectangels) (Daedallaser 2009)*

Strong investigations/ "reverse engineering" have been carried out to determine the pin-out of the original photodiodes, including microscopic imaging (Fig. 4-48) of the photo diode structure. Unfortunately, all attempts failed.

Fig. 4-48: *Microscopic images of the photo diode structure; the photo active area is marked with white circles*

117

As already been done with the Pioneer BDR 101 OPU setup, the original photodiode configuration was removed and replaced by an on-chip amplified photodiode (Fig. 4-49).
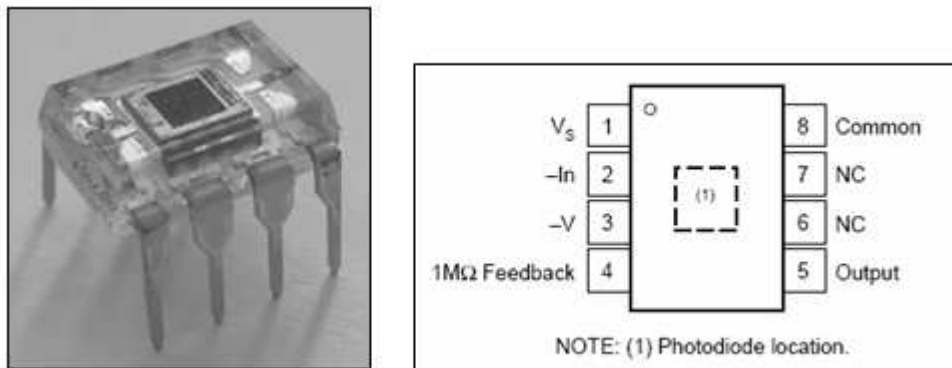
Fig. 4-49: *Burr Brown OPT 101 photodiode and its pin out*

Figure 4-50 shows the OPT 101 mounted into the PS3 OPU in the same position where the original photo diode detector had been located:

Fig. 4-50: *OPT 101 mounted in optical pickup unit (red circle)*

The signal conditioning is done analogous to the Pioneer BDR 101 system setup.

4.3.2.3. The triple wavelength Laser Diode

A "typical" laser diode is shown in Figure 4-51: The three pins are connected to the laser diode (LD) and the monitor diode (PD), which is located near the emitting area, to monitor the output of the LD.

Figure removed due to copyright restrictions

Fig. 4-51: *(Left, top): Laser diode in 5.6 mm metal housing (Conrad 2008) (Left, bottom): Widely-used pin-out of a laser diode ("common cathode"); (right): Opened laser diode with „animated" beam (WDR 2007)*

A laser diode (LD) is made out of a Double-Hetero (DH)-Structure (Fig. 4-52). This structure has a better charge carrier inclusion and thus a higher efficiency in comparison to the simple pn - structure.

When driven in forward-biasing mode, majority carriers are injected into the correspondingly doped fields. Already at small current densities, electrons and holes pile up in the field of the intrinsic layer. The recombination of the carrier pairs in this intrinsic layer leads to the radiation emission.
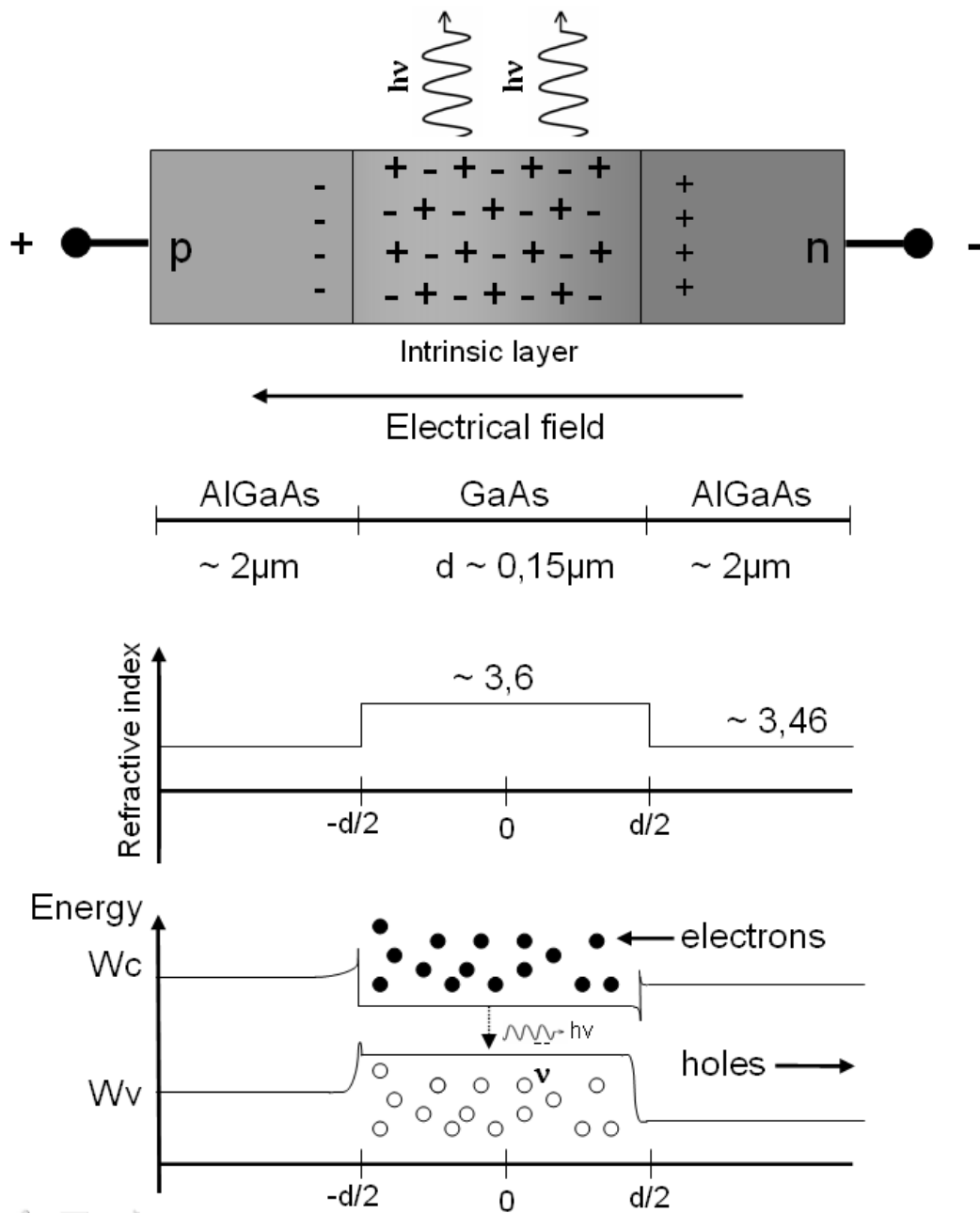
Fig. 4-52: *Scheme of a Double-Hetero (DH) structure*

Hereby the energy gap W_g between the valence band and the conduction band determines the frequency ν and/or wavelength λ of the main emission.

$$h\nu = \frac{h \cdot c}{\lambda} = W_g \quad respectively \quad \lambda \approx \frac{1.24 \; \mu m \cdot eV}{W_g} \tag{4.3.2.3.1}$$

Where "h" is Planck's constant

At small current densities, the valence and conduction bands are only filled a little more than in thermal balance. This imbalance through the added charge carriers is reduced by continuous recombination and radiation emission.

The spontaneous recombination is the dominating factor with all electrons involved and results in a wide spectral smearing of the emitted radiation. This process occurring at a light-emitting diode (LED) leads to a spectral width of several 10s of nm. At higher current densities, the population in the valence and/or conduction bands increases so strongly that the corresponding "quasi-Fermi-levels" are placed into the corresponding bands.

When the difference of the "quasi-Fermi-levels" in the active zone is bigger than the energy gap, a population inversion is reached. In this case, the first laser condition is fulfilled, in which the stimulated emission increases more than the spontaneous one so that amplification occurs. The second condition for the laser emission is the feedback of the radiation by the laser resonator. In the case of the DH-structure, this is formed by the intrinsic layer.

Due to the fact that the refractive index of this layer is higher than that of the surrounding material, the radiation is led in this layer by total internal reflection. The lateral dimensions of the layer lie in general in the range of one µm, so that a transversal, single-mode emission exists.

For simple Fabry-Perot-lasers, the fissured input/output surfaces of the diode laser crystal represent the mirrors of the laser waveguide and thus mark the resonator length. The reflectivity of the mirrors is given by the Fresnel equation:

$$R = \left(\frac{n_{HL} - n_{Air}}{n_{HL} + n_{Air}} \right)^2 \quad \Rightarrow \quad R \approx 0.31 \quad for \; n_{HL} = 3.5 \tag{4.3.2.3.2}$$

In case of a population inversion, energy in dimensions of the energy gap, which is induced through the high charge-carrier injection radiation, reaches into the resonator; this induces a charge carrier recombination, which results in an amplification of the radiation. If the amplification is higher in the active medium than the losses by absorption and transmission at the mirrors, it results in self-excitation of the laser resonator. At the input/output surfaces of the laser resonator, radiation escapes continuously.

The laser modes are determined by the spectral amplification of the material and the measurements of the resonator. The distance $\delta\lambda$ between two neighbouring resonator modes is stated (Brueckner (2007) :

$$\delta v = \frac{c}{2 \cdot n_{HL} \cdot L_{Re\,s}} \quad respectively \quad \delta\lambda = \frac{\lambda^2}{2 \cdot n_{HL} \cdot L_{Re\,s}} \qquad (4.3.2.3.3)$$

Where λ is the wavelength of the major emission and L_{Res} the length of the resonator.

For a laser with λ=670 nm, $L_{Res} \approx 0.3$ μm and n_{HL} = 3.5, a mode distance of $\delta\lambda \approx 0.21$ nm respectively $\delta v \approx 143$ GHz is reached. The width of the single lines becomes affected by many factors (see below). For laser diodes, a single line is in general less than 0.1 nm wide.

Figure 4-53 shows the output power vs. pump current and the different states of operation of a laser diode (a. – c) (Brueckner 2007).

Fig. 4-53: *Output power of a laser diode vs. pump current (Brueckner 2007)*

c.): With small pump currents, the spontaneous emission is dominant compared to the stimulated emission. The emitted photons are basically uncorrelated, they do not have any firm phase and frequency relationships to each other and they move in all possible directions. The emission spectrum is relatively wide with a Gaussian-shaped spectral distribution that corresponds to a light-emitting diode.

a.), b.): The output power P_e of the laser diode increases only slowly with the current. Above a lasing threshold current I_{th}, the amplification through the laser material is high enough so that laser emission occurs. P_e strongly increases and is linear with the current. The radiation is marked due to the fact that the stimulated emission predominates over the spontaneous emission and so the coherence of the radiation becomes very high. The photons are virtually all correlated, i.e. they have the same phase, wavelength and direction.

In the mid 1990s, Shuji Nakamura at Nichia Chemical Industries in Anan (Tokushima-ken, Japan) made a series of inventions and developed commercially - viable blue and violet semiconductor lasers based on gallium nitride (3.4 eV band gap) (Nakamura et al. 2000). This opened the door to new inventions e.g. optical discs with much greater memory densities, as the PS3 represents.

The PS3´s laser diode housing contains three laser diodes emitting at 780, 650, and 405 nm (for CD, DVD, and Blu-ray, respectively). These are connected in a CCC (Common Cathode Can) configuration. The case is the cathode of all three laser diodes as well as the monitor photodiode. The pin-out (Fig. 4-54) for the PS3 diode is shown below (Wright and Goldwasser 2008).

Figure removed due to copyright restrictions

Fig. 4-54: *Pin-out of the triple wavelength laser diode(3λ) used within the PS3 OPU*

Description of the Pin-out:

Data removed

Since the different laser diode emitters are located in one housing, the spatial arrangement of the single emitters within the housing was a big challenge for the manufacturers. Sony© decided to use a stacked alignment to ensure the linear beam output of all three emitters.

The patent for the stacked laser diode assembly can be seen at U.S. Patent #6956322: "Semiconductor light emitting device with stacked light emitting elements".

Figure 4-55 shows a close-up of the stacked emitters within the metal housing of the laser diode.

Figure removed due to copyright restrictions

Fig. 4-55: *Close-up of the front of the diode. You can see the multiple connections to the device (Rehwinkel 2008)*

A more detailed image (Fig. 4-56) of the stacked assembly was published by the Blu-Ray Disc Founders (2004) showing the single emitters and the beam output.

Figure removed due to copyright restrictions

Fig. 4-56: *(left) Stacked emitters in a triple wavelength laser diode; (right) beam output of the stacked diode structure (Blu-Ray Disc Founders 2004)*

4.3.2.3.1. Measurement of the optical characteristics of the PS3 3λ laser diode

The optical output power of the laser radiation has been measured with a Coherent Labmaster Ultima 33-0613 and a 13L16 "VIS" sensor.

The results are exemplary due to the high spread of standard factory models. Threshold currents vary.

Figure 4-57 shows the data gained for the Blue emitter:

Figure removed due to copyright restrictions

Fig. 4-57: *Plotted data of the optical output of the blue (405 nm) emitter*

Figure 4-58 shows the data gained for the Red emitter:

Figure removed due to copyright restrictions

Fig. 4-58: *Plotted data of the optical output of the red (650 nm) emitter*

4.4. Specification of BDR laser beam

Knowledge of the laser beam profile and the intensity distribution within the beam is essential for the design of the system for the structuring and characterisation of technical surfaces. Since the photo resist-covered substrate shall only be exposed in very small spots.

This chapter will explain how the laser beam diverging from the PS3 OPU has been characterised.

4.4.1. Methods of beam profiling/characterisation

Especially in the field of laser direct writing lithography it is necessary to gain exact knowledge about the shape and characteristics of the used laser beam, since a homogeneous power distribution is an essential parameter for qualitatively good and reproducible results in surface structuring.

Several "classical" methods for the characterisation of laser beams are already applied, such as (Magnes et al. (2008) :

- The knife edge method,
- The slit method,
- The pinhole method and
- The CCD camera method.

In fact, a laser beam ("standard TEM00", where TEM stands for: Transverse Electromagnetic Mode,) fades gradually due to its Gaussian profile (Fig. 4-59).
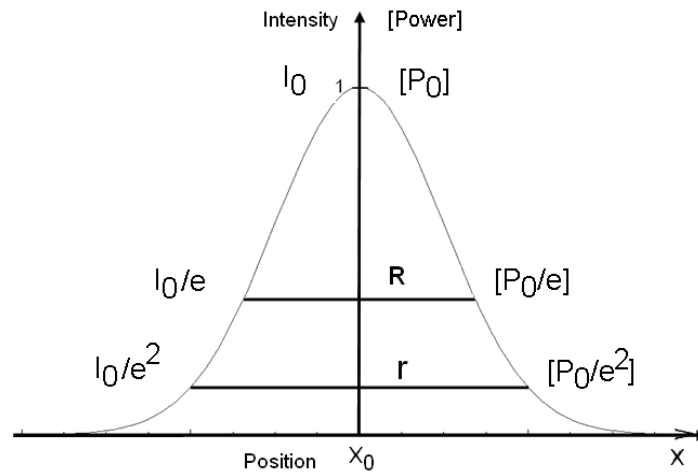
Fig. 4-59: *The theoretical power distribution within a TEM 00 laser beam can be described by a Gaussian profile*

Therefore it is necessary to determine what is known as the centre of the beam. Chapple (1994) describes the intensity profile I(x, y) as follows:

$$I(x, y) = I_0 \exp\left[-\frac{2((x-x_0)^2 + (y-y_0)^2)}{r^2}\right]$$

(4.4.1.1)

where x and y are the transverse Cartesian coordinates of any point, x_0 and y_0 mark the centre of the beam and r is the $1/e^2$ radius. This definition is often used in theory. McCally (1984) defines the Gaussian-shaped distribution of the intensity I(x, y) by means of the beam radius R belonging to the 1/e irradiance shown in Figure 131. The emitted power of the laser source can be determined by integrating the irradiance (I), namely the optical intensity I(x, y), over the affected cross sectional area A:

$$P = \int I dA$$

(4.4.1.2)

4.4.1.1. Knife edge method

To gain information about the power distribution across a cross-sectional plane of a laser beam, the use of the knife edge method is the simplest approach. Thereby, a sharp edged plate, e.g. a razor blade, is initially covering the whole laser beam in front of a power meter for continuous wave radiation or an energy meter for pulse operation. By precise line wise displacement of the knife edge mounted on a linear movement stage, more and more laser radiation reaches the sensor unit, until the whole beam is covering the sensing area. Figure 4-60 shows the result of this measurement procedure:
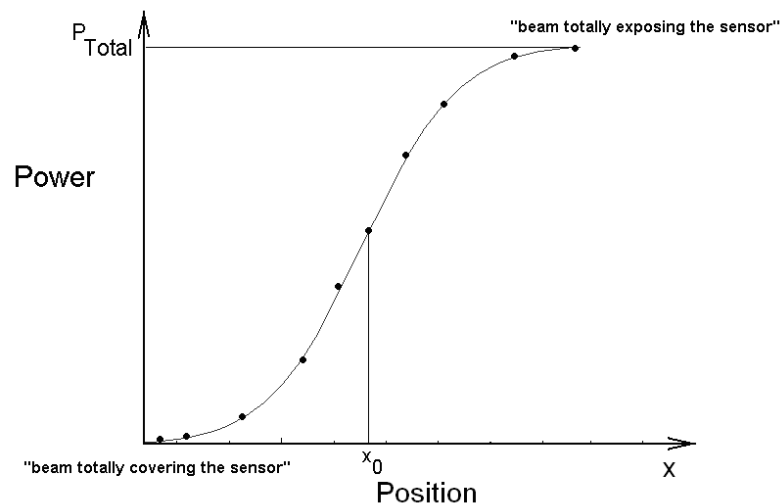
Fig. 4-60: *Integrated laser power measured using the knife edge method as a function of the cross sectional coordinate x.*

Due to the movement of the knife edge, the value of the detected power increases steadily. The derivative of this power function $P(x, y)$ yields the two-dimensional Gaussian profile of the power distribution across the laser beam (Fig. 4-55).

4.4.1.2. Slit method

A second possibility to determine the power distribution within a laser beam is similar to the knife edge method: Instead of a sharp-edged plate, a very narrow slit

is stepwise moved across the laser beam. As a precondition for valid measurements the opening of the slit has to be smaller than the diameter of the considered beam is. Typically, this opening is in the range of some microns.

Drawbacks of "traditional methods"

The knife edge - as well as the slit method - offers only a limited quantity of beam characteristics: local "hot-spots", i.e. areas of superior power, are undetectable due to the integrating measurement principle. Nevertheless, this method is suitable for quick measurements to determine the diameter and the course intensity profile of the considered laser beam.

4.4.1.3. Pinhole method

This method measures the intensity of irradiance through a very small hole in a plate (pinhole) facing the laser beam. The intensity of light passing through this pinhole is rather low, so that a photomultiplier tube (PMT) has to be used to detect the irradiance.

Due to the characteristics of a PMT, e.g. its relatively low signal-to-noise ratio (SNR), the collected data are corrugated. However the intensity distribution can be achieved within a local resolution of approximately 3 microns by applying a Gaussian fit. Therefore, by transversal scanning across a laser beam, a high-resolution image of the power distribution within the beam can be gained. Hot spots are detectable and more detailed features can be located.

4.4.1.4. CCD Camera method

Differing from the scanning methods described above, the usage of CCD (Charge-coupled Device) cameras for the inspection of laser spots will give a very quick impression of the power distribution within the beam in just a "single shot".

The quality of the image, e.g. the resolution, is directly depends on the size and number of pixels on the CCD-Sensor-chip. Typically, the pixel size is in the range of

6 microns^2, linked to a total number of pixels in the range of 1 to 2 megapixels. When using this method it must be noted that dust and other impurities on the CCD chip can result in image distortion and/or the misinterpretation of beam features. Moreover, care must be taken not to destroy the CCD chip with the incident laser beam. Figure 61 shows the result of such a scan across the focal spot of the PS3 OPU:
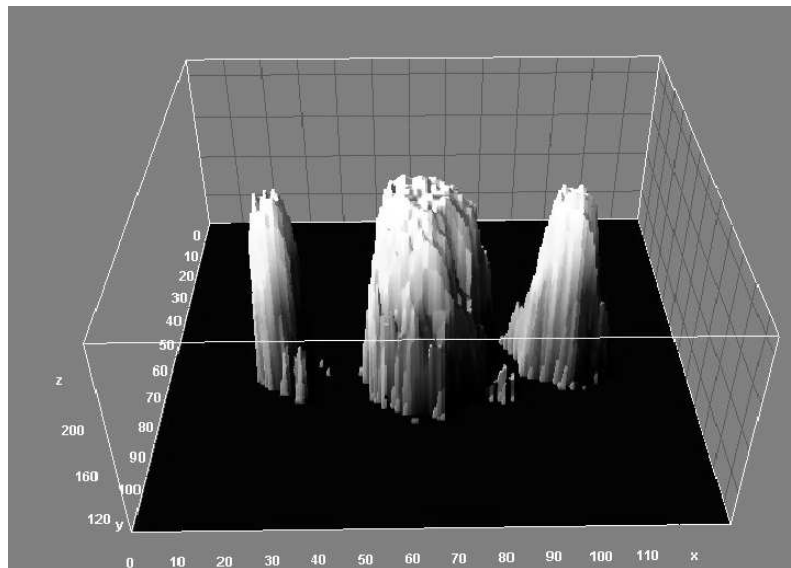
Fig. 4-61: Beam profile of the PS3 OPU (note the 2 "sub beams" next to the major beam in the middle)

Please not that the units are arbitrary due of the magnification of the focal spot. The smaller sub-beams next to the major beam in the middle are caused by the optical grating (Chapter 4.3.2.2.2) and do not emerge in the lithographic system for structuring and characterisation due to its dismounting otherwise these "sub-beams" would disturb the image. Furthermore note that the profile is "cut-off" due to sensor overload.

4.4.2. Beam characterisation by means of optical fibre tips

To overcome the limited resolution of the CCD and pinhole methods, respectively, a new intensity profile measurement technique has been developed.

Similar to the pinhole method described above, an optical fibre tip with an aperture of a few 100 nm is applied to collect light by scanning across a laser beam transversally. A photomultiplier tube (PMT) attached at the out-coupling end of the fibre detects the collected light during the scanning process so that a 2-dimensional image of the intensity distribution can be evaluated.

By changing the lateral position of the fibre tip, multiple cross-sectional planes can be scanned, leading to a 3-dimensional image of the intensity distribution e.g. within a focused laser beam. Former work of Herzog et al. 1997 and Lila et al. 1998 demonstrate the use SNOM fibre tips for the measurement of the beam properties of laser diodes close (some micron) to the out coupling facets of the laser active layer. The presented profiling technique however delineates from this methodology by using fibre tips in the far field of the focal area of a focussed laser beam.

4.4.2.1. Near-field coupling into the optical fibre

"Classical" approaches to depict the incoupling of light into the fibre tip fail, due to the very small opening of the fibre tip (aperture), in the range of some hundred nanometres, which is considerably smaller than the wavelength of the laser light being used.

To gain information originating from the near field (please refer to Chapter 3) and to transport this information into the far field, it is necessary to transform the evanescent fields into propagating fields. This could be done by putting a centre of scattering, in this case the very narrow tip, into the near field (Fig. 4-62). An electromagnetic model based on a finite element method (FEM) was generated with the aid of the simulation software CST MICROWAVE STUDIO® (CST, 2009) to show the field distribution along the thin fibre tip.
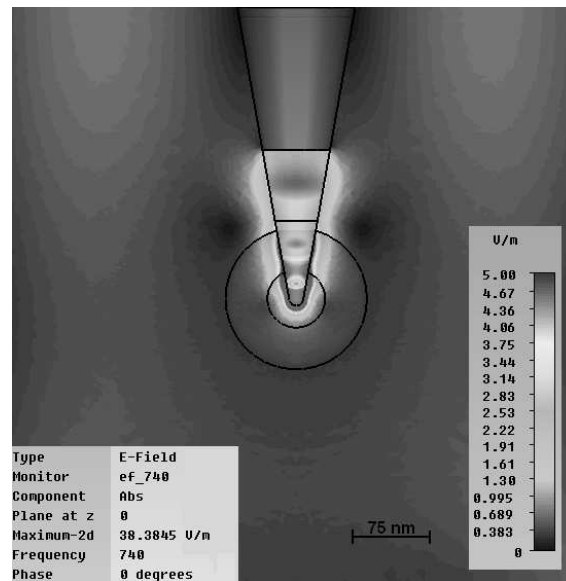
Fig. 4-62: *E-field in the near-field of the tip when illuminated by plane wave with field strength of 1 V/m, polarised along the axis of the tip*

Thereby Dipole-oscillations are generated at the boundary of this tip by means of the evanescent field (Fig. 4-63).

Fig. 4-63: *Cross-sectional view of an optical fibre tip with a cone angle"ϑ" and a radius from the aperture rim "r" .The associated electric field lines are plotted in logarithmic manner (Drezet et al. 2004)*

It has to be noted that the field within the tip is exponentially decreasing (refer to Appendix 5 for a detailed mathematical description of the field calculation) and,

133

because of this, only a very small part of the generated electrical field, in this example $5*10^{10}$ V/m directly at the tip, can be detected at the out-coupling end of the fibre by the PMT.

4.4.2.2. Setup

Figure 4-64 shows the schematic setup of the beam profiling test rig:
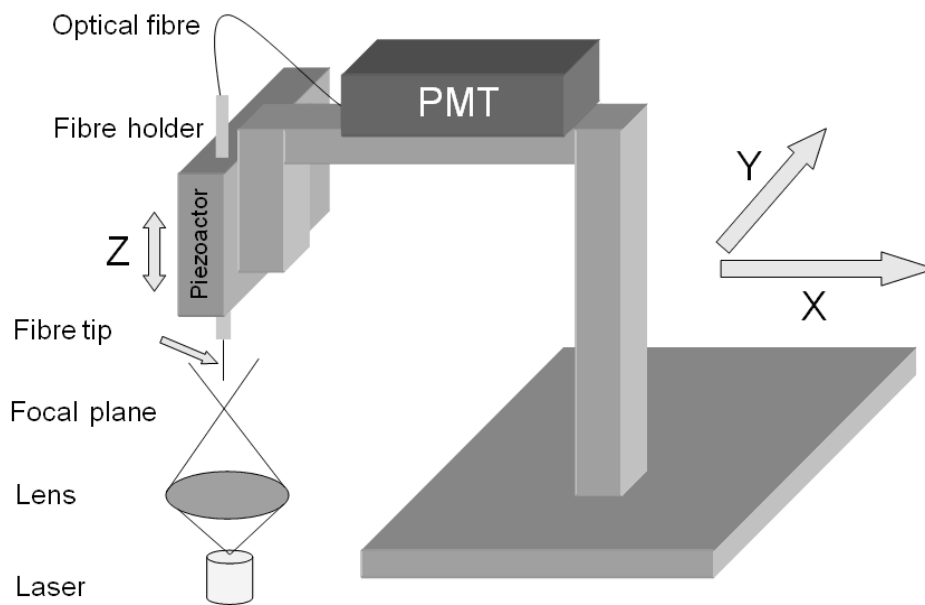
Fig. 4-64: *Schematic view of the beam profiling setup using SNOM fibre tip*

The PI P-854.00 piezoelectric actuator used in this setup has a displacement range of 25 μm for fine positioning and can also be roughly pre-positioned by a micrometer-screw. The detection of collected light is done by a Hamamatsu H5784 type photomultiplier tube (PMT) with an E5776 FC-type adaptor attached (Fig. 4-65).
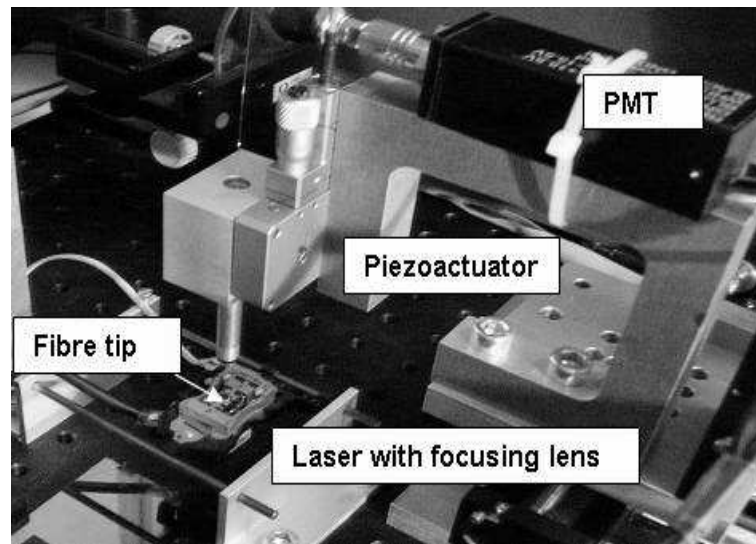
Fig. 4-65: *Detailed image of the beam profiling setup using SNOM fibre tip*

A fibre holder mounted on the piezoelectric actuator is used to lead and protect the optical fibre tip during the scanning process. A close-up view of the fibre tip in working position above the lens of an OPU is shown in Figure 4-66:
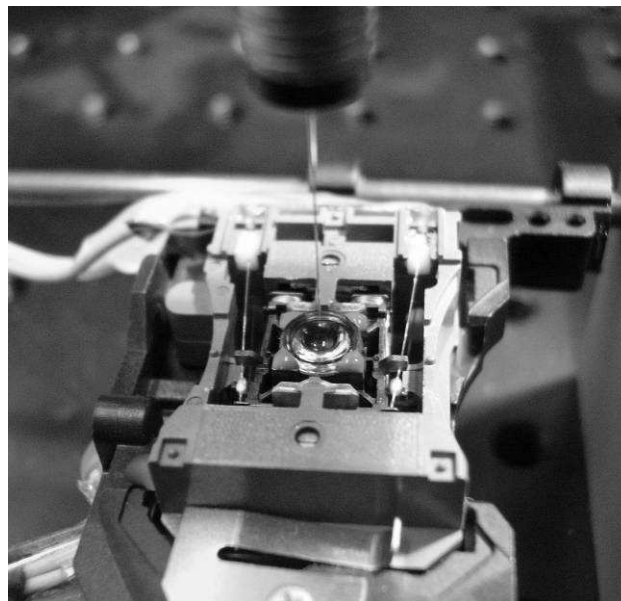
Fig. 4-66: *Fibre tip in working position above lens of a OPU*

After amplification (x10 by a transimpedance amplifier stage) and filtering of the collected intensity data, it is converted into digital data by means of a National Instruments 6025e PCI interface card.

4.4.2.3. Results gained by the beam profiling setup

By further development of the software that is used to control the translation stages of the SNOL system with a fibre tip (please refer to Chapter 3) it is possible to scan tomographically across the laser beam while collecting data (Fig. 4-67). This data can be displayed either in the scanning software itself or in newly-developed software that is based on OpenGl$^{©}$.
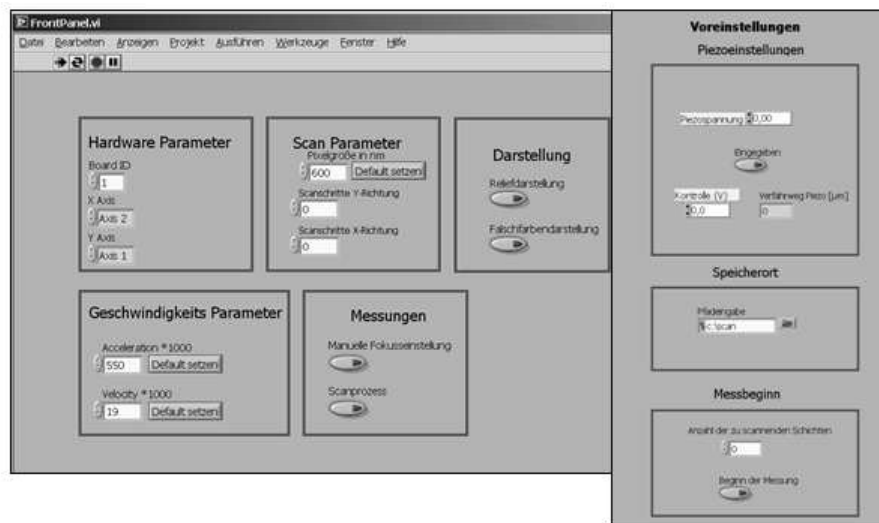
Fig. 4-67: *Screenshot of the scanning software´s user interface for the control of the beam profiling setup using SNOM fibre tip*

This newly-developed software allows the display of the data as a 3 dimensional image with the possibility to rotate the image in all degrees of freedom by using a mouse. Furthermore, different mathematical filters can be applied in order to improve the image quality.

Figs. 4-68 and 4-69 show images of profiles obtained by the beam profiling setup using a 405 nm Blu-ray OPU as the emitting laser source in different resolutions:

Fig. 4-68: *Image of a beam profile (resolution: 1000 nm (left); right: 5000 nm (right)) gained by the beam profiling setup using SNOM fibre tip*

Fig. 4-69: *Image of a beam profile gained by the beam profiling setup using SNOM fibre tip (resolution:525 nm)*

Figure 4-70 shows the same emitting source highly resolved; the Gaussian beam shape is visible:

Fig. 4-70: *Image of a beam profile obtained with the beam profiling setup using SNOM fibre tip (resolution: 150 nm)*

By scanning more slices, the single slices can be shown in an "overlaid" way, to watch the focus "moving" by the lateral change of the fibre tip (Fig. 4-71):

Fig. 4-71: *12-step scan through a laser focus (left); Same data in overlaid form (right)*

The results obtained verify the theoretical approaches regarding focal size (~500 nm) and shape (nearly Gaussian).

Summary

Confocal scanning, a technique for the structuring and characterisation of technical surfaces, has been described and different test rigs for laboratory evaluation shown. A reverse engineering procedure has been carried out to characterise the main component of the developed confocal system: an optical pickup unit (OPU) from a gaming console. The realisation of the confocal system has been described and, finally, a novel method for beam profiling has been introduced.

The next chapter will show a possible enhancement of the system's optical properties, increasing the resolution of the surface structuring and characterisation.

5. (Possible) Enhancement of the confocal setup for structuring and characterisation

To enhance the optical behaviour of the PS3 OPU to reach higher resolution (beneath the theoretical limit of 400-500 nm), it was decided to develop an adaptive enhancement to the focussing lens. This enhancement consists of a special lens (a solid immersion lens SIL) which is placed in front of the "original" focussing lens. By this, an increase in resolution can be expected. After a description of the theoretical background of the enhancement, a test rig to realize the enhancement will be described.

During the work, it has been found that the lens which was selected to be used was not adequate for this task. Furthermore, it has been found that a considerable research effort has been made within this field of technology by Philips Electronics N.V., with two PhD theses relating to the solid immersion lens-based technique being published (Zijp 2007; Eerenbeemd 2008). This technique appears to be the likely replacement for the recently-established Blu ray standard at some point in the future.

For this reason it was chosen to terminate the construction of the SIL system and push the design of a microcontroller-based system (Chapter 6) capable of using the "new" commercial SIL systems in the future. Moreover, it has been found that the resolution gained by the Blu ray system is adequate for the desired tasks and the need for an adaptive focal control and the ability to have a "Windows independent" system is more important.

5.1. General information

The diffraction-restricted resolution of optical instruments, here the lithography setup, was calculated by Abbe and Rayleigh using the wave character of light. This equation (Abbe 1873):

$$\Delta x = \frac{0,61 * \lambda}{NA} = \frac{1,22 * \lambda}{2 * n * \sin \Theta}$$

(5.1.1)

Testifies that the minimum distance Δx between two objects, at which both appear partially separated, is proportional to the wavelength λ and inversely proportional to the numeric aperture NA (formed by the refractive index n and the collection angle Θ) Consequently there are 2 parameters which can be varied to increase the resolution of the structures "written" into the photo resist surface:

- The wavelength of the focussed laser beam (λ),
- The focal diameter of the focussed laser beam achieved by increasing the numerical aperture (NA).

Decreasing the wavelength of the used laser source (here 405 nm) is not suitable for this application in order to maintain the small size of the apparatus, although there are other fields of lithography usage, e.g. the semiconductor industry, where shorter wavelengths have became common. Krypton-fluoride (KrF) Laser sources for example, working at a wavelength of 193 nm, or below, are state-of-the-art in this area (Stamm 2004), but require a lot of space and are more cost-intensive compared to 405 nm laser diodes.

Increasing the numerical aperture (NA) of the focussing system is the second way to achieve a better resolution.

According to the rules of the linear optics, no numeric aperture can be larger than 1 in air and so the minimum Δx is limited to 1.22*λ.

However this limitation can be bypassed by means of immersion. Immersion could be realized by:

- Liquid immersion. This involves putting water or oil into the gap between the focussing lens and the photo resist surface in order to raise the numerical aperture. This technique is widely used within the semiconductor industry (Ito and Okazaki, 2009) but is not adequate for the system used within this thesis due to the complex infrastructure of preventing the immersion liquid from becoming contaminated with air-borne particles.

Or

- Solid immersion. A lens with very high refractive index that is located very close to the surface of the medium (approx. ¼*λ, the so called "near-field") can achieve an NA bigger than 1.0. Such a lens is called Solid Immersion Lens (SIL).

5.2. Solid Immersion Lens (SIL)

Solid Immersion Lenses (SIL) typically consist of a hemisphere made out of glass with a high refractive index (Fig. 5-1).

Fig. 5-1: *Example of hemispherical SIL made of BK7- glass (diameter 2mm; height 1mm)*

The SIL (Fig. 5-1) is placed in front of a focusing lens so that the flat surface of the SIL and the focal plane of the focusing lens coincide (Fig. 5-2). Through this, the optical resolution (here, the smallest structure size) can be increased by the factor 1/n, where n is the index of refraction.
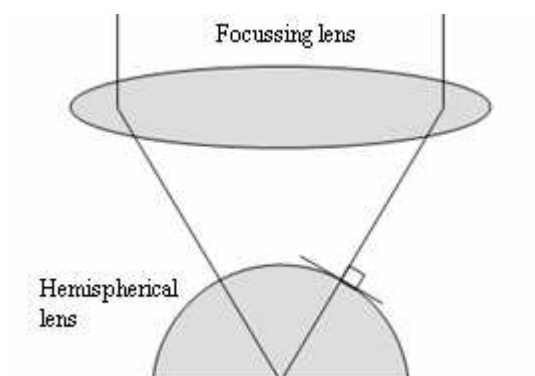
Fig. 5-2: *Solid immersion lens system with hemispherical lens*

A more complex design to form an SI-lens is called "super-hemispheric", and looks like an extended hemisphere (Figs. 5-3 and 5-4).
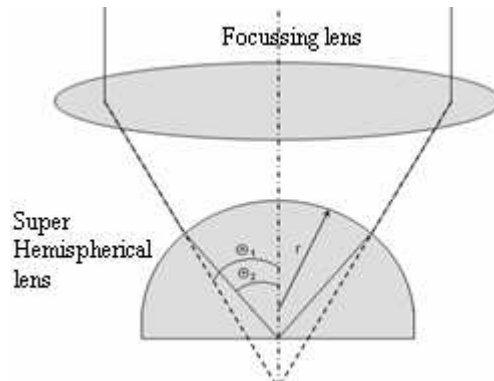
Fig. 5-3: *Solid immersion lens system with super-hemispherical lens*

Figure 5-4 shows an example of a super-hemispherical SIL made of diamond:

Figure removed due to copyright restrictions

Fig. 5-4: *Example of a super-hemispherical SIL made of diamond (engineering sample by Element Six Ltd. 2008)*

Optical systems using focussing lenses with high numerical apertures (NA), having short working distances, need small hemispherical SI-lenses to ensure that the focal plane "hits" the flat surface of the SIL. Therefore the positioning and manufacture of this SIL is more sophisticated. Using the "super-hemispherical" design can avoid this disadvantage and allows higher NA.

5.2.1. Optical path inside SIL

To understand what happens inside the SIL, it is appropriate to use a simplified model of a ray penetrating an interface between two media with different refractive indices (n_1, n2) (Fig. 5-5):
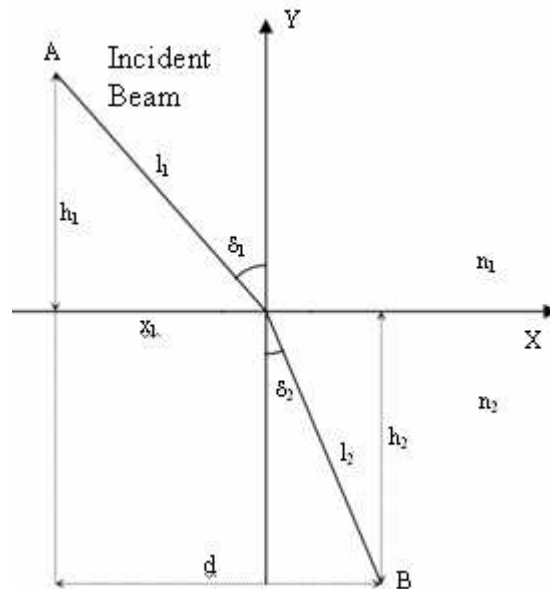
Fig. 5-5: *Beam refracted at boundary n_1-n_2*

The Fermat principle states that the optical path between two points has to be the most direct or the shortest way (Scheck 2009).

Observing the optical path (OP) from point A to B, it can be said:

$$OP\ (A{\rightarrow}B) = n_1{\cdot}l_1 + n_2{\cdot}l_2 \tag{5.2.1.1}$$

Using Pythagoras´ Theorem:

$$n_1 \cdot l_1 + n_2 \cdot l_2 = n_1\sqrt{h_1^2 + x_1^2} + n_2\sqrt{h_2^2 + (d - x_1)^2} \tag{5.2.1.2}$$

The direct path between the two points is marked by setting the derivation with respect to x_1 at zero:

$$\frac{dOP}{dx_1} = n_1 \frac{x_1}{\sqrt{h_1^2 + x_1^2}} - n_2 \frac{d - x_1}{\sqrt{h_2^2 + (d - x_1)^2}} \qquad (5.2.1.3)$$

$$= n_1 \cdot \frac{x_1}{l_1} - n_2 \cdot \frac{d - x_1}{l_2} = n_1 \cdot \sin(\delta_1) - n_2 \cdot \sin(\delta_2) = 0 \qquad (5.2.1.4)$$

This equation is called Snell´s Law. It states, that a wave (here a ray of laser light) is changing its direction, it is refracted, by propagating from one transparent medium into another transparent medium with a different refractive index. The ray is refracted towards the normal if it is travelling from a lower to a higher refractive index (lower optical density) and *vice versa* (Fig. 5-6). In simple words "Light takes the fastest way to get from point A to point B" (Hecht 2001).
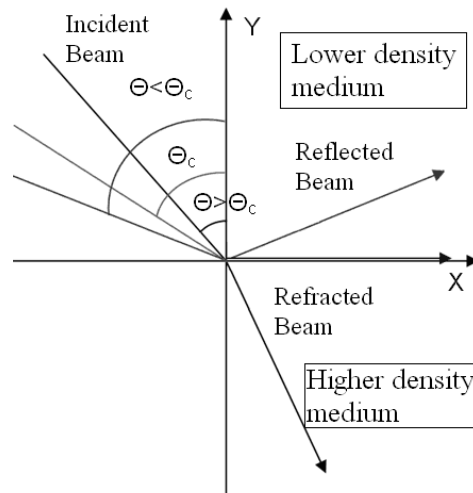
Fig. 5-6: *Beam path under different angles of incidence*

5.2.1.1. Total internal reflection

Snell´s Law only gives the direction of the refracted beam and it is only valid until the angle of incidence becomes critical. A SIL make use of this critical angle Θ_T to get a so-called "Total Internal Reflection" TIR. This angle can be calculated by applying the Fresnel equations (please refer to Appendix 3; →A3.3.10):

$$\Theta_T = \arcsin (n_t/n_e) \hspace{4cm} 5.2.1.1.1$$

This critical angle is equivalent to the angle within Snell´s Law at which $\sin\Theta_t$ becomes 1: The refracted light propagates parallel to the boundary. Returning to the SIL application, all light that is focused at angles larger than the critical angle Θ_T into the SIL is reflected back into the SIL by TIR (Fig. 5-7).
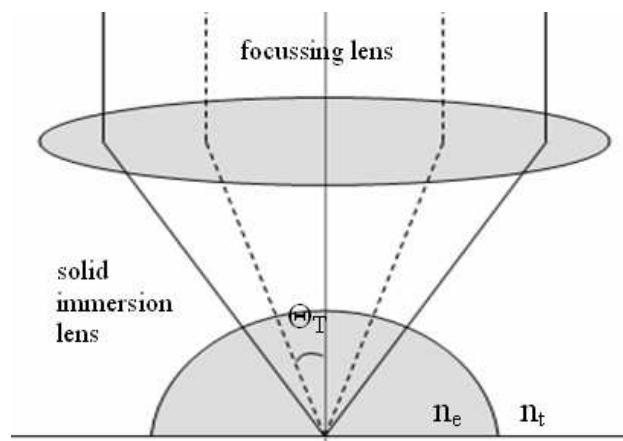
Fig. 5-7: *Beam path within a solid immersion lens using the refractive index of the SIL n_e and the refractive index of the surrounding media n_t as well as the critical angle Θ_T*

Θ_T is given by the refractive index of the SIL $n_e=1.77$ (Al_2O_3) and the refractive index of the media beneath/below the SIL, here air with $n_t=1$: $\Theta_T \sim 34{,}4°$. A practical example of TIR is given by figure 5-8 (University of Vienna 2010): Light transmitted under different angles through the interface can be observed and one light ray which is totally reflected occurs:

147

Fig. 5-8: *Light propagation under different angles of incidence*

Optical fibres represent another example of the use of TIR:

To transport light from one point to another, optical fibres make use of the TIR at the interface between their core and their cladding (Fig. 5-9):
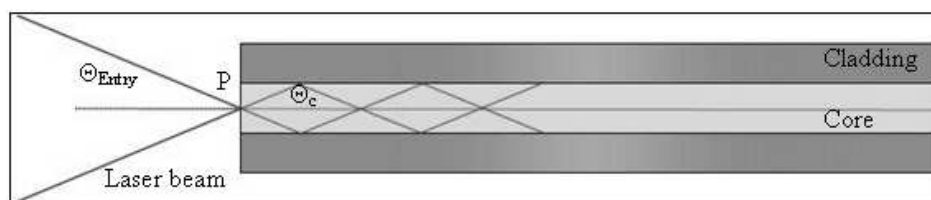
Fig. 5-9: *Schematic of light guidance inside an optical fibre*

The numerical aperture (NA) is the main parameter that specifies the optical fibre: It is a measure of the maximum angle of acceptance for which light will be guided along the fibre when the fibre is illuminated at its end.
It is given by Iizuka (2008):

$$NA = n \sin \Theta_c = \sqrt{n_1^2 - n_2^2}$$

(5.2.1.1.2)

Step index fibres consist of a core made of glass with a higher refractive index (n_1) surrounded by a cladding made of glass with a lower refractive index (n_2). Referring to Figure 5-9, the incident light ray will be guided through the core if it undergoes total internal reflection on the core-cladding boundary. In order to determine the numerical aperture, the incident angle Θ_{Entry} to the fibre end surface is calculated, so that the angle on the core-cladding boundary is the critical angle for reflection. When Θc is the critical angle:

(5.2.1.1.3)

$$n_1 \sin \Theta_c = n_2$$

Where n_1 is the refractive index of the core and n_2 the refractive index of the cladding. According to Snell´s law it can be stated for the point of entry **P**:

$$n \sin \Theta_{Entry} = n_1 \sin(90° - \Theta_c) = n_1 \cos \Theta_c = n_1 \sqrt{1 - \sin^2 \Theta_c} \qquad \text{(5.2.1.1.4)}$$

Where ´n´ is the refractive index of the surrounding media and by combining (5.2.1.1.3) and (4.2.1.1.4), it finally follows that:

(5.2.1.1.5)

$$n \sin \Theta_{Entry} = \sqrt{n_1^2 - n_2^2} = NA$$

5.2.2. Internal reflection and evanescent waves

The following pages will show the mathematical description of the electromagnetic waves at the back side of the SIL on which obviously no light appears. Considering the setup shown in Figure 5-10, the transmitted wave is given by Gross (2008):

$$\mathbf{E_t} \quad = \quad \mathbf{E_{t0}} \; e^{i(\mathbf{k_t}\cdot\mathbf{r} - \omega t)} \tag{5.2.2.1}$$

$\mathbf{k_t}\cdot\mathbf{r}$ can be described by the angle of refraction Θ_t as shown in Figure 5-10:

$$\mathbf{k_t}\cdot\mathbf{r} \quad = \quad k_{t\parallel}x + k_{t\perp}y = k_t \sin\theta_t x - k_t \cos\theta_t y = k_t x \sin\theta_t - i k_t y \sqrt{\frac{\sin^2\theta_e}{n^2} - 1} \tag{5.2.2.2}$$

Figure removed due to copyright restrictions

Fig. 5-10: *Propagation vectors concerning internal reflection at a boundary n_t/n_e (Gross 2008)*

The law of refraction $\sin\Theta_e / \sin\Theta_t = n$ was used to describe $\cos\Theta_t$ as follows:

$$\cos\theta_t \quad = \quad \sqrt{1 - \frac{\sin^2\theta_e}{n^2}} = i\sqrt{\frac{\sin^2\theta_e}{n^2} - 1} \tag{5.2.2.3}$$

As a matter of fact, the mathematical description of the phase holds a real value, hence an exponentially decreasing electromagnetic wave must exist on the back side of the Interface (here: SIL).

These electromagnetic waves are called evanescent waves. Based on the law of refraction, $\Theta_e > \Theta_t$ is $\sin^2\Theta_e/n^2 > 1$. Therefore, while within the range of total reflection (TIR), $k_{t\perp}$ only has an imaginary value:

$$k_{t\perp} \quad = \quad \pm ik_t \sqrt{\frac{\sin^2\theta_e}{n^2} - 1} = \pm i\beta \qquad (5.2.2.4)$$

The electrical field is defined by:

$$\mathbf{E_t}(x,y,t) \quad = \quad \mathbf{E_{t0}}\exp(-\beta y)\,\exp\!\left[i(k_{t\parallel}x - \omega t)\right] \qquad (5.2.2.5)$$

The electrical field is decreasing exponentially within a characteristic decay length:

$$\ell \quad = \quad \frac{1}{\beta} = \frac{1}{k_t\sqrt{\frac{\sin^2\theta_e}{n^2} - 1}} = \frac{\lambda_t}{2\pi}\left(\frac{\sin^2\theta_e}{n^2} - 1\right)^{-1/2} \qquad (5.2.2.6)$$

An oscillating motion, an evanescent wave, occurs parallel to the boundary layer (here in the x-direction). Its decay length is proportional to the wavelength within the optical thinner media; for n_e=1.5, n_t=1, Θ_T=41.8 and Θ_e=45 we get an decay length of l=λ/2. The evanescent wave rapidly decays with the shortening of the wavelength (Gross 2008).

5.2.3. Optical tunneling / Frustrated Total Internal Reflection (FTIR)

Evanescent waves can be experimentally detected by putting a rarer medium (air) between optically denser media (two prisms), a transmitted beam can be observed within the third medium (Fig. 5-11).
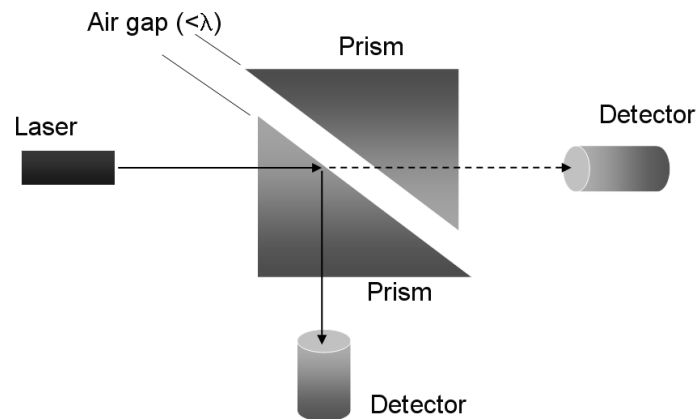
Fig. 5-11: *Experimental setup for evidence of FTIR using two prisms*

By putting a second prism towards the glass-air interface (red) of the first prism, a portion of light can "tunnel" from the "forbidden" area into the second prism (Fig. 5-12):

Fig. 5-12: *Scheme showing FTIR/optical tunnelling of light from the first prism (bottom) through the "forbidden" area(red) into the second prism (top) (Gross 2008)*

The amplitude of the "tunnelled" wave can be estimated by (5.2.2.5) (Gross 2008):

$$\mathbf{E}_{\text{tun}}(y) \quad \approx \quad \mathbf{E}_{\mathbf{t0}} \exp(-\beta d)) \tag{5.2.3.1}$$

Where **d** determines the width of the air gap between the two prisms. This approximation is only valid for big values of d, because for weaker d, the interface has to be seen as a multilayer system and the mathematical description becomes very complicated. The amplitude of the evanescent wave decays exponentially with increasing distance d, thus, no energy flux will occur in the direction of propagation. Hence, on the other side of the second prism, a wave exists with a certain energy density. This energy flux within the evanescent wave only occurs parallel to the boundary. Concerning the perpendicular wave components inside the intermediate medium (air) which can be extracted from (5.2.2.5):

$$E_z \quad = \quad E_{z0} \exp(-\beta y) \; \exp(i(k_{t\|}x - \omega t)) \tag{5.2.3.2}$$

By using **k × E= ω B**, the field components B_x and B_y can be defined, after this, the Pointing Vector S = 1 / μo (E × B) can be derived:

$$S_x = -\frac{1}{\mu_0} E_z B_y \quad \propto \quad E_z^2 \left(1 + \sqrt{1 - \sin^2 \theta_e} \right) \tag{5.2.3.3}$$

$$S_y = \frac{1}{\mu_0} E_z B_x \quad \propto \quad i E_z^2 \sqrt{1 - \sin^2 \theta_e} \tag{5.2.3.4}$$

The imaginary value of S_y states that no energy is transferred perpendicular to the boundary. A phase shift of $\Pi/2$ appears between E_z and B_x so that the average is zero. In contrast to this, no phase shift appears for E_z and B_y, so that energy can be propagated in the x-direction parallel to the surface (Gross 2008).

Summary

Following Maxwell's equations, an electromagnetic wave cannot change its direction at a boundary immediately. A standing wave will appear on the surface propagating to the following medium. The field strength inside the second medium is decreasing exponentially.

Therefore FTIR or the *optical tunnel effect* is only measurable as long as the width of the gap between the two prisms does not exceed the dimension of the used wavelength.

FTIR also occurs in Solid Immersion Lenses when moving them into a small distance from a surface consisting of a material with the same or higher refractive index. This realizes a diffraction-free resolution e.g. in order to expose a photo resist surface.

5.3. Distance regulation of the Solid Immersion Lens

Due to the exponentially decreasing power of the evanescent waves, a very small gap between the SIL and the photo resist-covered substrates is necessary. Within a distance of some hundred nanometres, the energy of light which is decoupled out of the SIL is sufficient to expose the photo resist. This distance must be kept constant in order to avoid damage to the lens or the substrate while moving the substrate beneath the lens. The use of a plate capacitor build into the lithographic device allows for distance detection and regulation by measuring the capacity between the plates and its change. Figure 5-13 shows the arrangement of the plates and Figure 5-14 gives an impression of the parts of the capacitor realized in the setup.
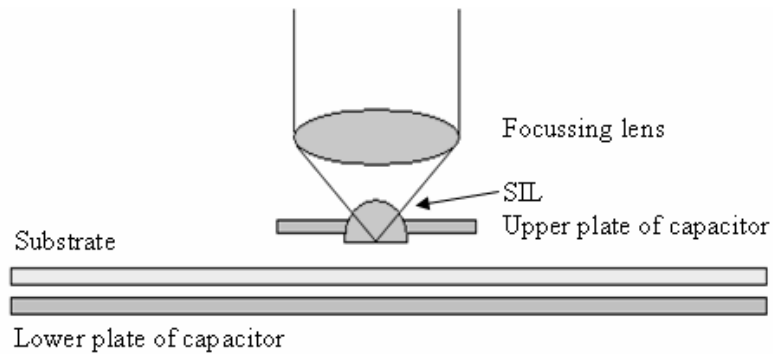
Fig. 5-13: *Scheme showing the capacitor plates and the lens system*
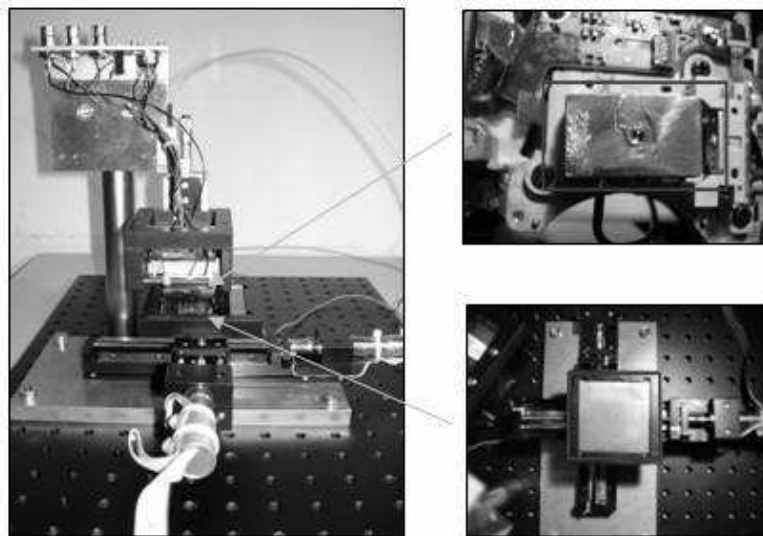
Fig. 5-14: *Figure showing the capacitor plates (red marking) within the setup*

5.3.1. Measurement of weak capacities

Each constellation of two electric conductors facing each other, even two wires lying next to each other, can be seen as a capacitor. The well-known plate capacitor is shown in Figure 5-15:
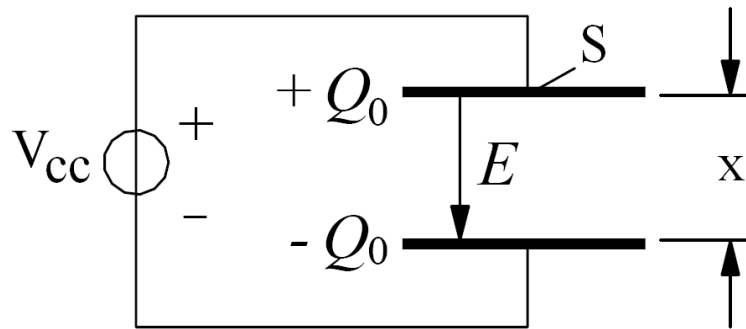
Fig. 5-15: *Scheme of a plate capacitor*

Two electrically conductive plates, with a surface area S facing each other in a distance x are connected to a power source. The operating voltage Vcc causes a charge current: electrons are moved from the one plate to the other by means of the power source.   A charge separation occurs and an electrical field E is generated between the two plates. The strengths of the electrical field E is given by E=V/d, where V is the actual voltage drop at the capacitor.

Certainly, this Voltage V gets to a maximum where V becomes Vcc and the capacitor is charged; one plate holds a charge $+Q_0$ and the other one $-Q_0$. The proportional coefficient C between Vcc and Q_0 is called the capacity (Dorf et al. 2001):

$$C = \frac{Q_0}{U_b}$$

(5.3.1.1)

Putting this in Farads:

$$[C] = F = \frac{A \cdot s}{V} = \frac{C}{V}$$

(5.3.1.2)

(F=Farad; A=Amperes; s=second; v=volts; C=Coulomb)

Within a vacuum, the capacity depends only on the surface area of the plates S and the distance x:

$$C \sim \frac{S}{x}$$

(5.3.1.3)

Using the proportionality constant ε_0, that is given by:

$$\varepsilon_0 = \frac{1}{\mu_0 \cdot c^2} = 8{,}8541 \cdot 10^{-12} \frac{As}{Vm}$$

(5.3.1.4)

With c=speed of light: 299.792.458 m/s and

μ_0= magnetic field constant: 1, 2566 $\cdot 10^{-6}$ H/m

This constant ε_0 is known as the electrical field constant. When putting an electrical insulator between the plates of the capacitor, the capacity is increased by $\varepsilon_r \geq 1$:

$$C = \varepsilon_0 \varepsilon_r \frac{S}{x}$$

(5.3.1.5)

where ε_r is the dielectric constant or relative permittivity and the product $\varepsilon = \varepsilon_0 \varepsilon r$ is called permittivity. Depending on the used isolator used, ε_r can hold different values; for example (National Physical Laboratory 2008):

Vacuum: ε_r =   1

Air (20°C): ε_r =   1,000576

Water (20°C): ε_r =   81

Glass: ε_r =   5-16

Ceramics: ε_r =   50-1000

Using the setup described in Figure 5-13, one can get capacity differences in the range of $\Delta C \sim 20 * 10^{-12}$ F= 20fF= 20 Femtofarad ; (For: Δx=100 nm; x=1 mm; ε_r=10).

5.3.1.1. Measuring bridges

An adequate method for measuring capacities is by using a measuring bridge (Fig. 5-16):
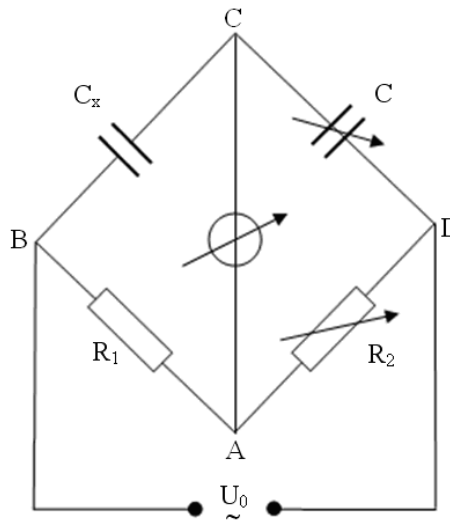
Fig. 5-16: *Measuring bridge for capacities*

The bridge is powered by an alternating voltage U_0, so that complex capacitive resistances occur. Unknown capacitor Cx can be defined by adjusting the bridge to zero (no current is flowing across the measuring instrument in the middle). This is done by the resistor R_2 and the capacitor C. According to Kirchhoff´s Laws (Paul 2001)("At any node (junction) in an electrical circuit, the sum of currents flowing into that node is equal to the sum of currents flowing out of that node" (1st law) and "The directed sum of the electrical potential differences (voltage) around any closed circuit must be zero" (2nd law)) we consider that (Paul 2001):

(Net: ABC) $\quad I_{CX} \cdot C_X = I_1 \cdot R_1 = 0$

(Net: CDA) $\quad I_C \cdot C = I_2 \cdot R_2 = 0$

$\hspace{11cm}$ (5.3.1.1.1)

By using $I_{CX}=I_C$ and $I_1=I_2$, it follows that:

$$C_X = \frac{R_1}{R_2} \cdot C$$

$\hspace{11cm}$ (5.3.1.1.2)

Using the complex resistances:

$$C_X = \frac{1}{i\omega C_x} \qquad C = \frac{1}{i\omega C}$$

$\hspace{11cm}$ (5.3.1.1.3)

Measurement bridges using alternating voltage are more interference-prone than bridges using direct voltage. The measurement can be disturbed by electric or magnetic fields around the circuit or other circumstances like the harmonic components of the operating voltage. Component tolerances and the resolution of adjustability of the used capacitor C and the resistor R2 are very important for determining very low capacities (1pF and below). This is the major issue using measurement bridges for the measurement of capacities and capacity changes in the range of some Femtofarads.

5.3.1.2. Measurement of capacities by LC oscillator

A more sophisticated way of defining weak capacities is given by a technique using an oscillator consisting of an inductor (L) and a capacitor (C). This circuit is using the capacity which has to be defined as a frequency-dependent component. Changing the capacity of the unknown capacitor (e.g. by changing the distance between the plates) results in a change of the resonance frequency of the oscillator. This frequency change can be measured and correlates with the capacity change caused by the distance variation of the plates.

The LC oscillator

The interconnection of a capacitor (C8) and an inductor (L1) results in an oscillating system (Fig. 5-17):
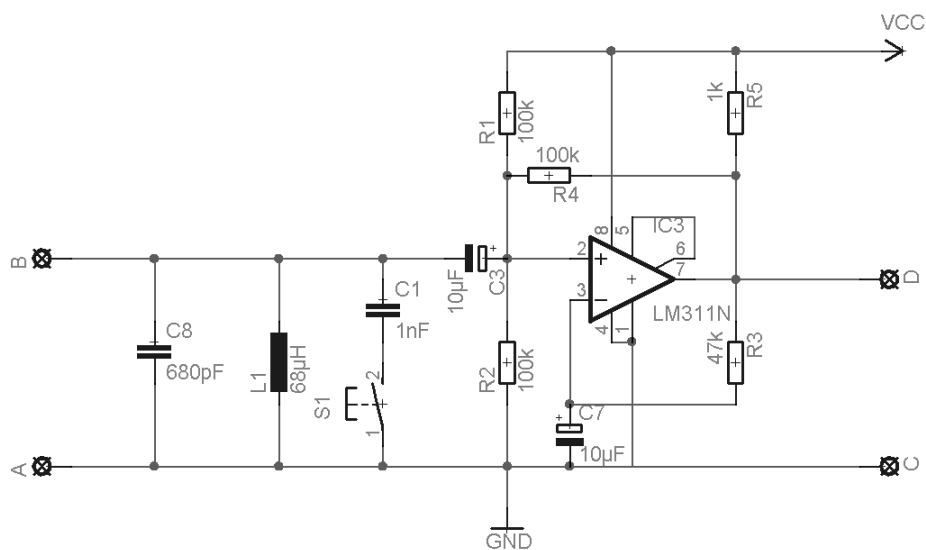
Fig. 5-17: *LC oscillator for the measurement of capacities (according to: Sprut 2008)*

The resonance frequency of such an oscillating system is defined by Paul (2001) as:

$$\omega_0 = \frac{1}{\sqrt{L \cdot C}} \quad \text{respect.} \quad f_0 = \frac{1}{2 \cdot \Pi \cdot \sqrt{L_1 \cdot C_8}}$$

(5.3.1.2.1)

Connecting an unknown capacity C_x to the circuit (terminals A and B) results in a decrease of the oscillating frequency, which can be measured by a frequency counter or an oscilloscope at terminals C and D. Calibration of the circuit can be done by adding a small, well-known capacity (here: C_1=1nF) to the input by pressing the switch S1. Thereby the frequency is changed to:

$$f_1 = \frac{1}{2 \cdot \Pi \cdot \sqrt{L_1 \cdot (C_8 + 1nF)}}$$

(5.3.1.2.2)

By increasing the difference between the unknown capacitor and the capacitor (C_1), the detune of the frequency becomes bigger. The real capacity of the circuit (including wire capacities and parasitic capacities) can be determined by the relationship of the frequencies:

$$C_{Circuit} = \frac{f_1^2}{f_0^2 - f_1^2} \cdot 1nF$$

(5.3.1.2.3)

Now, the detune of the frequency caused by the capacity C_x at the terminals A and B can be defined as:

$$C_x = \left[\frac{f_0^2}{f_1^2} - 1 \right] \cdot C_{Circuit}$$

(5.3.1.2.4)

(Where f_1 is the detuned oscillator frequency caused by the unknown capacitor C_x.)

5.3.1.3. Measurement of capacities by charge amplifier

Charge amplifiers, or better, charge to voltage amplifiers, convert a charge, e.g. from a plate capacitor, to a voltage proportional to that charge.

The input of such an amplifier commonly consists of a differential amplifier with a capacitor (C_f) in its feedback chain (Fig. 5-18):
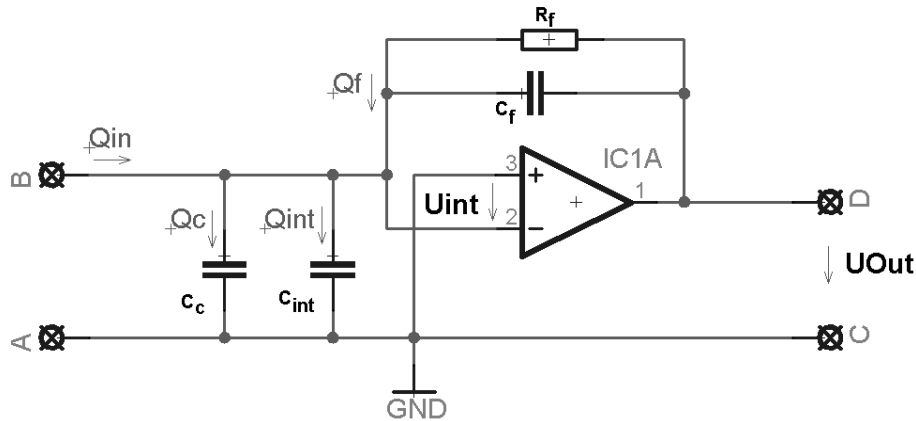
Fig. 5-18: *Scheme of an input stage from a charge amplifier*

The unknown capacity, which is connected to terminals A and B, delivers a charge Q_{in} to the point of summation, the inverting input of the operational amplifier. This charge is dispersed to the capacity of the cables C_c, the internal capacity of the OP-amp C_{int} and the capacity of the feedback chain C_f. According to Kirchhoff's Law one can summarize for the input (Paul 2001) that:

$$Q_{in} = Q_c + Q_{int} + Q_f$$

(5.3.1.3.1)

using $C = \dfrac{Q}{U} \rightarrow Q = C \cdot U$, and replacing C_c, C_{int} and C_f follows:

$$Q_{in} = U_{int} \cdot (C_c + C_{int}) + U_f \cdot C_f$$

(5.3.1.3.2)

Due to the fact, that the voltage difference will be zero at the input of the OP-amp, the input-voltage U_{int} should be on ground level. With $U_{int}=0$ one gets:

$$U_{Out} = U_f = \frac{Q_{in}}{C_f}$$

(5.3.1.3.3)

So, the output voltage from a charge amplifier depends only on the charge at the input and the feedback capacitor. The parasitic and cable capacities can be disregarded. The feedback resistor R_f should stabilize the circuit and avoid drift at the output. Note that the scheme in Figure3 only shows the input circuit, other circuits for signal conditioning, like further amplification, filtering and integration follow.

5.3.1.3.1. Measurement of capacities by GEMAC CVC 2.0 circuit

An integrated circuit combining all components for the measurement of weak capacities by means of a charge amplifier (Fig. 5-19) has been developed by GEMAC mbH, Chemnitz, Germany. Originally designed for capacitive position sensors, the ASIC (Application Specific Integrated Circuit) is able to detect weak capacitive differences down to 500 Attofarad (5 $\cdot 10^{-16}$ F).

Fig. 5-19: *Circuit diagram of GEMAC CVC 2.0 (Gemac 2009)*

A measuring circuit, based on the CVC 2.0 for evaluation purposes, has been realized by means of the Eagle$^{©}$ electronic layout software (Fig. 5-20):
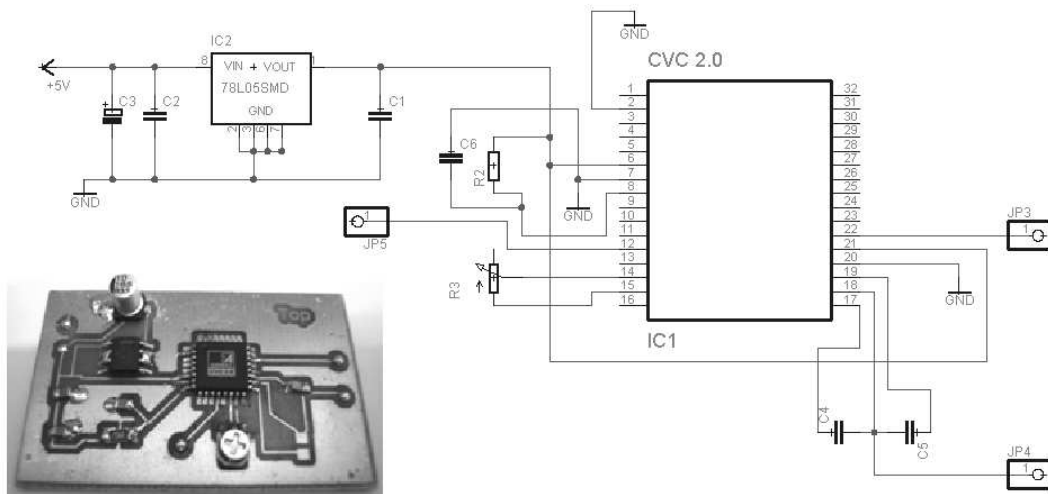
Fig. 5-20: *Schematic and image of CVC 2.0 measuring circuit*

This circuit has been positively tested within the SIL setup for distance detection and has shown a good linearity between output voltage of the CVC 2.0 measurement circuit and the distance variation between the substrate surface and the SIL assembly.

163

5.4. Height variation of the SIL Device

In order to vary the position of the Solid Immersion Lens relative to the substrate, depending on the height information gained by the capacitance measuring, a piezo-driven actuator is being used. Figure 5-21 shows the SIL Setup with the actuators and the optical head:

Actuator with micrometer screw and piezo drive

Optical head consisting of focussing lens, laser and SIL

Substrate (here: mirror for showing the reflection of the SIL
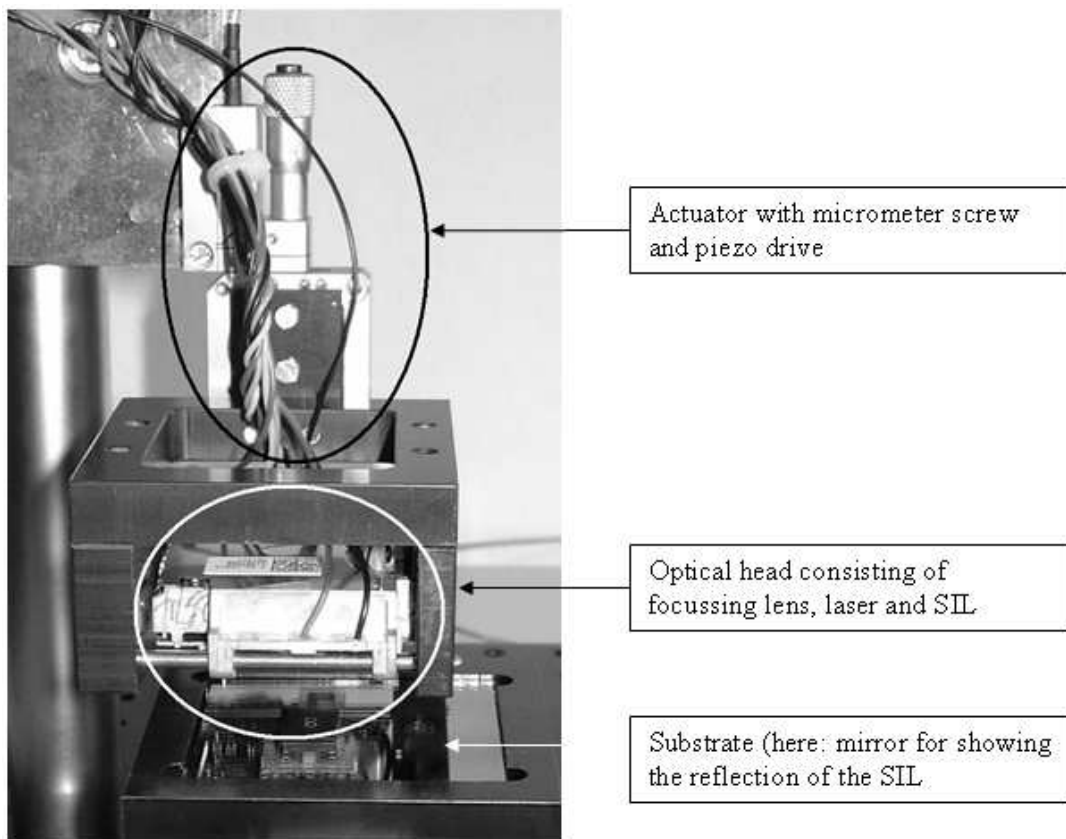
Fig. 5-21: *Picture showing SIL setup with actuator and optical head*

The actuator used in this setup, PI-P853.00, has a range of 25 µm for fine positioning and can also be positioned by a micrometer-screw more roughly within a range of 6 mm. All necessary components of the Solid Immersion Setup are attached to this actuator and can be precisely moved towards the photo resist-covered substrate. The actuator is powered by an integrated low voltage (-20 V up to 120 V) piezo driver (LVPZT) controller unit (PI E-503). This can be controlled via a serial bus from a PC, in this case directly by Labview©. Alternatively a voltage in the range of -2 V up to 12 V DC can be applied to gain a corresponding output voltage of -20 V-120 V.

5.4.1. Distance regulation between the Lenses

The main prerequisite of a Solid Immersion Lens (SIL) setup is the adequate alignment of the two lenses involved. This alignment ensures the coincidence of the focal plane of the focusing lens and the flat surface of the SIL (Fig. 5-22).
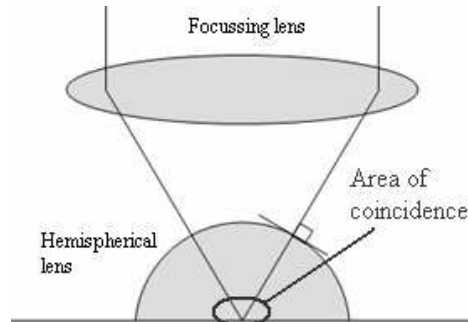
Fig. 5-22: *Solid immersion lens system with hemispherical lens showing the area of coincidence*

This alignment is done by the moving coil actuator at the Optical Pickup Unit (OPU) (refer to Chapter 4). The amplified signal is A/D converted by a National Instruments[©] USB Interface (NI 6009) and processed by Labview[©].Figure32 shows the typical graph, which occurs when the pickup (with the focussing lens) is moved towards the SIL: the point of coincidence of the focal plane of the focussing lens and the flat surface of the SIL is marked in Figure 5-23.
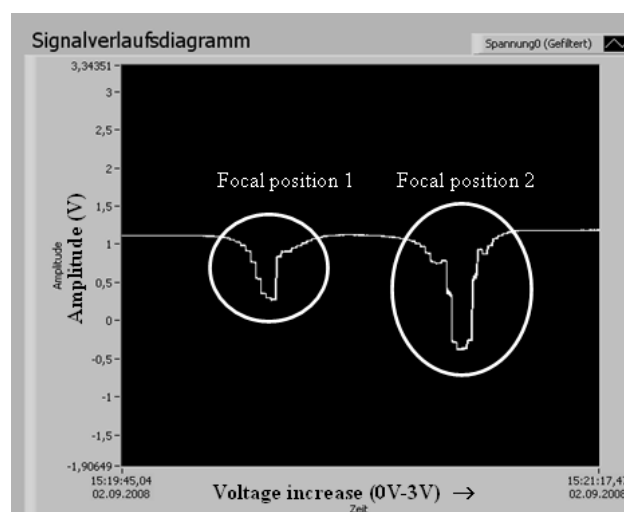
Fig. 5-23: *Graph showing the backscattered signal while moving the focussing lens towards the SI-Lens*

165

Please note that the signals are amplified by a transimpedance amplifier (an inverting amplifier) and the course of the graph is "in reality" inverted. Nevertheless, one is only interested in the minimum (-maximum) values.
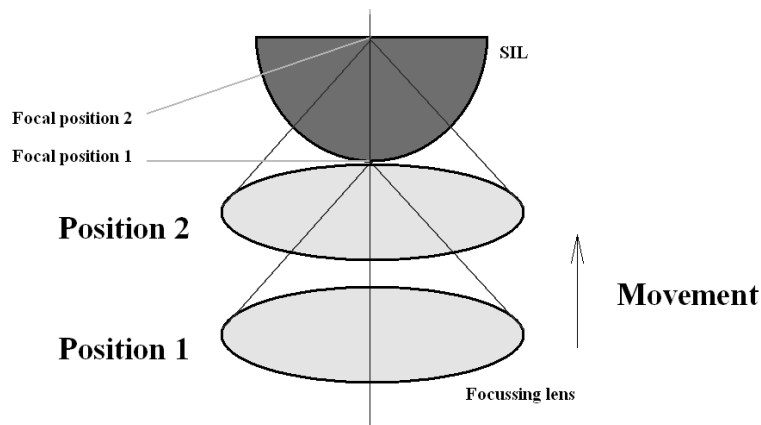
Fig. 5-24: *Illustration showing the change of the focal positions, while moving the focussing lens towards the SI-Lens*

Considering the course shown in Figure 5-23, the first minimum describes the focus striking the rounded side of the SIL (the side facing the focussing lens) and the second minimum, the focus striking the plane side of the SIL. This behaviour is illustrated in Figure 5-24.

5.5. SIL-based technology as the next generation of optical storage

Although the current standard for optical storage and playback technology, Blu ray, has just been launched, and the market analysts are watching, if the consumers respond to this technology as they did when the DVD standard was introduced, the research for the 4th generation of optical storage can be considered to have already started.

Especially, Philips Electronics N.V. is working on this technology and two published PhD theses show how the technology will be implemented (Zijp 2007 and Eerenbeemd 2008) Eerenbeemd is presenting the complete theoretical background of this innovation including the field calculations and optical simulation while the thesis of Zijp deals with a technology option for the next generation of optical storage based on SIL technology and with the possibility of holding a constant distance between the SIL and the surface of the optical disc. Figure 5-25 shows two types of actuators that have been used within his research.

Fig. 5-25: *a) NA=1.9 lens mounted in a two-axis actuator, b) NA=1.9 lens mounted in a three axes actuator that enables control of the θ– tilt angle (Zijp 2007).*

It is obvious that the "mechanical" outline of this technology will be similar to what is known by the optical disc systems used so far (please refer to Chapter 4 for the figures showing the Blu ray OPU). Therefore, it was decided to develop the system for surface structuring and characterisation so that these special types of OPU may be implemented in the future, to make the entire system "SIL- Ready".

Summary

This chapter has presented a possible enhancement of the confocal system described in Chapter 3. Due to the lack of necessary "key" equipment and the fact that a very strong research effort is already taking place within this field of engineering, it was decided to develop the confocal system and its peripheral components in a way such that the SIL technology can be implemented in the confocal system in the future. The next chapter will introduce the development of the confocal system's microcontroller-based peripheral environmen

6. Microcontroller (µC) implementation into the confocal setup

The current chapter deals with the integration of the confocal device (PS3 optical pickup unit) into a microcontroller-based system. This system has been developed due to the necessity for a standalone device without the Windows/Labview latency times caused by "windows internal" procedures (hard disc accesses etc.). Latency times like these have led to errors concerning the uniformity of the structuring. Moreover, a µC-based adaptive focal control will be presented. The entire setup is controlled by software written in C#, allowing the user to have full access to the individual hardware components to either structure a photo resist-covered surface with a desired pattern or to characterise an "unknown" surface. A strong focus on the possibility of making the system open for the next generation of optical storage, such as the SIL technology described in the last chapter, has been maintained.

6.1. Overview of the system components

The system consists of three main components connected by a USB interface to a host computer (Fig. 6-1):

- The ARM µC part for focal control and data acquisition for surface characterisation,
- The LPG (laser pattern generator) microcontroller device for providing the pattern data to the laser diode for surface structuring and
- The USI 2 device for controlling the stepper motors of the translation stages.

In the following sub-chapters, the necessary system components will be introduced in greater detail.
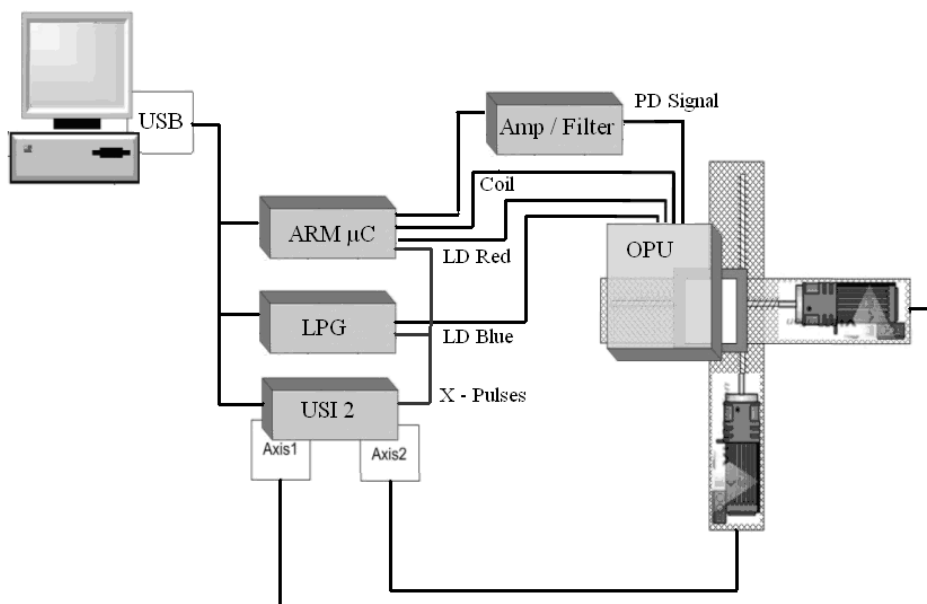
Fig. 6-1: *Schematic overview of the components used for the µC based setup*

A metal base has been used to mount the PS3 optical pickup unit (OPU) above the translation stage (Fig. 6-2).

The 650 nm and 405 nm emitters of the laser diode, the photo diode detectors (one for the blue and one for the red signal) as well as the actuator supplies are located at a connection terminal (Fig. 6-3).
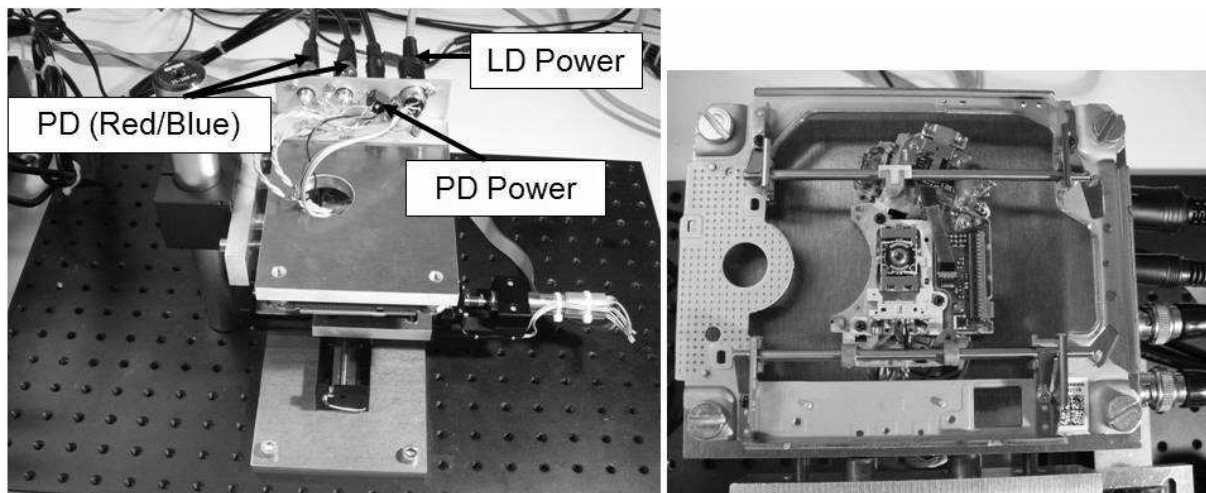
Fig. 6-2: *Left: PS3 OPU mounted onto a metal base above the translation stages (with the "older" servo motors attached to the stages). right: bottom view of OPU*
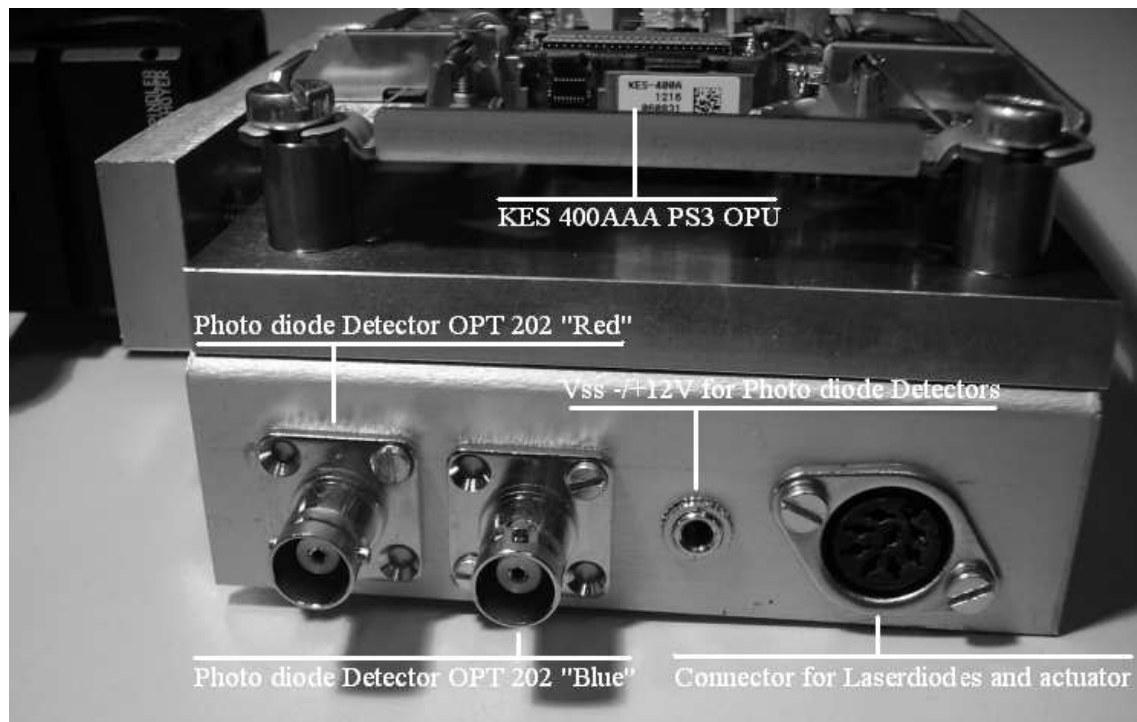
Fig. 6-3: *Connection terminal of the mounted PS3 OPU*

6.2. The ARM μC based focal control

While scanning the technical object by means of the confocal system, the laser beam illuminates its surface and the photodiodes within the pickup detect the backscattered light. To achieve a high resolution, it is necessary that the laser spot is as small as possible, e.g. that the focus lies exactly on the surface. Formerly, this was realised with the aid of a second computer, which was connected in parallel to the photo diode monitoring the intensity of backscattered light, in order to adjust the position of the focusing lens by changing the voltage applied to the actuator coil. By permanent (manual) increase of the driving voltage, the lens moves downward towards the object surface. Starting out of focus (too far away from the surface), the lens then became in focus and, as it continued its descent to the surface, finally became out of focus again (too near to the surface) (Fig.6-4).
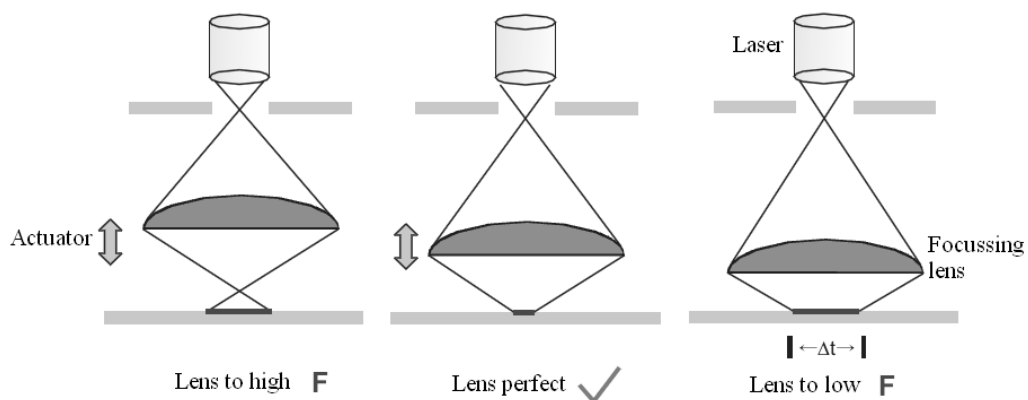
Fig. 6-4: *Variation of the focal spot size (x) by changing the driving voltage*

The detected photo diode signal is shown in Fig 6-5:
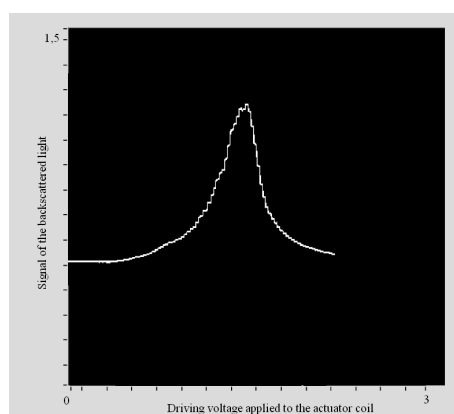
Fig. 6-5: *Position of the focusing lens (detector voltage) vs. driving voltage*

This manual procedure was time-consuming and not "state-of-the-art". Thus, a microcontroller-based test rig was developed to automate this focussing process. Figure 6-6 shows the required test rig in the form of a "black box".
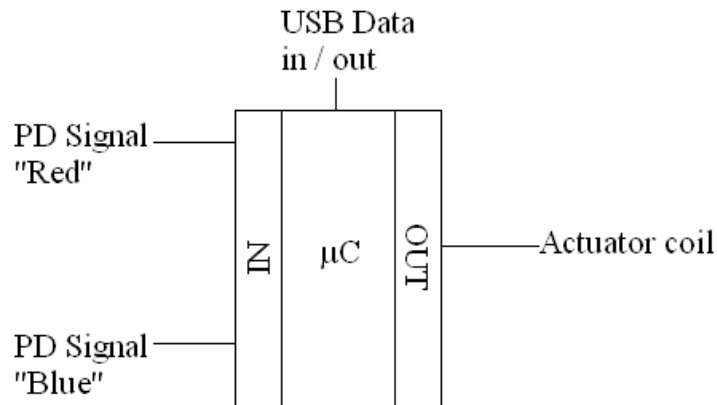
Fig. 6-6: *Schematic of input /output structure of the µC device*

The hardware platform is represented by an Olimex STM-P103 evaluation board (Fig. 6-7) holding an ARM 32 bit CORTEX M3 microcontroller (please refer to Appendix 7 for more information on this board).
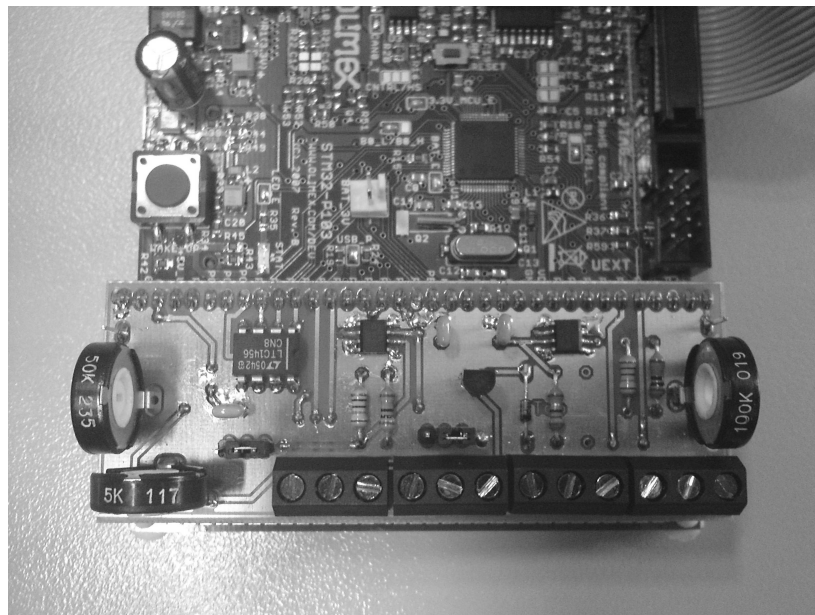
Fig. 6-7: *Olimex STM-P103 evaluation board with add-on circuitry*

Necessary peripheral circuitry, including amplification of the photo diode signal and the analogue /digital conversion of the output data for the actuator coils, was mounted directly to the evaluation board.

The process of "finding the focal position" was done by:

- Putting the lens into "zero" position (0V at the coil),

- Activating the laser diode 405 nm (Blue),

- Lens steps down one increment (1 mV at the coil),

- Conversion and storage of detector signal ,

- Delay,

- Lens steps down another increment and

- Iterate until lens is completely moved downward.

Since the lens may oscillate while moving down, due to its mounting in a "spring-like" arrangement, a delay-time is important. This whole procedure takes about 15 s and the stored data show the characteristic "focal-curve" (Fig. 6-8):
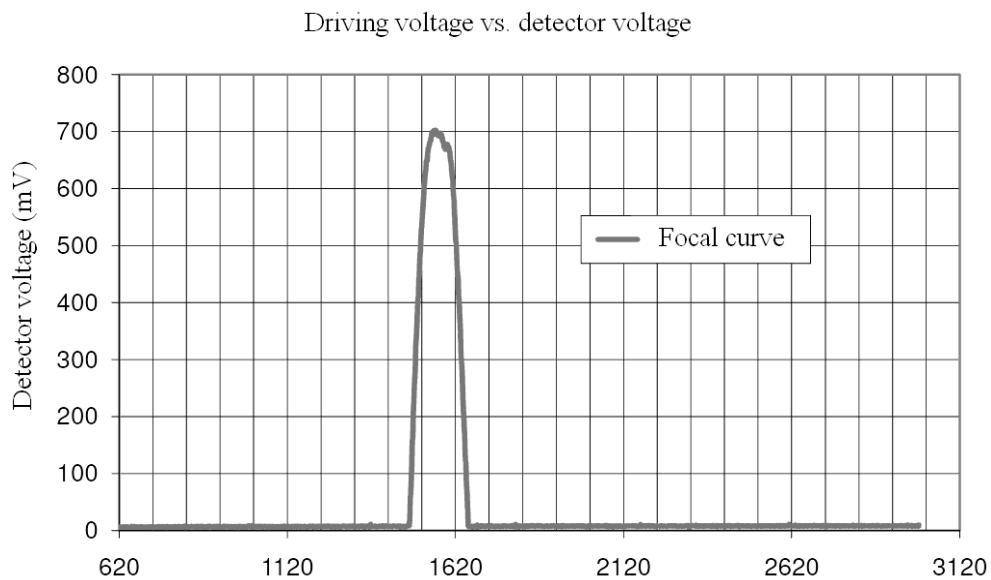
Fig. 6-8: *Diagram showing the "focal curve", note that the driving voltage is represented by the number of increments sent to the actuator (one increment = 1 mV)*

After this procedure, the optimal position of the focussing lens (detector voltage ~700 mV and driving voltage ~ 1500 mV in Figure 6-8) is determined by the controller and the voltage applied to the actuator coil is incremented until the "final" focal position of the lens is reached (Fig. 6-9).

Putting optic into focal position
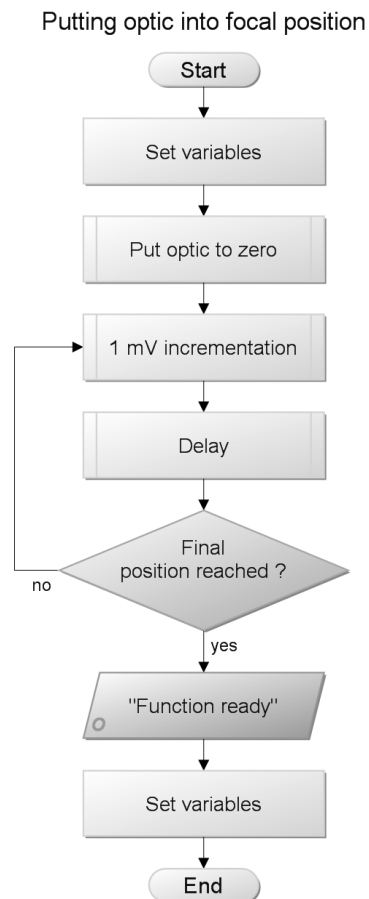
Fig. 6-9: *Structure of focal driving procedure*

6.2.1. Focal control

Whilst the substrate is moving beneath the focussing lens, irregularities in the thickness of the photo resist layer result in a varying distance between surface and lens. Thus results in errors during the exposure process (Fig. 6-10).
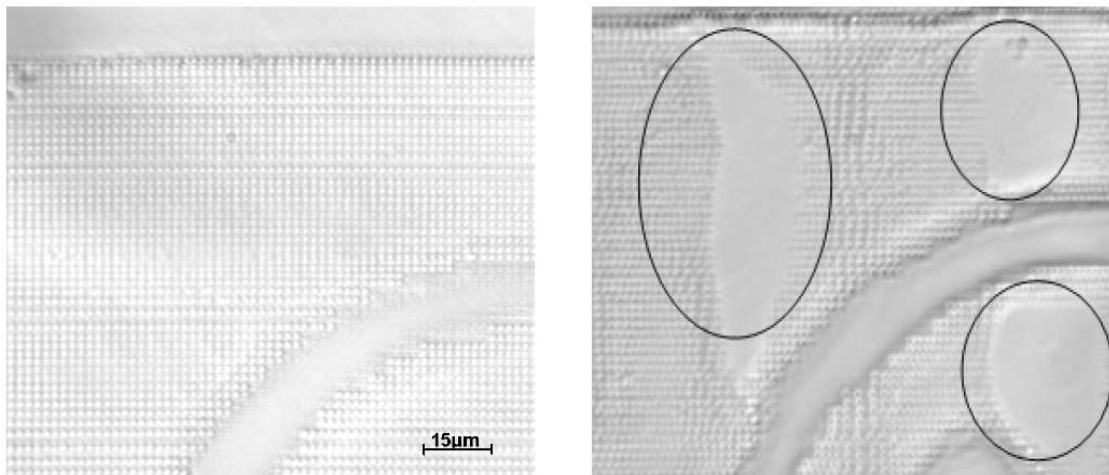
Fig. 6-10: *Structured photo-resist: left: error-free resist layer; right: faulty photo resist layer*

The idea of an adaptive focal control (AFC) comprises involves the use of the 650 nm "red" emitter. Due to the fact that the photo resist does not absorb "red" light (please refer to Fig. 2-8), the 650 nm emitter can be used for AFC without affecting the exposure.

At a glance:

- The focussing lens is moved to the focal position (refer to the last chapter),

- The 405 nm emitter is deactivated; the focussing lens remains at the position,

- Activation of the 650 nm emitter,

- Detector voltage of the 650 nm emitter is stored and taken as the reference (set point) and

- Regulation of the actuator coils according to the stored 650 nm detector voltage (set point).

Regulation using the 650 nm detector signal is possible, because the wavelength difference between 405 nm and 650 nm is constant and the signal of the 650 nm detector is changing relative to the 405 nm signal. The first attempt at regulation involved the use of a software-based PID controller. Due to the oscillating control path (the lens is spring mounted within the OPU), which acts as a classical spring-mass system (Fig. 6-11), the parameterisation of the PID controller (Parts to relocate were: P = proportional; I = integral and D = differential) was very hard.
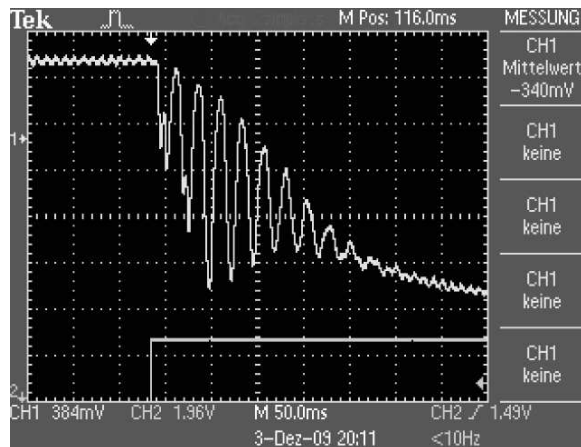
Fig. 6-11: *Step function response (lens was moved from zero to the focal position)*

It was decided to use another strategy: Considering, that the changes within the photo resist covered surface are small in comparison to the complete working distance of the lens actuator (nearly 1 mm), the upper region of the graph (Fig. 6-12 left) can be linearised (Fig. 6-12 right).
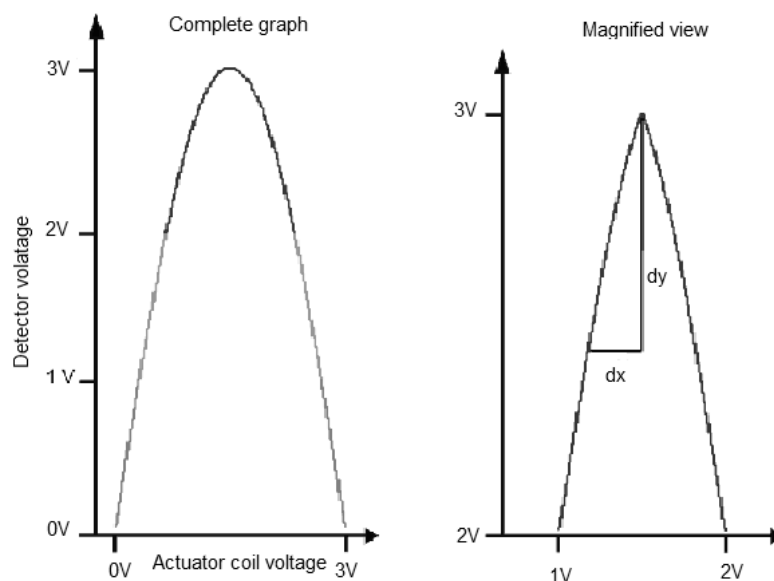
Fig. 6-12: *Scheme of the focal graph (focal curve) with simplified linearization*

This leads to the following linear equation:

$$y = \frac{\Delta y}{\Delta x} * x + 0 \qquad\qquad (5.2.1.1)$$

For example:

The focal position is reached at 3 V (y) corresponding to a voltage applied to the actuator coil of 1.5 V (x). As a result of irregularities within the photo resist surface, the detector voltage decreases by 0.5 V (Δy). Δx, the voltage which has to be applied to the actuator coils to readjust the lens into the focal position, is wanted:

$$y = \frac{\Delta y}{\Delta x} * x \Rightarrow \Delta x = \frac{x}{y} * \Delta y \qquad\qquad (5.2.1.2)$$

$$\Delta x = \frac{1.5V}{3V} * 0.5V = 0.25V \qquad\qquad (5.2.1.3)$$

A voltage of 0.25 V must be applied to the actuator coil to readjust the focal position of the focussing lens.

6.2.2. The ARM µC based surface characterisation

To gain information about the topography of an unknown surface, the laser beam is led grid-wise across the surface (Fig. 6-13) and the reflected light which is detected by the photo detector is analogue /digital converted by the microcontroller and stored within a file on the host computer.
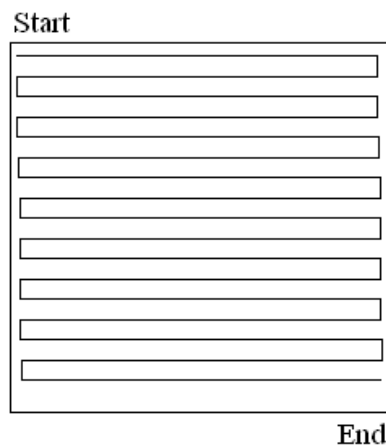
Fig. 6-13: *Schematic view of scanning strategy*

Data collection is done depending on the clock pulses given to the stepping motors (Fig. 6-14). This ensures a synchronous and homogenous image of the surface, avoiding trapezoidal images which may occur when steps or data are lost. After each line (while the motor is moving back to the beginning of the next line), the data stored within the RAM of the microcontroller (20 kB, but not fully available, due to stored variables) is sent to the host computer.
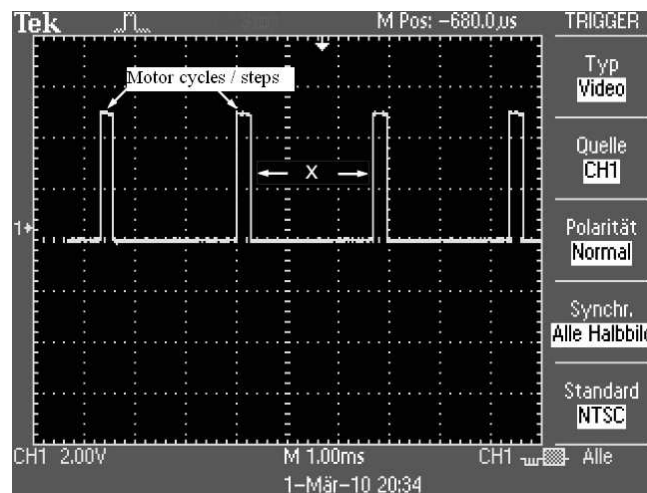
Fig. 6-14: *Diagram showing the motor cycles and the time between each of the cycles/step (x≈2,3ms)*

179

The maximum number of data points collectable in one line is theoretically limited to 8000 (16 kB available RAM; stored within unsigned-short-Int variables (16Bit)). Figure 6-15 shows the structure chart of the software while performing a surface scan. Please note that the data collected at each point can result from the averaging-out of several values since the time for data collection is 2, 72 µs and the time between 2 data points is 2.3 ms.
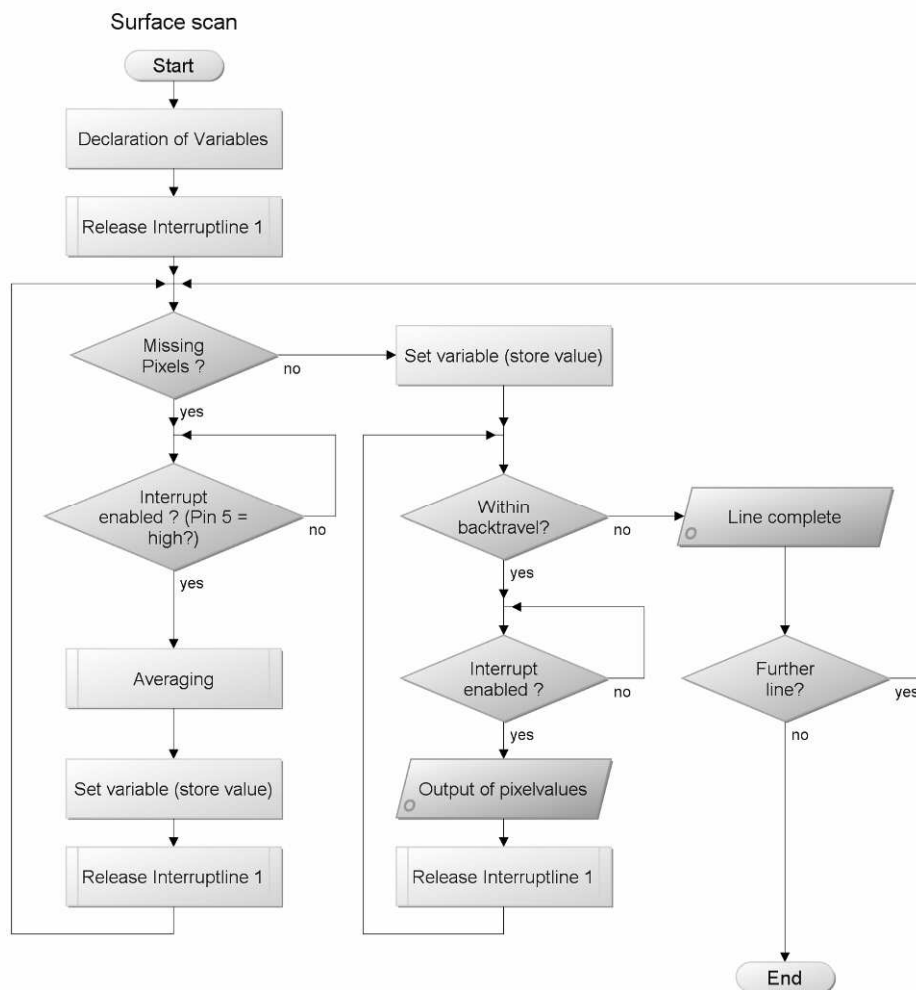
Fig. 6-15: *Structure chart of software while performing a surface scan*

All the pixels (data points) of each line are collected by this procedure. While being in back travel, the interrupts (clock pulses for the stepping motors) are also counted as well, to guarantee a perfect alignment of the motor according to the previous line. The data is sent to the host computer stepwise after each back travel interrupt (step).

6.3. The laser pattern generator (LPG) microcontroller device

The Labview-based system for surface structuring and characterisation has drawbacks concerning the quality of the produced structures since the exposure process is very time-critical. Latency times caused by hard disc accesses or windows internal processes have led to errors concerning the uniformity of structuring and to the development of a hardware-based system for providing the pattern data to the laser diode.

6.3.1. Pattern Data

An 8-Bit Bitmap (Fig. 6-16) represents the desired structure that is intended to be exposed. Each pixel of the Bitmap is exposed onto the photo resist surface with a resolution of 256 grey-scale steps.
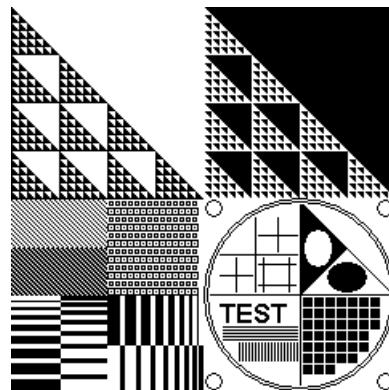
Fig. 6-16: *Example of an 8-Bit test pattern (240x240pixel)*

The control software (chapter 6.5) is sending this Bitmap data line-wise to the LPG microcontroller device (Fig.6-17), which generates pulses for the laser diode depending on the position of the substrate.

6.3.2. Laser pattern generator (LPG) Hardware

A schematic view of the LPG is given by Figure 6-17 (please refer to Appendix 6.1 for detailed schematics). After conversion of the data from USB to UART data, the first line of the pattern is stored into the SRAM of the LPG. The LPG is now in the "ready state": the data is transferred pixel-by-pixel (pixel = a data point on the Bitmap) to the laser driver via the DA converter on each pulse ("logic high") of the stepping motor controller.
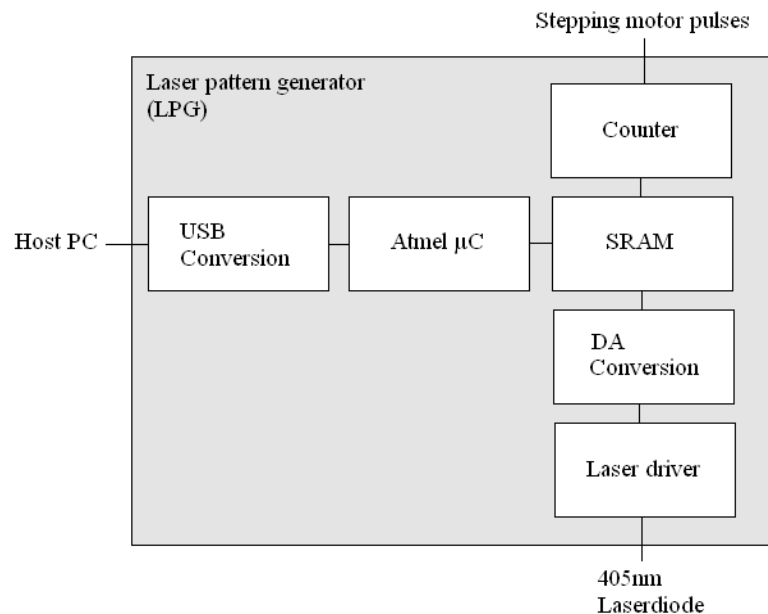
Fig. 6-17: *Schematic view of the LPG Hardware components*

After each line, a handshake (the" E" for Execute command) is given to the host computer for sending the next line. When no stepping motor pulses occur at the input, no laser light pulses will be generated.

6.3.2.1. Laser driver for common-cathode laser diodes

Laser diodes are very sensitive to voltage- and current-peaks and thus a special driving circuit has to be used providing the generated pixel data to the laser diode. Referring to Chapter 4, the used laser diode has three emitters, all mounted together in one housing, and connected in a "common cathode" arrangement. This means, all anodes are separated while all cathodes are connected together to the metal housing.

Unfortunately no driving circuit could be found on the market since these are intended for the use of the 'diode connected in common-anode' arrangement, for singe laser diode supply only, lack any triggered inputs or are simply too expensive (CWE 2010, Thorlabs 2010).

To fulfil all the requirements, the circuit shown in Figure 6-18 has been developed:
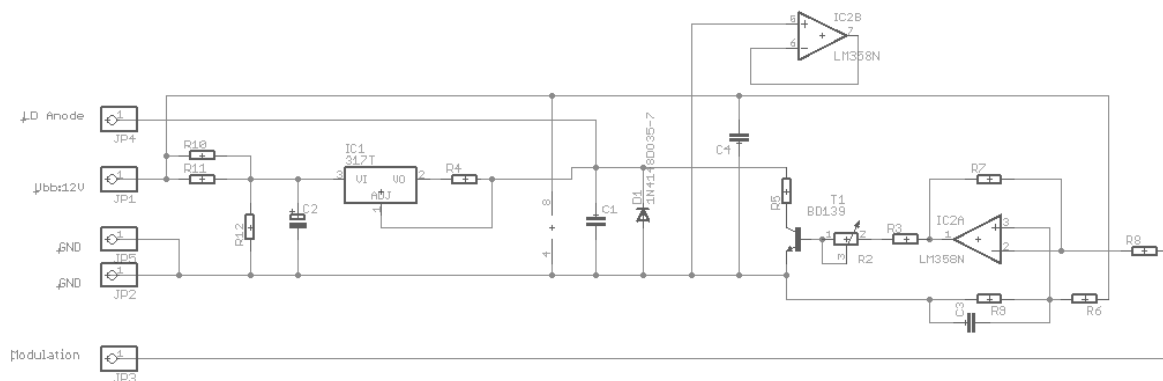
Fig. 6-18: *Electronic circuit for driving common cathode laser diodes*

The laser diode is connected directly to the output of the constant current converter (IC1), while the triggering voltage, provided by the DA converter ("Modulation"-Pin), is connected to an operation amplifier (IC2A), which is powering a transistor (T1). This transistor regulates the output voltage of a constant current converter (IC1) across the load resistor (R5). A 'logic high' at the modulation input pin results in a complete opening of the transistor and the complete darkening of the laser diode. IC2B is for putting the input resistance of the entire circuit to a higher level (some 100 kΩ) and the maximum output current is set to 30mA by R4.

6.4. Stepping motor interface "USI 2"

To ensure a correct alignment of the photo resist-covered substrates beneath the focussing lens for surface structuring (or characterisation), high-resolving actuators are needed. In this thesis, translation stages (refer to Chapter 3) consisting of jackscrews moved by stepping motors (formerly servo motors had been used, but for economic purposes they were replaced) are used. Stepping motors are synchronous electric motors, which can break down a 360º rotation into several steps. The number of steps to perform a full rotation can be e.g. 24, 48, 96 or even 400. As long as a stepping motor is not overloaded, it can be controlled precisely without a feedback mechanism, like encoders (which were used by the servo motors). Thus, closed-loop peripheral components, necessary within the former system, can be omitted; making the system more "clear" and economical. (Please refer to Appendix 8 for detailed information about the stepping motors used.)

Calculation of theoretical resolution:

The lead screw has a pitch of 80 threads per inch and the used stepping motor holds 400 steps per rotation. This results in a resolution of: (25, 4 mm/80)/400 = 793.75 nm ~ <u>800 nm</u>

By using other stepping motors, e.g. with attached gear heads, the resolution can be enhanced. Although the resolution can be seen theoretically, the thermal expansion of the used material, aluminium, is (Tipler and Mosca 2008):

$$\Delta L \approx \alpha * L_0 * \Delta T \tag{6.4.1}$$

With

ΔL :   length difference;

α :   coefficient of thermal expansion, here: Al: $23 * 10^{-6}\ K^{-1}$

L_0 :   length before thermal change, here 100 mm

ΔT :   temperature change, here 1° C

<u>$\Delta L \approx 2,3\ \mu m$ (considering a length ´L_0´ of 100 mm; ~23 nm at L_0 1 mm)</u>

The resolution and linearity of the translation stages has been proven by applying an inductive precision dial gauge (Millitron 1240, resolution 100 nm) and is displayed in Fig. 6-19, showing no irregularities within movement.

184

The chart displays displacement (mm) versus time (s), with annotations:
- Displacement: 1000 steps right
- Displacement: 1000 steps left
- Stepsize: 794 nm
- Speed: 260 µm / s
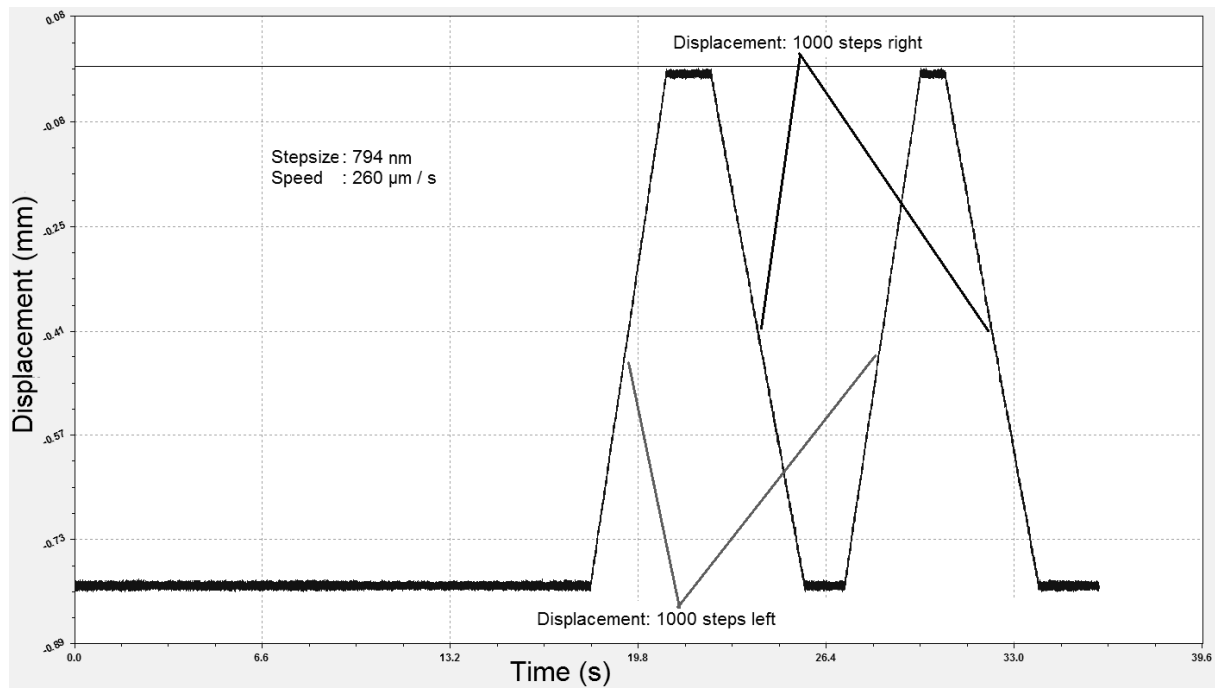
Fig. 6-19: Diagram showing the linear movement of a translation stage over an displacement of ~800µm (two cycles)

The two stepping motors (x and y) are controlled by software which interconnects by USB to a microcontroller-based device, the USI 2 (Fig.6-20). This device is commercially available from the Company ELV and is very cost-efficient, since its retail price is about 40 Euro.

Figure removed due to copyright restrictions

Fig. 6-20: *Stepping motor interface USI2 from ELV (ELV 2009)*

A very simple control set is used to control the attached stepping motors, for example, to move motor 1 by 255 steps in the left direction, the following command line is sent to the USI 2:   <STX> <'l'> <255> <0> <ETX>;

With „l" for left-Motor 1 (whereas "L" moves motor 2 in left direction.

Depending on the stepping motors used (please refer to Appendix 8 for details on the used stepping motors), the duration of scanning an area of 255 pixels square (resolution 1

185

micron/step) for surface structuring or characterising an surface topography is approximately 15-20 minutes.

6.5. Control software

The confocal device for structuring and characterisation of technical surfaces is completely controlled by software written in C#. Figure 6-21 gives an impression of the main screen:

Fig. 6-21: *Screenshot of the main screen of the controlling software*

All necessary data can be adjusted within this screen:

- Either structuring mode (start LPG) or characterisation mode ("Scan Pattern") can be selected,

- The translation stages can be moved manually to position the substrate,

- The number of steps for the motors can be changed for the use of different types of motors,

- The pattern, which has to be exposed into photo resist, can be loaded and displayed,

- The pitch size ("Gridsize") is being displayed, showing the smallest increment of movement.

Furthermore, a Fourier transformation can be applied to pattern data; thus, diffractive optical elements (DOE) can be checked to see if they are correct before exposure (Fig.6-22):
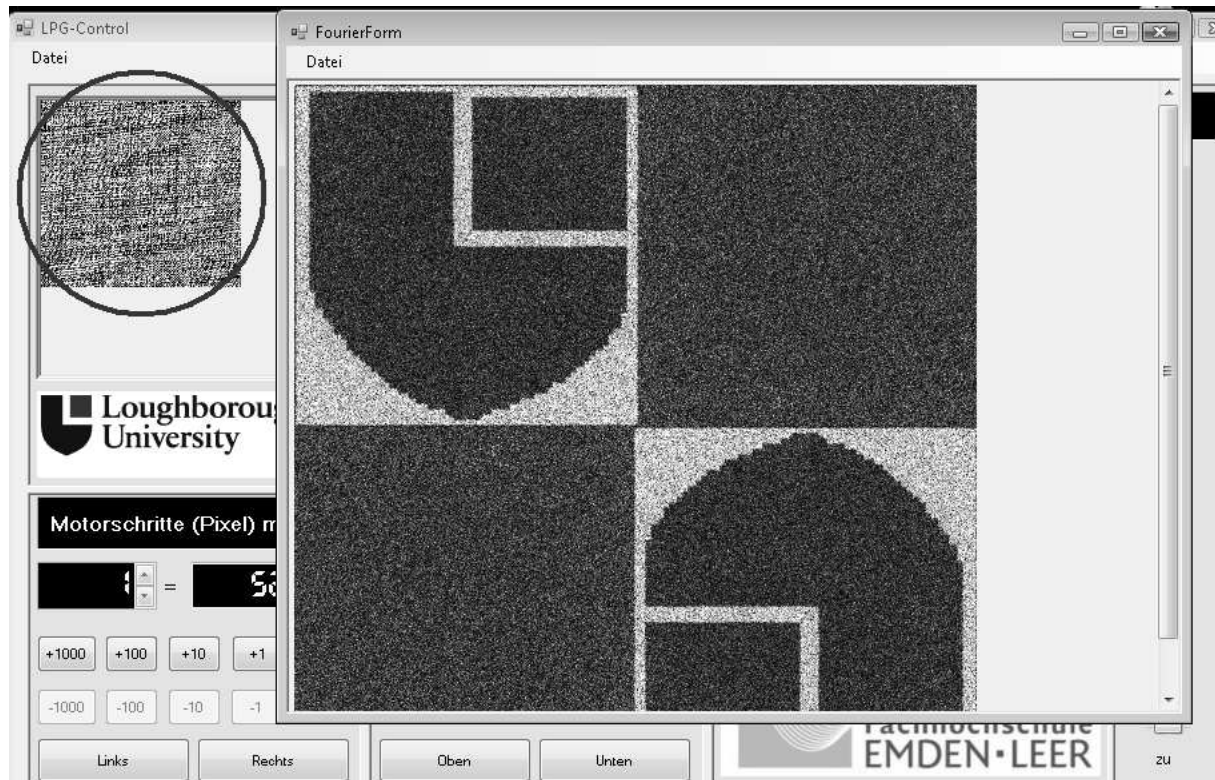
Fig. 6-22: *Example of Fourier transformation of a DOE pattern: image in red circle shows the DOE pattern; the transformed signal is showing the Loughborough emblem*

Within "Scan" mode, the software is capable of controlling the stepping motors in order to scan an area line-wise, while collecting and storing the data gained from the reflected light.

6.6. Results of the structuring by means of the confocal device

Several different patterns have been written (i.e. exposed) into photo resist-covered surfaces by means of the developed confocal lithography system (chapter 6.1):

The glass substrates (2"x 2"), coated with Shipley Microposit S1805 photo resist (layer thickness approx. 500nm), had been loaded onto the substrate holder (Fig. 6-23; mounted to the translation stages) and moved beneath the optical pickup unit (OPU), accordingly to the desired pattern.
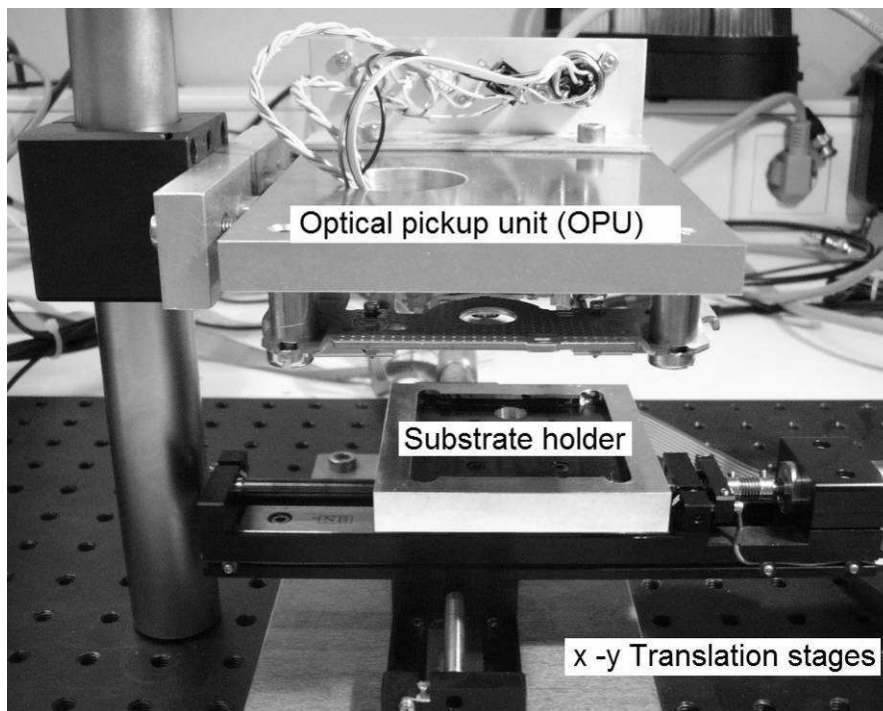
Fig. 6-23: Detailed view of the primary components of the confocal lithography system

This sub-chapter will show examples of this work. For the calculation on the illumination doses, please refer to Chapter 2.1.1.1.2. Microscopic as well as atomic force microscopic (AFM) tools had been used to verify the results of surface structuring.

6.6.1. Test structure

This test structure (Fig. 6-24) was created to evaluate the resolution and the rectilinearity of the patterns produced by the confocal lithography system.
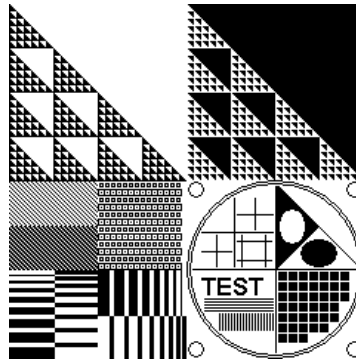
Fig. 6-24: *Original image of the test structure (BMP Data 240x240 pixel)*

Figures 6-25 - 6-27 show microscopic images of the test structure written into the photo resist

Parameters: Velocity of substrate movement: v: 150μm / s; Exposure dose: D: 270mJ / cm^2
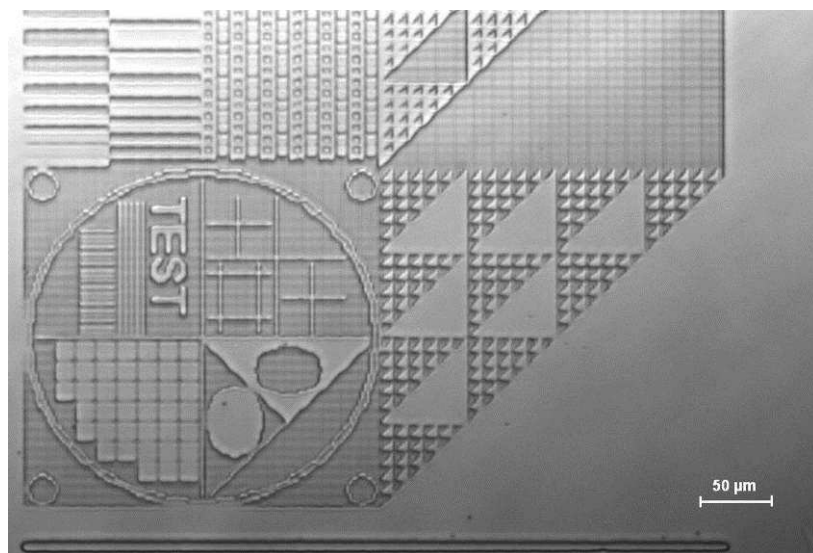
Fig. 6-25: *Overview microscopic image of the test structure written into photo resist*
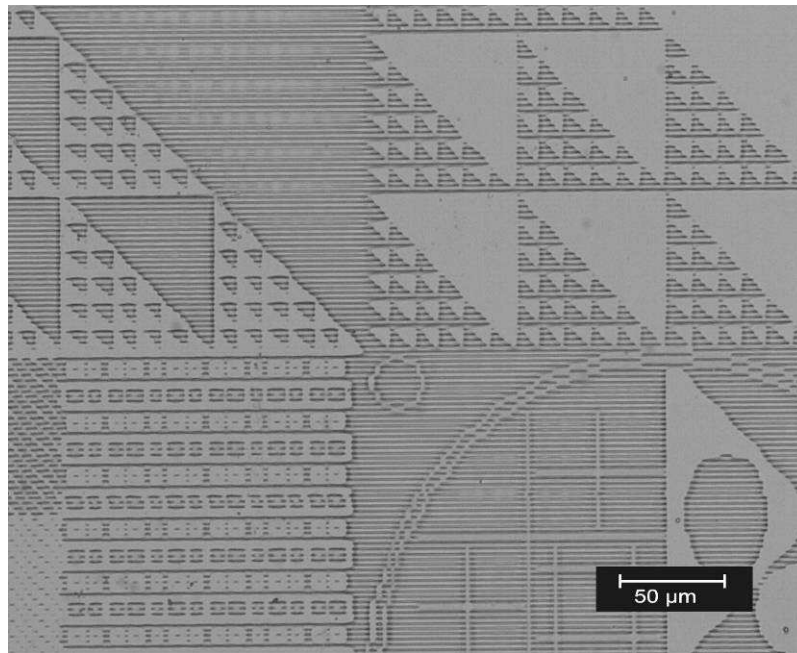
Fig. 6-26: *Microscopic image of the test structure written into photo resist*

The previous figures 6-24 and 6-25, above, show a very good linearity of the lines within the written test pattern. It has to be noted, that the lines appear slightly separated (Fig. 6-26); this is intended to show the minimum line width, respectively the resolution of the lithographic system.
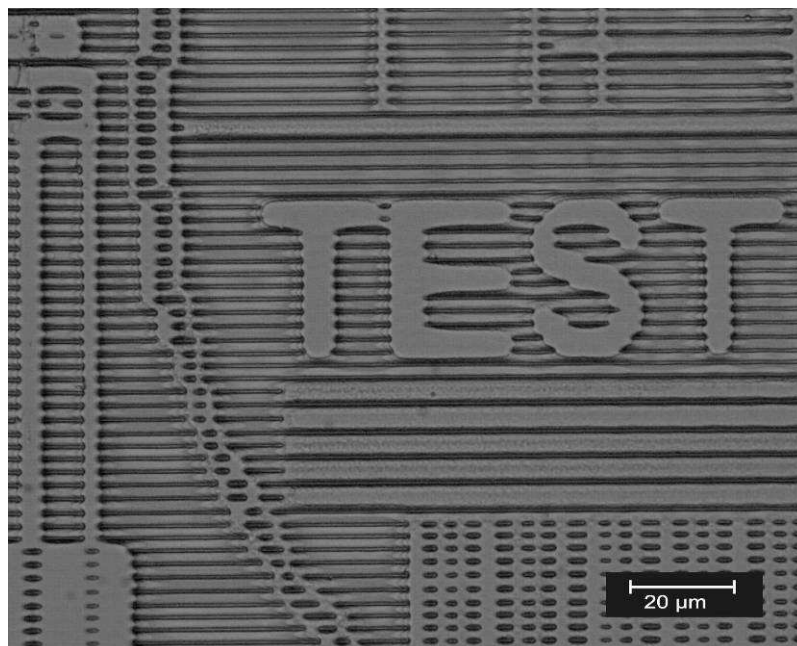
Fig. 6-27: *Detailed microscopic image of the test pattern written into photo resist*

Figure 6-28 is shows a detailed view of the written test pattern imaged by a commercial atomic force microscope (AFM) (Bruker/ SIS Nanos).
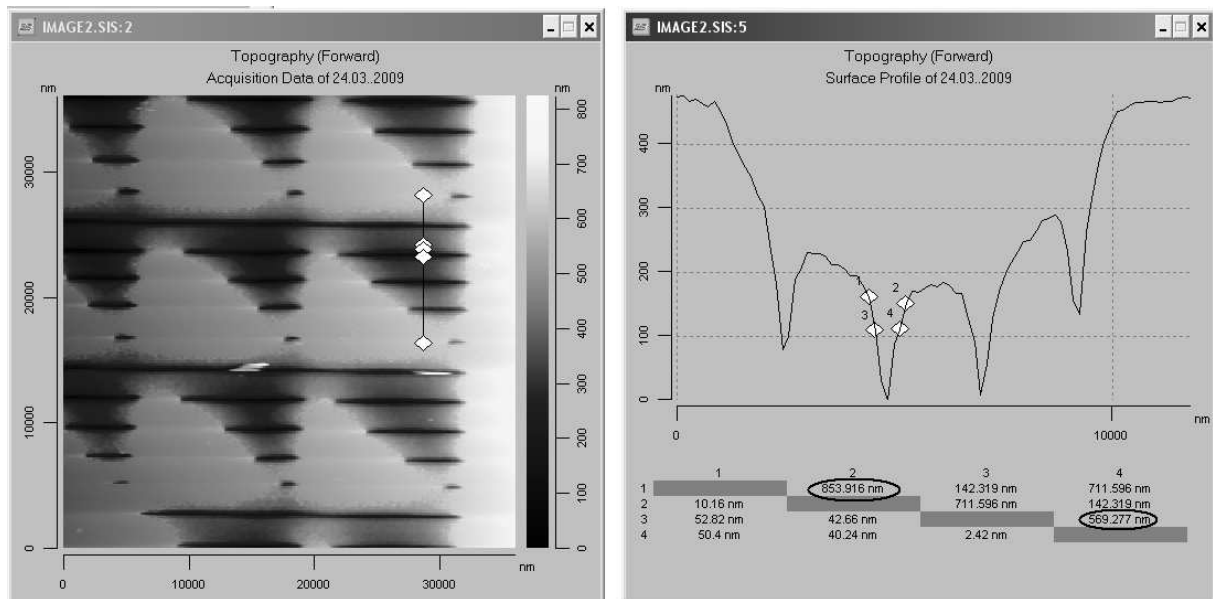
Fig. 6-28: *Atomic force microscopic image of a part of the test pattern (Fig. 6-23) written into photo resist (left) and the surface profile of a line of interest (right)*

Measurements of the AFM images show a minimum line width of 570 nm – 850 nm. This result meets the prospects concerning the resolution applied to the system. Moreover, the results show a sufficient rectilinearity of the patterns written by the confocal system.

6.6.2. Grating (please refer to Chapter 2.2.1)

This optical grating consists of approx. 330 line-pairs per millimeter (lp/mm). This grating has been inspected by a light microscope (Fig. 6-29) as well as with an atomic force microscope (Fig. 6-30).

Parameters: Velocity of substrate movement: v: 150µm / s; Exposure dose: D: 270mJ / cm^2
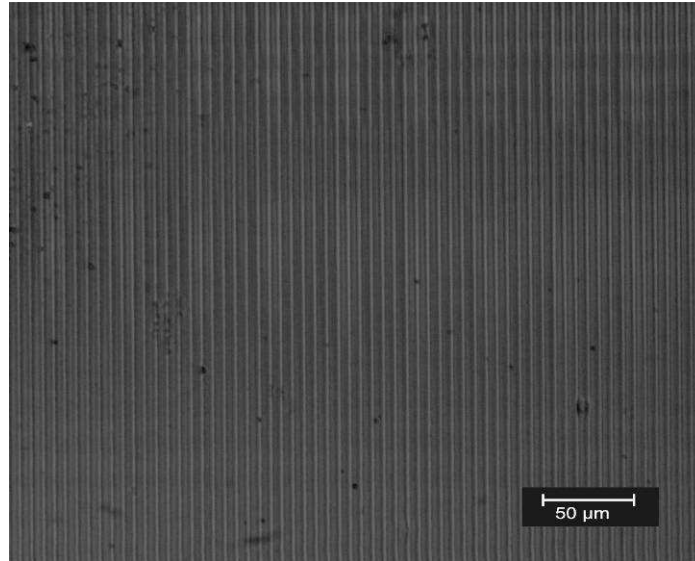
Fig. 6-29: *Microscopic image of the optical grating written into photo resist*
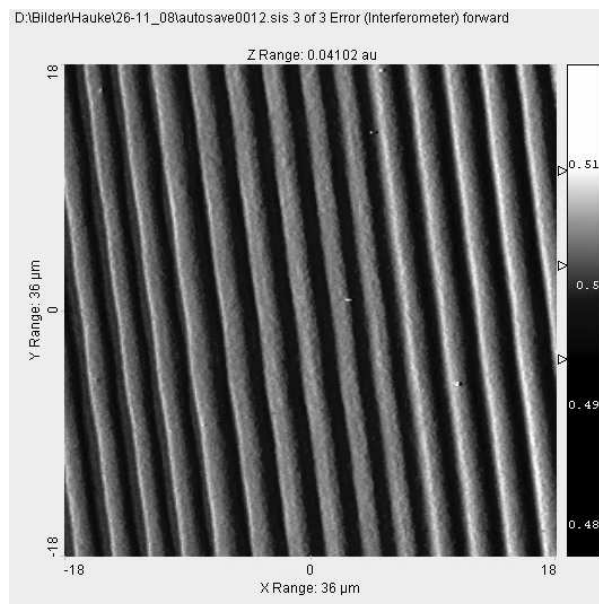
Fig. 6-30: *Atomic force microscopic image of the test pattern written into photo resist*

The three dimensional AFM images (Fig.6-31) show the continuous profile of the line structure as well as its height characteristic:
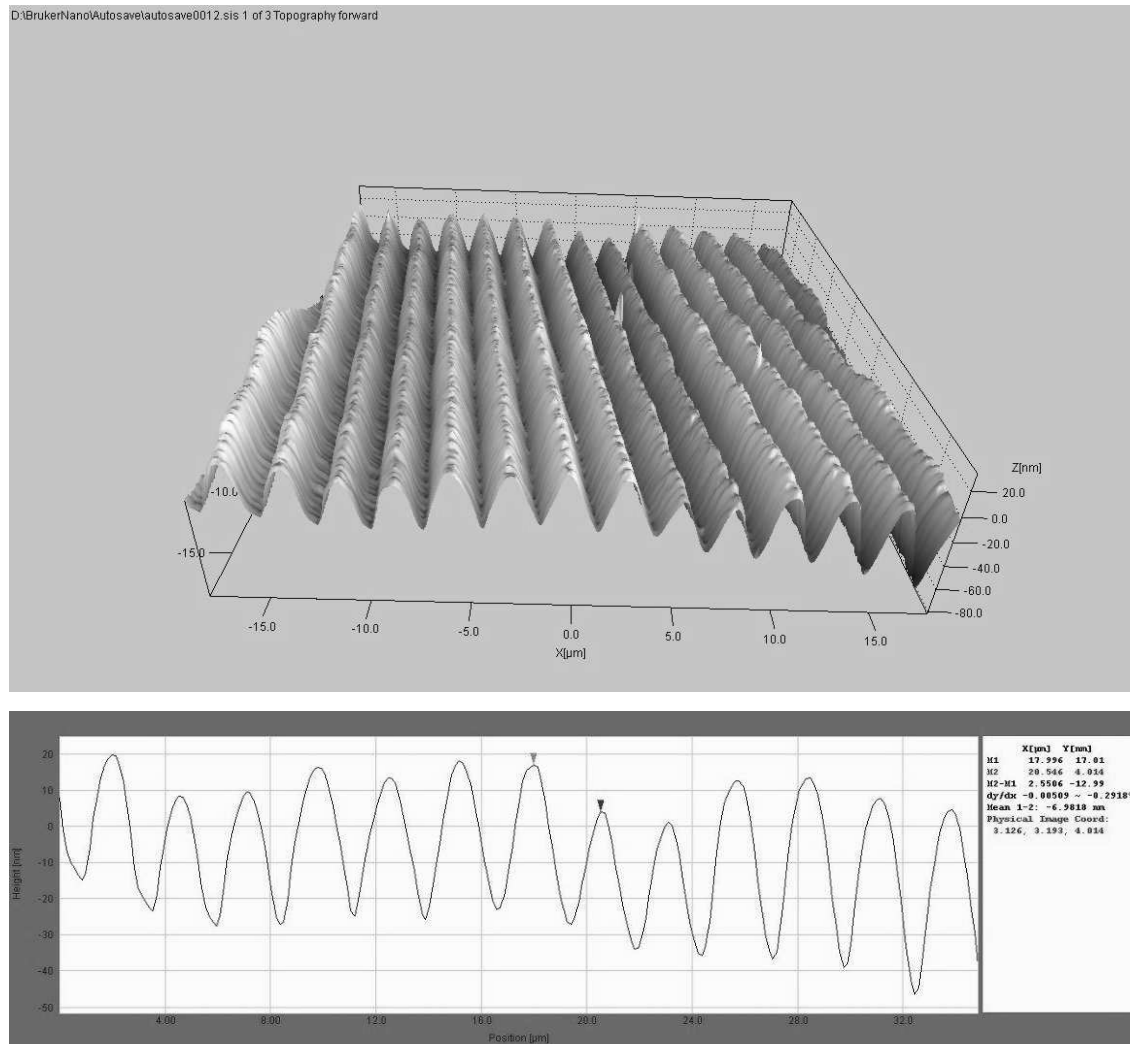
Fig. 6-31: *3- Dimensional image of the test pattern written into photo resist taken by atomic force microscopy (AFM), and a line scan across a part of the pattern showing the height characteristic /profile*

The AFM results represent a steady, uniform structuring of the line pattern with a continuous profile, important for e.g. diffractive optical elements.

6.6.3. Diffractive optical elements (DOE) (refer to Chapter 2.3)

6.6.3.1. Loughborough University Emblem

To show the capability of the system for the production of DOE´s, the emblem of the University of Loughborough (Fig. 6-32) was transformed into a DOE by means of the IFTA software described in Chapter 2 (Fig. 6-33) and exposed into photo resist by using the developed confocal lithographic system.
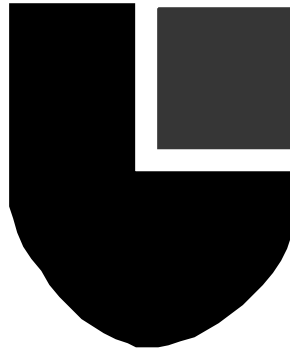
Fig. 6-32: *Original image of the Loughborough emblem*
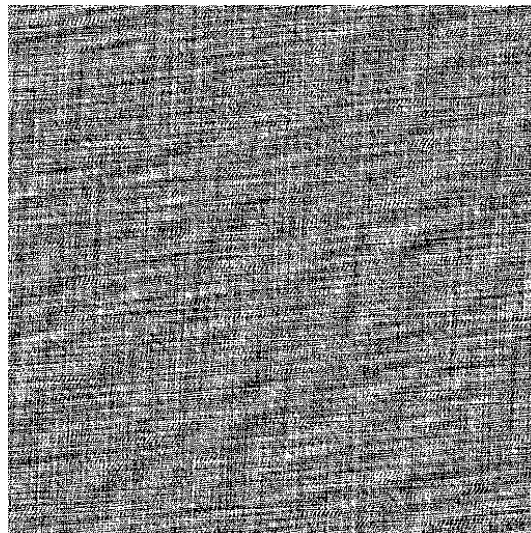
Fig. 6-33: *Computer generated DOE of the Loughborough image*

The qualitatively good transfer of the digital pattern (Fig. 6-33) to a structured resist surface is shown by a microscopic image in Figure 6-34.

Parameters: Velocity of substrate movement: v: 150µm / s; Exposure dose: D: 270mJ / cm^2
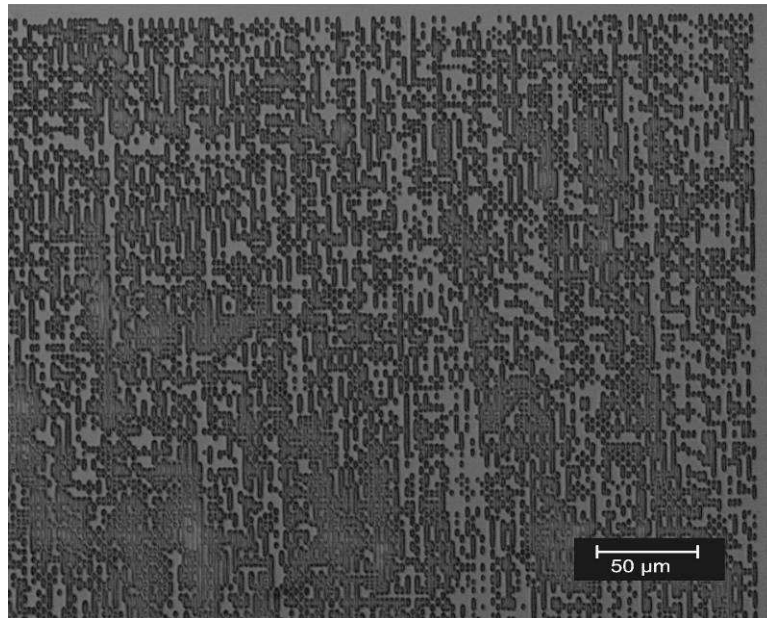
Fig. 6-34: *Microscopic image of a part of the Loughborough DOE written into photo resist*

To gain information about the size and the three-dimensional behaviour of the written structures, AFM measurements were carried out. Figure 6-35 shows a detailed view (30 microns square) of the resist structures.
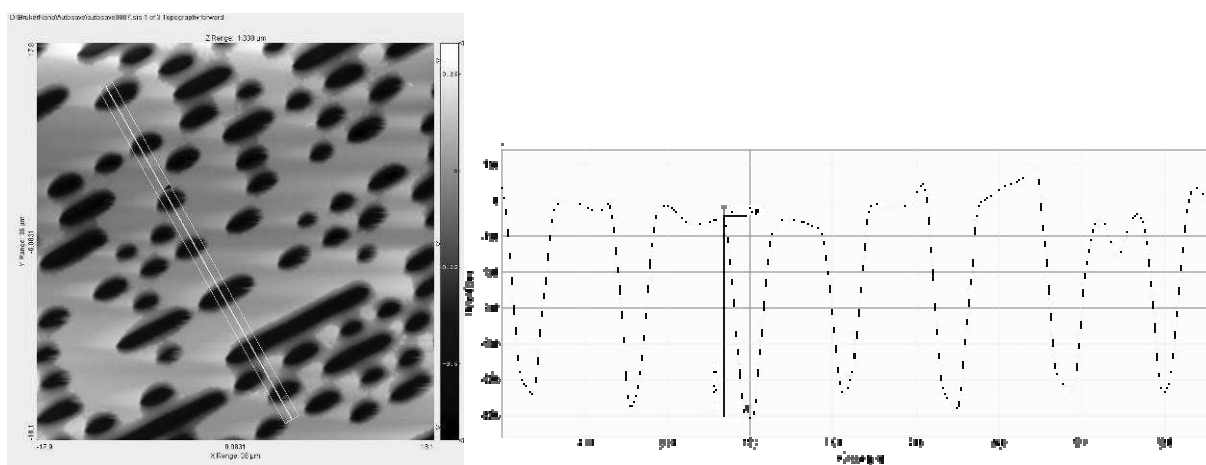
Fig. 6-35: *2-Dimensional image of a part of the written Loughborough DOE taken with AFM (left) and a line scan showing the profile of the written structure (right)*

Moreover a structure height of 560 nm and a structure width of 2 µm are shown by a line scan (Fig.6-35, right) along a part of the written structure.

To reconstruct the original image of a DOE, it has to be illuminated by means of a laser; Figure 6-36 represents a diffraction pattern of the written DOE under illumination by a 650 nm (HeNe) laser beam. The Loughborough emblem is well recognisable.
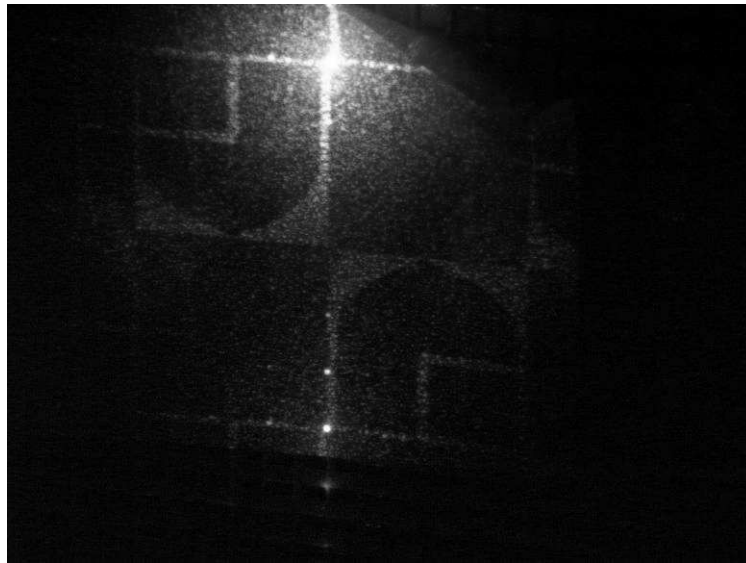
Fig. 6-36: *Figure showing the diffraction pattern of the written DOE while illumination with laser light*

This example proved the suitability of the confocal lithographic system for the production of DOE´s. The quality of transfer of the digital DOE pattern to the resist structure as well as the line width and line depth of the resist structure fully meets the prospects concerning the confocal system.

6.6.3.2. DOE Sample

Another sample showing the resolution and accuracy of the lithography system is shown by the following series of pictures (Fig. 6-37):

> **Parameters**: Velocity of substrate movement: v: 150µm / s; Exposure dose: D: 270mJ / cm^2
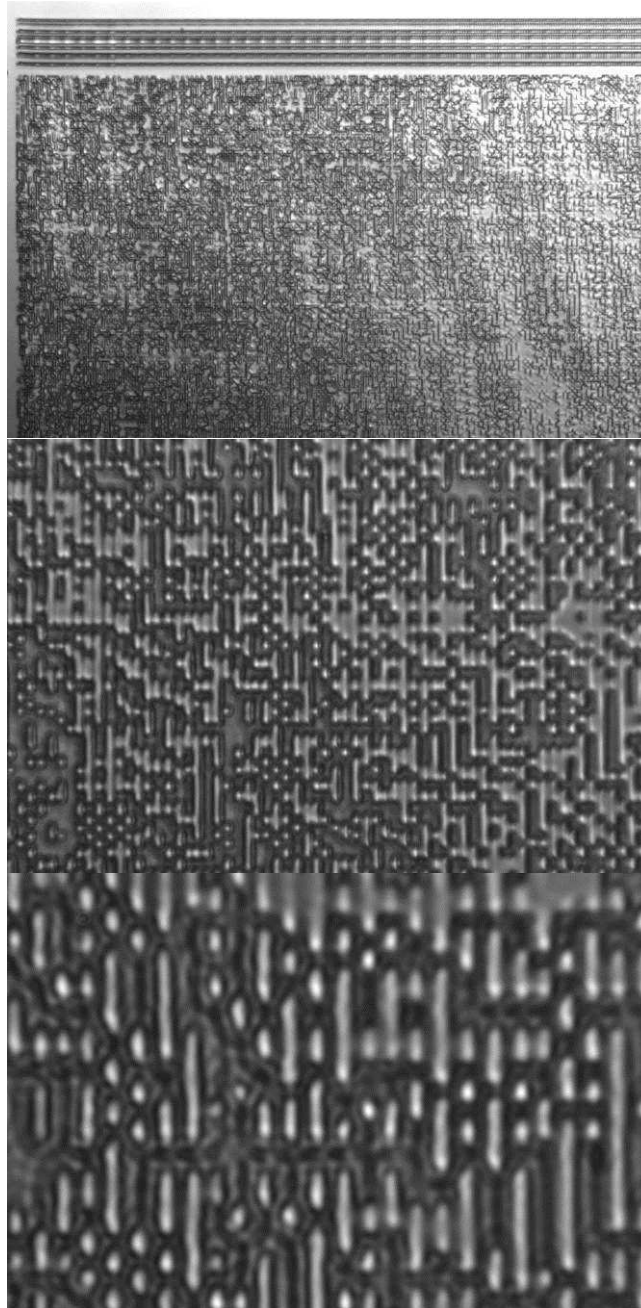
Fig. 6-37: *Another DOE sample magnified 10x, 40x ,100x*

The examples of surface structuring shown in Figure 6-37 also validate the capability of the confocal lithographic setup for the production of with highly accuracte DOE´s .

6.6.4. Dammann Grating (refer to Chapter 2.3.3)

Dammann gratings are used for the beam splitting of laser beams. These beam splitters produce an array of spots with equal intensity. Figure 6-38 illustrates an example of such a grating:
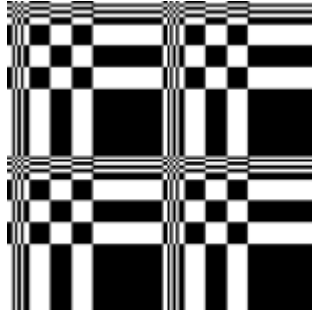
Fig. 6-38: *Original image of the Dammann grating for beam splitting*

Figure 6-39 shows the result of structuring the photo resist covered substrate with the Dammann grating pattern:

Parameters: Velocity of substrate movement: v: 150µm / s; Exposure dose: D: 270mJ / cm^2
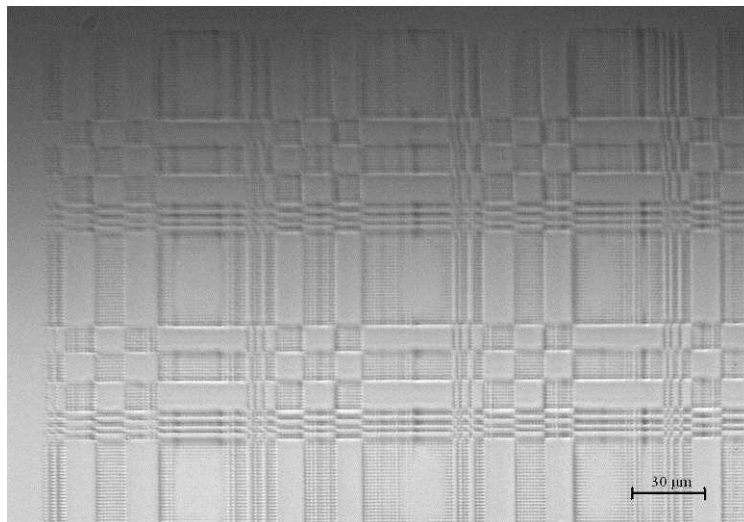
Fig. 6-39: *Dammann grating written into photo resist*

Figure 6-40 shows the diffraction pattern of the produced Dammann grating under illumination by with a laser beam.
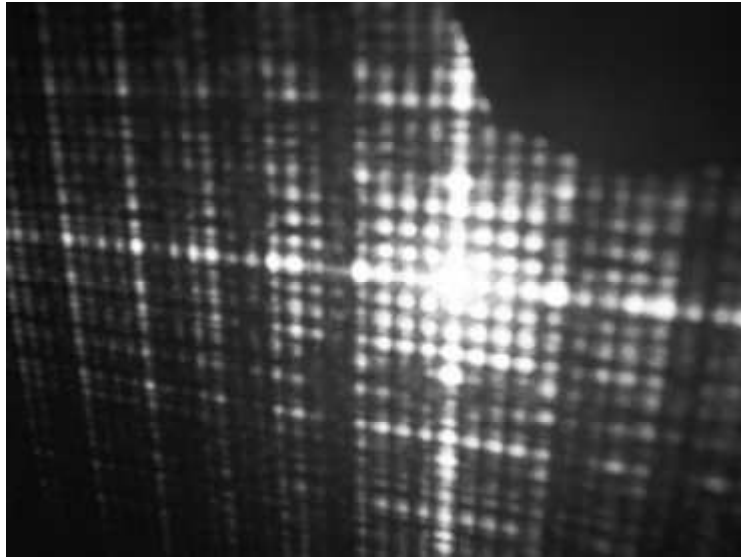
Fig. 6-40: *Figure showing the diffraction pattern of the written Dammann grating under illumination by laser light*

The array of light spots is clearly visible. It must be noted that the diffraction efficiency is not as good as possible, since the bright spot in the centre of the array (the zero order diffraction) should not exist. This can be remedied by using thicker resist layers. Nevertheless, it can be stated that the confocal lithography system is well-suited to the production of Dammann gratings.

6.6.5. Structured technical surfaces (refer to chapter 2.2.2)

Another important field of the use of lithography purposes is the structuring of technical surfaces with special functions. This sub- chapter will give some examples.

6.6.5.1. Functional surfaces / Sharkskin-like structure (refer to chapter 2.2.2.)

This example of a functional surface adapts the characteristic features of sharkskin; it should prevent the sticking of micro organisms and enhance the hydrodynamic properties of e.g. vehicles (like ships) which are covered with these structures. Figure 6-41 shows an example of such a structure:
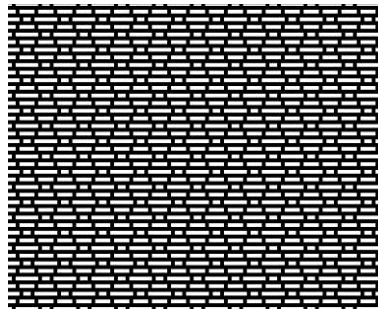
Fig. 6-41: *Original image of the sharkskin-like pattern (according to Hoipkemeier-Wilson et al. 2004)*

Figure 6-42 shows a microscopic image of the pattern written into photo resist.

Parameters: Velocity of substrate movement: v: 150µm / s; Exposure dose: D: 270mJ / cm^2
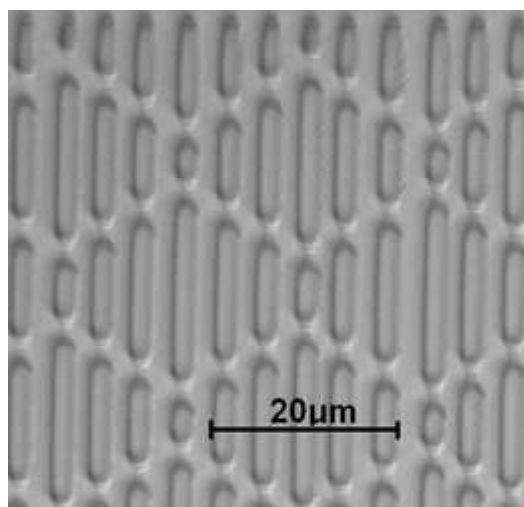
Fig. 6-42: *Microscopic image of the sharkskin-like pattern written into photo resist*

A clean adequate transfer of the digital sharkskin pattern to the resist surface has been achieved by means of the confocal lithography system.

The subsequent process would comprise the transfer of the structure (by etching) into the glass substrate, to make a stamp. With the aid of this stamp, the structure can be duplicated into a surface, like paint or silicone.

6.6.5.2. Micromechanics (refer to chapter 2.2.4)

The last example of the structuring of technical surfaces shows a gearwheel for micro-mechanical purposes. Figure 6-43 shows the computer-generated image of this wheel:

Fig. 6-43: *Original image of a gearwheel (schematic, only exemplary purposes)*

Figure 6-44 shows the result when this gearwheel structure is written into a photo resist surface by mean of confocal scanning. In combination with the results presented in 6.6.5.1, the suitability of the developed confocal lithography system for the production of technical surfaces is confirmed.

Parameters: Velocity of substrate movement: v: 150µm / s; Exposure dose: D: 270mJ / cm^2
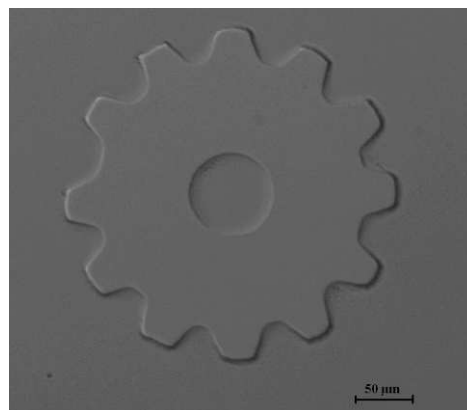
Fig. 6-44: *Microscopic image of the gearwheel written into photo resist*

6.7. Results of the characterisation by means of the confocal device

For evaluation of the lateral resolution of the confocal device, a test pattern with a defined grid size of 9,87 µm, utilised for the calibration of scanning electron microscopes (SEM) has been used (Fig. 6-45). This pattern is commercially available from a German company (Plano GmbH 2009).
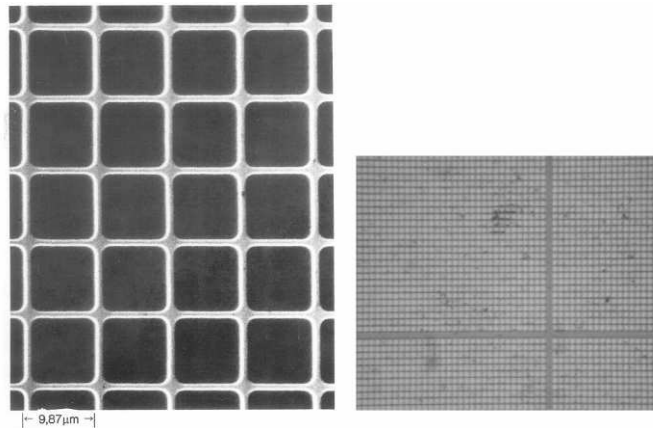
Fig. 6-45: *SEM test structure "S1930": Scanning electron beam microscopy (SEM) image (left); light microscopic image (right)*

By grid-wise scanning of the surface with the 405 nm laser beam, an image of the surface can be produced (the non-uniformity of the single rectangles is caused by a temporarily inaccurate linear stage). The first influencing factor is the step size in which the pattern is scanned. For example Figure 6-46 is scanned by 2 µm steps (which means that the distance between 2 consecutive data points is 2 µm):
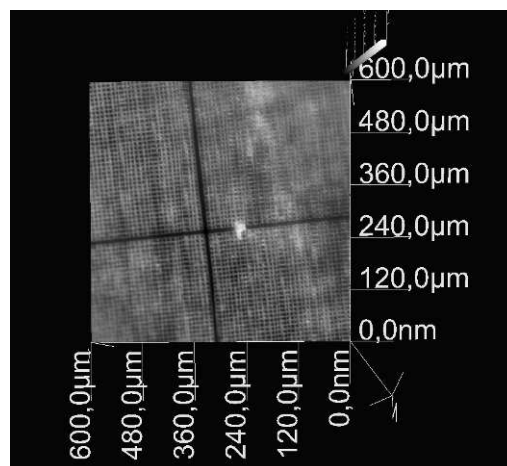
Fig. 6-46: *2-dimensional image of the scanned test structure with a step size of 2µm*

In addition, the topography shown in Figure 6-47 is processed with step sizes of 525 nm:
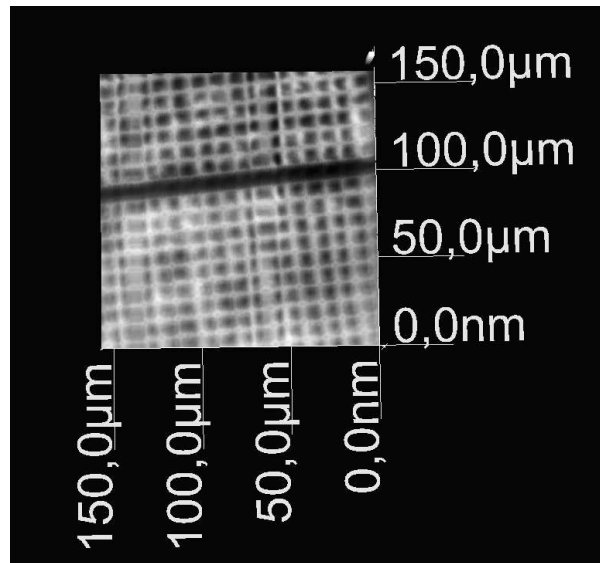
Fig. 6-47: *2-dimensional image of the scanned test structure with a step size of 525 nm*

The second influence is given by the resolution of the gained image which is strongly dependant on the position of the focusing lens, which has to be in the focal range (Fig.6-46):
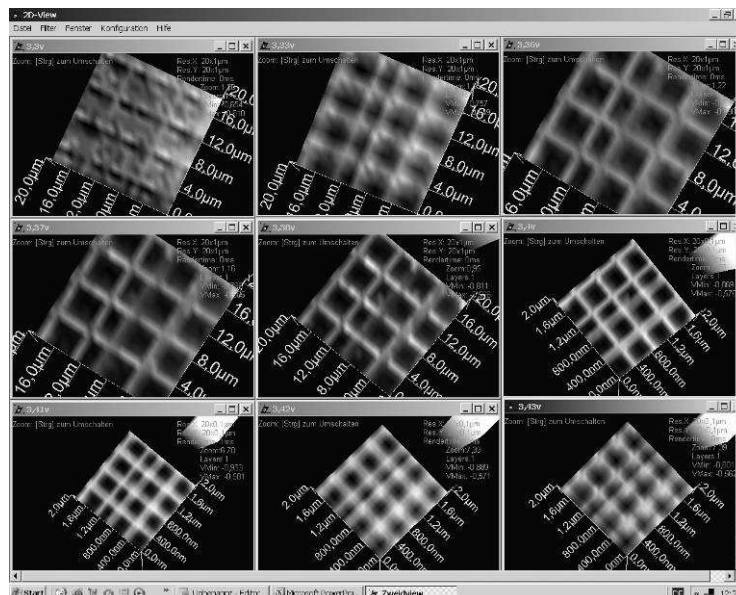
Fig. 6-48: *Varying position of the focusing lens and the produced surface images*

By using the optimal focal position of the lens, sharp images (Figs. 6-47 and 6-48) of the surface can be gained (please note that some impurities remain on the surface although it was cleaned before operation):
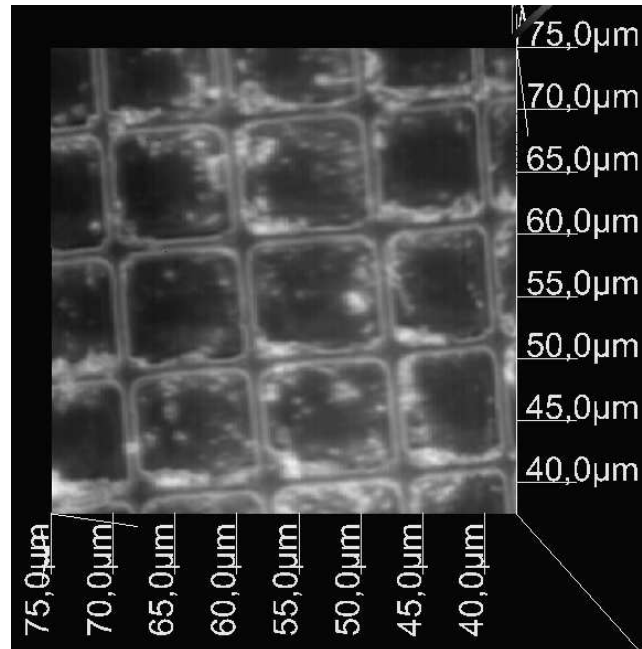
Fig. 6-49: *Image of the SEM test structure gained by confocal scanning*
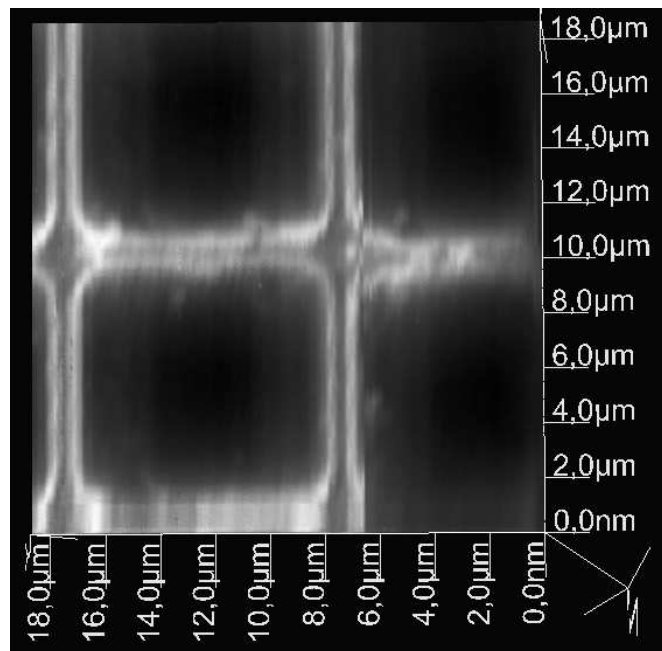
Fig. 6-50: *Detailed view of the SEM test structure gained by confocal scanning*

The imaging software (written for this work) is also capable of showing the measuring data in three-dimensional arrangement. Units in "z-"direction (colours) are arbitrary (Fig. 6-49):
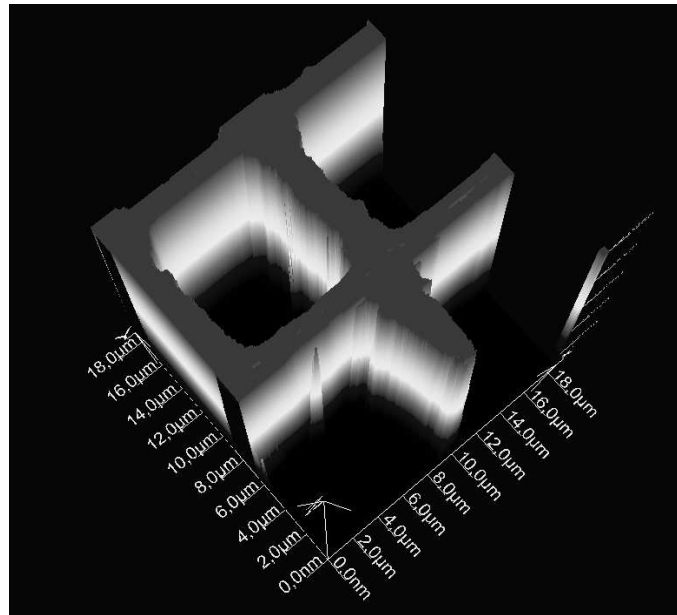
Fig. 6-51: *3- dimensional image of the measuring data gained by confocal scanning*

Figure 6-50, obtained by using a commercial atomic force microscope (AFM) (Bruker/ SIS Nanos), is intended to verify the grid size (9,87 µm) of the test structure in comparison with the results gained by confocal scanning:
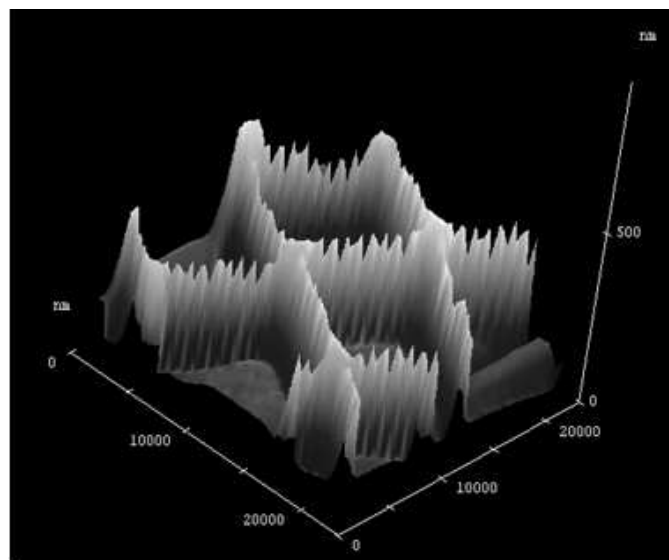
Fig. 6-52: *3-dimensional image of the test structure obtained by using an AFM*

To quantify the results of surface characterisation gained with the confocal device and to compare these results with the outcome of a commercial AFM, the surface profile of both results was extracted to determine the grid size (9,87 µm) of the test structure. Accordingly, the surface data displayed in Fig. 6-50 were converted into the Software "Gwyddion" (an open source data analysis tool) to define two "lines of interest" (Figure 6-53).
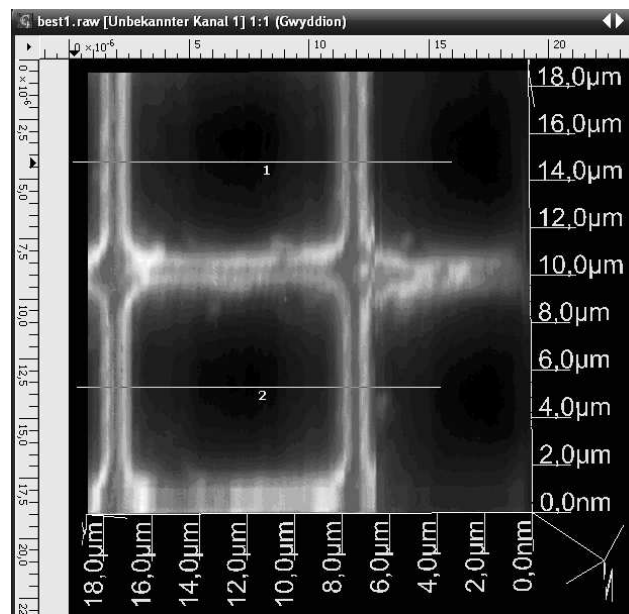
Fig. 6-53: *Test structure data loaded into "Gwyddion" software with two lines of interest (marked as "1" and "2") along the structure*

Figure 6-54 shows the extracted surface profile along the two lines of interest (LOI) marked in Figure 6-53 (line 1 = black and line 2 = red) and the calculated distances between characteristic points of the profile, representing the grid size of the test structure:
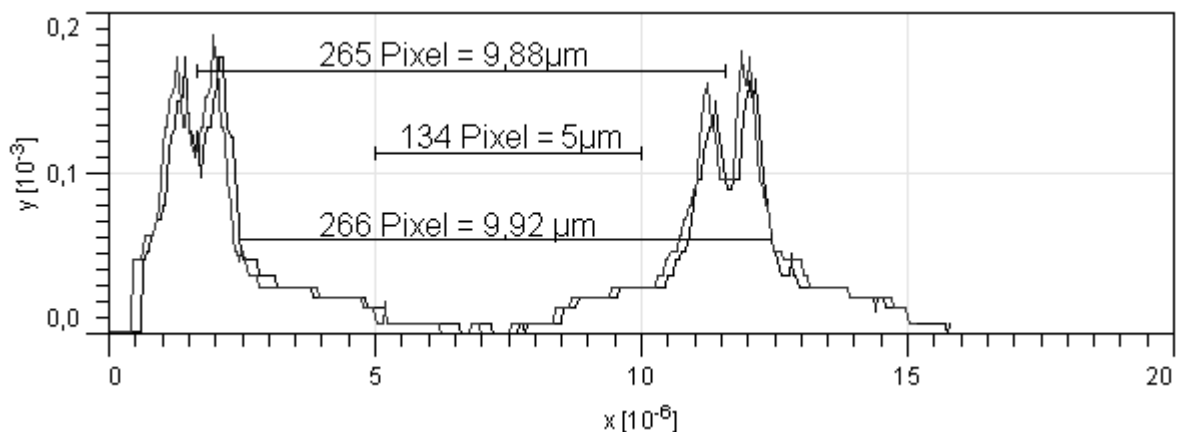
Fig. 6-54: *Extracted surface profile of the test structure gained by confocal scanning (top-top: 9,88µm; btm-btm: 9,92µm)*

In addition to the results gained by confocal scanning, Figure 6-55 shows the topography of the test structure obtained by AFM as well as the position of the associated line of interest:
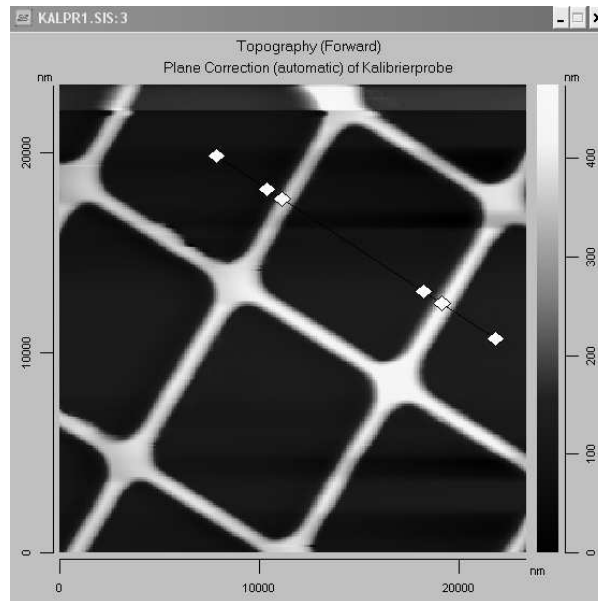
Fig. 6-55: *Topography and associated line of interest (LOI) of test structure obtained by AFM*

Figure 6-56 shows the extracted surface profile along the line of interest marked in Figure 6-55 and the calculated distances between characteristic points of the profile, representing the grid size of the test structure:
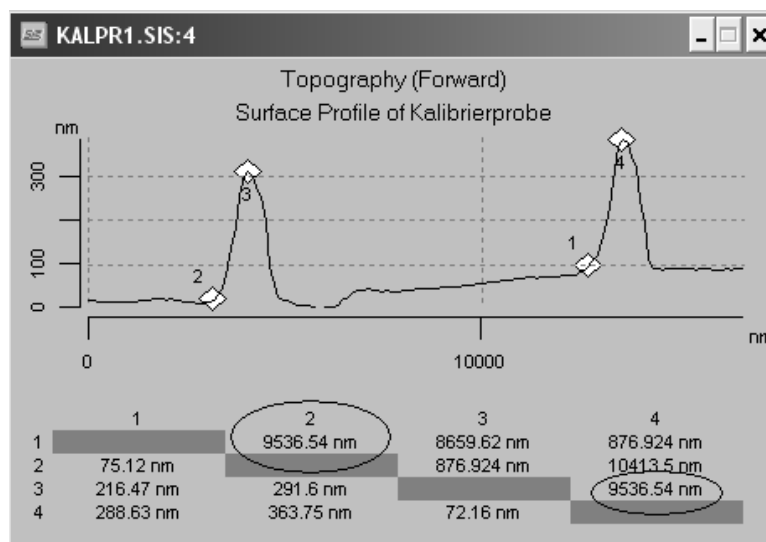
Fig. 6-56: *Extracted surface profile of the test structure gained by AFM (top-top: point 3-4; btm-btm: point 2-1)*

Comparing the grid size given by the results of confocal scanning and AFM with the measurement values stated in the measurement protocol of the manufacturer of the test

structure shown in Figure 6-57:
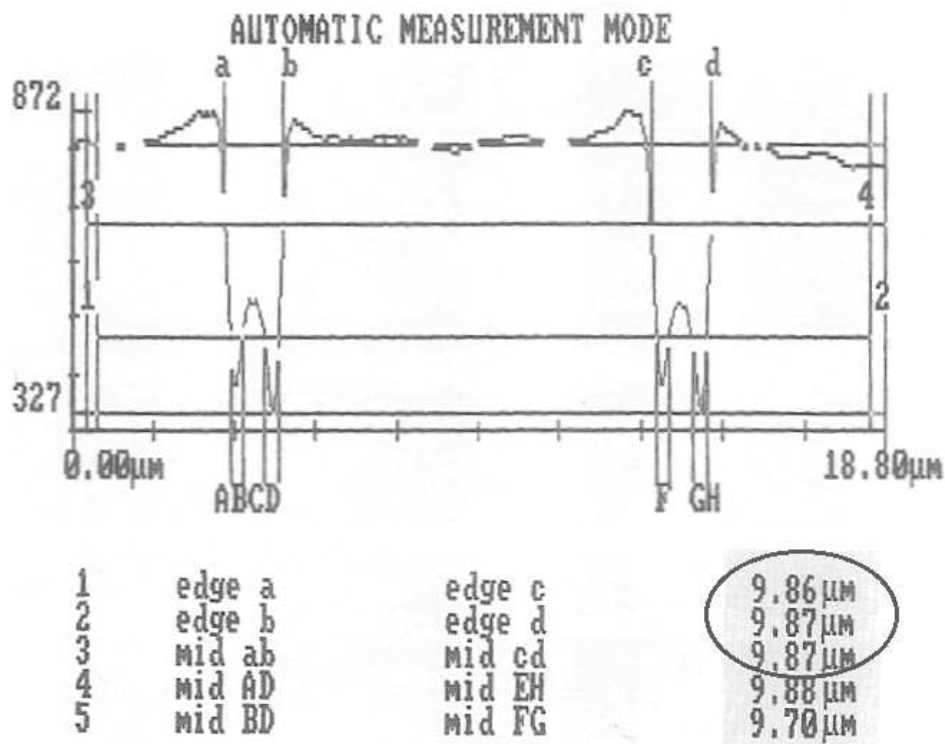
Fig. 6-57: *Grid dimensions given within the measurement protocol of the manufacturer (Plano 2009)*

it is obvious that the results of confocal scanning differ less from the manufacturer values than the results of AFM measurements (Table 6).

Table 6: Résumé of the obtained results identifying the differences between the quantitative measurements techniques (all values in μm):

	Manufacturer	Confocal	AFM	Δ Confocal	Δ AFM
Top-top	9,87	9,88	9,54	0,01	0,33
Btm-btm	9,86	9,92	9,54	0,06	0,32

The presented examples have demonstrated the appropriateness of the developed confocal system for surface structuring as well as characterisation of technical surfaces. The user of this system is able to produce surface structures and additionally to examine unknown surface profiles with high resolution and precision with results comparable to professional expansive equipment, on a low cost basis.

7. Discussions, Conclusions and Future Work

An environment for the micro- and submicrostructuring of technical surfaces by means of serial laser lithography - specifically, laser direct writing - has been developed. This development, the confocal system, further allows an optical scanning across an unknown surface to characterise its topography. A novel method of beam profiling, capable of characterising beam spots within the range of the diffraction limit, has been invented during this research. This method makes use of optical fibre tips applied within the scanning near-field optical lithography (SNOL) system, producing tomographical scans of the beam spot.

A wide range of operation within the fields of surface structuring and characterisation is covered by this device. Various patterns have been written into photo resist-coated substrates to structure their surface. Beginning with diffractive optical elements (DOE) for projection usage, followed by Dammann gratings for two-dimensional beam shaping and optical gratings for light guidance as well as producing technical surfaces imitating the properties of sharkskin or simple micro-mechanical structures, the technique has shown itself to be flexible and widely-applicable.

As the examples of surface structuring in Chapter 6.6 and the examples of surface characterisation in Chapter 6.7 have demonstrated, the developed confocal setup is very suitable to characterise and structure optical surfaces. The structured surfaces show a very precise transfer of the desired Bitmap pattern into the photo resist layer. In addition, the produced optical grating has proved the capability of the system to produce continuous surface profiles.

A comparison of the results gained by scanning a Scanning Electron Microscope (SEM) test structure to a commercial atomic force microscope (AFM) represents the quality of surface characterisation by means of the confocal setup.

Compared with the SNOL setup described in Chapter 3, the operation of the confocal system is much faster and offers a safer operation, due to the fact, that there is a greater distance between the lens of the confocal system and the object's surface.

Nevertheless, the SNOL system has the potential to structure smaller areas with a high resolution down to hundreds of nanometres.

Compared to other production techniques, the confocal system is highly cost-efficient, enabling laboratories to realise small batches of structured surfaces. The total costs of the confocal system ranges from 8 k€ up to 10 k€ compared to some 100 k€ for ion-beam or electron beam systems.

An increase in resolution can be gained by adapting Solid Immersion Lens (SIL) units, the designated successor of the Blu-ray optical disc technology. The SIL technology is being developed diligently and is intended to be commercially launched within the second half of this decade. Thus the system was developed without optimisation for a special purpose or application and it is constructed to be "SIL-ready".

Further enhancement of the system would include the application of faster stepping motors using micro-stepping mode for faster and more precise operation and/or adding a camera into the beam path of the optical pickup unit (OPU) for a more convenient alignment of the focussing lens above a surface.

Even though the developed system was intended to, and is capable of producing (as well as characterising) structures down to 750 nm, a very sophisticated goal would be to combine the high resolution of the scanning near-field optical lithography system (SNOL) with the fast and safe operation of the confocal device within one setup. A further idea would be to expose ("write") the "rough"- structures with the confocal device and write the smaller "sub-structures" by means of SNOL within a subsequent process.

This would require a very precise alignment of the substrate, for example with the aid of alignment marks, to ensure a coincidence of the "major"- structure written by means of the confocal system and the "sub"- structure written by means of SNOL.

Considering the novel method for beam profiling, measurement with calibrated light/laser sources can be carried out to gain quantitative instead of qualitative results.

References

Abbe, E. (1873); Beiträge zur Theorie des Mikroskops und der Mikroskopischen Wahrnehmung. Found in: Archiv für Mikroskopische Anatomie 9, 1873, 413-468.

Ash E.A., Nicholls G. (1972); Super-resolution Aperture Scanning Microscope; Nature 237; 510-512

Bartolini, R. A. (1977); Holography recording materials; Applied physics; Vol.20; 209-227

BBC (2008); Online resource:
http://news.bbc.co.uk/2/hi/technology/6135452.stm;
Accessed: [05.05.2008]

Bennet (2006); The Authoritative BD FAQ: III; Online resource:
http://www.emedialive.com/articles/readarticle.aspx?articleid=11632;
Accessed: [05.12.2009]

Bentley, J; (2002); Semi-custom DUV Micro-Objectives for OEM Applications; SPIE Conference; Online resource:
http://clearcurve.com/semiconductoroptics /pdf/Bentley_Hi-res_20020309.pdf;
Accessed: [12.02.2010]

Betzig, E., Finn, P. L., Weiner, S. J. (1992); Combined shear force and near-field scanning optical microscopy; Appl. Phys. Lett. 60; 2484

Betzig, E., Trautman, J.K., Wolfe, R., Gyorgy, E.M., Finn, P.L., Kryder, M.H., Chang, C.H. (1992); Near-field magneto-optics and high density data storage; Appl. Phys. Lett. 61, 142-144

Bloomfield, L.A. (2008); How Everything Works: Making Physics out of the Ordinary; Online resource:

http://howthingswork.virginia.edu/compact_disc_players.html;

Accessed: [19.06.2009]

Blu-Ray Disc Founders (2007); White paper Blu-ray Disc Format General Blu-ray Disc Association Administration; 3855 SW 153rd Dr.; Beaverton, OR 97006 USA

BRDAA (2010); Blu-ray Disc Association Administration; 3855 SW 153rd Dr.; Beaverton, OR 97006 USA

Brückner, H.J. (2007); Laboratory project documentation "laser diode"; FHOOW Emden; 2005

Burr Brown Corporation (2007); OPT 202 Datasheet, Monolithic photodiode with on- chip transimpedance amplifier

Chapple, P.B., (1994); Beam waist and M2 measurement using a finite slit; Opt. Eng., 33, 2461-2466

Conrad Catalogue (2008); Conrad Elekrtronic; Klaus-Conrad-Str. 1;92240 Hirschau; Germany

Cotton, D., Fell, C., Belcher, W., and Dastoor, P. C. (2008); The origin of fine structure in near-field scanning optical lithography of an electroactive polymer; J. Phys. D: Appl. Phys. 41; 195107

Credgington, C., Fenwick, O., Charas, A., Morgado, J., Suhling, K., Cacialli, F. (2010); High-Resolution Scanning Near-Field Optical Lithography of Conjugated Polymers; Adv. Funct. Mat. 20, 2842-2847

CT Magazine (1998); Number 7; Heise Verlag Heise Zeitschriften Verlag; Postfach 111428; 20414 Hamburg; Germany

CST Microwave Studio (2009); CST AG; Bad Nauheimer Str. 19; 64289 Darmstadt; Germany

CWE Catalogue (2010); Contact Wavelength Electronics, Inc.; 51 Evergreen Dr.; Bozeman, MT 59715; USA

Daedallaser (2009); Online resource: http://www.daedallasers.com/kes-400a.html; Accessed: [05.12.2009]

Datarius (2010); Online resource: http://www.datarius.com/news/white_paper-PDF/wp-bd-stamper-correlation-0408.pdf; Accessed: [15.11.2010]

Datasheet Shipley Microposit (2006); Rohm and Haas; 100 Independence Mall West; Philadelphia; Pa 19106; USA

Dammann,H; Gortler,K (1971); High-Efficiency In-Line Multiple Imaging by Means of Multiple Phase Holograms Opt. Commun. 3, 312

Damask, Jay N. (2004); Polarization Optics in Telecommunications; Springer. pp. 221–223

Dorf, Richard C.; Svoboda, James A. (2001). Introduction to Electric Circuits (5th ed.). New York: John Wiley and Sons, Inc.

Drezet, A., Nasse, M.J., Huant, S., Woehl, J.C., (2004), The optical near-field of an aperture tip; Europhys. Lett., 66 (1), 41–47

Dzur, B. (2007); Grundlagen der Oberflächentechnik; PhV-OT-Handout, 09/2007; TU Ilmenau; Kirchhoff-Bau K 3013; Postfach 100565; 98684 Ilmenau; Germany

Eerenbeemd, J.M.A. (2008); PhD. Thesis: Near-Field Optical Recording on Cover-Protected Discs; TU Delft; The Netherlands

Element Six Ltd. (2008); Kings Ride Park, Berkshire, SL5 8BP, UK.

213

ELV Catalogue (2009); ELV Elektronik AG; Maiburger Straße 29 - 36; 26789 Leer; Germany

Encyclopaedia Britannica (2009a); Article: Lithography; Encyclopaedia Britannica Online;
Accessed: [06/ 05 /2009]

Encyclopaedia Britannica (2009b); Article: MEMS; Encyclopaedia Britannica Online;
Accessed: [16/ 10 /2009]

Encyclopaedia Britannica (2009c); Article: Numerical aperture; Encyclopaedia Britannica Online;
Accessed: [03/ 05 /2009]

Endyn (2010); Endyn Energy Dynamics3144 S. Main St.; Ft. Worth, Texas 76110; USA; Online resource:
http://www.theoldone.com/articles /
Accessed: [16/ 10 /2010]

EPJ- European Physical Journal A (2002); Nr.3, Page 40
Fienup, J.R. (1980); Iterative method applied to image reconstruction and to computer generated holograms; Opt. Eng. 193; 297–305

Essaidi N., Chen Y., Kottler V., Cambril E., Mayeux C., Ronarch N., Vieu C. (1998); Fabrication and characterisation of optical fiber nanoprobes for scanning near field optical microscopy, Applied Optics, 37(4), 609-15

Gabor, D. (1971); HOLOGRAPHY, 1948-1971 Nobel Lecture; Imperial Colleges of Science and Technology; London;UK

Gemac (2009); Datasheet CVC 2.0; Gemac GmbH; Zwickauer Straße. 227; 09116 Chemnitz Germany

Goldberg, B.B., Unlu, M.S., Herzog, W.D., Ghaemi, H.F.,Towe, E. (1995); Near-field optical studies of semiconductor heterostructures and laser diodes; IEEE Journal of Selected Topics

in Quantum Electronics; Vol. 1, No. 4, 12/1995; 1073

Gross, R (2008); Licht als elektromagnetische Welle; Walther Meißner Institut; Walther-Meißner-Straße 8; 85748 Garching; Germany

Guillou, D. (2010); IC Mechanics, Inc.; New Manufacturing Methodology Substantially Reduces Smart MEMS Costs: An innovative capping technology opens doors to broader applications Online resource:
http://archives.sensorsmag.com/ articles/ 1203/20/ main.shtml;
Accessed: [14/ 02/2010]

Haase, C. and Stiebig, H. (2007) ; Thin-film silicon solar cells with diffractive elements; SPIE Newsroom. DOI: 10.1117/2.1200602.0150

Haumann, C., Pelargus, Ch., Frey, H. G., Ros, R., Anselmetti, D. (2005); Stand-alone device for the electrolytic fabrication of scanning
near-field optical microscopy aperture probes; Rev. of scientific instruments 76,033704

Hecht, B., Sick, B.; Wild, U.; Deckert, V.; Zenobi, R.; Martin, O. J.; Pohl, D. W.; (2000); Scanning near-field optical microscopy with aperture probes: Fundamentals and applications. - Jour. Chem. Phys., 112 7761

Hecht, E. (2001); Optics; Addison Wesley; 4. Edition

Heidelberg Instruments Mikrotechnik GmbH (2010); Tullastrasse 2; D-69126 Heidelberg; Germany Online resource:
http://www.himt.de/en/technology/optical-components.php
Accessed: [12.02.2010]

Herzog, W. D., Uenlue, M. S.,Goldberg, B. B., Rhodes, G. H., Harder, C. H. (1997); Beam divergence and waist measurements of laser diodes by near-field scanning optical microscope; Appl. Phys. Lett. 70 (6)

Hoipkemeier-Wilson, L., Schumacher J.F., Brennan, A.B. (2004); Antifouling Potential of Lubricious, Micro-engineered, PDMS Elastomers against Zoospores of the Green Fouling Alga Ulva (Enteromorpha); Biofouling, Volume 20, Issue 1 February 2004 , pages 53 – 63

Hoppe, S., Ctistis, G., Paggel, J., Fumagalli, P. (2004); Spectroscopy of the shear force interaction in scanning near-field optical microscopy; Ultramicroscopy 102 (2005) 221–226

Iizuka , K. (2008); Engineering Optics; Springer

Imlau, M. (2003); Script 24. April 2003 "CD-ROM" (ß-Version); Department of physics; University of Osnabrueck; Germany

Ito, T. and Okazaki, S. (2009); Pushing the limits of lithography; Nature 406, 1027-1031

JGU-Johannes Gutenberg Universität (2010); Online resource:

http://www.quantum.physik. uni-mainz.de/de/lectures/ 2007/ss07 _physik _III/index.html;

Accessed: [14/ 01/2010]

John Grossman Collection of Antique Images (2009); Online resource: http://johngrossmancollection.com /_wsn/page13.html;

Accessed: [13/ 04/ 2009]

Kluth, O. (1999); Texture etched ZnO:Al coated glass substrates for silicon based

thin film solar cells; Thin Solid Films 351 247-253

Klocke (2007); The Nanomotor, Technical manual; Klocke Nanotechnik GmbH;GmbH, Aachen ;2007

Komma, Y.; Compatible Objective Lens for Blu-ray Disc and Degital Versatile Disc Using Diffractive Optical Element and Phase-Step Element which Corrects both Chromatic and Spherical Aberrations; Japanese Journal of Applied Physics; Vol. 43, No. 7B, 2004, pp. 4768-4771

Kramper, P. (2002); PH.D. Thesis: Mikroskopie und Spektroskopie an photonischen Kristallen:

Einschluss von Licht auf Subwellenlängen-Bereiche; University of Konstanz; Germany

Krausch, G., Wegscheider, S., Kirsch, A., Bielefeldt, H., Meiners, J. C., Mlynek, J.(1995); Near-field microscopy and lithography with uncoated fiber tips: a comparison; Opt. Comm. 119, 283

Kreischer Optics (2007), Ltd. 729 Oak Drive, IL, USA; Online resource:
http://www. kreischer.com/ aspheres/primer.html;
Accessed: [01.05.2007]

Lambelet, P. (1998); Chemically etched fiber tips for near field optical microscopy: a process for smoother tips; Applied Optics, 37(31), 7289-92

Lee, Y.I., Park, K.H.; Lee, J.; Lee, C., Yoo, H.J.; Kim, C.H. (1997); Dry Release for Surface Micromachining with HF Vapor-Phase Etching; Journal of microelectromechanical systems, Vol. 6, No. 3

Leggett, G. J.(2006); Scanning near-field photolithography—surface photochemistry with nanoscale spatial resolution; Chem. Soc. Rev., 2006, 35, 1150–1161

Lila, N. H., Saib, D. P., Yeha, F. C., Changa, C. S., Tsonga, T. T., Hilangc, M. F., Liuc, C. J. (1998); Near-field optical characterisation of visible multiquantum—well semiconductor lasers; SPIE Vol. 3285;pp.59-65

Madsen S., Holme N. C. R., Ramanujam P. S., Hvilsted S., Hvam J. M., Smith S. (1998); Optimizingthe fabrication of aluminum coated fiber probes and their application to optical near fieldlithography, Ultramicroscopy, 71(1-4), 65-71

Magnes, J. Odera, D.,Hrtke, J.,Fountain, M., Florence, L., Davis, V. (2008); Quantitative and Qualitative Study of Gaussian Beam Visualization Techniques; eprint arXiv:physics/0605102; arXiv:physics/0605102v1; Online resource:
http://arxiv.org/PS_cache/physics/pdf/0605/0605102v1.pdf
Accessed: [21.08.2009]

Maruyama, K. (1995); A hybrid achromatic objective; Proc. SPIE, 2577, 123-129

Marti, O; Nahfeld mit fast-atomarer Auflösung; Hand-out; Universität Ulm; 89069 Ulm; Germany

Menz, W. and Mohr, J. (1997) ; Mikrosystemtechnik für Ingenieure; VCH-Wiley

McCally, R.L., (1984) Measurement of Gaussian beam parameters, Appl. Opt., 23, 2227

Microchemicals Technical Information (2007); Microchemicals GmbH; Schillerstrasse18; 89077 Ulm; Germany

Micronic Laser Systems AB (2010); P.O Box 3141; Nytorpsvägen 9; 183 03 Täby, Sweden

MIT (2010); Massachusetts Institute of Technology; Gas Turbine Laboratory; Online resource: http://www.rcuniverse.com/magazine/reviews/marsh/image21.jpg
Accessed: [11.01.2010]

Monos; University Leiden (2009); Huygens Laboratory; P.O. Box 9504; 2300 RA Leiden
Online resource:
http://www.molphys.leidenuniv.nl /monos/students/pdf/smon02.pdf;
Accessed: [07.08.2009]

Muranishi M., Sato K, Hosaka S., Kikukawa A., Shintani T., Ito K., (1997); Control of aperture size of optical probes for scanning near field optical microscopy using focused ion beam technology, Japanese Journal Appl. Phys, 36(7B), L942-4

Nadim M., Williams K. (2004); An Introduction to MEMs Engineering; Artech House Publishers; UK

Nakamura, S., Fasol, G., Stephen J. (2000); The Blue Laser Diode: The Complete Story, Springer; 2nd edition, October 2, 2000

National Physical Laboratory (2008); Serco House 16 Bartley Wood Business Park Hook Hampshire RG27 9UY United Kingdom Online resource:

http://www.kayelaby.npl.co.uk/ general_physics/2_6/2_6_5.html

Accessed: [11.04.2008]

Newport (2004); Newport main catalogue; "Technical Information optical fibres" Newport Corporation; 1791 Deere Avenue; Irvine, CA 92606; USA

Nexus (2009); NEXUS Market Analysis for MEMS and Microsystems III; WTC Wicht Technologie Consulting; Frauenplatz 5; 80331 München; Germany

Olsen, K. E. (1996); Holographic multi-stereogram constructed from computer images: Applied 3-D printer; University of Bergen, Norway; Online resource: http://www.fou.uib.no/fd/1996/h/404001/kap02.htm

Accessed: [14/ 02/2010]

Olympus (2009); Olympus Cooperation; 3500 Corporate Parkway Center Valley, PA 18034-0610; USA; Online resource:

http://www.olympus-global.com /en/corc/history/camera/auto.cfm;

Accessed: [11/ 10/2009]

Paesler, M.A. and Moyer, P.J. (1996); Near-Field Optics; Theory, Instrumentation and Applications. Wiley, Canada

Paul, Clayton R. (2001); Fundamentals of Electric Circuit Analysis; John Wiley & Sons

Pioneer Cooperation Japan (2008); Blu-ray Disc/DVD/CD Writer BD-R/RE, DVD-R/RW, DVD+R/+RW, CD-R/RW Online product overview; Online resource:

http://wwwbsc.pioneer.co.jp/product-e/ibs/

Accessed: [20.09.2008]

Plano GmbH (2009); Ernst Befort Str 12; 35578 Wezlar; Germany

Pohl, D.W., Denk, W., Lanz, M. (1984); Optical stethoscopy: Image recording with resolution $\lambda/20$; Appl. Phys. Lett. 44: 651

Rehwinkel J. (2008); Online resource:

www.vitriol.com

Accessed: [11.06.2008]

Reuk (2009); Online resource:

http://www.reuk.co.uk/40-Percent-Efficiency-PV-Solar-Panels.htm;

Accessed: [10/ 03/ 2009]

Ruiter, A. G. T., Veerman, J. A., van der Werf, K. O., van Hulst , N. F., (1997); Dynamic behavior of tuning fork shear-force feedback; Appl. Phys. Lett. 71 (1)

Scarrf T. (2010); Dublin institute of technology; School of Electronic and communications engineering; Online resource:

http://www.electronics.dit.ie/staff/tscarff

Accessed: [18/ 01/2010]

Scheck, F.(2009); Theoretische Physik 3. Klassische Feldtheorie; Springer

Siegman, A. E. (1986); Lasers. University Science Books. pp. 664–669

Schlarb, A; (2003); PhD thesis; Scherkraft- und optische Nahfeldmikroskopie; University Duisburg-Essen; Germany

Sony Cooperation (2008a); Online resource:

 http://www.scee.presscentre.com/content/detail.asp?released= 4268&newsareaid=2;

Accessed: [05.05.2008]

Sony Cooperation (2008b); Online resource:

http://www.scee.presscentre.com/Content/Detail.asp?ReleaseID=4317&NewsAreaID=2;

Accessed: [05.05.2008]

Sprut (2008); Messgerät für Kapazität und Induktivität; Joerg Bredendiek, Hückelhoven,

Germany; Online resource:

http://www.sprut.de/electronic/pic/projekte/lcmeter/lcmeter.htm

Accessed: [03.07.2008]

Stamm, U. (2004); Extreme ultraviolet light sources for use in semiconductor lithography—state of the art and future development; J. Phys. D: Appl. Phys. 37 3244

Stankovic, S (2002); Diffraktive Optische Elemente für moderne mikrooptische Systeme ; University of Darmstadt, Germany; Online resource:

http://deposit.dnb.de/cgibin/dokserv?idn=965146863&dok_var=d1&dok_ext=pdf&filename=965146863.pdf

Accessed: [14/ 01/2007]

Stöckle, R, Fokas, C, Deckert,V Zenobi R (1999); High quality near field optical probes by tube etching; Applied Physics Letters,75(2)

Suh Y., Zenobi R. (2000); Improved Probes for Scanning Near Field Optical Microscopy; Advanced Materials, 12(15), 1139

Tanaka, Y., Komma, Y., Shimizu Y.(2003); Tech. Dig. ISOM2003, Nara, Th-G-04; 222

Thoma, C. (2006); Anlage zum Abschlussbericht EFRE 2005.151„Verbund Lasertechnik"; FHOOW Standort Wilhelmshaven

Thorlabs (2010); Thorlabs Catalogue 2010; New Jersey; 435 Route 206 North; Newton, NJ 07860; USA

Tipler, A. , Mosca, G.; (2008); Physics for Scientists and Engineers, Sixth Edition, Volume 1; New York, NY; Worth Publishers; 666-670

Toppan (2009); Toppan printing Co. LTD.;1-5-1, Taito, Taito-ku, Tokyo; Japan Online resource: http://www.toppan.co.jp/english/products_service/pdf/photomask.pdf

Accessed: [26/ 11 /2009]

Tokai optical co. Ltd. (2007); Japan;

Online resource: http://www.tokai.com/ images/content/Aspheric-design. jpg;

Accessed :[05.2007]

Toshiba (2009); 1-1, Shibaura 1-chome, Minato-ku, Tokyo 105-8001, Japan; Online resource: http://www.toshiba.co.jp/about/press/2008_02/pr1903.htm; Accessed: [22.03.2009]

University Leiden (2009); Online resource:

http://www.molphys.leidenuniv.nl /monos/students/pdf/smon02.pdf;

Accessed: [07.08.2009]

United States Patent 5890796; Laser illuminated lighting system utilizing a diffractive optical element

United States Patent Application Publication #2006/0067196 A1: "Optical pickup and optical disk drive using same" (Sony)

United States Environmental Protection Agency EPA (2010); Office of Compliance Sector Notebook Project: Profile of the Fabricated Metal Products Industry; available at: http://www.epa.gov/compliance/resources/publications/assistance/sectors/notebooks/fab metsn.pdf, Accessed: [26/ 1 /2010]

University of Cape Town (2010); The electron microscope unit;

Online resource: http://sbio.uct.ac.za/Webemu/gallery/descriptions.php;

Accessed: [13/ 01/2010]

University of Neuchâtel (2009); IMT - Applied Optics; Online resource:

http://www-optics.unine.ch/former/microoptics/cantilever_ SNOM/ cantilever_SNOM.html

Accessed: [20/ 09/2009]

University of Rochester (2010); Chem 421: Introduction to Polymer ChemistryThe Chemistry of Photo resists; Online resource:

http://chem.chem.rochester.edu/~chem421/polymod2.htm

Accessed: [06/ 05/2010]

University of vienna (2010); Online resource :

https://elearning. mat.univie.ac.at/physikwiki/images/a/ac/Totalreflexion_k.jpg;

Accessed [05.05.2010]

USA Today (2008); Online resource:

http://www.usatoday.com/tech/gaming/2006-11-17-ps3-debut_x.htm;

Accessed: [05.05.2008]

Vawter, R. (2009); Physics Net; Western Washington University; USA

Veerman, J. A., Otter A. M., Kuipers. L., van Hulst, N. (1998); High definition aperture probes for near-field optical microscopy fabricated by focused ion beam milling; Applied Phys. Let. 72-24

WDR   (2007);   Westdeutscher   Rundfunk;   Köln;   Germany;   Online   resource: http://www.wdr.de/themen/forschung/physik/terahertz_strahlen/img /laserdiode _40jpg; Accessed: [20.06.2007]

Webb R.H. (1996); Confocal optical microscopy; Rep. Prog. Phys. 59 427–471

Wiki (2008); Online resource:

http://en.wikipedia.org/wiki/PlayStation_3;

Accessed: [05.05.2008]

Wright and Goldwasser (2008); Dissection of a Blu-ray Reader Assembly;

Online resource: http://repairfaq.cis.upenn.edu/Misc/Blu-ray/site1/diode.html;

Accessed: [11/ 6 /2008]

Wyrowski,F.,   Bryngdahl,   O.   (1988);   Iterative   Fourier-transform   algorithm   applied   to

computer holography; JOSA A, Vol. 5, Issue 7, pp. 1058-1065

Yamada, H. (2004); Unaxis;

Online resource: http://www.epcos.org /library/papers/ pdf_2004/02pp_yamada.pdf

Accessed: [01.11.2008]

Yariv, A. and P. Yeh, P. (1984); Optical Waves in Crystals; John Wiley & Sons, New York, p. 374.

Young, I.T., Vliet, R., J. Mullikin, J., F. Boddeke, F., Netten, H. (1993); Depth-of-Focus in microscopy, in: SCIA'93, Proc. of the 8th Scandinavian Conference on Image Analysis, Tromso, Norway, 1993, 493-498

Zemax (2009); ZEMAX Development Corporation; 3001 112th Avenue NE; Suite 202;

Bellevue; WA 98004-8017; USA

Zengerle, R. (2006); Mikrosystemtechnik 1; 6.Schichtabtragung durch Ätzen; Albert-Ludwigs-Universität Freiburg; Georges-Köhler-Allee 106; 79110 Freiburg; Germany

Ziel, R. (2007); Funktionsprinzip REM-EDX; Online resource:

http://de.wikipedia.org/w/index.php?title=Datei:Funktionsprinzip_REM.gif

Accessed: [14/ 07/2009]

Zijp, F. (2007); Near-field optical data storage; HBO Eindhoven; The Netherlands

Appendix

Software of the "Pioneer BDR 101" setup

An 8 Bit Bitmap picture is fractionised by the software into 256 grey levels, in order to expose it pixel by pixel into a photo resist. This is done by moving the linear stages point by point, and sending out an impulse at the positions given by the bitmap. Hereby the pixel is exposed into the resist layer. After developing of the photo resist the structure can be transferred through different etching mechanisms into the glass permanently. The necessary operating parameters:

- Trigger voltage (0-10V, default value: 1,4V) for the triggering of one
- Laser pulse signals
- Board ID (Number of the built-in NI-Motioncontrol-Cards, default: 1)
- Board ID (Number of the built-in NI-Motioncontrol-Cards, default: 1)
- Step wide / Pixel size (Default value: 600 nm)
- Acceleration (0 to 8x10^6 [Impulse/ s^2], (Servo parameter)
- Velocity (of 0 to 2x10^4 [Impulse/ s]) (Servo parameter)
- Denomination of the axes to be used (Default: X = Axis2 and Y = Axis1)

will be predefined with the given values at program start. These values can be changed later during system operation. The program offers the possibility of a manual shift of the X/Y-tables and a precise control on basis of the 8 Bit Bitmaps, to expose this picture into a resist layer by means of an optical fibre tip. The exposure is divided into several steps:

- Manual procedure: Moving to desired position, so that the glass substrate can be illuminated on a defined region
- Reading in data: Reads in 8 Bits Bitmap and indicates the gray-scale values in a table. Furthermore the height and the width in pixel are indicated.
- Lithography: Represent the screen for the illumination process. Some item data as well as the progress are indicated on this screen.

The front panel

— *The start screen*

The start screen (Fig. 1) is subdivided into three columns:

- To the hardware parameters: Board ID, X and Y axis
- To the speed parameters: Acceleration and velocity
- The Litho Parameters: Pixel size and trigger voltage

These parameters are explained in detail within the following:

Board ID

The board ID declares which PCI- card is supposed to be used; this is only important if several cards (Motion Controller 7344) are built into the computer.

X- and Y- Axis

The parameters X- and Y- Axis indicate at which port of the servo-booster the both axes are connected. The servo controller used in the construction has 4 connection options for servo motors. 2 ports are needed for the excitation.

Acceleration

The acceleration is measured in Counts/ s^2 * 1000, at what a Count corresponds to a movement of 75 nm. The default value (Default) is 550 * 1000 Counts/ s^2. This value is resetet onto its default value by pressing of the "Default" Button.

227

Velocity (Speed)

Acceleration is measured in Counts/ s * 1000, at what a Count corresponds to a movement of 75 nm. The default value (Default) is 19 * 1000 Counts/ s. This value is resetet onto its default value by pressing of the "Default" Button.

Pixel size

The pixel size indicates the distance in nanometres of the single pixels to each other. The default value (Default) is here 600 nm .This value is resettet onto its default value by pressing the "Default" Button.

Trigger voltage

The trigger voltage is the voltage, with that of the lasers is powered. The default value (Default) is 1,4V. This value is resetet onto its default value by pressing the "Default" Button.

Write operation : Start

By pressing of this button the loading procedure of a bitmap and the subsequent exposure of this onto the photoresist is initiated.

Manual positioning: Start

Through activity of this button a new surface is opened in order to position the x-y stages manually.

Lithography routine

After all parameters on the start surface are adapted and by pressing the "Start" button, a surface is opened (as shown in Fig. 2) to read in the 8 Bit bitmap data. The bitmap is analyzed by its gray-levels and the levels are indicated in a table. Furthermore the width and the height of the bitmap are indicated.
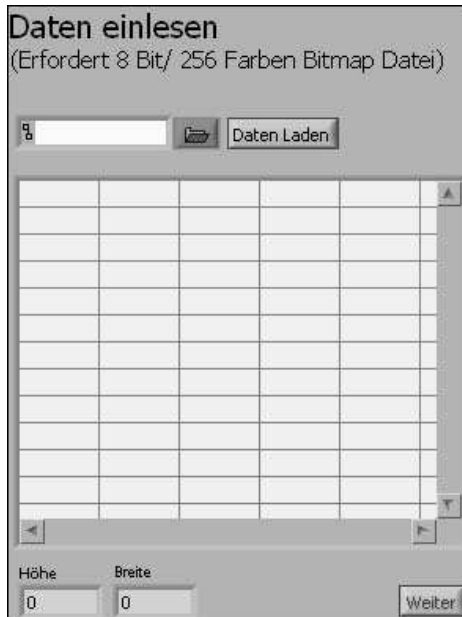
– "Reading in Data" screen

By pressing "weiter" the next screen (Fig. 3) appears showing some of the important parameters in the lithography process:
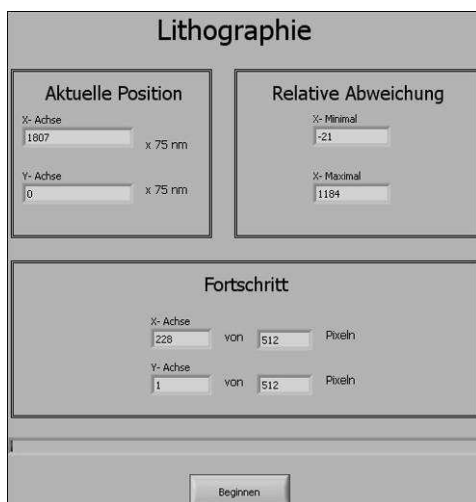
– *Lithography routine*

- The current position ("Aktuelle Position")

- The relative positioning error ("Relative Abweichung")

- And the progress of writing ("Fortschritt")

These parameters are explained in detail within the following:

Lithography: Current position

The column shows, according to the reference position, the current position of the linear stages. The distances of the x- and the y-axis are indicated in counts. A count corresponds to 75 nm.

Lithography: Relative deviation

This column is used for error analysis. It is possible to indicate the relative deviation by means of the "X-Minimal" and "X-Maximal" values. If the deviation is too high, the lithography process can be aborted, and started with other parameters again.

Lithography: Start

By pressing the "Beginnen" button the process starts and the laser exposes the picture into the photoresist

Lithography: Progress

Describes the progress of operation.

Hardware of the "Pioneer BDR 101" setup

Motion control card (PCI-7344) from National Instruments

Figure removed due to copyright restrictions

–   Motion control card (PCI-7344) for the servo motor

The card 7344 from National Instruments facilitates the connection of up to 4 servo or step engines.

- PID update rate range: 62.5 to 500 µs/sample

- Max PID update rate: 62.5 µs/axis

- Multi-axis synchronization: < 1 update sample

- Encoder feedback: ±1 quadrature count

- Long-term velocity accuracy: Oscillator based, ±100 ppm

- Velocity range: 1 to ±20,000,000 counts/s

- Acceleration/deceleration: 4,000 to 128,000,000 counts/s2

Digital/ Analog IO Card (6025e) from National Instruments

$-$ Digital/ Analog IO card (6025e) to control the exposure of photo resist layer

With the aid of this card the laser is switched on and off, to expose only the desired points into the photo resist layer. While collecting data in characterisation mode it converts the voltage from the photodiode. This card has the following inputs/outputs:

- 2 x   Analog Outputs (12Bit)
- 32 x   Digital I/O Pins
- 2 x   24Bit Counters

Servo Controller (MC - 4SA) from National Aperture, Inc. (NAI)
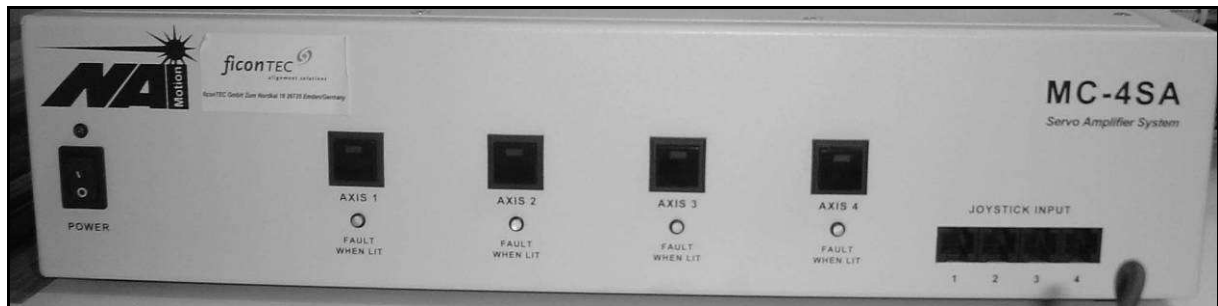
–   Servo Controller (MC - 4SA) from NAI

The servomotor signals that are distributed from the motion control card (NI PCI-7344) are processed and amplified through the servo controller. Furthermore, the servo controller uses the encoder signals from the servomotors to provide a precise and regular operation. This is done by a PID closed-loop circuit.

The front of the servo booster offers the possibility to deactivate single or several axes. To control selected axes manually, it is possible to connect a joystick to the servo controller at the front panel.

- Motor control input voltage: ±10 VDC across 300 K ohms

- Encoder voltage output: +5 VDC

- Max output power (Standard): 6 Watts

- Output voltage range: ±12 VDC

- Slew rate: 8 V /μS, maximum

- Voltage gain (Av): 1.2

233

Laser diode controller LDC 200 from Thorlabs

Figure removed
due to copyright
restrictions

−   Laser diode controller LDC 200 to control the laser diodes current

This controller drives the laser diode within the Blu-ray pickup depending on the input level it gets from the computer via its BNC input.

It is very important to operate the laser diode this way in order to avoid damage through overcurrent and to ensure the constant stability of emission, in order to expose the photo resist with the correct dose of light.

-       Control range (continuously variable) 0 ... ± 200 mA

-       Setting accuracy ± 0.1 mA

-       Resolution 10 µA

-       Accuracy ± 0.1mA

-       Compliance voltage > 6 V

Digital/ Analog IO USB Interface (6009) from National Instruments

Figure removed due to copyright restrictions

– Digital/ Analog IO USB Interface (6009)

The distance between lens and object surface is controlled by means of this interface due to the change of voltage applied to the coils, depending on the signal from the photodiode.

- 14-Bit, 48 kS/s Low-Cost Multifunction DAQ

- 8 analog inputs (14-bit, 48 kS/s)

- 2 analog outputs (12-bit, 150 S/s); 12 digital I/O; 32-bit counter

- Bus-powered for high mobility; built-in signal connectivity

- Compatible with LabVIEW, LabWindows/CVI, and Measurement Studio for Visual Studio .NET

Linear Servo stages MM-4-EX80 from National Aperture, Inc. (NAI)

Figure removed
due to copyright
restrictions

— Linear Stages (MM-4-EX80) to positionate the substrate

The used servo motors are characterized as follows:

- Gear ratio: 66:1

- Impulse Encoder: 74, 9 nm

- Repeatability: 100 nm

- Travel range: 80mm

- Precision: +/-500nm / 25mm

Two of these motors are arranged in x/y order in this setup. On the upper stage a rectangular fixture is mounted to hold the glass substrates.

Fresnel equations

Originally, the Fresnel equations had been derived from the elastic light theory by A.Fresnel (1821).Nowadays they are derived from the electromagnetic theory of light. This derivation has been carried out many times in the past. In order to prevent "reinventing the wheel": a very clear way of derivation, including the mathematical behaviour of total internal reflection (TIR), freely adapted by, but according to R.Gross from the Walther-Meißner Institute, Germany is shown:

Light at dielectric boundaries

The Fresnel equations describe the reflection, respect. the transmission of electromagnetic waves at a dielectric boundary. In our case this boundary is given by the intersection of the media of which the SIL consists and the media beneath it (here: air). The equations can be derived from the Maxwell's theory of electromagnetism:

Assuming the perpendicular incidence of a wave, the mathematical boundary conditions are:

$$E_{e0} + E_{r0} \quad = \quad E_{t0} \tag{3.1.1}$$

$$B_{e0} + B_{r0} \quad = \quad B_{t0} \tag{3.1.2}$$

where **E** describes the strength of the electric field, and **B** the magnetic flux density of the associated electromagnetic wave.

From Maxwell's equation: $\nabla \times E = \dfrac{-\partial B}{\partial t}$ follows: $B = \dfrac{1}{\omega}(k \times E)$. The wave number **k** is defined by: $k = 2\Pi/\lambda$ and the angular frequency **ω** by $\omega = 2\,\Pi\,\upsilon$. **υ** describes the frequency of waves: $\upsilon = \omega/k$.

Using this relationship, and substituting **B** and **E** within (3.1.2).With $k_r = -k_e$ and $k_i = n_i\,\omega/c$ one get:

$$n_e E_{e0} - n_e E_{r0} = n_t E_{t0} \tag{3.1.3}$$

After eliminating E_{t0} from the equation, the strength of the reflected field is given by:

$$E_{r0} = \frac{n_e - n_t}{n_e + n_t} E_{e0} = r\, E_{e0}$$ (3.1.4)

and

and:

$$E_{t0} = t\, E_{e0}$$ (3.1.5)

The coefficient of reflection **r**, respect. the coefficient of transmission **t** is defined by equation (3.1.14) : If light is travelling from an optic denser media onto the boundary layer, **r** becomes >0.E_r and E_e are pointing into the same direction, viz. they are "in phase".

The coefficient of reflection becomes <0, if the light is propagating from a optical thinner media towards the boundary layer, thus the electric field are antiparallel.

A phase shift of Π occurs between the propagating and the reflected wave: they oscillate out of phase. If only the intensity is necessary, the phase is irrelevant and we get for the grade of reflection for perpendicular incidence:

$$R = \left(\frac{n_e - n_t}{n_e + n_t} \right)^2 = \left(\frac{1 - n}{1 + n} \right)^2$$ (3.1.6)

Concerning the reflected intensity, the side from which the light is heading the boundary is insignificant. The grade of reflection (refer to 3.2.2) is only depending of the change of the refractive indices **n**. Using an air to glass interface, for example a window, with n_{glass}=1.5, 4% of the incident light is reflected. By higher refractive indices, the grade of reflection increases, e.g. diamond (n=2.41) reflects 17% of the incident light. If the light, respect. the waves, are not propagating in an perpendicular way to the boundary, things are looking a little bit different:

Two extremes can be distinguished:

1st case:
$$\mathbf{E} = \mathbf{E}_{\parallel} = -\mathbf{u_n} \times (\mathbf{u_n} \times \mathbf{E})$$

The electric field is parallel to the boundary and perpendicular to the plane, given by the wave vectors. The corresponding coefficients of reflection and transmission are defined by $r_{\perp}$

and t⊥.This case is called transversal electric polarisation (TE).

2$^{\text{nd}}$ case:
$$\mathbf{B} = \mathbf{B}_\parallel = -\mathbf{u_n} \times (\mathbf{u_n} \times \mathbf{B})$$

The magnetic field is parallel to the boundary and perpendicular to the plane, given by the wave vectors. This case is called transversal magnetic polarisation (TM).Due to the fact that the electric field is parallel to the plane given by the wave vectors, the coefficients of reflection and transmission are called: $r_\parallel$ and $t_\parallel$.

Figure removed due to copyright restrictions

Fig.7: *Illustration of TE and TM polarisation at a boundary [R.Gross]*

Considering the first case, the continuity of the tangential component of **E** gives us:

$$E_e + E_r \;\; = \;\; E_t \tag{3.1.7}$$

For the continuity of the tangential component for **H**:

$$-H_e \cos\theta_e + H_r \cos\theta_r \;\; = \;\; -H_t \cos\theta_t \tag{3.1.8}$$

Depending on Faraday´s law follow:

$$\mathbf{k} \times \mathbf{E} \quad = \quad \omega\,\mu_0\mathbf{H} \tag{3.1.9}$$

therefore:

$$k\,E \quad = \quad \omega\mu_0 H \tag{3.1.10}$$

from (3.2.1.7) is derived:

$$-k_e E_e \cos\theta_e + k_r E_r \cos\theta_r \quad = \quad -k_t E_t \cos\theta_t \tag{3.1.11}$$

So one of the three amplitudes within (3.1.6) can be eliminated:

By eliminating E_t and by using $n_i = ck$ and $n = n_t/n_e$ the amplitude reflection coefficient of the component perpendicular to the plane of incidence follows:

$$r_\perp \quad = \quad \left.\frac{E_r}{E_e}\right|_{\mathbf{TE}} = \frac{\cos\theta_e - n\cos\theta_t}{\cos\theta_e + n\cos\theta_t} \tag{3.1.12}$$

Using Snell´s law $n = \dfrac{\sin\Theta_e}{\sin\Theta_t}$ the refractive index can be eliminated from the equation:

$$r_\perp \quad = \quad \left.\frac{E_r}{E_e}\right|_{\mathbf{TE}} = -\frac{\sin(\theta_e - \theta_t)}{\sin(\theta_e + \theta_t)} \tag{3.1.13}$$

The TM-polarisation; viz. **B** parallel to the boundary can be derived the same way:

$$r_{\parallel} \;=\; \left.\frac{E_r}{E_e}\right|_{\mathbf{TM}} = -\,\frac{n\cos\theta_e - \cos\theta_t}{n\cos\theta_e + \cos\theta_t}$$ (3.1.14)

Using Snell´s law one can eliminate the refractive index and we get:

$$r_{\parallel} \;=\; \left.\frac{E_r}{E_e}\right|_{\mathbf{TM}} = -\,\frac{\tan(\theta_e - \theta_t)}{\tan(\theta_e + \theta_t)}$$ (3.1.15)

Fig.6 describes the relationship between the coefficient of reflection and the angle of incidence (for TE and TM polarisation).The left part shows waves propagating from an optical thinner media, and the right part shows waves propagation from an optical thicker media to a boundary. By increasing the angle of incidence, the coefficient of reflection increases also. For great angles it rises to 1: The critical angle (angle of total internal reflection, TIR) is reached even below 90 degrees by propagation from a denser media.

Figure removed
due to copyright
restrictions

Fig.8: *Amplitude reflection coefficient for air-glass (n=1.5) interface: left: propagation form thinner media (external reflection); right: propagation from optical denser media (internal reflection) [R.Gross]*

The amplitude transmission coefficient can be determined analogues by eliminating E_r within (3.1.6):

$$t_\perp = \left.\frac{E_t}{E_e}\right|_{\textbf{TE}} = \frac{2\cos\theta_e}{\cos\theta_e + n\cos\theta_t} \tag{3.1.16}$$

respectively:

$$t_\perp = \left.\frac{E_t}{E_e}\right|_{\textbf{TE}} = \frac{2\cos\theta_e\sin\theta_t}{\sin(\theta_e + \theta_t)} \tag{3.1.17}$$

and:

$$t_\parallel = \left.\frac{E_t}{E_e}\right|_{\textbf{TM}} = -\frac{2\cos\theta_e}{\cos\theta_t + n\cos\theta_e} \tag{3.1.18}$$

finally :

$$t_\parallel = \left.\frac{E_t}{E_e}\right|_{\textbf{TM}} = -\frac{2\cos\theta_e\sin\theta_t}{\sin(\theta_e + \theta_t)\cos(\theta_e - \theta_t)} \tag{3.1.19}$$

Grade of reflection and transmission

By using the energy theorem, the reflected or transmitted power of the light, respect. the grade of reflection or grade of transmission can be determined:

The reflected power (W_r) and the transmitted power (W_t) shall give summarized the incident power (W_e): $W_e = W_r + W_t$.

With $R = W_r/W_e$ follows:

$$R_\| = |r_\||^2 \quad \text{and} \quad R_\perp = |r_\perp|^2 \tag{3.2.1}$$

Using $T = W_t/W_e$ one get:

$$T_\| = 1 - |r_\||^2 \quad \text{and} \quad T_\perp = 1 - |r_\perp|^2 \tag{3.2.2}$$

It has to be noticed that the size of the area $A \propto d$ which is illuminated by a bunch of light waves d changes according to the refraction to $A' \propto d'$ (Fig.7):

$$T^W = \frac{W_t}{W_e} = \frac{I_t A'}{I_e A} = \frac{I_t \cos\theta_t}{I_e \cos\theta_e} = \frac{n_t \cos\theta_t}{n_e \cos\theta_e} |t|^2 \tag{3.2.3}$$

or:

$$T^I = \frac{I_t}{I_e} = T^W \frac{\cos\theta_e}{\cos\theta_t} = |t|^2 \frac{n_t}{n_e} \tag{3.2.4}$$

243

Fig.9: *Grade of reflection for air-glass (n=1.5) interface: left: propagation form thinner media (external reflection); right: propagation from optical denser media (internal reflection) [Wikipedia encyclopaedia]*

Total internal reflection (TIR)

By eliminating the angle of refraction Θ_t from (3.1.11) and (3.1.13) by mains of Snell´s law we gain the four Fresnel equations as a function of Θ_e and n:

$$r_\perp = \frac{\cos\theta_e - \sqrt{n^2 - \sin^2\theta_e}}{\cos\theta_e + \sqrt{n^2 - \sin^2\theta_e}} = -\frac{\left(\cos\theta_e - \sqrt{n^2 - \sin^2\theta_e}\right)^2}{(n^2 - 1)} \tag{3.3.1}$$

$$r_\parallel = -\frac{n^2\cos\theta_e - \sqrt{n^2 - \sin^2\theta_e}}{n^2\cos\theta_e + \sqrt{n^2 - \sin^2\theta_e}} \tag{3.3.2}$$

$$t_\perp = \frac{2\cos\theta_e\sqrt{n^2 - \sin^2\theta_e} - 2\cos\theta_e^2}{(n^2 - 1)} \tag{3.3.3}$$

$$t_\parallel = \frac{2n\cos\theta_e}{n^2\cos\theta_e + \sqrt{n^2 - \sin^2\theta_e}} \ . \tag{3.3.4}$$

In the following, the notation: external reflection for n>1 and internal reflection for n<1 (n: relative index of refraction), will be used.

Recap:

1. For a perpendicular incidence follows: $\quad r_\parallel = r_\perp = \frac{n_e - n_t}{n_e + n_t}$

The coefficients for reflection and transmission are equal, due to the fact, that the plane of incidence could not be defined.

2. For angles of incidence $\Theta_e \to 90°$ we get $r_\parallel = r_\perp \to -1$. This states, that all light heading to a boundary is reflected regardless of the size of $r_\parallel$ and $r_\perp$ at $\Theta_e = 0$. This behaviour can be observed for example in large corridors: The floor may look like a mirror, by looking at it under very flat angles ($\Theta_e = 90°$).

3. In case of external reflection, the term $\sqrt{n^2 - \sin^2\theta_e}$ within (3.3.1) and (3.3.2) always becomes bigger than 0:
The relationship between reflected and incident field amplitude has for both polarisations a real value.

245

4. The coefficient of reflection is always negative (3.2.3.1) for TE-polarisation at external reflection (n^2-1>0): A phase shift of Π occurs for all angles (see blue graph in Fig.6).Therefore the strengths of field for the reflected and incident wave head to opposite directions.

5. Using TM-polarisation, the phase shift changes from Π to zero (zero crossing of the $r_\parallel$ (Θ_e) graph, see red graph in Fig.8) at the **Brewster angle**:

By setting the numerator of (3.2.3.2) to zero:

$$n^2 \cos \theta_B = \sqrt{n^2 - \sin^2 \theta_B}$$

(3.3.5)

and therefore:

$$n^2 \cos^2 \theta_B = 1 - \frac{\sin^2 \theta_B}{n^2}$$

(3.3.6)

by substitution of 1 by $\sin^2 + \cos^2$ follows:

(3.3.7)

$$(n^2 - 1) \cos^2 \theta_B = (1 - \frac{1}{n^2}) \sin^2 \theta_B$$

finally one can get:

(3.3.8)

$$\frac{\sin^2 \theta_B}{\cos^2 \theta_B} = \tan^2 \theta_B = \frac{n^2 - 1}{1 - 1/n^2} = n^2$$

(3.3.9)

or:

$$\theta_{\text{Brewster}} \equiv \theta_B = \arctan n$$

(3.3.10)

$R_\parallel$ becomes 0 at the Brewster angle and no reflection occurs. This is given, if the

denominator in (3.1.13) and (3.1.15) diverges: either the angle of incidence $\tan(\Theta_b+\Theta_t)$ becomes ∞ or $\Theta_B+\Theta_t=90$. This would imply that the refracted beam and the reflected beam are perpendicular to each other. For light heading form air (n~1) to glass (n=1.5), for example, the Brewster angle is 56.3° .

The physical behaviour of reflection at the Brewster angle can be declared by the processes at/in the surface of the boundary layer:

Electrons within the affected media are stimulated to oscillate by means of the incident electromagnetic waves (polarization due to displacement of excess charges). Conglomerates of oscillating (in direction of polarisation) atomic dipoles generate secondary waves. These waves are reflected under the angle of reflection according to the laws of regular reflection (angle of incidence = angle of reflection) see Fig.10.

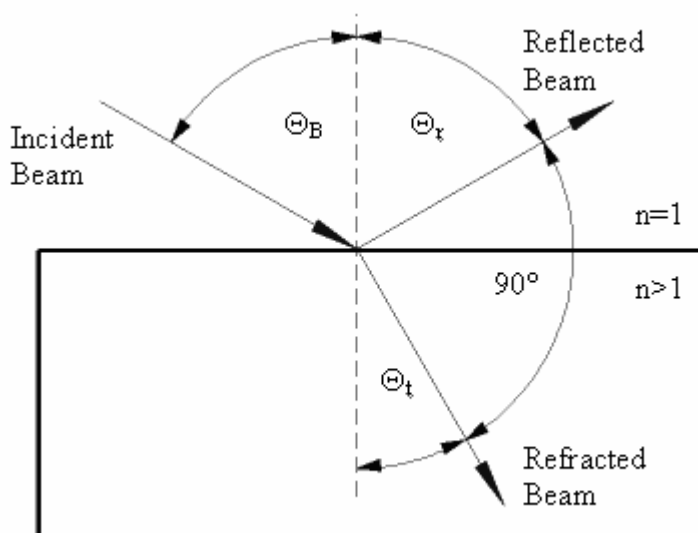**Fig.10:** *Sketch showing the Brewster angle Θ_B and the angle of the transmitted beam Θ_t*

A practical application of using the Brewster angle is given by so called Brewster-windows. These windows are commonly used in gas lasers for out coupling of light from the cavity. Parallel polarised light can pass this window without any loss, while perpendicular polarised light is partially reflected (Fig.11).

Fig.11: *Brewster window for out coupling of laser beam at a He-Ne laser tube [repairfaq]*

6. For internal reflection, the outcome for n^2-$\sin^2\Theta_e$ within the equations (3.3.1 $\rightarrow$ 3.3.4) becomes negative for all angles bigger than Θ_T=arcsin n.

The critical angle or angle of Total Internal Reflection (TIR) is defined by:

$$\theta_T \equiv \arcsin\left(\frac{n_t}{n_e}\right) = \arcsin n \tag{3.3.10}$$

Phase variation and Total Internal Reflection (TIR)

Considering external reflection (n_e<n_t) the phase is given by the algebraic sign of the coefficients of reflection- respect. transmission. From Fig.8 follows that, for external reflection, the phase shift of the perpendicular component is always -Π for all angles of incidence. The parallel component undergoes a phase shift of -Π until it reaches the Brewster angle and than skips to +Π.So the relative phase variation is 0 until the Brewster angle is reached and than skips to Π.

For internal reflection (n_e>n_t) the phase behaviour is comparable: Until the Brewster angle is reached the phase shift is 0 and than it skips to -Π. But at total internal reflection (TIR) the

amplitude reflection coefficients have a complex (imaginary) value.

To define this phase shift, the equations (3.3.11) and (3.3.12) can be written in their exponential form:

$$r_\perp = e^{-i\delta_\perp} = \frac{ae^{-i\alpha}}{ae^{+i\alpha}} = e^{-i2\alpha} \tag{3.4.1}$$

$$r_\parallel = -e^{-i\delta_\parallel} = -\frac{ce^{-i\gamma}}{ce^{+i\gamma}} = e^{-i2\gamma} \tag{3.4.2}$$

By comparison of the variables $r_\parallel$ and $r_\perp$ one can get:

$$ae^{-i\alpha} = \cos\theta_e - i\sqrt{\sin^2\theta_e - n^2} \tag{3.4.3}$$

$$ae^{i\alpha} = \cos\theta_e + i\sqrt{\sin^2\theta_e - n^2} \tag{3.4.4}$$

$$ce^{-i\gamma} = n^2\cos\theta_e - i\sqrt{\sin^2\theta_e - n^2} \tag{3.4.5}$$

$$ce^{i\gamma} = n^2\cos\theta_e + i\sqrt{\sin^2\theta_e - n^2} \tag{3.4.6}$$

with:

$$\delta_\perp = 2\alpha \quad \text{und} \quad \delta_\parallel = 2\gamma \tag{3.4.6}$$

The phase shift is:

$$\tan\frac{\delta_\perp}{2} = \frac{\sqrt{\sin^2\theta_e - n^2}}{\cos\theta_e} \tag{3.4.7}$$

$$\tan\frac{\delta_\parallel}{2} = \frac{\sqrt{\sin^2\theta_e - n^2}}{n^2\cos\theta_e} \tag{3.4.8}$$

Fig 17 shows the phase difference given by: $\Delta=\delta_\parallel-\delta_\perp$:

Fig.17: *Phase shift at Total Internal Reflection (TIR) for glass (n=1.5)-air (n=1) interface*

This phase shift results in an effect called "Goos-Haehnchen"- effect:

If polarised light is being total reflected a local shift **x** of the beam occurs depending on the phase, polarisation and critical angle Θ_T (Fig.17):

Fig.18: *Scheme showing the "Goos-Haehnchen"- effect [Meschede, D. (2005); Optik, Licht und Laser,;B.G. Teubner / GWV Fachverlage Wiesbaden]*

Lorentz force

This law describes the behaviour of a conductor (wire) with current passing through within a magnetic field:

Fig.23: *Scheme of a conductor within magnetic field [Wikipedia encyclopaedia]*

Considering that all charge carriers within the wire are travelling with the same velocity $\vec{v}$, the so called drift velocity, the electrical current can be determined by:

$$I = \frac{\Delta Q}{\Delta t}$$

(4.1)

251

Where ΔQ is the complete charge, which is moved through the wire within the time Δt. So N can be seen as the amount of charge carriers Q which are transported inside the wire whilst Δt. With ΔQ=N·Q one get:

$$I = \frac{N \cdot Q}{\Delta t}$$

<div align="right">(4.2)</div>

Multiplication of (3.3.2) with l and respecting that Δt is the period of time in which all charge carriers are moved by the distance l gives (by using $\frac{l}{\Delta t} = v$) :

$$I \cdot l = \frac{N \cdot Q \cdot l}{\Delta t}$$

<div align="right">(4.3)</div>

$$I \cdot l = N \cdot Q \cdot v$$

<div align="right">(4.4)</div>

Acknowledging the prefix of Q results in the fact, that $\vec{I}$ and Q·$\vec{v}$ are equiaxially and can be written in an vectorial form:

$$\vec{I} \cdot l = N \cdot Q \cdot \vec{v}$$

<div align="right">(4.5)</div>

The whole magnetic force generated by a magnetic field with a magnetic flux $\vec{B}$ belongs to the section l of the wire:

$$F_{Total} = l \cdot \vec{I} \times \vec{B} \tag{4.6}$$

$$F_{Total} = N \cdot Q \cdot \vec{v} \times \vec{B} \tag{4.7}$$

Considering that this force affects all charge carriers equally follows:

$$\vec{F} = Q \cdot \vec{v} \times \vec{B} \tag{4.8}$$

A force $\vec{F}$ appears when an object with a charge Q is moved with a velocity $\vec{v}$ inside a magnet field with a magnetic flux $\vec{B}$.

[Höfling, O.; Physics; Duemmler]

Calculation of dipoles at small openings

Considering that the opening of the fibre tip produces small electric dipoles:

$$\vec{E}_{Dipole} = \frac{1}{4\pi\varepsilon_0}\{k^2(\vec{n}\times\vec{p})\times\vec{n}\frac{1}{r} + [3\vec{n}(\vec{n}\cdot\vec{p}) - \vec{p}](\frac{1}{r^3} - \frac{ik}{r^2})\}\exp i(\omega t - \vec{k}\cdot\vec{r})$$

(5.1)

With: ε_0= vacuum permittivity; $\vec{n}$=unit vector; $\vec{k}$= wave vector: 2π / λ; ω= angular frequency of the oscillation and using the dipole-moment $\vec{p}$:

$$\vec{p} = (\frac{\varepsilon - 1}{\varepsilon + 2})\, a^3\vec{E}_{in}$$

(5.2)

With: a=diameter of the opening; ε_r=relative permittivity

The following terms for the far field (r << λ/2) and the near field (r >> λ/2) can be derived, and one gets not-propagating as well as propagating field components:

$$\vec{E}_{Near\,field} = \frac{3\vec{n}(\vec{n}\cdot\vec{p}) - \vec{p}}{4\pi\varepsilon_0 r^3}\exp i(\omega t - \vec{k}\cdot\vec{r})$$

(5.3)

Respectively:

$$\vec{E}_{Far\,field} = \frac{k^2(\vec{p} - \vec{n}(\vec{n}\cdot\vec{p}))}{4\pi\varepsilon_0 r}\exp i(\omega t - \vec{k}\cdot\vec{r})$$

(5.4)

The propagating field is directly linked to the near field and can be detected afar. The simulation of the electrical field generated by a plane wave of 1 V/m, heading to a fibre tip, is shown in Fig 3. Based on an optical power of 10mW dispersed on an area of 1 square micron, (which is a rather big area), one get by using:

$$I = S \cdot v = \frac{1}{2}E_0\,D_0\,c/n = \frac{1}{2}\varepsilon_0\,n^2\,E_0^2\,c/n$$

(5.5)

with:

I= Optical Intensity; S=Pointing vector; v=velocity; E_0=electrical field; D_0= electric induction density; n= index of refraction (here air: 1.0); ε_0= vacuum permittivity (rounded: 10^{-11} F/m)

$$E_0 = \sqrt{\frac{2I}{\varepsilon_0 nc}} \quad = 10^{10} \, V/m \tag{5.6}$$

Schematics of Hardware components

LPG µC device

Data removed

Add on board for ARM µC focal control device

Data removed

Common cathode laser diode driver

Data removed

The ARM µC evaluation board

(The following pages are extracted from the user's manual and should only give a brief overview of the evaluation board. This manual is © 2008 Olimex Ltd.)
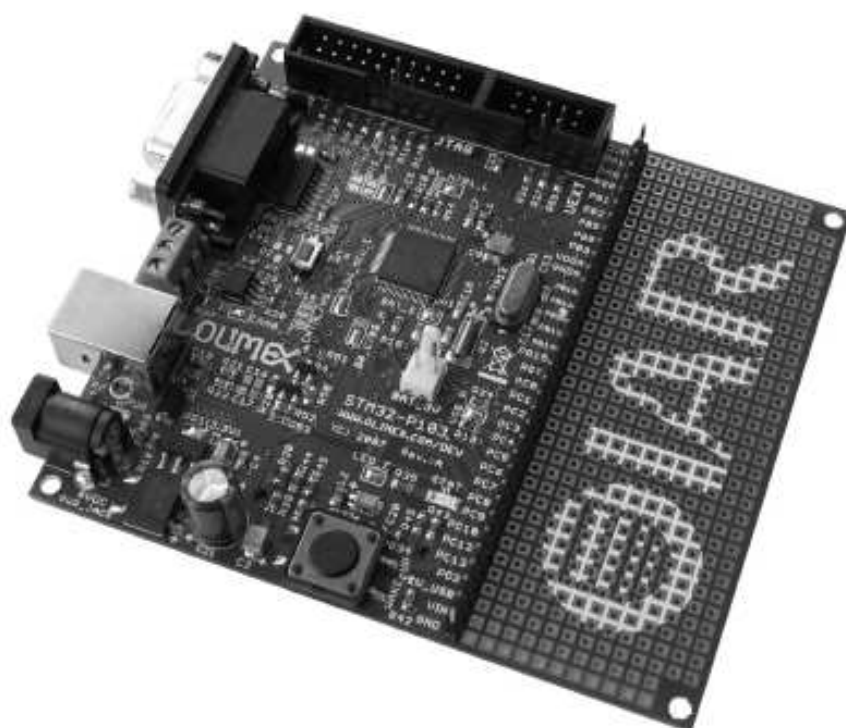
STM-P103 development board

Users Manual

INTRODUCTION:

STM32-P103 board is development board which allow exploring the complete features of the new ARM Cortex M3 STM32F103RBT6 microcontrollers produced by ST Microelectronics Inc.

The board have SD/MMC card connector and allow USB Mass storage device demo to be evaluated. The RS232 driver and connector allow USB to Virtual COM port demo to be evaluated. The CAN port and driver allow CAN applications to be developed. The UXT connector allow access to all other UEXT modules produced by OLIMEX like MOD-MP3, MOD-NRF24LR, MOD-NOKIA6610 etc to be connected easily. In the prototype area customer can solder his own custom circuits and to interface them to USB, CAN, RS232 etc.

BOARD FEATURES:

- CPU: STM32F103RBT6 ARM 32 bit CORTEX M3™
- JTAG connector with ARM 2x10 pin layout for programming/debugging with ARM-JTAG, ARM-USB-OCD, ARM-USB-TINY
- USB connector
- CAN driver and connector
- RS232 driver and connector
- UEXT connector which allow different modules to be connected (as MOD-MP3, MOD-NRF24LR, etc)
- SD-MMC connector
- backup battery connector
- user button
- RESET button
- status LED
- power supply LED
- on board voltage regulator 3.3V with up to 800mA current
- single power supply: takes power from USB port or extension connector pin
- 8 Mhz crystal oscillator
- 32768 Hz crystal and RTC backup battery connector
- extension headers for all uC ports
- RESET button
- status LED
- power supply LED
- on board voltage regulator 3.3V with up to 800mA current
  single power supply: takes power from USB port or power supply jack
- PCB: FR-4, 1.5 mm (0,062"), soldermask, silkscreen component print
- Dimensions: 100 x 90mm (3.94 x 3.5")

ELECTROSTATIC WARNING:

The STM32-P103 board is shipped in protective anti-static packaging. The board must not be subject to high electrostatic potentials. General practice for working with static sensitive devices should be applied when working with this board.

BOARD USE REQUIREMENTS:

Cables: 1.8 meter USB A-B cable to connect to USB host.
Hardware: ARM-JTAG, ARM-USB-OCD, ARM-USB-TINY or other ARM JTAG compatible tool
Software: ARM C compiler and debugger software, the possible options are:
  - free open source platform: GNU C compiler + OpenOCD and Eclipse (support all low cost Olimex JTAG debuggers)
  - commercial solution EW-ARM from IAR Systems AB, require expensive J-LINK debugger
  - CrossWorks from Rowley (supports all Olimex low cost JTAG debuggers).

## BOARD LAYOUT:

SCHEMATIC:

STM32-P103
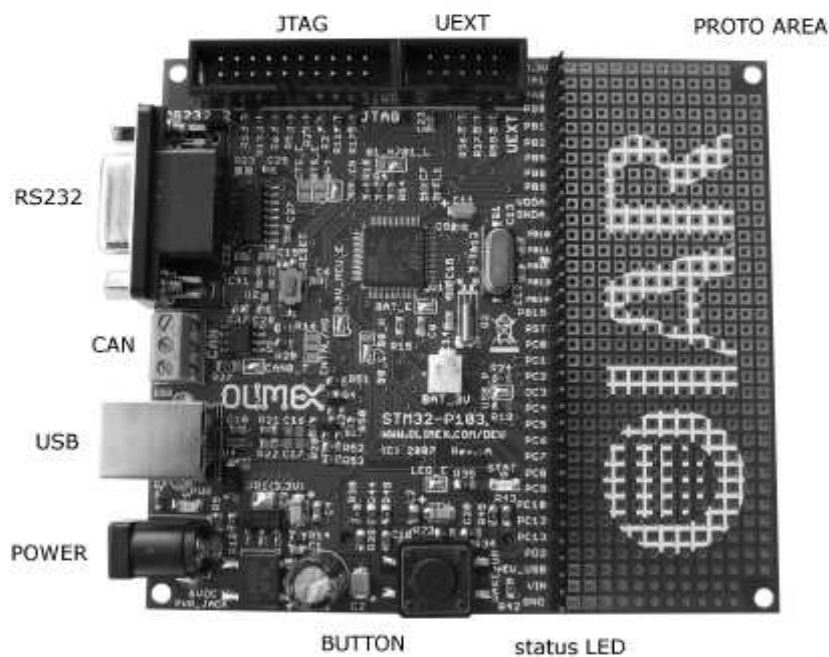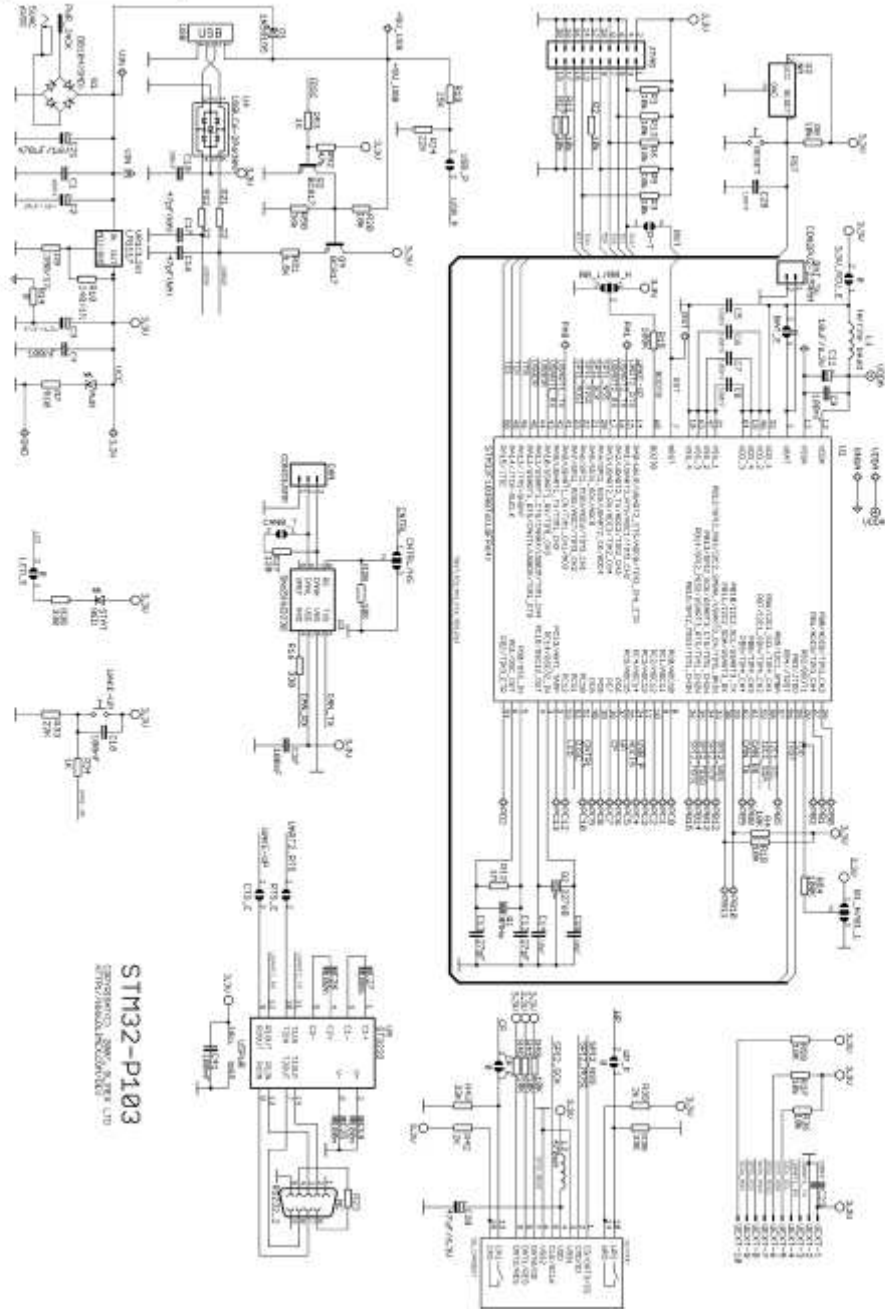
PROCESSOR FEATURES:

STM-P103 board use ARM 32-bit Cortex™-M3 CPU **STM32F103RBT6** from ST Microelectronics with these features:
- CPU clock up to 72Mhz
- FLASH 128KB
- RAM 20KB
- DMA x7 channels
- RTC
- WDT
- Timers x3+1
- SPI x2
- I2C x2
- USART x3
- USB x1
- CAN x1   (multiplexed with USB so both can't be used in same time)
- GPIO up to 51 (multiplexed with peripherials)
- 2 ADC 12-bit
- operating voltage 2.0-3.6V
- temperature -40C +85C

STM32F103xx performance line block diagram
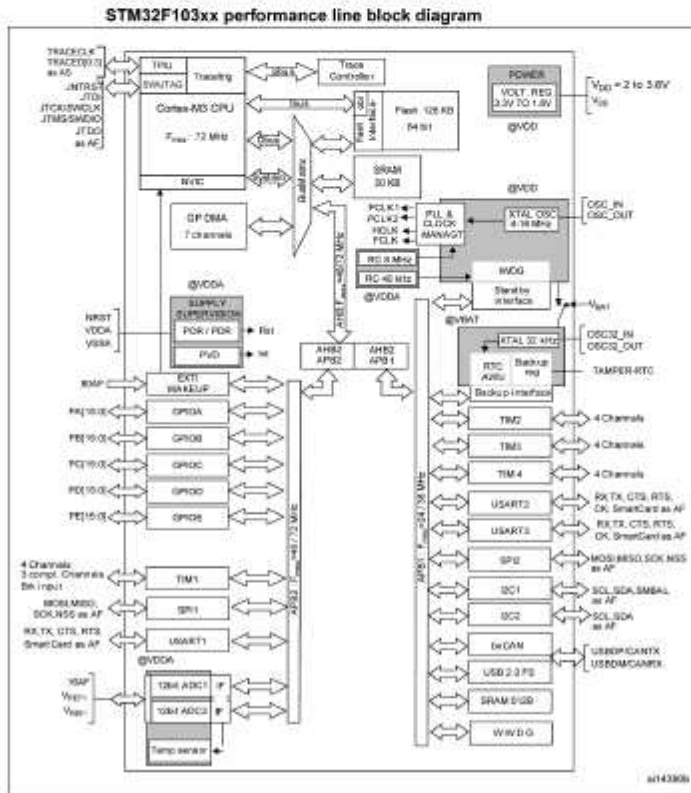
1. T_A = –40 °C to +105 °C (junction temperature up to 125 °C).
2. AF = alternate function on I/O port pin.
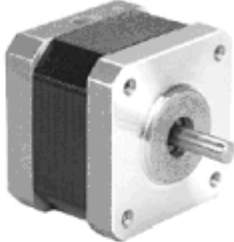
MECHANICAL DIMENSIONS:
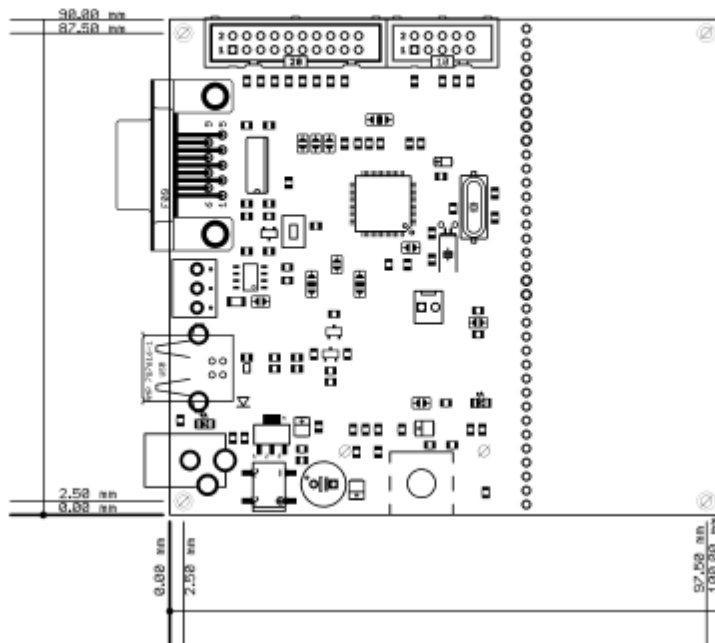
Stepping motor datasheets

The **17HA4401** motor manufactured by Moons (Shanghai Moons' Electric Co. Ltd; No. 168 Mingjia Rd.;North Minhang Industrial Park; Minhang District; SHANGHAI) :

17HA SERIES 0.9°

Key Features

■ High Accuracy
■ Low Noise
■ Smooth Movement

General Specifications

Bi-polar

Model Number	Resistance per Phase	Inductance per Phase	Rated Current	Holding Torque		Detent Torque		Rotor Inertia	
	ohm	mH	A	mNm	oz-in	mNm	oz-in	g.cm²	oz-in²
17HA0403-44N	8	11	0.43	90	12.75	8	1.13	20	0.11
17HA4401-05N	3.1	3.6	0.87	180	25.50	12	1.70	38	0.21
17HA4402-16N	20	23	0.5	220	31.16	12	1.70	38	0.21
17HA7402-06	6.6	7	0.65	70	9.92	5	0.71	15	0.08
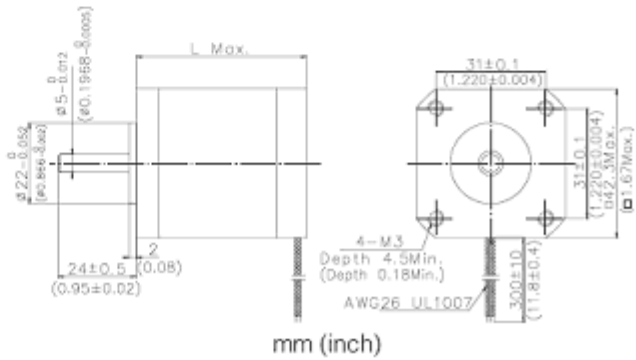
Uni-polar

Model Number	Resistance per Phase	Inductance per Phase	Rated Current	Holding Torque		Detent Torque		Rotor Inertia	
	ohm	mH	A	mNm	oz-in	mNm	oz-in	g.cm²	oz-in²
17HA0601N	8	4	0.43	50	7.08	8	1.13	20	0.11
17HA4605N	3.1	2.3	0.87	160	22.66	12	1.70	38	0.21
17HA4606N	20	13	0.5	200	28.33	12	1.70	38	0.21
17HA7602	6.6	2.9	0.65	30	4.25	5	0.71	15	0.08

Motor Wiring Diagram —> Page A-8

Mechanical Dimension

Model Number	L	Mass
	mm (in.)	kg (lb.)
17HA0**N	28 (1.10)	0.19 (0.42)
17HA4**N	34.3 (1.35)	0.23 (0.51)
17HA7**	20 (0.79)	0.12 (0.26)

mm (inch)

The **P542-M48-G06** geared stepper motor manufactured by Mclennan (Mclennan Servo Supplies Ltd.Unit 1, The Royston Centre; Lynchford Road, Ash Vale, Surrey, UK):
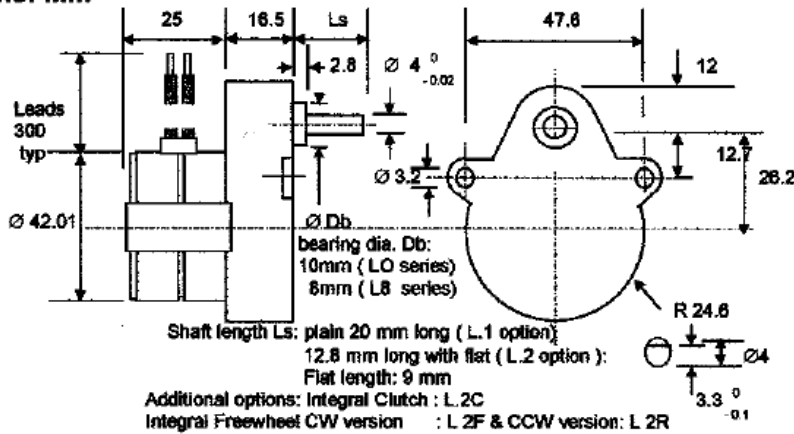
Geared Stepper Motor

The P5-M48 series provides a combination of optimum performance and price for use in instrumentation applications which require digital control of position and speed. Features include:

- High performance permanent magnet stepper motor
- Precision Ovoid gearhead incorporating metal gears for optimum torque transmission
- Wide range of standard gear ratio options from stock
- Choice of output shaft options
- Optional integral freewheel and clutch
- Special shaft and gear ratios to meet customer special requirements

Dimensions: mm

Leads 300 typ

Ø 42.01

Ø Db
bearing dia. Db:
10mm (LO series)
8mm (L8 series)

Shaft length Ls: plain 20 mm long (L.1 option)
12.8 mm long with flat (L.2 option):
Flat length: 9 mm
Additional options: Integral Clutch : L.2C
Integral Freewheel CW version : L 2F & CCW version: L 2R

P542-M48 geared stepper motor performance

Geared Stepper Motor	Ratio	Steps per rev. at output	Holding Torque (Ncm)	Max Working Torque (Ncm)	Typical Working Torque (Ncm)
P542-M48 -G01....	25:6	200	19.8	13.5	6.0
-G03	25:4	300	29.7	20.3	9.0
-G04	25:3	400	39.6	27.0	12.0
-G05	10:1	480	42.9	29.3	13.0
-G06	25:2	600	53.6	36.6	16.3
-G08	50:3	800	71.5	48.7	21.7
-G09	20:1	960	85.8	58.5	26.0
-G11	25:1	1,200	100.0	73.1	32.5
-G14	100:3	1,500	100.0	97.5	43.3
-G16	125:3	2,000	100.0	100.0	54.2
-G17	50:1	2,400	100.0	100.0	65.0
-G19	125:2	3,000	100.0	100.0	72.5
-G21	250:3	4,000	100.0	100.0	90.0
-G23	125:1	6,000	100.0	100.0	100.0
-G27	250:1	12,000	Use P535-M48 series for ratios of 250:1 and above		

Standard Versions:		P542-M482U	P42-M481U		Step rate @	
Number of phases		4	4		typical working	
Rated voltage (L/R Drive)		12	5		torque	
Current per phase	(mA)	230	550		L/R :	300 Hz
Resistance per phase	(Ohms)	52.4	9.1		L/4R:	550 Hz
Inductance per phase	(mH)	51.7	8.1			

Publications

(In chronological order; only those listed where Main author = Hauke Buse)

DGAO Proceedings 2006

Production of Diffractive Optical Elements by means of nearfield lithography

H.Buse, F.Ahnepohl, F.Buchmüller, R.Parkin*, H.Kreitlow

Fachhochschule Oldenburg / Ostfriesland / Wilhelmshaven Constantiaplatz 4 26723 Emden
* Mechanical and Manufacturing Engineering / Loughborough University Leicestershire LE11 3TU UK

mailto:hauke.buse@fho-emden.de

In order to increase the diffraction efficacy of Diffractive Optical Elements (DOEs), the production of substructures, with structure widths in the sub-micron range, is necessary. A possibility to that represents the Scanning Nearfield Optical Lithography (SNOL).

1 Introduction

Limits of optical resolution due to diffraction ("Abbe limit") can be bypassed through the use of Scanning Nearfield Optical Lithography (SNOL). As shown in Fig.1, only those object information are out spreading-capable beyond the nearfield, which originate structure sizes larger $\lambda/2$.
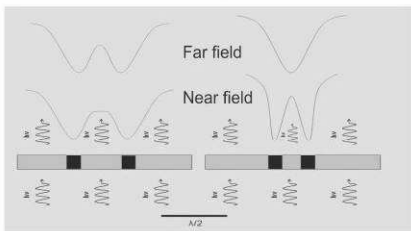
Fig.1 Nearfield principle

SNOL is used to expose the photo resist layer. Thereby a small fibre tip (Fig. 2), which is led over the surface by few 10nm in a distance, is used.
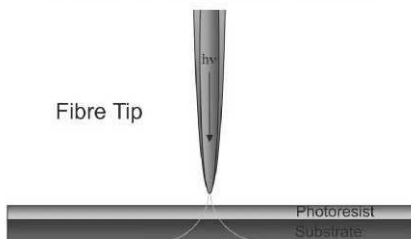
Fig.2 Scheme of SNOL

Structures within the sub-micron range can be produced by the small aperture (approx. 100 nm) of a fibre tip, and the small distance to the surface.

2 Construction of the SNOL-system

The laser beam from a He-Cd laser is guided to the photo resist layer through an optical fibre with a shaped tip, and intensity controlled via an acousto-optic modulator (AOM). The distance regulation of the fibre tip occurs via shear-force interaction.
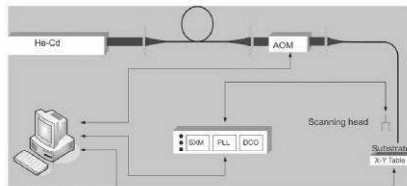

Fig.3 Block diagramm SNOL

The fibre tip is forced to oscillate by a ditherpiezo. If the distance to the surface is smaller than 30 nm, the oscillation of the tip is subdued by the shear force interaction. This damping is measured by a tuning fork.

Fibre tip production

To produce the tips, the coating of the monomode optical fibre is not removed before its immersion in hydrofluoric acid (40%).
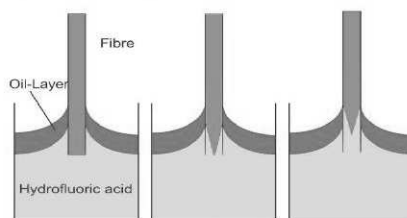

Fig.3 Sketch of fibre production process

265

Due to gravitive degradation of the glass products, a concentration slope arises in the hydrofluoric acid which causes convection. The convection carries the hydrofluoric acid into the upper zone of the tip which develops thus conically (Fig.5)
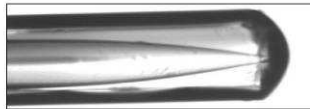

Fig.4 *Fibre top after the etching*

After the etching the residual coating is removed chemically (Fig.6) and the tip metalized. The aperture at the fibre tip is created by etching of the metal layer and/or through a lift-off procedure in a further process step.
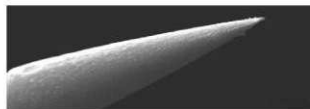

Fig.5 Fibretip after coating removal

3 Lithography on confokal basis

An alternative to the mentioned procedure to expose the photoresist represents the lithography by means of a confocal construction (Fig.7/8). With this, it possible to structure a photo resist layer also in the sub micrometer range and to characterize the result
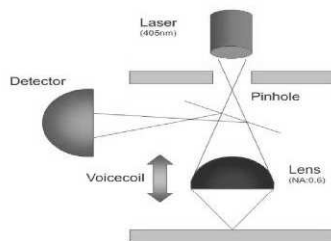
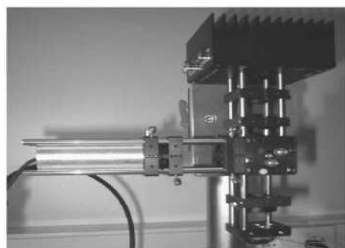

Fig. 7 Principle of the confocal setup

Fig. 8 The confocal setup

The used laser has a wavelength of $\lambda=405nm$. Fig. 9 shows the Scan of a commercially produced moire grating (Grid: 80 line pairs / mm).
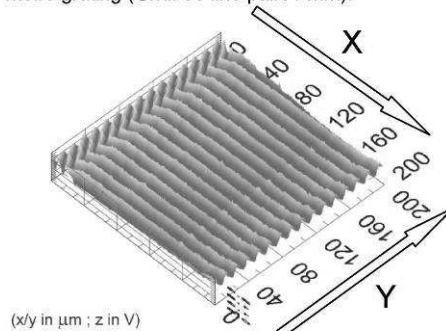

(x/y in µm ; z in V)

Fig. 9 *Scan of a moire grating*

4 Results

It has been shown, that the SNOL-system as well as the confocal system is adequate to produce structures smaller than 800nm (Fig.10+11).With finer apertures of the fibre tips, structure sizes of 400nm shall be realized.
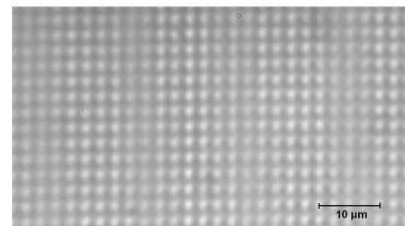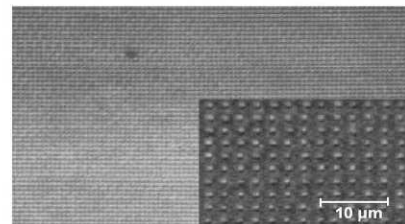

Fig.10 *DOE structure made with SNOL*

Fig.11 DOE structure made with confocal-system

Literature

[1] Suh Y, Zenobi R, Improves Probes for Scanning Near Field Optical   Microscopy, Advanced Materials, 12(15), 1139, (2000)

[2] Physik Journal 1 (2002) Nr.3,Seite 40

Einsatz der Nahfeldlithografie /-mikroskopie zur Strukturierung bzw. Charakterisierung von DOE´s sowie zur Vermessung von Laserstrahlprofilen

H.Buse, F.Buchmüller, R.Parkin*, H.Kreitlow

Fachhochschule Oldenburg / Ostfriesland / Wilhelmshaven Constantiaplatz 4 26723 Emden

* Loughborough University Leicestershire LE11 3TU UK

Die Herstellung von Diffraktiv Optischen Elementen erfolgt durch Mikrostrukturierung von Oberflächen optischer Bauteile mithilfe lithografischer Verfahren mit Ortsauflösungen im Bereich einiger Mikrometer. Um den Beugungswirkungsgrad dieser DOEs zu erhöhen ist darüber hinaus die Bildung von Unterstrukturen notwendig, die Strukturbreiten im Submikrometerbereich erfordern.

Es wird sowohl über die Entwicklung eines SNOL- und eines Konfokalsystems, mit denen diffraktive Optiken (DOE) mit Strukturbreiten im Mikrometer- bzw. Submikrometerbereich hergestellt und charakterisiert werden können, als auch über die Herstellung der benötigten Faserspitzen für das SNOM/SNOL Verfahren berichtet.

1 Einführung

Diffraktiv Optische Elemente (DOE´s) transformieren eine optische Wellenfront in eine beliebig anders gestaltete Wellenfront. Sie sind im Allgemeinen ebene optische Bauteile mit kleinen Abmessungen, sowie geringem Gewicht, und sind multifunktional und in der Regel kostengünstig herstellbar.

Im Vergleich zu den refraktiven Optiken, welche die Brechung des Lichts verwenden, nutzen DOE das Phänomen Beugung an einer Mikrostruktur und das Überlagern von Lichtwellen zu einem Interferenzmuster (Hologramm). Die Berechnung der diffraktiven Mikrostrukturen erfolgt mit Hilfe des sog. IFT-Algorithmus. Mit diesem wird aus der vorliegenden optischen Wellenfront und der transformierten Wellenfront die für die Transformation benötigte Mikrostruktur berechnet.

Abb. 1 *Prinzip des IFT-Algorithmus zur Berechnung diffraktiver Strukturen*

Abb. 2 *Von der IFTA Software berechnete Intensitätsverteilung der beugenden DOE- Struktur (rechts) und des aus einem Gaussstrahl gebeugten Grauwertbildes (Mitte)*

2 Umgehung des Beugungslimits

Klassische Verfahren zur Übertragung von Mikrostrukturen in (Fotolack-) Oberflächen wie z.B. die Maskenlithografie oder auch direkt schreibende Verfahren (Laser Pattern Generator) sind aufgrund von Beugungseffekten mit einer Auflösungs-limitierung behaftet, welche durch die Abbe Gleichung beschrieben werden kann:

Hierbei ist die kleinste mögliche Ortsauflösung Δx proportional zur verwendeten Belichtungswellen-länge λ und umgekehrt proportional zur numeri-schen Apertur NA der Belichtungsoptik.

$$\Delta x = \frac{0{,}61 * \lambda}{NA}$$

Durch den Einsatz des Scanning Nearfield Optical Lithography (SNOL) -Systems kann die Begrenzung der optischen Auflösung umgangen werden.

Wie in Abb.3 zu erkennen ist, sind nur diejenigen Objektinformationen über das Nahfeld hinaus ausbreitungsfähig, die einer Struktur größer $\lambda/2$ entstammen.
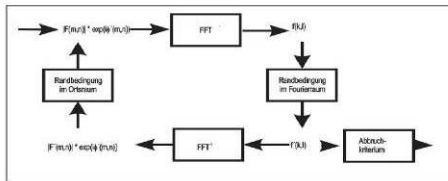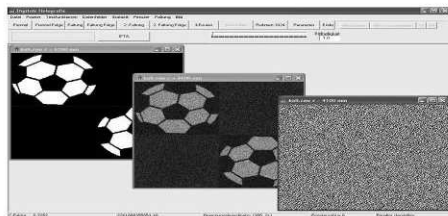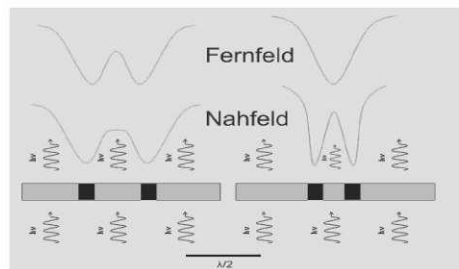

Abb. 3 *Prinzip des Nahfeldes*

Das SNOL-System wird zum Belichten der Fotolack-schicht eingesetzt. Dabei wird eine ausgezogene Lichtleitfaserspitze mit einer Apertur von ca. 100nm (Abb. 4) benutzt, die in einem Abstand von wenigen

10nm über die Fotolackoberfläche geführt wird. Dadurch können Strukturen im Sub-Mikrometerbereich erzeugt werden.
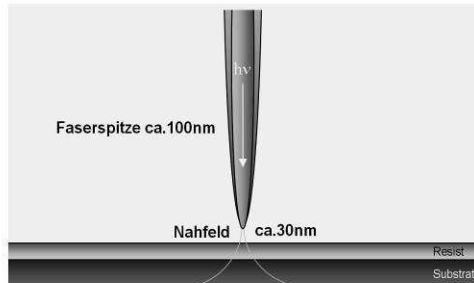

Abb. 4 *Schema der Belichtung mit SNOL-Faserspitze*

Faserspitzenherstellung

Zur Spitzenherstellung wird die äußere Ummantelung (Coating) einer Monomode Glasfaser vor dem Eintauchen in 40%ige Flusssäure nicht entfernt.
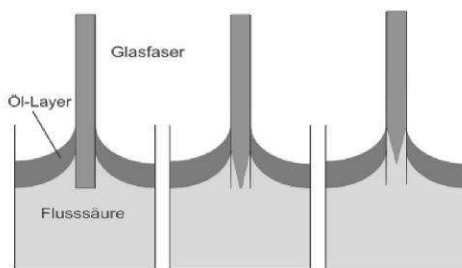

Abb. 5 *Prinzipskizze zur Spitzenherstellung durch Ätzen*

Aufgrund gravitiver Entfernung der Glasabbau-produkte entsteht ein Konzentrationsgefälle in der Flusssäure, die eine Konvektion hervorruft. Die Konvektion fördert die Flusssäure in den oberen Randbereich der Spitze, die sich somit kegelförmig ausbildet (Abb.5)
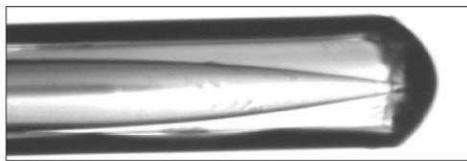

Abb. 6 *Faserspitze nach dem Ätzen*

Im Anschluss an das Ätzen wird das verbleibende Coating chemisch entfernt (Abb.6) und die Spitze metallisiert. Durch Anätzen bzw. Lift-Off - Verfahren wird in einem weiteren Prozessschritt die benötigte kleine Apertur von ca. 100nm am Ende der Faserspitze geschaffen.
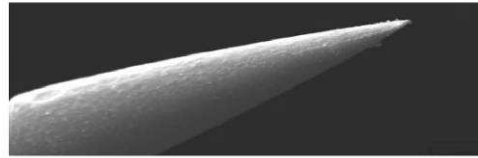

Abb. 7 *Faserspitze nach dem Entfernen des Coatings*

3 Lithografie auf SNOL- Basis

Über einen Akustooptischen Modulator (AOM), zur Steuerung der Lichtintensität wird der Laserstrahl eines He-Cd Lasers über eine Lichtleitfaser mit ausgezogener Spitze auf das mit Fotolack beschichtete Substrat gelenkt. Die Abstands-regelung der Faserspitze erfolgt über Scherkraft-Wechselwirkung.
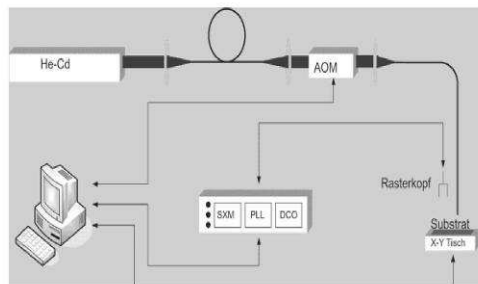

Abb. 8 *Blockschaltbild des SNOL- Systems*

Dabei wird die Faserspitze mittels eines Zitterpiezos in Schwingungen versetzt. Ab einem Abstand der kleiner ist als 30nm, wird die Schwingung der Spitze durch die Scherkraft-Wechselwirkung gedämpft. Diese Dämpfung wird durch einen Stimmgabel-Piezo gemessen.
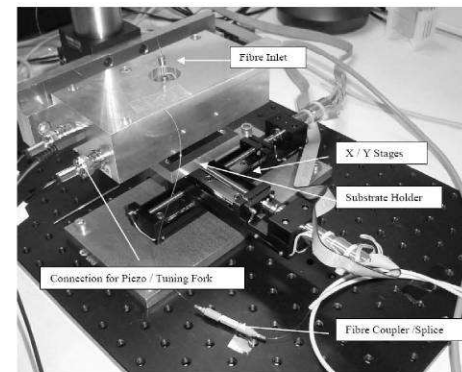

Abb. 9 *SNOL- Systems mit X-Y Positioniereinheit*

Mit Hilfe dieses Systems wurde die folgende Testmikrostruktur mit einer Auflösung von ca. 800nm geschrieben (Abb.10).
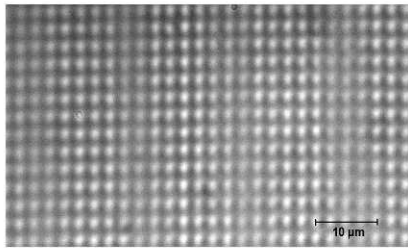
Abb. 10 *Mit SNOL geschriebene DOE – Struktur eines Punktrasters (Punktdurchmesser: 800nm)*

4 Charakterisierung von Foki mittels SNOL-Faserspitzen

Zur räumlichen Vermessung von Laserstrahlen und deren Foki stehen diverse Verfahren zur Verfügung (z.B. Schneidenverfahren). Gemeinhin sind diese jedoch nur bei relativ schwach fokussierten Strahlen anwendbar. Bei Fokussierungen unter hohen Aperturen und im Bereich des Beugungslimits versagen sie. Durch den Einsatz einer Faserspitze, welche mit Hilfe einer Feinpositioniereinrichtung dreidimensional durch den zu prüfenden Fokus bewegt wird, kann eine höhere Auflösung erreicht werden. Abb. 11 zeigt den grundsätzlichen Aufbau, bestehend aus Piezofeintrieb zum schichtweisen Scannen der Faserspitze und dem Fotomultiplier (PMT) zur Detektion des mittels einer Linse (NA=0.65) fokussierten Laserlichtes.
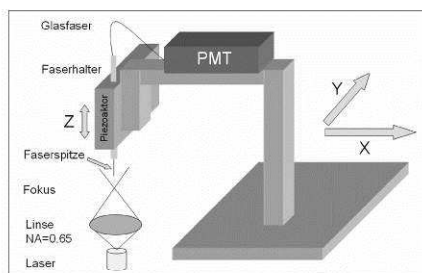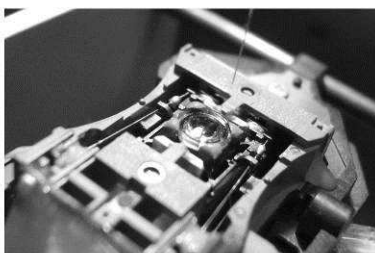

Abb. 11 *Aufbau zur Fokusvermessung*

Abb. 12 *Strahlquelle mit Fokussierlinse und Faserspitze*

Mit diesem Aufbau wurde das Strahlprofil einer fokussierten Laserdiode vermessen. Das Schirmbild

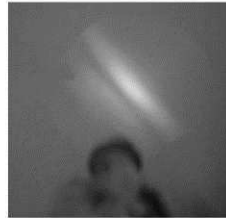der Diode ist in Abb. 13 dargestellt und zeigt das ovale Profil der Abstrahlcharakteristik.

Abb. 13 *Schirmbild der Abstrahlcharakteristik der verwendeten Laserdiode*

Nach Detektion und Aufbereitung wird das Signal bildgebend dargestellt. Das Strahlprofil kann sowohl 2- als auch 3-dimensional visualisiert werden. Abb. 14 zeigt jeweils einen Grobscan des Fokus mit einer Auflösung von: 1 Teileinheit =30µm
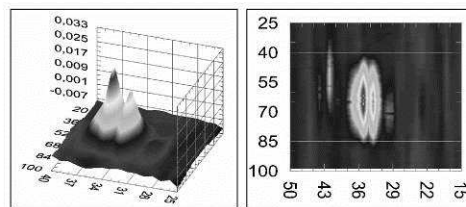

Abb. 14 *2D/3D-Darstellung der mittels Faserspitze vermessenen Abstrahl-Charakteristik der Laserdiode*

5 Lithografie auf konfokaler Basis

Eine Alternative zu dem genannten Fotolack-Belichtungs-Verfahren stellt die Lithografie mittels eines konfokalen Systems dar (Abb.15).
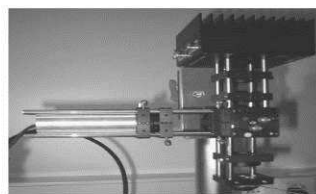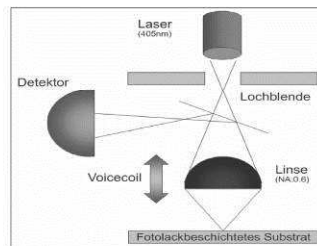

Abb. 15 *Prinzip und Aufbau des Konfokalsystems*

Mit diesem ist es möglich eine Fotolackschicht ebenfalls im Submikrometerbereich zu strukturieren und das Ergebnis zu charakterisieren. Der verwendete Laser besitzt eine Wellenlänge von λ=405nm.
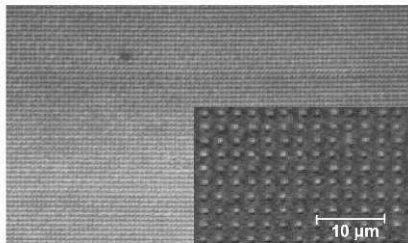

Abb. 16 *Mit Konfokal- System geschriebenes DOE –Testmusters (Graukeil mit Punktdurchmessern von ca. 800nm)*

Die nachfolgenden Abbildungen 17 und 18 zeigen die rasterkraftmikroskopische (AFM) Charakterisierung eines einzelnen Punkts aus dem Punktraster- Testmuster von Abb.16.
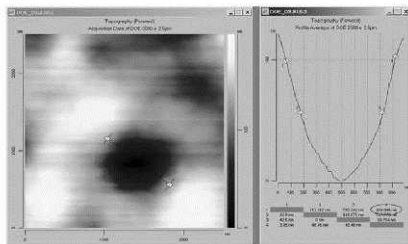

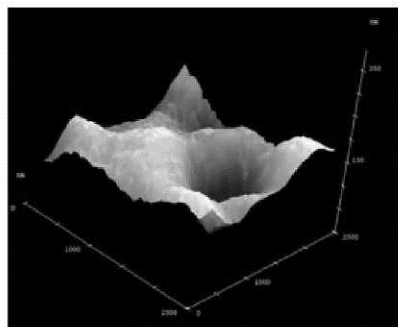**Abb. 17** *2D-Darstellung der AFM-Charakterisierung des Testmusters aus Abb.16*

Abb. 18 *3D-Darstellung der AFM-Charakterisierung des Testmusters aus Abb.16*

6 Charakterisierung technischer Oberflächen auf konfokaler Basis

Neben der Strukturierung technischer Oberflächen lassen sich, wie auch bei dem SNOM-System Oberflächentopografien darstellen.
Abb. 19 zeigt den Scan eines kommerziell gefertigten Moiregitters (Grid: 80 line pairs / mm).
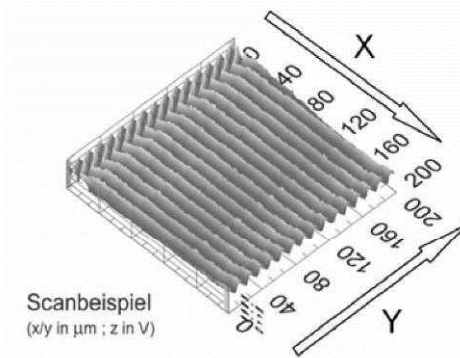
Abb. 19 *Scan eines Moiregitters*

Bisher wurden mit diesen Verfahren (SNOL, Konfokal) Strukturen mit Ortsauflösungen im Bereich von ca. 800nm realisiert. Zukünftig sollen durch Verwendung anderer Optiken und weiter optimierter Faserspitzen kleinere Strukturen für diffraktive Optiken erstellt und ihre Mikrostruktur charakterisiert werden.

Literatur

[1] Suh Y, Zenobi R, Improves Probes for Scanning Near Field Optical Microscopy, Advanced Materials, 12(15), 1139, (2000)

[2] Physik Journal 1 (2002) Nr.3,Seite 40

Charakterisierung von Laserstrahlfoki mittels SNOM- Faserspitzen und Anwendungen einer 405nm Optical Pickup Unit

H.Buse, T. Sobczak , F.Buchmüller, R.Parkin*, H.Kreitlow

Fachhochschule Oldenburg / Ostfriesland / Wilhelmshaven Constantiaplatz 4 26723 Emden
* Mechanical and Manufacturing Engineering / Loughborough University Leicestershire LE11 3TU UK

mailto:hauke.buse@fho-emden.de

Die etablierten Verfahren zur Strahlprofilvermessung sind nur bei kleinen Aperturen anwendbar. Durch das vorgestellte System kann hierfür eine höhere Auflösung erreicht werden. Dieses System wurde zur Strahlvermessung u.a. an einer 405nm Optical Pickup Unit erprobt, die zur Oberflächen- Charakterisierung und zur Strukturierung von Photolackschichten modifiziert wurde.

1 Grundlagen

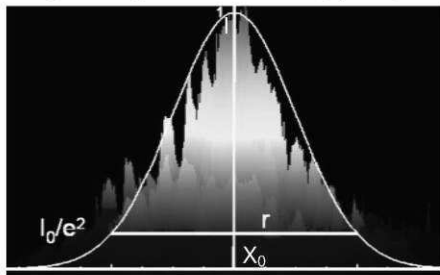Das ideale Profil eines TEM00 Laserstrahls hat eine gausförmige Intensitätsverteilung (Abb.1).

Abb. 1 *Messdatendarstellung im Vergleich mit einem Gaussprofil*

Die Intensitätsverteilung I(x,y) eines solchen Strahls wird von Chapple [1] wie folgt beschrieben:

$$I(x,y) = I_0 \exp\left[-\frac{((x-x_0)^2 + (y-y_0)^2)}{r^2} \right]$$

Wobei I_0 die Maximalintensität am Punkt x_0 darstellt und r den Radius an der Stellen I_0/e^2.

2 Vermessungsverfahren

Die klassischen Strahlvermessungsverfahren wie z.B. das Schneidenverfahren oder die Charakterisierung mittels CCD Kameras sind in der Literatur hinreichend beschrieben und werden hier nicht weiter behandelt. Ihnen gemein ist die Limitierung seitens der Ortsauflösung bzw. die Integrale Messmethodik beim Schneidenverfahren, die eine Auflösung von lokalen Maxima (sog. "Hot-Spots") nicht erlaubt.

3 Fokusvermessung mit Glasfaserspitzen

Der grundsätzliche Aufbau des Messsystems mit Glasfaserspitzen ist in Abb.2 dargestellt. Hierbei dient die Spitze (Apertur ~100nm) einer Monomode Glasfaser (vgl. [3]) als Messwertaufnehmer, welche hochauflösend dreidimensional durch den zu vermessenden Laserstrahl geführt wird.
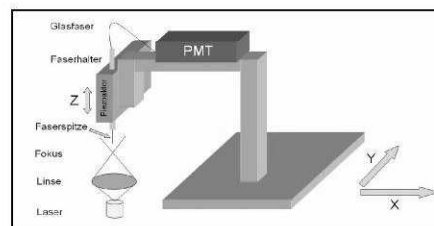

Abb. 2 *Schematischer Aufbau des Systems*

Ergebnisse von Messungen mit diesem System sind in Abb.3 beispielhaft für den Strahlaustritt einer Blu-Ray© Optical Pickup Unit (OPU; 405nm) zu sehen.
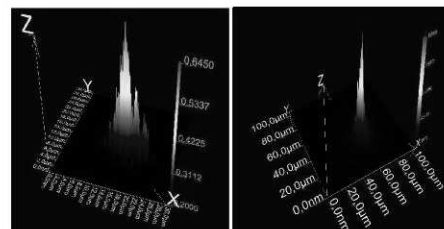

Abb. 3 *Strahlprofil einer Blu-Ray Optical Pickup Unit (Auflösung 150nm/div + 1µm/div)*

4 Oberflächencharakterisierung via 405nm OPU

Die unter Punkt 3 charakterisierte Optical Pickup Unit (OPU), deren schematischer Aufbau in Abb.4 (rechts) dargestellt ist, wird verwendet um Topografien technischer Oberflächen zu ermitteln.
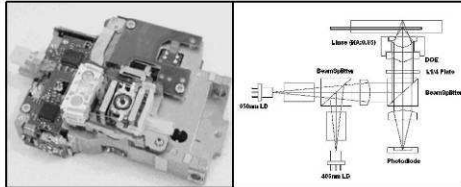

Abb. 4 *Optical Pickup Unit (OPU)*

Als Beispiel dient hier eine Teststruktur für Rasterelektronenmikroskope (REM) der Firma Plano (S1930). Abb. 5 (links) zeigt eine REM Aufnahme dieser Struktur, im rechten Bild ist die 2D Darstellung der mit der 405nm OPU erhaltenen Messergebnisse zu sehen
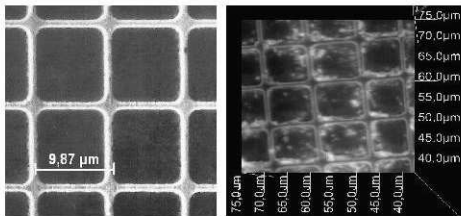

Abb. 5 *Teststruktur S1930*

Einen dreidimensionalen Eindruck vermittelt Abb.5: Im linken Bereich ist die rasterkraftmikroskopische Aufnahme (AFM) der Struktur dargestellt, rechts das 3D Bild der mit dem hier entwickelten System gewonnenen Messdaten.
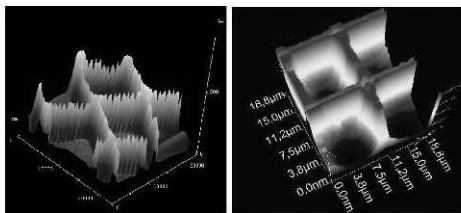

Abb. 6 *Dreidimensionale Ansichten der Test Struktur S1930*

5 Oberflächenstrukturierung via 405nm OPU

Über die Verwendung zur Oberflächencharakterisierung hinaus wurde der Einsatz der OPU zur Mikro- und Nanostrukturierung von Photolackoberflächen evaluiert. Beispiele zur Strukturierung sim im Folgenden die Nachbildung einer Haifischhaut,

eines Graustufen-Punktrasters und eines Dammangitters (Fan-Out Element) zur Strahlteilung.

a.) Haifischhaut ähnliche Struktur (vgl.[4]) , die zum Einen die Anhaftung von Seepocken minimieren, und somit zum Verzicht auf umweltschädliche Antifoulings beitragen kann, und zum Anderen strömungsgünstige Eigenschaften besitzt.
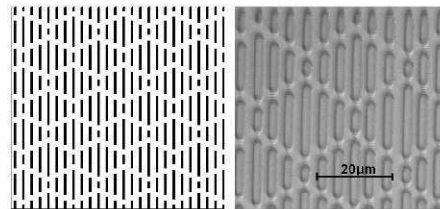
Abb. 7 *Haifischhautstruktur, links: Computermodell, rechts :Mikroskopische Aufnahme der Fotolackstruktur*

b.) Graustufen-Punktraster
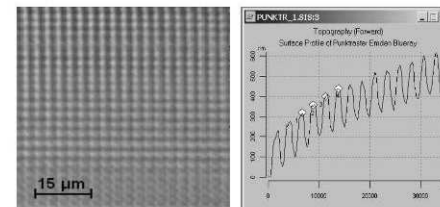
Abb. 8 *Graustufenstruktur, links: Mikroskopische Aufnahme, rechts: AFM Höhenverlauf*

c.) Damman Gitter zur Strahlteilung
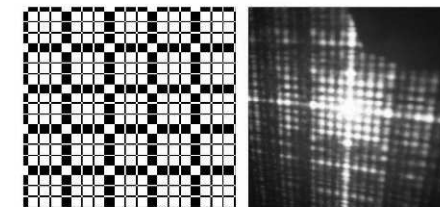
Abb. 9 *Dammanngitter, links Computermodell, rechts: Beugungsbild der Struktur*

Literatur

[1] P.B.Chapple, Opt. Eng. 33, 2461 (1994)

[2] R.L.McCally, Appl. Opt. 23, 2227 (1984)

[3] H.Buse,F.Ahnepohl,F.Buchmüller,R.Parkin, H.Kreitlow DGAO Proceedings 107 (2006)

[4] Anthony B. Brennan et al. , Biofouling, 22(1), 11-21 (2006)

TI-Technologie Informationen 2-2007

(Published by the technology transfer institutes of the Universities of Lower Saxony)

Struktur einer Haifischhaut und synthetische Nachahmung (Quelle: BMBF)

Fachhochschule
Oldenburg/Ostfriesland/Wilhelmshaven
Institut für Lasertechnik Ostfriesland
Prof. Dr. Horst Kreitlow
Dipl.-Ing. Hauke Buse
hauke.buse@fho-emden.de

Transferstelle: Tel. 04921.807-1385

Vorbild Natur – Oberflächen mit Haifischhaut-Effekt
Mikrostrukturierung technischer Funktionsoberflächen

Oberflächen, wie sie in der Natur zum Beispiel bei der Haifischhaut oder den Lotusblättern vorkommen, eignen sich als Vorbild für mikrostrukturierte Funktionsoberflächen technischer Bauteile. Anwendung finden sie unter anderem als Ersatz von umweltschädlichen Antifouling-Anstrichen bei der Beschichtung von Schiffsrümpfen (Maßnahme gegen den Bewuchs) und zur Verrin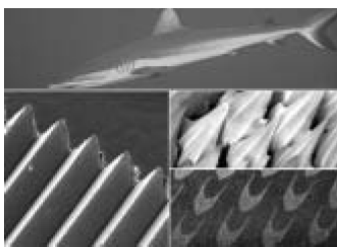gerung des Strömungswiderstandes. Entsprechende Masken oder Werkzeuge zur Realisierung solcher Oberflächen lassen sich mit verschiedenen lithografischen Verfahren herstellen, mit denen Fotolacke strukturiert werden können.

Werden Ortsauflösungen gefordert, deren Strukturgröße im Bereich unter einem Mikrometer liegen, wird die Fotolackbelichtung durch das Phänomen der Beugung erschwert. So lassen sich unter Verwendung sichtbaren Lichts nur Strukturen bis zu etwa einem halben Mikrometer Breite realisieren. Die Anwendung eines Scanning Nearfield Optical Lithography Systems (SNOL) macht es möglich, das Beugungslimit bei der Strukturierung zu umgehen.

An der Fachhochschule Oldenburg/Ostfriesland/Wilhelmshaven, Standort Emden, wurde ein SNOL-System in Verbindung mit einer XY-Positioniereinheit entwickelt, mit dem Strukturen im Sub-Mikrometerbereich hergestellt werden können. Dies wird durch eine ausgezogene Lichtleitfaserspitze mit einer Apertur (Öffnungsblende) von zirka 100 Nanometern erreicht, die in einem Abstand von etwa zehn Nanometern über die Fotolackoberfläche geführt wird. Dadurch können Strukturgrößen im Sub-Mikrometerbereich erzeugt werden, bei denen herkömmliche Verfahren versagen. ■

Implementation and application of a „triple wavelength laser diode into a lithography setup

H.Buse, T. Sobczak, S.Ernst, R.Parkin*, H.Kreitlow

Fachhochschule Oldenburg / Ostfriesland / Wilhelmshaven Constantiaplatz 4 26723 Emden
* Mechanical and Manufacturing Engineering / Loughborough University Leicestershire LE11 3TU UK

mailto:hauke.buse@fho-emden.de

In directly writing lithography systems, better control of the focal position of the "writing beam" can be gained by implementing a laser diode, emitting 3 different wavelengths (405nm, 650nm and 780nm). This facilitates the realization of higher resolution, improved reproducibility and better quality of the structures.

1 Fundamentals

Lithography on confocal basis (Fig.2) is one alternative possibility to expose photo resist surfaces within lithography processes using focussed laser beams (Fig.1).
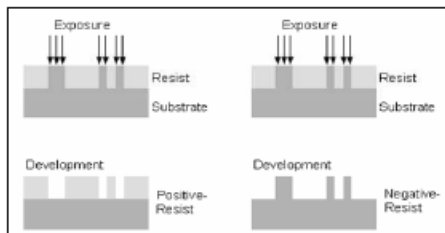
Fig. 1 Principle of lithography process

The reflected light from the resist-surface (focal plane) is used to control the distance or the focal position of the "writing beam", respectively.
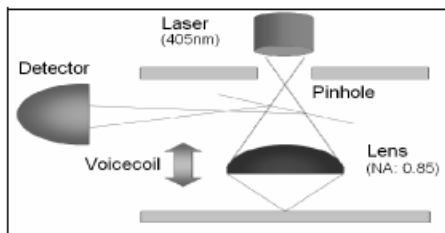
Fig. 2 Scheme of a confocal system

2 Implementation

The resist coated substrate, which has to be structured, is located below the focussing lens on an X-Y table. The X-Y table is controlled pointwise by Labview© according to the desired pattern (Fig.3).
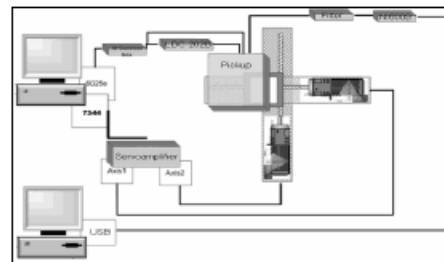
Fig. 3 Laser lithography setup

The laser diode used within the setup emits 3 wavelengths (3λLD; Fig.4), from which the 405nm is used to structure the photo resist. To control the focal position of the „writing beam", the signal of the reflected light of the 650nm laser diode is sent to a computer via an USB Interface.
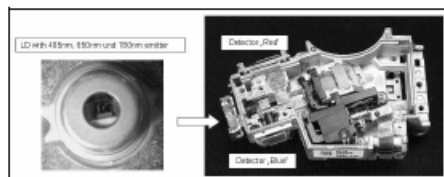
Fig. 4 Optical unit with 3λ laser diode at the left (Pictures © Leslie Wright / Samuel Goldwasser)

3 Application and results

A homogeneous, planar and error-free photo-resist layer (Fig.5) is highly important for proper structuring of technical surfaces.
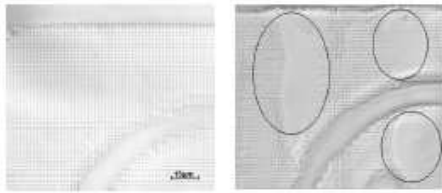
Fig. 5 Structured photo-resist: left: error-free resist layer; right: faulty photo resist layer

Errors within the photo resist layer caused by different resist heights are shown in Fig.5. These height differences result in constant distance changes between the resist surface and the focussing lens: Therefore a uniform exposure of the resist is not possible. Fig.6 shows the signal of the 650nm laser diode: A linear increasing unevenness of the resist layer causes a saw tooth signal.

Fig. 6 Signal response of the 650nm laser diode

Intention of a control unit is to minimize this effect by adjusting the actuator (voice coil) based on the signal gained by the 650nm diode.

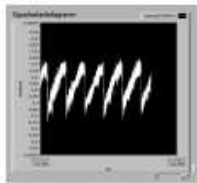Fig.7 shows structured surfaces: A diffractive optical element (DOE) here: Dammangrating (used to split laser beams) at the left and a section of a computer generated hologram (CGH) at the right.
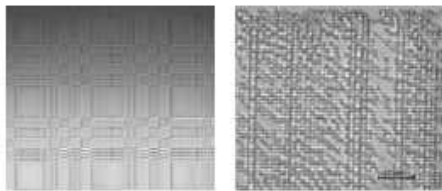

Fig. 7 Structured photo resist: left: DOE (Dammangrating); right: CGH (used for projection purposes)

Further development

Near field optical techniques are suitable to bypass the limitation of optical resolution caused by diffraction. By this, smaller structures can be realized. Solid immersion systems make use of the frustrated total internal reflection (FTIR) at a boundary layer. In solid immersion lens (SIL) systems, a hemispherical lens (or a more complex shaped "super hemispherical lens") is placed in front of the focussing lens of the confocal optical unit (see

Fig.2) , so that the focal plane of the focussing lens coincides with the planar surface of the SI- lens (Fig.8).
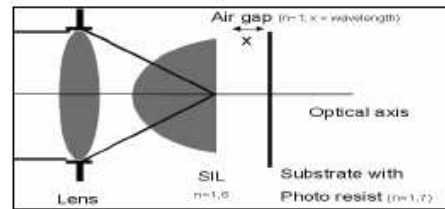
Fig. 8 Functional scheme of structuring optics with solid immersion lens (SIL)

If this lens-system is brought close to a surface (air gap/ boundary layer <λ), evanescent waves propagate beyond the boundary layer (Fig.9) [1]. This process is called FTIR and can be used to structure photo resist surfaces with high resolution or, by using information gained by the reflected light, to characterize surfaces and their topographies.
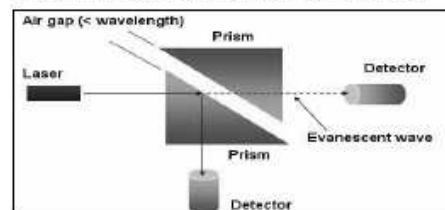
Fig. 9 Principle of frustrated total internal reflection (FTIR)

Fig.10 (left) shows an example of a laboratory SI-setup used for data storage realized by Philips N.V. The picture on the right displays a solid immersion lens made out of diamond produced by Element Six Ltd.
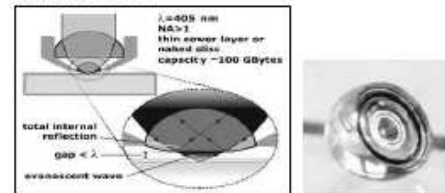
Fig. 10 Left: SI-lenses for data storage (© Philips N.V); right: Example of SI-lens (© Element Six Ltd.)

In our running experiments these lens systems are tested for Nano- and microstructuring.

Literature

[1] J.Tominaga, T.Nakano; Optical Near- field Recording (2005)

275

Lasers in Engineering (in evaluation process)

Method for characterisation of laser beams diverging from large NA by means of optical fibre tips

H.Buse, S.Ernst, R.Parkin*, H.Kreitlow

Fachhochschule Oldenburg / Ostfriesland / Wilhelmshaven; Constantiaplatz 4; 26723 Emden; Germany

* Mechanical and Manufacturing Engineering / Loughborough University Leicestershire LE11 3TU UK

Abstract:

Especially in the field of laser direct writing lithography it is necessary to gain exact knowledge about the shape and characteristics of the illuminating laser beam, whilst a homogeneous power distribution is an essential parameter for good and reproducible results in surface structuring.

We present a way of characterisation the power distribution within focussed laser beams by scanning its focal plane with optical fibre tips, commonly used for scanning near field optical microscopy.

Compared to established profiling techniques, this technique is suitable for locally high resolved characterisation of very small focal apertures, e.g. beams diverging from lenses of DVD or BluRay© devices with numerical apertures (NA) in the range of 0.6 up to 0.85. The presented technique has been used to characterise a laser beam emerged by a modified optical pickup unit (OPU) applied to laser direct writing processes for structuring photo resist surfaces.

Method for characterisation of laser beams diverging from large NA by means of optical fibre tips

1. General

Especially in the field of laser direct writing lithography it is necessary to gain exact knowledge about the shape and characteristics of the used laser beam, whilst a homogeneous power distribution is an essential parameter for qualitatively good and reproducible results in surface structuring.

Several "classical" methods in characterisation of laser beams are already applied, such as:

- Knife edge method
- Slit method
- Pinhole method
- CCD camera method

These techniques will be shortly explained in section 2.

In fact, a laser beam ("standard TEM00") fades gradually, due to its Gaussian profile (Figure 1). Therefore it is necessary to determine what is known as the centre of the beam.

Chapple [1] describes the intensity profile I(x, y) as follows:

$$I(x, y) = I_0 \exp\left[-\frac{2((x-x_0)^2 + (y-y_0)^2)}{r^2}\right]$$

where x and y are the transverse Cartesian coordinates of any point, x_0 and y_0 mark the centre of the beam and r is the $1/e^2$ radius. This definition is often used in theory.

McCally [2] defines the Gaussian distribution of the intensity I(x, y) by means of the beam radius R belonging to the 1/e irradiance shown in Figure 1 (left).

2

The emitted power of the laser source can be determined by integrating the irradiance (I), respectively the optical intensity I(x, y), over the affected cross sectional area A:

$$P = \int I dA$$

2. Techniques of beam profiling

Knife edge method

To gain information about the power distribution across a cross sectional plane of a laser beam, the usage of the knife edge method is the most simple approach. Thereby, a sharp edged plate, e.g. a razor blade, is initially covering the whole laser beam in front of a power meter for continues wave radiation or an energy meter for pulse operation. By precise line wise displacement of the knife edge mounted on a linear movement stage, more and more laser radiation reaches the sensor unit, until the whole beam is covering the sensing area.

Figure 1 (right) shows the result of this measurement procedure: Due to the movement of the knife edge the value of the detected power increases steadily. The derivative of this power function P(x, y) yields the two dimensional Gaussian profile of the power distribution across the laser beam (Figure 1, left).

Slit method

A second possibility to determine the power distribution within a laser beam is similar to the knife edge method: Instead of a sharp edged plate, a very narrow slit is stepwise moved across the laser beam. As a precondition for valid measurements the opening of the slit has to be smaller than the diameter of the considered beam is. Typically this opening is in the range of some microns.

3

Drawbacks of "traditional methods"

The knife edge- as well as the slit method offer only a limited quantity of beam characteristics: local "hot-spots", i.e. areas of superior power, are undetectable due to the integrating measurement principle. Nevertheless this method is suitable for quick measurements to determine the diameter and the course intensity profile of the considered laser beam.

Pinhole method

This method measures the intensity of irradiance through a very small hole in a plate (pinhole) facing the laser beam. The intensity of light passing through this pinhole is rather low, so that a photomultiplier tube (PMT) has to be used to detect the irradiance.

Due to the characteristic of a PMT, e.g. its relatively low signal to noise ration (SNR), the collected data are corrugated. However the intensity distribution can be achieved within a local resolution of approximately 3micron by applying a Gaussian fit. Therefore by transversal scanning across a laser beam, a high resolution image of the power distribution within the beam can be gained. Hot spots are detectable and more detailed features can be located.

CCD Camera method

Differing from the scanning methods described above, the usage of CCD (Charge-coupled Device) cameras for the inspection of laser spots will give a very quick impression of the power distribution within the beam by just a "single shot".

The quality of the image, e.g. the resolution, is directly depending on size and number of pixels on the CCD-Sensor-chip. Typically the pixel size is in the range of 6 microns^2, linked to a total number of pixels in the range of 1 to 2 mega pixels. By using this method it must be noted, that dust and other impurities on the CCD chip can result in image distortion and/or

4

Drawbacks of "traditional methods"

The knife edge- as well as the slit method offer only a limited quantity of beam characteristics: local "hot-spots", i.e. areas of superior power, are undetectable due to the integrating measurement principle. Nevertheless this method is suitable for quick measurements to determine the diameter and the course intensity profile of the considered laser beam.

Pinhole method

This method measures the intensity of irradiance through a very small hole in a plate (pinhole) facing the laser beam. The intensity of light passing through this pinhole is rather low, so that a photomultiplier tube (PMT) has to be used to detect the irradiance.

Due to the characteristic of a PMT, e.g. its relatively low signal to noise ration (SNR), the collected data are corrugated. However the intensity distribution can be achieved within a local resolution of approximately 3micron by applying a Gaussian fit. Therefore by transversal scanning across a laser beam, a high resolution image of the power distribution within the beam can be gained. Hot spots are detectable and more detailed features can be located.

CCD Camera method

Differing from the scanning methods described above, the usage of CCD (Charge-coupled Device) cameras for the inspection of laser spots will give a very quick impression of the power distribution within the beam by just a "single shot".

The quality of the image, e.g. the resolution, is directly depending on size and number of pixels on the CCD-Sensor-chip. Typically the pixel size is in the range of 6 $microns^2$, linked to a total number of pixels in the range of 1 to 2 mega pixels. By using this method it must be noted, that dust and other impurities on the CCD chip can result in image distortion and/or

4

misinterpretable beam features. Moreover, care must be taken not to destroy the CCD chip by the incident laser beam.

3. Beam characterisation by means of optical fibre tips

To overcome the limited resolution of the CCD- and pinhole method, respectively, a new intensity profile measurement technique has been developed.

Similar to the pinhole method described above, an optical fibre tip with an aperture of a few 100 nm is applied to collect light by scanning across a laser beam transversally. A photomultiplier tube (PMT) attached at the out-coupling end of the fibre detects the collected light during the scanning process so that a 2-dimensional image of the intensity distribution can be evaluated.

By changing the lateral position of the fibre tip, multiple cross sectional planes can be scanned, leading to a 3-dimensional image of the intensity distribution e.g. within a focused laser beam.

3.1 Near-field coupling into the optical fibre

"Classical" approaches to depict the incoupling of light into the fibre tip fail, due to the very small opening of the fibre tip (aperture), in the range of some hundred nanometres, which is considerable smaller than the wavelength of the laser light within the focus. Due to this very small opening, one can talk about the so called "near field"

To gain information originating from the near field and to transport this information into the far field, it is necessary to transform the evanescent fields into propagating fields. This could be done by putting a centre of scattering, in this case the very narrow tip, into the near field. Thereby dipole- oscillations are generated at the boundary of this tip by means of the evanescent field (Figure 2).

5

$$\vec{E}_{Dipole} = \frac{1}{4\pi\varepsilon_0}\{k^2(\vec{n}\times\vec{p})\times\vec{n}\frac{1}{r} + [3\vec{n}(\vec{n}\cdot\vec{p}) - \vec{p}](\frac{1}{r^3} - \frac{ik}{r^2})\}\exp i(\omega t - \vec{k}\cdot\vec{r})$$

With: ε_0= vacuum permittivity; $\vec{n}$=unit vector; $\vec{k}$= wave vector: $2\pi / \lambda$; ω= angular frequency

of the oscillation and using the dipole-moment $\vec{p}$:

$$\vec{p} = (\frac{\varepsilon - 1}{\varepsilon + 2})\, a^3 \vec{E}_{in}$$

With: a=diameter of the opening; ε_r=relative permittivity

The following terms for the far field (r << λ/2) and the near field (r >> λ/2) can be derived,

and one gets not-propagating as well as propagating field components:

$$\vec{E}_{Near\,field} = \frac{3\vec{n}(\vec{n}\cdot\vec{p}) - \vec{p}}{4\pi\varepsilon_0 r^3}\exp i(\omega t - \vec{k}\cdot\vec{r})$$

Respectively:

$$\vec{E}_{Far\,field} = \frac{k^2(\vec{p} - \vec{n}(\vec{n}\cdot\vec{p}))}{4\pi\varepsilon_0 r}\exp i(\omega t - \vec{k}\cdot\vec{r})$$

The propagating field is directly linked to the near field and can be detected afar. The

simulation of the electrical field generated by a plane wave of 1 V/m, heading to a fibre tip, is

shown in Fig 3. Based on an optical power of 10mW dispersed on an area of 1 square micron,

(which is a rather big area), one get by using:

$$I = S \cdot v = \frac{1}{2}\,E_0\,D_0\,c/n = \frac{1}{2}\,\varepsilon_0\,n^2\,E_0^2\,c/n$$

with:

I= Optical Intensity; S=Pointing vector; v=velocity; E_0=electrical field; D_0= electric induction

density; n= index of refraction (here air: 1.0); ε_0= vacuum permittivity (rounded: 10^{-11} F/m)

$$E_0 = \sqrt{\frac{2I}{\varepsilon_0 nc}} \quad = 10^{10}\,\text{V/m}$$

6

It has to be noted that the field within the tip is exponentially decreasing (refer to formula n) and by this only a very small part of the generated electrical field, in this example $5*10^{10}$ V/m directly at the tip, can be detected at the out coupling end of the fibre by the PMT.

3.2 Setup

The PI P-854.00 piezoelectric actuator used in this setup has a displacement range of 25μm for fine positioning and can also be pre-positioned by a micrometer-screw more roughly. The detection of collected light is done by a Hamamatsu H5784 type photomultiplier tube (PMT) with an E5776 FC type adaptor attached (Figure 4)

A fibre holder mounted to the piezoelectric actuator is used to lead and protect the optical fibre tip during the scanning process. After amplification (x10 by transimpedance amplifier stage) and filtering of the collected intensity data it is converted into digital data by means of a National Instruments 6025e PCI interface card.

3.3 Fibre tip production

For this application the optical fibre type used to produce the tips is a single mode fibre manufactured by Newport. Its cut-off wavelength is optimised for the use of lasers in the wavelength range of 400nm -500nm.

There are two possibilities to develop the conic tip of an optical fibre according to the requests of a Scanning near field optical lithography (SNOL) - fibre tip:

The optical fibre tip can be realised by:

- Pulling methods
- Chemical etching

During the pulling procedure the optical fibre is preloaded before it is heated up locally with a CO2-laser or a heating-film and forced to melt. As the melting process begins, the puller stretches the optical fibre with additional force apart, so that the fibre is tapert first and finally

7

283

tears itself generating two tips.

The properties of the optical fibre tips produced this way vary on the different parameters of the puller - as for example the pulling force.

Commonly, all pulled SNOL-tips show a very lean geometry (e.g. Figure 4, left).

This is especially disadvantageous for the considered application, because this lean structure tends to bend and oscillate. More rigid fibres, which have tips with higher cone angle, are more suitable Furthermore, these fibre tips feature a very small transmission of 10^{-5} to 10^{-6} due to the long shape of the tip, in which the light is evanescent (exponentially decreasing). Larger cone angles and correspondingly a higher transmission up to 10^{-2} is reached by etched SNOL- fibre tips as used in this work.

Several etching methods exist to produce fibre tips. The procedure used here is the so called "tube-etching". After cleaning of the optical fibre by means of ethanol, the fibre is immersed into hydrofluoric acid. (Figure 5)

The following chemical reactions take place to the silicon contained in the fibre - and/or with the germanium at doped fibres:
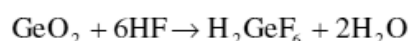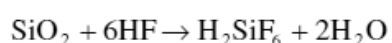
$$SiO_2 + 6HF \rightarrow H_2SiF_6 + 2H_2O$$

$$GeO_2 + 6HF \rightarrow H_2GeF_6 + 2H_2O$$

Tube-Etching is a further development of the standard etching-method, invented by Turner in 1984, published by Stoeckel et al. and Lambelet et al. [4, 5, 6]

This procedure improves the production of considerably smoother tip surfaces. At the tube-Etching procedure the coating of the optical fibre is not removed before the etching process. Due to gravity drawn degradation of the glass products, a concentration slope arises in the hydrofluoric acid, which causes convection. The convection carries the hydrofluoric acid into the upper zone of the tip that develops thus conically.

To prevent corrosion by hydrofluoric acid fumes at the upper regions the fibre, a light mineral oil was used as a solvent to realise a separate phase above the hydrofluoric acid. The

8

temperature during the production of the tips corresponded to room temperature. By completion of the tube-etching process the coating of the optical fibre is removed by dichlorine methane and the tip can be metallized, leaving a small aperture.

4. Results

A test rig has been build using optical fibre tips for automized 3-dimensional intensity profile scanning (Figure 3). With this it is possible to gain information about the spatial power distribution within laser beams. Due to the small aperture of the fibre tip even very small focal regions can be profiled with high local resolution. Corresponding software was developed to control the moving x-y stage, as well as the z actuator automatically using Labview$^©$. Therefore, it is possible to scan across the laser beam tomographically, while collecting intensity data. The data can either be displayed or visualised by means of the scanning software itself. Applying a new developed software based on OpenGl$^©$,

the intensity data can be displayed in a 3 dimensional image (Figure 7) with the opportunity to rotate the direction of view in all degrees of freedom. Furthermore, different mathematical filters can be applied to improve image quality.

By scanning more cross sectional planes, single slices can be shown in an "overlayed" way, to observe the focus "moving" due to the lateral change of the fibre tip (Figure 8)

3. Conclusion

A novel method for high resolving beam characterisation especially for small aperture lasers has been described. With this automized 3- dimensional serial scanning method it is possible to gain information about the spatial power distribution within a laser spot.
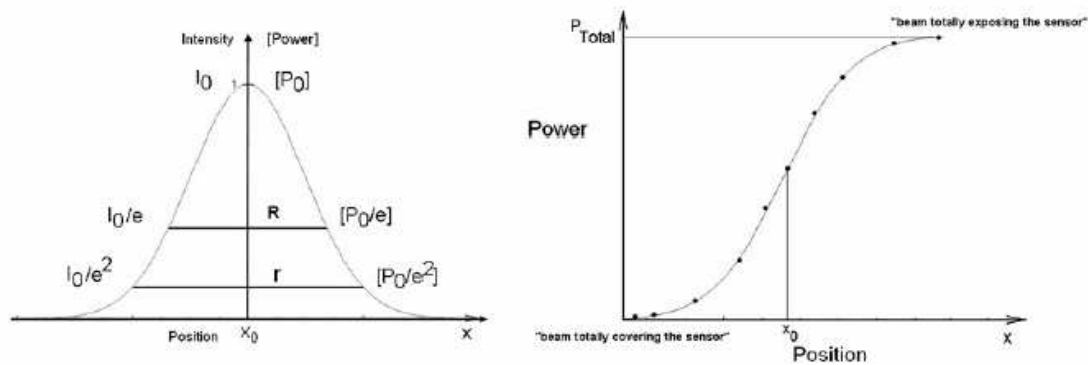
9

4. Figures / Artwork

Figure 1: [left] *Theoretical power distribution within a TEM 00 laser beam can be described by a Gaussian profile* [right] *Integrated laser power measured with the knife edge method as a function of the cross sectional coordinate x.*
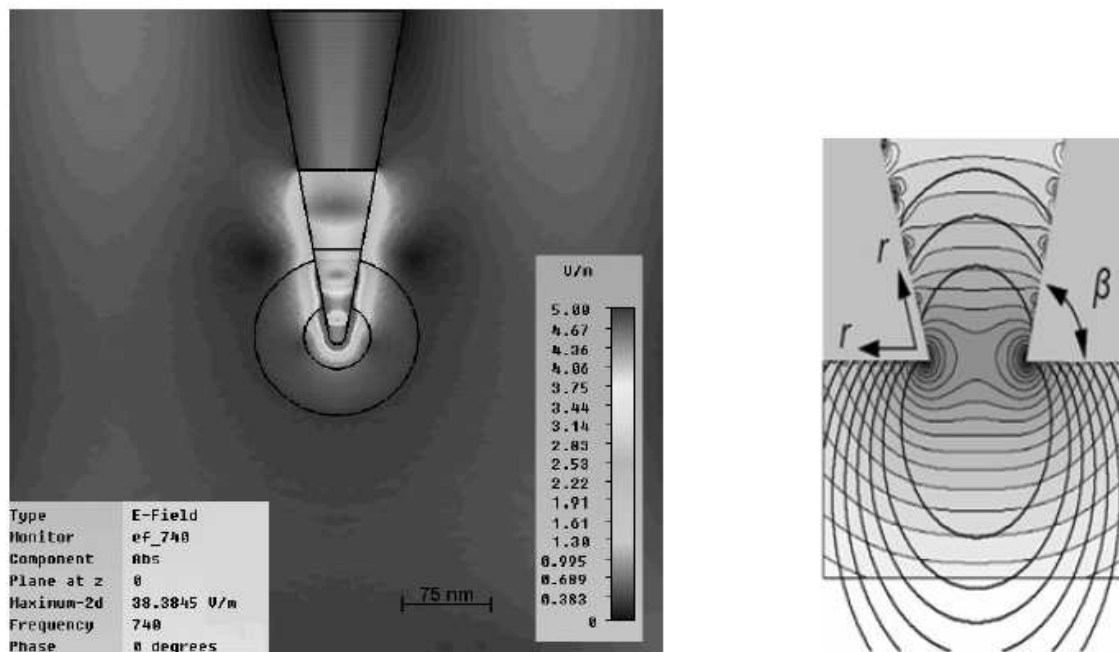

Figure 2: [left] *E-field in the near field of the tip when illuminated by plane wave with field strength of 1 V/m, polarised along the axes of the tip* [right] *Cross-sectional view of an optical fibre tip with an cone angle"β" and an radius from the aperture rim"r" .The associated electric field lines are plotted in logarithmic manner* [3]

10

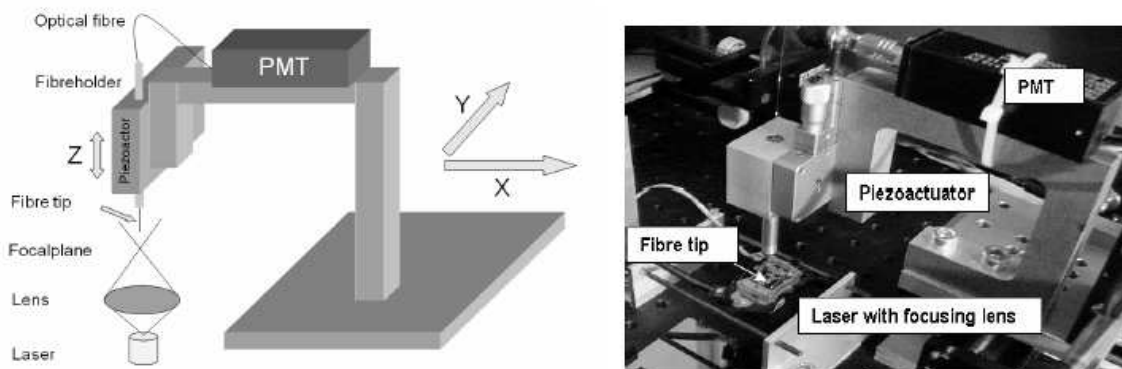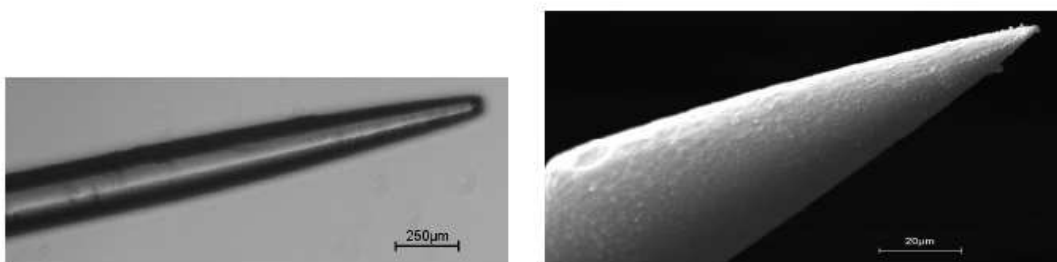**Figure 3:** *Principle and picture of the setup for high resolving laser beam profiling*

Figure 4: *Comparison of a fibre tip produced by the pulling method* [**left**] *and a fibre tip produced by etching* [**right**]
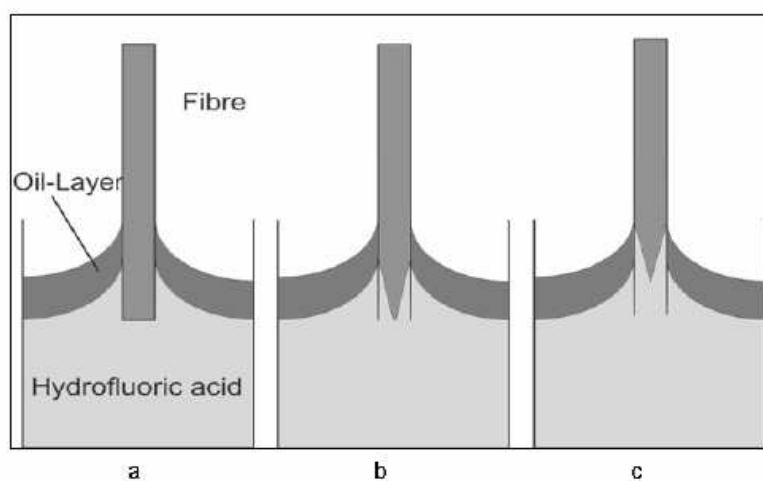

Figure 5: *Schematic representation of the „tube- etching method"*
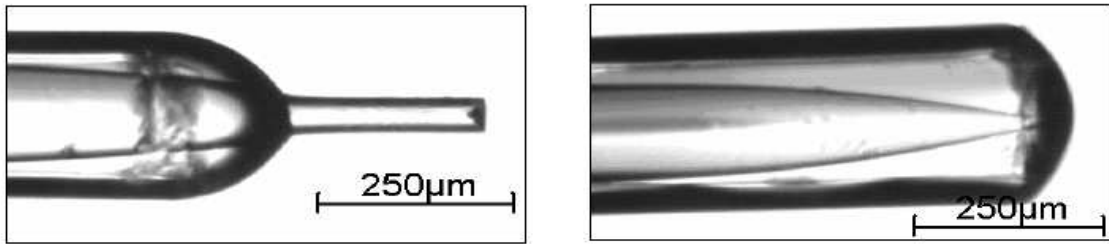
11

Figure 6: [left] *Fibre tip generated by the etching method after 60min etching time (please refer to Figure 4 "b")* [right] *Fibre tip generated by the etching method after 120min etching time (please refer to Figure 4 "c")*
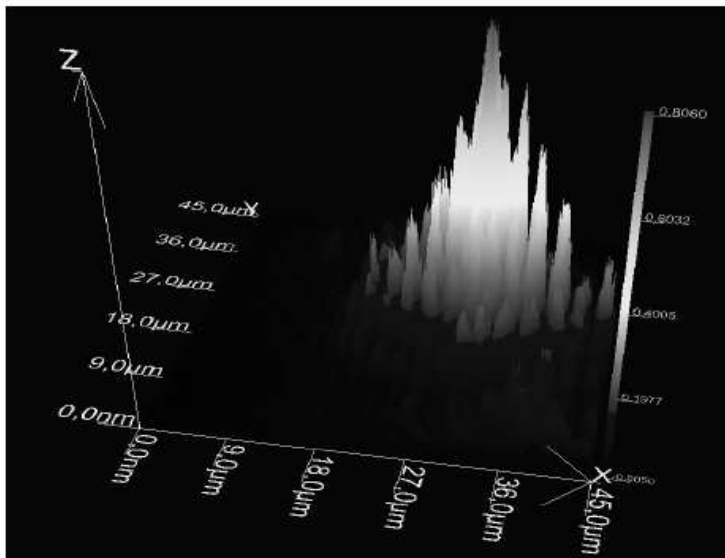

Figure 7: *Beam profile of a DVD optical pickup unit (OPU) gained with the fibre tip based system (resolution: 150nm)*
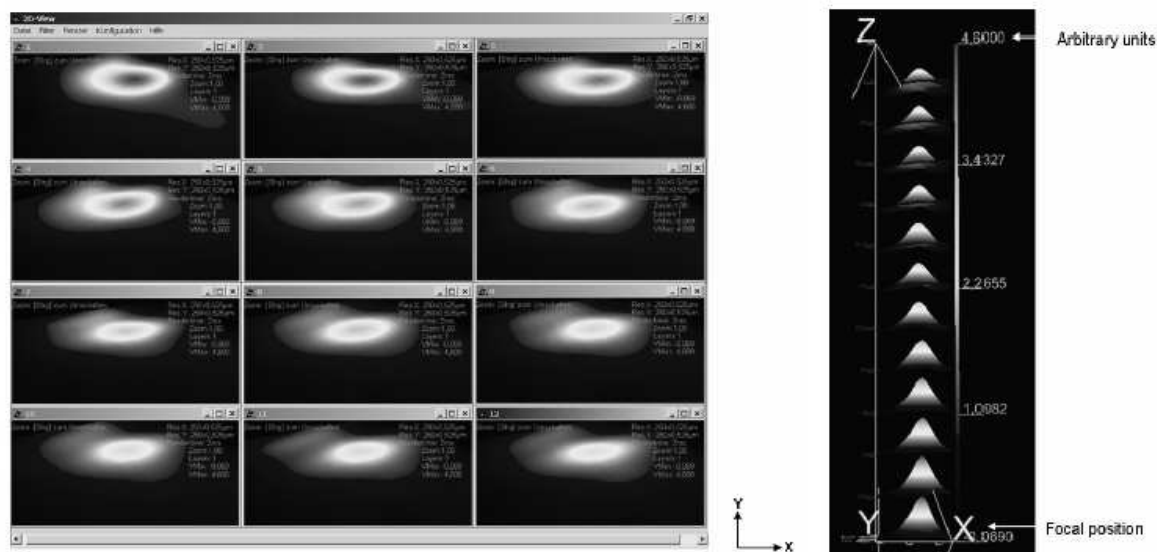
12

Figure 8: [left] *12- step lateral scan through a (TEM00) laser focus of a DVD optical pickup unit (OPU) gained with the fibre tip based system (transversal view)* **[right]** *(lateral view)*

5 Literatures:

[1]   Chapple, P.B., (1994), Beam waist and M2 measurement using a finite slit, Opt. Eng., 33, 2461-2466

[2]   McCally, R.L., (1984) Measurement of Gaussian beam parameters, Appl. Opt., 23, 2227

[3]   Drezet, A., Nasse, M.J., Huant, S., Woehl, J.C., (2004), The optical near-field of an aperture tip; Europhys. Lett., 66 (1), 41–47

[4]   Stockle, R., Fokas, C., Deckert, V., Zenobi, R., Sick, B., Hecht, B., Wild, U.P., (1999), High quality near field optical probes by tube etching, Applied Physics Letters, 75(2), 160-2

[5]   Lambelet, P., Sayah, A., Pfeffer, M., Philipona, C., Marquis Weible, F., (1998), Chemically etched fiber tips for near field optical microscopy: a process for smoother tips, Applied Optics, 37(31), 7289-7292

[6]   Suh, Y., Zenobi, R., (2000), Improved Probes for Scanning Near Field Optical Microscopy, Advanced Materials, 12(15), 1139-1142

13

6.0 Keywords: Near field, far field, laser beam, focus, focal plane, fibre tip, pinhole, knife edge

7.0 Nomenclature:

I= Intensity [W/m]

P=Power [W]

A=Area [m^2]

λ=Wavelength [m]

E=Energy [W/s]

ε= Vacuum permittivity [$A^2 \cdot s^4 \cdot kg^{-1} \cdot m^{-3}$]

ε_r=Relative permittivity [$A^2 \cdot s^4 \cdot kg^{-1} \cdot m^{-3}$]

$\vec{n}$=Unit vector

$\vec{k}$=Wave vector: $2\pi / \lambda$

t=Time [s]

ω= Angular frequency of the oscillation [s^{-1}]

$\vec{p}$=Dipole-moment [$A \cdot m^2$]

a=Diameter of the opening [m]

14

291